NOVEL INSIGHT INTO THE DIAGNOSIS AND TREATMENT OF CARDIO(THORACIC) DISEASES IN DOGS AND CATS

EDITED BY: Ryou Tanaka and Zeki Yilmaz
PUBLISHED IN: Frontiers in Veterinary Science

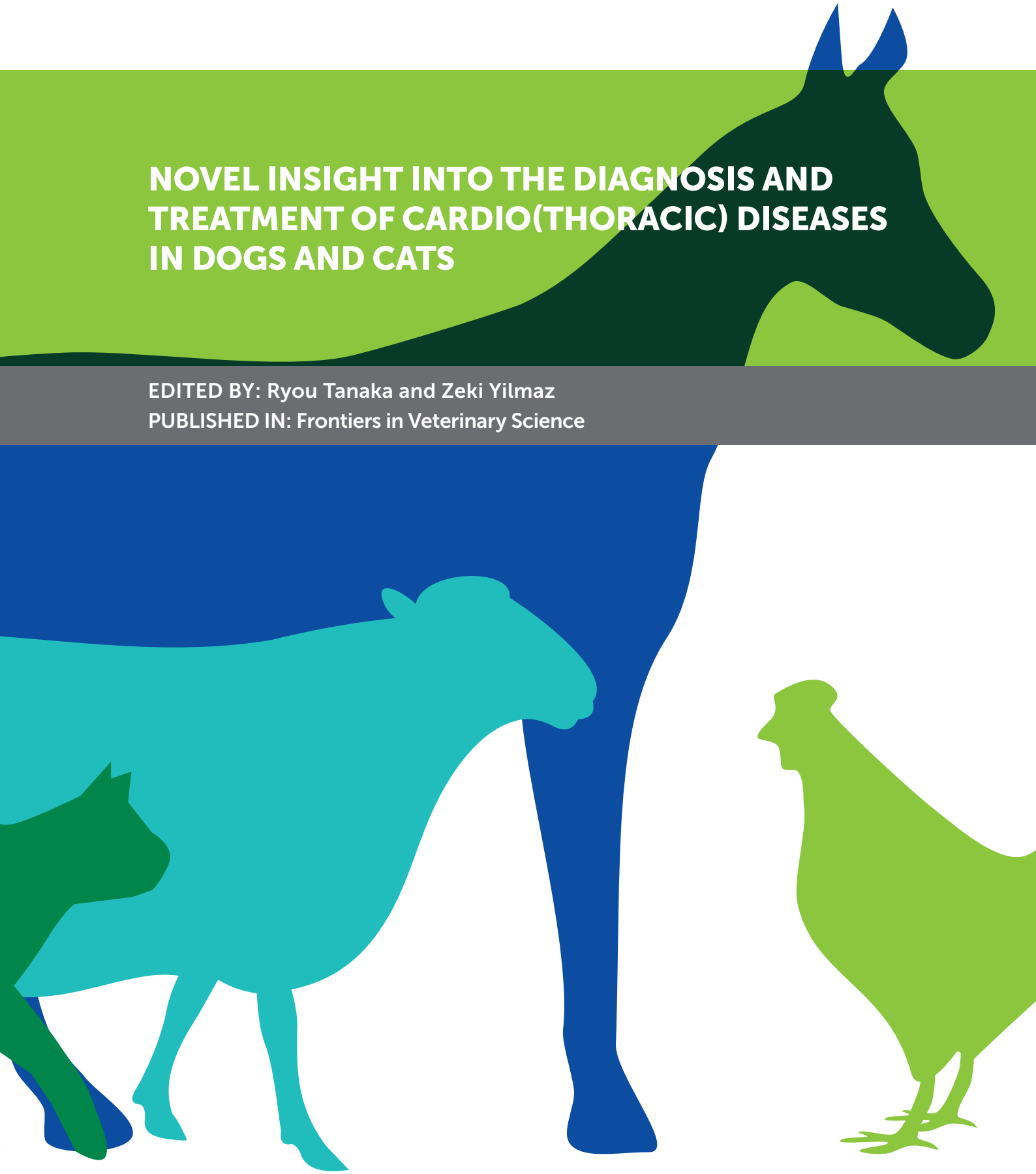

frontiers Research Topics

ISSN 1664-8714
ISBN 978-2-88976-304-7
DOI 10.3389/978-2-88976-304-7

About Frontiers

Frontiers is more than just an open-access publisher of scholarly articles: it is a pioneering approach to the world of academia, radically improving the way scholarly research is managed. The grand vision of Frontiers is a world where all people have an equal opportunity to seek, share and generate knowledge. Frontiers provides immediate and permanent online open access to all its publications, but this alone is not enough to realize our grand goals.

Frontiers Journal Series

The Frontiers Journal Series is a multi-tier and interdisciplinary set of open-access, online journals, promising a paradigm shift from the current review, selection and dissemination processes in academic publishing. All Frontiers journals are driven by researchers for researchers; therefore, they constitute a service to the scholarly community. At the same time, the Frontiers Journal Series operates on a revolutionary invention, the tiered publishing system, initially addressing specific communities of scholars, and gradually climbing up to broader public understanding, thus serving the interests of the lay society, too.

Dedication to Quality

Each Frontiers article is a landmark of the highest quality, thanks to genuinely collaborative interactions between authors and review editors, who include some of the world's best academicians. Research must be certified by peers before entering a stream of knowledge that may eventually reach the public - and shape society; therefore, Frontiers only applies the most rigorous and unbiased reviews.
Frontiers revolutionizes research publishing by freely delivering the most outstanding research, evaluated with no bias from both the academic and social point of view. By applying the most advanced information technologies, Frontiers is catapulting scholarly publishing into a new generation.

What are Frontiers Research Topics?

Frontiers Research Topics are very popular trademarks of the Frontiers Journals Series: they are collections of at least ten articles, all centered on a particular subject. With their unique mix of varied contributions from Original Research to Review Articles, Frontiers Research Topics unify the most influential researchers, the latest key findings and historical advances in a hot research area! Find out more on how to host your own Frontiers Research Topic or contribute to one as an author by contacting the Frontiers Editorial Office: frontiersin.org/about/contact

NOVEL INSIGHT INTO THE DIAGNOSIS AND TREATMENT OF CARDIO(THORACIC) DISEASES IN DOGS AND CATS

Topic Editors:
Ryou Tanaka, Tokyo University of Agriculture and Technology, Japan
Zeki Yilmaz, Department of Internal Medicine, Faculty of Veterinary Medicine, Turkey

Citation: Tanaka, R., Yilmaz, Z., eds. (2022). Novel Insight Into the Diagnosis and Treatment of Cardio(thoracic) Diseases in Dogs and Cats.
Lausanne: Frontiers Media SA. doi: 10.3389/978-2-88976-304-7

Table of Contents

frontiers | Frontiers in Veterinary Science

EDITORIAL
published: 09 May 2022
doi: 10.3389/fvets.2022.914602

Editorial: Novel Insight Into the Diagnosis and Treatment of Cardio(Thoracic) Diseases in Dogs and Cats

Lina Hamabe[1], *Meriç Kocatürk*[2], *Zeki Yilmaz*[2]* *and Ryou Tanaka*[1]

[1] Department of Veterinary Surgery, Tokyo University of Agriculture and Technology, Fuchu, Japan, [2] Department of Internal Medicine, Faculty of Veterinary Medicine, Bursa Uludag University, Bursa, Turkey

Keywords: echocardiography, color Doppler, cardiac biomarker, two-dimensional tissue tracking echocardiography, RV function, pulmonary arterial wave reflection

Editorial on the Research Topic

Novel Insight Into the Diagnosis and Treatment of Cardio(Thoracic) Diseases in Dogs and Cats

Improved diet, management, and health care of companion animals have led to increased life expectancy, as a result, cardiac diseases have become pivotal causes of death for both dogs and cats. For such reason, a major objective has become to increase the quality of life by reducing the expansion of cardiac diseases via early detection of diseases and provision of effective treatment.

Conventional echocardiography and cardiac biomarkers, such as N-terminal pro-B type natriuretic peptide (NT-ProBNP) and cardiac troponin I (cTnI), are the most routinely applied method of diagnosing cardiac disorders. While they provide a diagnosis when cardiac dysfunction is prominent, prediction or early diagnosis of cardiac dysfunction prior to the development of overt clinical symptoms is challenging. This Research Topic aims to provide the recent trends in the diagnosis and treatment of cardiothoracic diseases in dogs and cats. It presents 9 peer-reviewed research articles, which explore the diagnosis and treatment of cardiothoracic diseases with emphasis on novel echocardiographic techniques and bio-fluid analysis of cardiac biomarkers.

Two-dimensional speckle tracking echocardiography (2D-STE) is an advanced echocardiographic technique that allows comprehensive analysis of myocardial function by quantifying myocardial deformation. There is growing evidence that the parameters of this deformation analysis are superior to the conventional parameters for the early diagnosis of myocardial dysfunction (1). Suzuki et al. evaluated the relationship between congestive heart failure (CHF) and myocardial function in cats with cardiomyopathies using 2D-STE. The results revealed left atrial enlargement and decreased left ventricular apical circumferential strain in cats with CHF, suggesting a possible association with progression from sub-clinical cardiomyopathy to CHF. Furthermore, evaluation of the right ventricle (RV) demonstrated increased end-diastolic RV internal dimension and decreased RV longitudinal strain in cats with CHF, also indicating an association with the onset of CHF in cats with cardiomyopathy.

In recent years, the importance of RV function has become apparent, and it is now known to play a critical role in the pathophysiology of various cardiovascular diseases. Yuchi et al. evaluated the RV myocardial adaptation associated with increased pulmonary arterial pressure (PAP) in a canine model of chronic pulmonary hypertension (PH) using 2D-STE. In the acute phase of PH, temporal reduction of RV longitudinal strain was observed as a result of acute rise in PAP, which improved with progressive RV hypertrophy, indicative of RV adaptive remodeling. In the chronic phase, RV dilation and reduction in RV longitudinal strain were observed, suggestive of RV maladaptive

OPEN ACCESS

Edited and reviewed by:
Carmel T. Mooney,
University College Dublin, Ireland

***Correspondence:**
Zeki Yilmaz
zyilmaz@uludag.edu.tr

Specialty section:
This article was submitted to Comparative and Clinical Medicine, a section of the journal Frontiers in Veterinary Science

Received: *07 April 2022*
Accepted: *21 April 2022*
Published: *09 May 2022*

Citation:
Hamabe L, Kocatürk M, Yilmaz Z and Tanaka R (2022) Editorial: Novel Insight Into the Diagnosis and Treatment of Cardio(Thoracic) Diseases in Dogs and Cats. Front. Vet. Sci. 9:914602. doi: 10.3389/fvets.2022.914602

remodeling and myocardial dysfunction. Such results suggest that the RV longitudinal strain is reflective of the intrinsic RV myocardial contractility during the PH progression, which could not be detected by conventional echocardiography.

Pulmonary arterial wave reflection (PAWR) analysis, which can be performed non-invasively via wave intensity analysis of the Doppler echocardiography, is a novel technique that gives valuable information on pulmonary artery hemodynamics in PH (2). Yoshida et al. investigated the changes observed before and after mitral valvuloplasty in dogs with PH caused by myxomatous mitral valve disease (MMVD) using PAWR, which demonstrated mitral valvuloplasty as an effective treatment of PH secondary to MMVD.

Cardiac biomarkers are of great importance in the early diagnosis and treatment of cardiac diseases, which include but are not limited to metabolic by-products, enzymes, proteins, peptides, and microRNAs (miRNAs). A prospective, multicenter case-control study by Valente et al. measured the plasmatic concentration of asymmetric dimethylarginine (ADMA) and symmetric dimethylarginine (SDMA) in dogs with various stages of MMVD. The results revealed that ADMA, a biomarker of endothelial dysfunction, was significantly associated with LA enlargement, whereas SDMA, a biomarker of renal dysfunction, was significantly correlated with serum creatinine level.

The intestinal microbiota is known to play a key role in the physiological process of mammals, and alteration of intestinal microbiota has been associated with various diseases (3). Araki et al. compared the intestinal microbiota between dogs with MMVD and healthy dogs using 16S rRNA gene amplicon sequencing. While echocardiographic and radiographic parameters showed significant differences, diversity, and composition of intestinal microbiota showed no significant differences among the groups.

Proteomic and peptidomic analysis allow evaluation of changes in protein and peptide compositions, and previous study on serum proteomics in dogs with MMVD has shown that dogs with different stages of CHF showed different serum protein compositions (4). Similarly, Petchdee et al. investigated serum peptidomics in dogs with MMVD, which demonstrated the presence of peptides including mitogen-activated protein kinase, kallikrein, and tenascin-C in the group with progressed MMVD. Additionally, Sukumolanan et al. compared serum peptidomic profile of cats with sarcomeric gene mutations and normal cats, and revealed that expression of three peptides, including FOXO1, CYP3A132 and AGAP2, were increased in cats with sarcomeric gene mutations.

Altered expressions of circulating miRNAs have been reported in various cardiac diseases in humans, and anticipated as novel cardiac biomarkers as they can be found in serum or plasma in a stable form (5). A study by Ro et al. investigated circulating levels of 11 miRNAs in serum samples of dogs with cardiac diseases, which found that cfa-miR-130b was able to accurately distinguish dogs with cardiac diseases from healthy dogs. Sukumolanan et al. developed a loop-mediated isothermal amplification assay (LAMP) coupled with a lateral flow dipstick (LFD) test to detect myosin-binding protein C3 A31P (*MYBPC3-A31P*) missense mutation in Maine Coon cats, which is a genetic deviation associated with the development of hypertrophic cardiomyopathy (HCM). This novel test was able to distinguish between cats with *MYBPC3-A31P* wild-type and *MYBPC3-A31P* mutant-type from blood samples, which has excellent potential as a novel screening test.

This Research Topic of studies has illustrated the current understanding of the diagnosis and treatment of cardiothoracic diseases in dogs and cats. We hope that these articles will inspire and encourage further studies on the advancement of novel echocardiographic techniques and bio-fluid analysis of cardiac biomarkers.

AUTHOR CONTRIBUTIONS

All authors listed have made a substantial, direct, and intellectual contribution to the work and approved it for publication.

REFERENCES

1. Hamabe L, Mandour AS, Shimada K, Uemura A, Yilmaz Z, Nagaoka K, et al. Role of two-dimensional speckle-tracking echocardiography in early detection of left ventricular dysfunction in dogs. *Animals.* (2021) 11:2361. doi: 10.3390/ani11082361
2. Yoshida T, Matsuura K, Seijirow G, Uemura A, Yilmaz Z, Tanaka R. Non-invasive assessment of pulmonary artery wave reflection in dogs with suspected pulmonary hypertension. *Front Vet Sci.* (2021) 8:659194. doi: 10.3389/fvets.2021.659194
3. Mondo E, Marliani G, Accorsi PA, Cocchi M, Di Leone A. Role of gut microbiota in dog and cat's health and diseases. *Open Vet J.* (2019) 9:253–8. doi: 10.4314/ovj.v9i3.10
4. Saril A, Kocaturk M, Shimada K, Uemura A, Akgün E, Levent P, et al. Serum proteomic changes in dogs with different stages of chronic heart failure. *Animals.* (2022) 12:490. doi: 10.3390/ani12040490
5. Xu J, Zhao J, Evan G, Xiao C, Cheng Y, Xiao J. Circulating microRNAs: novel biomarkers for cardiovascular diseases. *J Mol Med.* (2012) 90:865–75. doi: 10.1007/s00109-011-0840-5

Conflict of Interest: The authors declare that the research was conducted in the absence of any commercial or financial relationships that could be construed as a potential conflict of interest.

frontiers in Veterinary Science

ORIGINAL RESEARCH
published: 16 August 2021
doi: 10.3389/fvets.2021.727155

Right Ventricular Myocardial Adaptation Assessed by Two-Dimensional Speckle Tracking Echocardiography in Canine Models of Chronic Pulmonary Hypertension

Yunosuke Yuchi, Ryohei Suzuki, Haruka Kanno, Takahiro Teshima, Hirotaka Matsumoto and Hidekazu Koyama*

Laboratory of Veterinary Internal Medicine, Faculty of Veterinary Science, School of Veterinary Medicine, Nippon Veterinary and Life Science University, Musashino, Japan

OPEN ACCESS

Edited by:
Zeki Yilmaz,
Faculty of Veterinary Medicine, Turkey

Reviewed by:
Domenico Caivano,
University of Perugia, Italy
Enrica Zucca,
University of Milan, Italy

***Correspondence:**
Ryohei Suzuki
ryoheisuzuki@nvlu.ac.jp

Specialty section:
This article was submitted to Comparative and Clinical Medicine, a section of the journal Frontiers in Veterinary Science

Received: *18 June 2021*
Accepted: *22 July 2021*
Published: *16 August 2021*

Citation:
Yuchi Y, Suzuki R, Kanno H, Teshima T, Matsumoto H and Koyama H (2021) Right Ventricular Myocardial Adaptation Assessed by Two-Dimensional Speckle Tracking Echocardiography in Canine Models of Chronic Pulmonary Hypertension. Front. Vet. Sci. 8:727155. doi: 10.3389/fvets.2021.727155

Background: Pulmonary hypertension (PH) is a life-threatening disease in dogs characterized by an increase in pulmonary arterial pressure (PAP) and/or pulmonary vascular resistance. Right ventricle adapts to its pressure overload through various right ventricular (RV) compensative mechanisms: adaptive and maladaptive remodeling. The former is characterized by concentric hypertrophy and increased compensatory myocardial contractility, whereas the latter is distinguished by eccentric hypertrophy associated with impaired myocardial function.

Objectives: To evaluate the RV adaptation associated with the increase of PAP using two-dimensional speckle tracking echocardiography.

Animals: Seven experimentally induced PH models.

Methods: Dogs were anesthetized and then a pulmonary artery catheter was placed via the right jugular vein. Canine models of PH were induced by the repeated injection of microspheres through the catheter and monitored pulmonary artery pressure. Dogs were performed echocardiography and hemodynamic measurements in a conscious state when baseline and systolic PAP (sPAP) rose to 30, 40, 50 mmHg, and chronic phase. The chronic phase was defined that the sPAP was maintained at 50 mmHg or more for 4 weeks without injection of microspheres.

Results: Pulmonary artery to aortic diameter ratio, RV area, end-diastolic RV wall thickness, and RV myocardial performance index were significantly increased in the chronic phase compared with that in the baseline. Tricuspid annular plane systolic excursion was significantly decreased in the chronic phase compared with that in the baseline. The RV longitudinal strain was significantly decreased in the sPAP30 phase, increased in the sPAP40 and sPAP50 phases, and decreased in the chronic phase.

Conclusions: Changes in two-dimensional speckle tracking echocardiography-derived RV longitudinal strain might reflect the intrinsic RV myocardial contractility during the PH progression, which could not be detected by conventional echocardiographic parameters.

Keywords: dog, right ventricular remodeling, right ventricular strain, right ventricular-arterial coupling, wall stress, myocardial function

INTRODUCTION

Pulmonary hypertension (PH), a life-threatening disease in dogs, is characterized by increased pulmonary arterial pressure (PAP, normal range: systolic PAP; 15–25 mmHg, mean PAP; 10–15 mmHg, and diastolic PAP; 5–10 mmHg) and/or pulmonary vascular resistance (1, 2). The disease would be caused by various diseases in dogs, including pulmonary arterial disease, left heart disease, respiratory disease, hypoxia, pulmonary embolic disease, parasitic disease, or some combination of these (1). Recent studies have reported that PH was one of the risk factors for the worse outcome especially in dogs with myxomatous mitral valve disease and respiratory disease/hypoxia (3, 4). Considering the structural characteristics of the right ventricle, the right ventricular (RV) pressure overload would critically impact RV function and cardiac output (5). In humans, to compensate for low cardiac output due to increased PAP, the right ventricle responds through two compensatory mechanisms: adaptive and maladaptive remodeling (6–9). The former is characterized by concentric hypertrophy and increased compensatory myocardial contractility, whereas the latter is distinguished by eccentric hypertrophy associated with impaired myocardial function. Therefore, to estimate the progression of PH, the change in RV myocardial function and remodeling associated with increasing RV pressure overload must be evaluated.

Currently, various echocardiographic variables are used as clinical, non-invasive tools to assess RV function in veterinary medicine; specifically, two-dimensional speckle tracking echocardiography (2D-STE) enables quantitative, non-invasive assessment of the intrinsic RV myocardial function (10–12). However, studies that have assessed the relationship between invasively measured PAP and echocardiographic variables for RV function in the same individuals are limited (13, 14). Furthermore, almost all these studies have evaluated the association in the acute phase of RV pressure overload in anesthetized dogs (13, 14), although in majority of the cases, PH runs a chronic course and various RV adaptations are exhibited.

We hypothesized that 2D-STE indices would reflect the changes in RV function associated with RV adaptation, and there would be differences in RV function between the acute and chronic phase of RV pressure overload. This study aimed to assess RV morphology and function associated with the increase in PAP during the process of creating model dogs with chronic PH.

Abbreviations: 2D-STE, two-dimensional speckle tracking echocardiography; 3seg, only right ventricular free wall analysis; 6seg, right ventricular global analysis; CV, coefficient of variation; PA:Ao, pulmonary artery to aortic diameter ratio; PAP, pulmonary arterial pressure; PH, pulmonary hypertension; RV CO, right ventricular cardiac output; RV FACn, right ventricular fractional area change normalized by body weight; RV MPI, right ventricular myocardial performance index; RV s', tissue Doppler imaging-derived peak systolic myocardial velocity of lateral tricuspid annulus; RV SV, right ventricular stroke volume; RVEDA index, end-diastolic right ventricular area normalized by body weight; RVESA index, end-systolic right ventricular area normalized by body weight; RV-SL, right ventricular longitudinal strain; RV-SrL, right ventricular longitudinal strain rate; RVWTd, end-diastolic right ventricular wall thickness; TAPSEn, tricuspid annular plane systolic excursion normalized by body weight.

MATERIALS AND METHODS

Our prospective, experimental study consisted of procedures that were performed in accordance with the Guide for Institutional Laboratory Animal Care and Use in Nippon Veterinary and Life Science University and was approved by the ethical committee for laboratory animal use of the Nippon Veterinary and Life Science University, Japan (approval number: 2019S-56).

Animals

Seven laboratory male beagles (body weight: 9.1 ± 1.5 kg, age: 1.0 ± 0.2 years) were used in this study. All dogs were determined to be healthy based on a complete physical examination, blood tests, thoracic and abdominal radiography, transthoracic and abdominal ultrasonography, and oscillometric method-derived blood pressure measurement.

Study Preparation

The study dogs were administered butorphanol tartrate (0.2 mg/kg, IV) (Meiji Seika Pharma Co. Ltd., Tokyo, Japan), midazolam hydrochloride (0.2 mg/kg, IV) (Maruishi Pharmaceutical. Co., Ltd., Osaka, Japan), heparin sodium (100 IU/kg, IV) (AY Pharmaceuticals Co. Ltd., Tokyo, Japan), and cefazolin sodium hydrate (20 mg/kg, IV) (LTL Pharma Co. Ltd., Tokyo, Japan) as pre-anesthetic medication. They were then anesthetized intravenously with propofol (Nichi-Iko Pharmaceutical Co., Ltd., Toyama, Japan), maintained with 1.5–2.0% isoflurane (Mylan Seiyaku Ltd., Osaka, Japan) mixed with 100% oxygen. The end-tidal partial pressure of carbon dioxide was monitored and maintained between 35 and 45 mmHg by manual ventilation at a rate of 8–12 breaths per minute. The anesthetized dogs were placed in left lateral recumbency and the right lateral neck region was clipped, prepared aseptically, and draped. An ∼5.0-cm surgical cutdown was performed over the right jugular furrow to exteriorize the right jugular vein. Then an 8-Fr multipurpose catheter (Atom Medical Corp., Tokyo, Japan) was placed in the main pulmonary artery under fluoroscopic guidance. The right side of the neck was sutured, and all the dogs

completely recovered from anesthesia through the conventional method (15).

Creating Model Dogs With Chronic PH and Hemodynamic Measurements

The PAP was measured using circulatory function analysis software (SBP2000, Softron, Tokyo, Japan). The conscious dogs were restrained in the most stable position, and the PAP (systolic, mean, and diastolic) was measured invasively by calibrating with the atmospheric pressure. The average value of PAP calculated from nine consecutive cardiac cycles was considered as "baseline" data and used for the statistical analysis. After baseline PAP measurements were taken, microspheres measuring between 150 and 300 μm in diameter (Sephadex G-25 Coarse, Cytiva, Tokyo, Japan) were injected repeatedly and the peripheral pulmonary artery was embolized via the prepared catheter (16, 17). The time points at which systolic PAP (sPAP) rose to ∼30, 40, and 50 mmHg were defined as "sPAP30," "sPAP40," and "sPAP50," respectively. Each time point was at least 2 days after injection of the microspheres to eliminate the acute effects of microspheres on RV function. When the sPAP was maintained at 50 mmHg or more for 4 weeks without injection of microspheres, the time point was defined as "chronic" and the same examinations as those carried out at the other time points were performed. At each time point, the systemic arterial pressure was measured for all dogs using the oscillometric method. The dogs were sedated using butorphanol tartrate (0.1 mg/kg, IV) and midazolam hydrochloride (0.1 mg/kg, IV) to perform the microsphere injection, PAP measurements, and echocardiography when necessary.

Echocardiographic Assessment of the Right Heart

Echocardiography was performed in all dogs on the same day as the hemodynamic measurements were taken at all time points. Conventional 2D and Doppler examinations were performed by a single investigator (RS) using a Vivid 7 or Vivid E95 echocardiographic system (GE Healthcare, Tokyo, Japan) and a 3.5–6.9 MHz transducer. A lead II electrocardiogram was recorded simultaneously and the images were displayed. Data obtained from at least five consecutive cardiac cycles in sinus rhythm from the dogs that were manually restrained in right and left lateral recumbency were stored. The images were analyzed using an offline workstation (EchoPAC PC, Version 204; GE Healthcare, Tokyo, Japan) by a single observer (YY).

For studying the right heart morphology, the end-diastolic and end-systolic RV areas (RVEDA and RVESA) along with the end-diastolic RV wall thickness (RVWTd) were measured using the left apical four-chamber view optimized for the right heart (RV focus view), as described previously (18–20). Each variable except for the RVWTd was measured by tracing the endocardial border of the right ventricle and normalized by body weight (20).

$$\text{RVEDA index} = \frac{(\text{RVEDA } [\text{cm}^2])}{(\text{body weight } [\text{kg}])^{0.624}}$$

$$\text{RVESA index} = \frac{\text{RVESA } (\text{cm}^2)}{\text{body weight } (\text{kg})^{0.628}}$$

The RVWTd was measured as the largest diameter of the RV free wall at end-diastole using the B-mode method. Additionally, the ratio of pulmonary artery to aortic diameter (PA:Ao) was obtained from the right parasternal short-axis view at the level of the pulmonary artery, as described previously (21).

Tricuspid annular plane systolic excursion (TAPSE), RV fractional area change, peak systolic change (RV FAC), tissue Doppler imaging-derived peak systolic myocardial velocity of lateral tricuspid annulus (RV s'), RV myocardial performance index (RV MPI), RV stroke volume (RV SV), and RV cardiac output (RV CO) were measured as indicators of RV systolic function, as described previously (19, 20, 22). All RV functional variables were obtained from the RV focus view. The TAPSE was measured using the B-mode method as described previously (23–25). The TAPSE and RV FAC were normalized by body weight using the following formula (22, 25):

$$\text{TAPSEn} = \frac{(\text{TAPSE } [\text{cm}])}{(\text{body weight } [\text{kg}])^{0.284}}$$

$$\text{RV FACn} = \frac{(\text{RV FAC } [\%])}{(\text{body weight } [\text{kg}])^{-0.097}}$$

The RV MPI was obtained from the tissue Doppler imaging-derived lateral tricuspid annular motion wave using the following formula:

$$\text{RV MPI} = \frac{(\text{b} - \text{a})}{\text{a}}$$

where a is the duration of the systolic tricuspid annular motion wave, and b is the interval from the end of the late diastolic tricuspid annular motion wave to the onset of the early diastolic tricuspid annular motion wave (19). The RV SV was calculated by multiplying the velocity-time integral of the pulmonary artery flow and the cross-sectional area of the pulmonary trunk obtained from the right parasternal short-axis view at the level of pulmonary artery, as described previously (26). The RV CO was obtained using RV SV and heart rate calculated by mean R-R intervals obtained from the same cardiac cycle used for RV SV measurement.

If the dogs had tricuspid valve or pulmonary valve regurgitation, we classified these severities as mild, moderate, or severe using color Doppler and continuous wave Doppler methods, as described previously (27, 28).

Two-Dimensional Speckle Tracking Echocardiography

All 2D-STE analyses were performed by a single investigator using the same ultrasound machine and evaluated by the same investigator using the same offline workstation as that used for standard echocardiography. The strain and strain

rate were obtained from the RV focus view using the left ventricular four-chamber algorithms (23, 29). The region of interest for 2D-STE was defined by manually tracing the RV endocardial border. Only RV free wall analysis (3seg) was performed by tracing from the level of the lateral tricuspid annulus to the RV apex for the longitudinal strain (RV-SL_{3seg}) and strain rate (RV-SrL_{3seg}) (**Figure 1A**). Right ventricular global analysis (6seg) was also performed by tracing from the lateral tricuspid annulus to the septal tricuspid annulus (including the interventricular septum) *via* the RV apex for the 6seg longitudinal strain (RV-SL_{6seg}), and strain rate (RV-SrL_{6seg}) (**Figure 1B**). Manual adjustments were made to include and track the entire myocardial thickness over the cardiac cycle when necessary. When the automated software could not track the myocardial regions, the regions of interest were retraced and recalculated. The RV-SL was defined as the absolute value of the negative peak value obtained from the strain wave (23, 30). The RV-SrL was obtained from the strain rate wave and was defined as the absolute value of the negative peak value during systole (30–32).

Variability of Intra- and Inter-Observer Measurements

Intra-observer measurement of variability was performed by a single observer who performed all the echocardiographic and radiographic measurements (YY). The baseline RV morphological and functional indices were obtained from the seven dogs. All measurements were performed on two different days at >7-day intervals using the same cardiogram and cardiac cycles. A second blinded observer (HK) measured the same indices for the determination of inter-observer variability using the same echocardiogram and heart cycles.

Statistical Analysis

All statistical analyses were performed using the commercially available EZR software, version 1.41 (Saitama Medical Center, Jichi Medical University, Saitama, Japan) (33). All continuous data were reported as median (interquartile range).

The normality of data was tested using the Shapiro–Wilk test. Continuous variables were compared between each timepoint by means of repeated measures analysis of variance with subsequent pairwise comparisons using the Bonferroni-adjusted paired *t*-test for normally distributed data or Friedman rank sum test with subsequent pairwise comparisons using the Bonferroni-adjusted Wilcoxon signed rank sum test for non-normally distributed data.

Variability of intra- and inter-observer measurements was quantified by the coefficient of variation (CV), which was calculated using the following formula:

$$\text{CV}\ (\%) = \frac{(\text{standard deviation})}{(\text{mean value})} \times 100$$

Intra- and inter-class correlation coefficients (ICC) were also used to evaluate the measurement variability. Low measurement variability was defined as CV < 10.0 and ICC > 0.7. Statistical significance was set at $P < 0.050$.

RESULTS

Creating PH Model Dogs

The dogs were administered repeated microsphere infusions for 2.2 ± 1.0, 6.9 ± 3.8, 14.9 ± 5.7, and 50.9 ± 13.1 weeks to meet the definition of sPAP30, sPAP40, sPAP50, and chronic, respectively. The median total dose of microspheres was 1.24 mg/kg (range: 0.93–1.37). There was no significant change in body weight. Two dogs required sedation with butorphanol tartrate and midazolam hydrochloride to perform echocardiography and for taking PAP measurements at each timepoint. None of the dogs showed any clinical symptoms associated with PH, including syncope, dyspnea, lethargy, ascites, and pleural effusion throughout this study protocol.

Hemodynamic Measurements

The hemodynamic data obtained from all seven model dogs were included in the statistical analysis. **Table 1** shows the results of hemodynamic parameters in the PH model dogs. With the rise in sPAP, the mean PAP also increased in the sPAP30, sPAP40, sPAP50, and chronic phases compared with the baseline ($P = 0.012$, $P = 0.018$, $P < 0.001$, and $P = 0.021$, respectively) parameters. The diastolic PAP was significantly increased in the sPAP50 and chronic phases compared with the baseline and sPAP30 values (sPAP50: $P = 0.003$ and $P = 0.004$, respectively; chronic: $P = 0.013$ and $P = 0.023$, respectively). There were no significant changes in systolic, mean, and diastolic systemic arterial pressure and heart rate with increased sPAP.

Echocardiographic Measurements

In this study, the echocardiographic data obtained from all seven model dogs were included in the statistical analysis. All the dogs had mild pulmonary valve regurgitation at baseline, sPAP30, and sPAP40 phases, and that was progressed to moderate at sPAP50 and chronic phases in four dogs (57%). Additionally, three dogs (43%) had mild tricuspid valve regurgitation at each timepoint.

Table 2 shows the results of echocardiographic parameters for RV morphology and function. The PA:Ao value was significantly higher in the sPAP50 phase than the baseline values and those of the sPAP40 phase ($P = 0.034$ and $P = 0.038$, respectively). This value was also significantly elevated in the chronic phase compared with those in the baseline, sPAP30, and sPAP40 phases ($P = 0.021$, $P = 0.004$, and $P = 0.010$, respectively). The RVEDA index and RVESA index were significantly increased in the chronic phase compared with those in the sPAP30 phase ($P = 0.041$ and $P = 0.048$, respectively). The RVWTd was significantly higher in the sPAP50 phase compared with that in baseline phase ($P = 0.042$). This value was also significantly elevated in the chronic phase compared with those in the baseline and sPAP30 phases ($P = 0.002$ and $P = 0.047$, respectively). The TAPSEn and RV MPI were significantly worse in the chronic phase compared with the baseline values ($P = 0.008$ and $P = 0.003$,

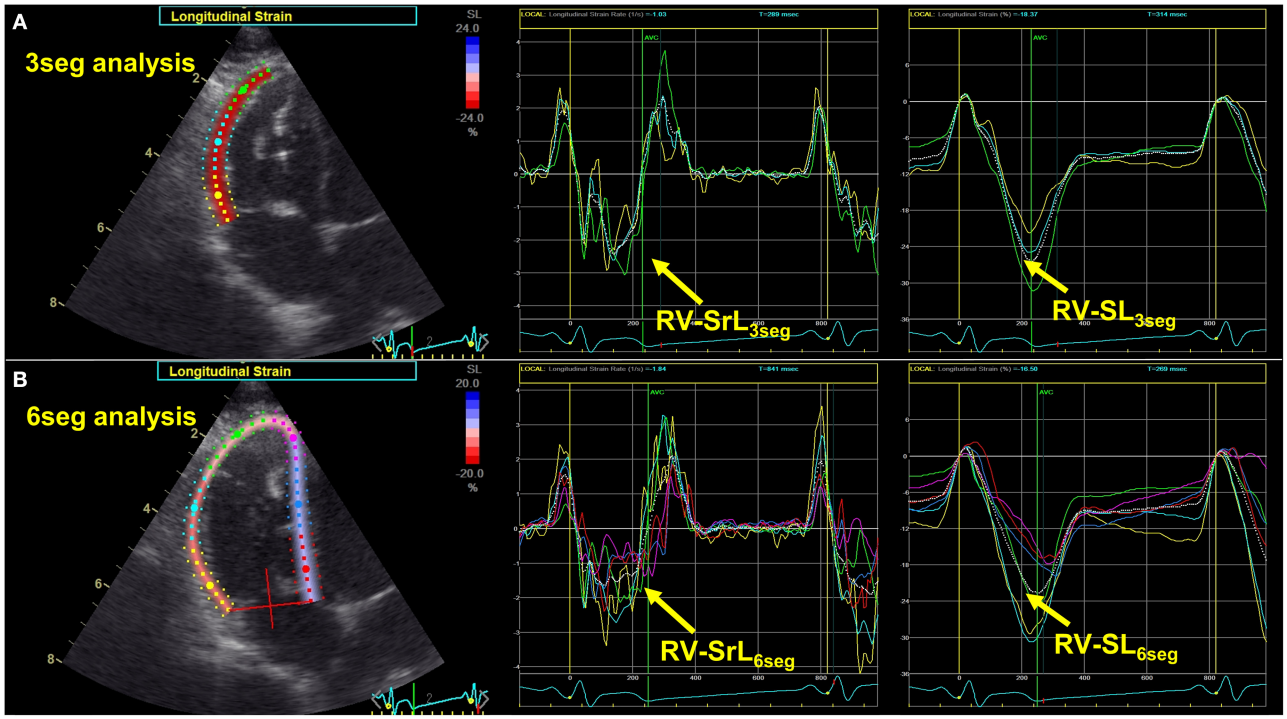

FIGURE 1 | Two-dimensional speckle tracking echocardiography-derived right ventricular longitudinal strain and strain rate (RV-SL and RV-SrL, respectively). **(A)** RV-SL and RV-SrL of the right ventricular free wall ($RV\text{-}SL_{3seg}$ and $RV\text{-}SrL_{3seg}$, respectively). **(B)** RV-SL and RV-SrL of the global right ventricle ($RV\text{-}SL_{6seg}$ and $RV\text{-}SrL_{6seg}$, respectively).

TABLE 1 | Changes in hemodynamic parameters during the process of creating canine models of chronic embolic pulmonary hypertension.

Variables	Baseline	sPAP30	sPAP40	sPAP50	Chronic
Pulmonary arterial pressure (mmHg)					
Systole	20.0 (17.3, 24.6)	33.0 (30.0, 34.6)[a]	42.3 (40.4, 47.8)[ab]	52.4 (50.7, 52.9)[abc]	51.4 (50.3, 65.9)[abc]
Mean	12.8 (11.0, 15.0)	16.8 (16, 20.4)[a]	21.7 (18.3, 23.9)[ab]	29.4 (27.9, 33.7)[abc]	30.1 (29.3, 31.9)[abc]
Diastole	6.4 (5.1, 9.0)	8.8 (8.3, 12.6)	11.8 (7, 17.2)	16.1 (15.4, 18.8)[ab]	16.3 (15.2, 19.4)[ab]
Systemic arterial pressure (mmHg)					
Systole	126 (116, 134)	124 (113, 137)	132 (116, 136)	130 (130, 131)	128 (120, 142)
Mean	92 (88, 97)	91 (78, 106)	97 (81, 107)	99 (91, 102)	93 (82, 98)
Diastole	80 (70, 82)	75 (65, 87)	82 (64, 93)	80 (73, 88)	69 (60, 77)
Heart rate (bpm)	88 (81, 115)	99 (91, 120)	102 (82, 124)	94 (64, 112)	84 (81, 100)

Continuous variables were displayed as median (interquartile range).
[a] *The value is significantly different from the Baseline ($P < 0.050$).*
[b] *The value is significantly different from the sPAP30 ($P < 0.050$).*
[c] *The value is significantly different from the sPAP40 ($P < 0.050$).*

respectively). The RV SV was significantly higher in the chronic phase compared with that in the sPAP30 phase ($P = 0.016$), whereas, RV FACn, RV s', and RV CO showed no significant changes with increased sPAP.

The results of 2D-STE indices are summarized in **Figures 2**, **3**. The $RV\text{-}SL_{3seg}$ and $RV\text{-}SL_{6seg}$ were significantly decreased in the sPAP30 phase compared with the baseline values ($P = 0.047$ and $P = 0.040$, respectively). Additionally, $RV\text{-}SL_{3seg}$ was significantly lower in the chronic phase compared with those in the baseline, sPAP40, and sPAP50 phases ($P = 0.012$, $P = 0.010$, and $P = 0.011$, respectively) (**Figure 2A**). However, $RV\text{-}SL_{6seg}$ was significantly reduced in the chronic phase compared with those in the baseline and sPAP40 phases ($P = 0.047$ and $P = 0.044$, respectively) (**Figure 2B**). The $RV\text{-}SrL_{3seg}$ and $RV\text{-}SrL_{6seg}$ were significantly lower in the chronic phase compared with those in the sPAP50 and sPAP40

TABLE 2 | Changes in echocardiographic parameters during the process of creating canine models of chronic embolic pulmonary hypertension.

Variables	Baseline	sPAP30	sPAP40	sPAP50	Chronic
PA:Ao	0.80 (0.78, 0.81)	0.78 (0.76, 0.81)	0.78 (0.74, 0.79)	0.92 (0.85, 0.93)[ac]	0.97 (0.96, 0.99)[abc]
RVEDA index ($cm^2/kg^{0.624}$)	1.43 (1.11, 1.44)	1.08 (0.91, 1.17)	1.02 (0.96, 1.27)	1.08 (0.96, 1.14)	1.47 (1.28, 1.63)[b]
RVESA index ($cm^2/kg^{0.628}$)	0.77 (0.60, 0.85)	0.73 (0.55, 0.82)	0.72 (0.52, 0.82)	0.65 (0.60, 0.72)	0.99 (0.88, 1.10)[b]
RVWTd (mm)	3.7 (3.4, 3.8)	4.0 (3.8, 4.2)	4.4 (3.9, 4.9)	4.9 (4.5, 5.0)[a]	5.6 (5.2, 6.1)[ab]
RV FACn (%/$kg^{-0.097}$)	53.7 (49.1, 61.0)	47.9 (46.3, 50.2)	44.0 (42.7, 56.6)	47.7 (41.6, 50.1)	37.1 (36.7, 40.0)
TAPSEn (mm/$kg^{0.33}$)	6.2 (5.9, 6.6)	5.5 (3.9, 5.9)	6.2 (6.0, 6.6)	5.9 (5.3, 6.4)	4.6 (4.3, 5.5)[a]
RV s' (cm/s)	11.0 (10.6, 12.2)	11.8 (9.8, 14.0)	13.1 (11.6, 14.8)	13.4 (11.6, 14.7)	9.1 (7.6, 11.0)
RV MPI	0.41 (0.36, 0.43)	0.41 (0.39, 0.56)	0.55 (0.43, 0.64)	0.55 (0.44, 0.62)	0.72 (0.68, 0.76)[a]
RV SV (mL)	18.5 (16.1, 19.4)	15.0 (10.9, 16.6)	15.5 (13.4, 17.6)	16.9 (15.7, 21.7)	21.8 (20.8, 23.4)[b]
RV CO (L/min)	1.5 (1.3, 2.2)	1.5 (1.4, 1.6)	1.5 (1.3, 1.9)	1.5 (1.4, 1.6)	1.8 (1.7, 2.1)

PA:Ao, pulmonary artery to aortic diameter ratio; RV CO, right ventricular cardiac output; RV FACn, right ventricular fractional area change normalized by body weight; RV MPI, right ventricular myocardial performance index; RV s', tissue Doppler imaging-derived peak systolic myocardial velocity of lateral tricuspid annulus; RV SV, right ventricular stroke volume; RVEDA index, end-diastolic right ventricular area normalized by body weight; RVESA index, end-systolic right ventricular area normalized by body weight; RVWTd, end-diastolic right ventricular wall thickness; TAPSEn, tricuspid annular plane systolic excursion normalized by body weight.

Continuous variables were displayed as median (interquartile range).

[a] The value is significantly different from Baseline ($P < 0.050$).

[b] The value is significantly different from sPAP30 ($P < 0.050$).

[c] The value is significantly different from sPAP40 ($P < 0.050$).

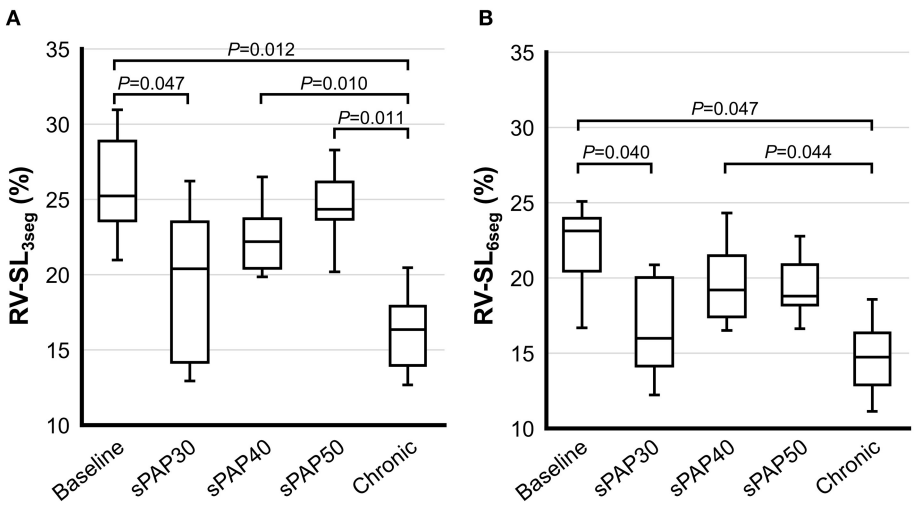

FIGURE 2 | Box and whisker plots of the right ventricular longitudinal strain (RV-SL) obtained from two-dimensional speckle tracking echocardiography. The bottom of the box is 25%, the middle line is the median, the top of the box is 75%, and the whiskers represent the range. **(A)** RV-SL of the right ventricular free wall ($RV\text{-}SL_{3seg}$). **(B)** RV-SL of the global right ventricle ($RV\text{-}SL_{6seg}$).

phases, respectively ($P = 0.028$ and $P = 0.039$, respectively) (**Figure 3**).

Intra- and Inter-Observer Measurement Variability

The results of intra- and inter-observer measurement variability for the echocardiographic indices assessed in this study are summarized in **Table 3**. Considering the intra-observer measurement variability, all the echocardiographic parameters showed low measurement variability. Further, all the echocardiographic indices except for RVESA, RV FAC, and RV MPI showed low measurement variability based on CV and ICC.

DISCUSSION

We created model dogs with chronic pre-capillary PH with moderately increased PAP and substantial right heart remodeling and compared the changes in RV function associated with increased PAP that was measured invasively in conscious dogs. In the acute phase, 2D-STE-derived RV systolic function was temporarily decreased due to the acute rise in PAP; however, it improved with RV hypertrophy; this may be a sign of RV adaptive remodeling. In contrast to the acute phase, RV systolic dysfunction assessed by RV-SL and RV dilatation were observed in the chronic phase of PH, which could be because of RV maladaptive remodeling and myocardial dysfunction.

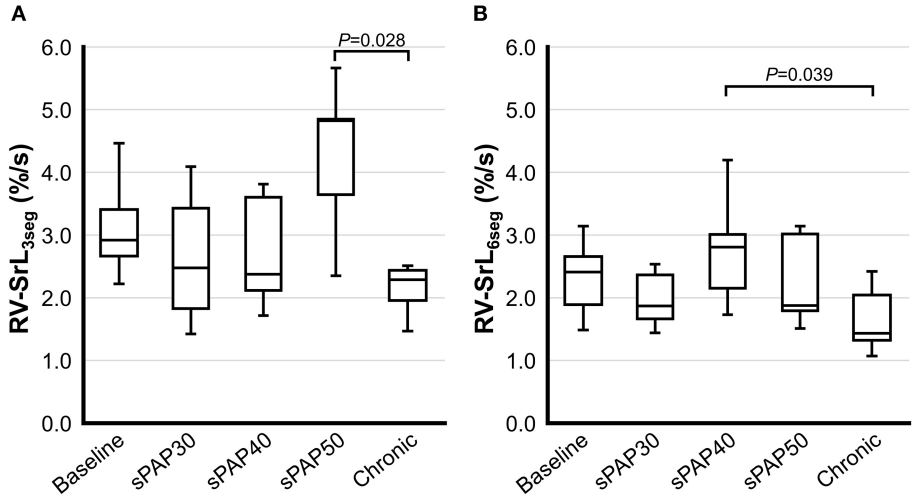

FIGURE 3 | Box and whisker plots of the right ventricular longitudinal strain rate (RV-SrL) obtained from two-dimensional speckle tracking echocardiography. The bottom of the box is 25%, the middle line is the median, the top of the box is 75%, and the whiskers represent the range. **(A)** RV-SrL of the right ventricular free wall ($RV\text{-}SrL_{3seg}$). **(B)** RV-SrL of the global right ventricle ($RV\text{-}SrL_{6seg}$).

TABLE 3 | Inter- and intra-observer measurement variability for echocardiographic parameters evaluated in this study.

Variables	Intra-observer			Inter-observer		
	CV (%)	ICC	*P*	CV (%)	ICC	*P*
PA:Ao	4.2	0.94	< 0.001	5.9	0.80	0.012
RVEDA	4.1	0.99	< 0.001	8.6	0.82	< 0.001
RVESA	5.8	0.94	< 0.001	11.4	0.66	0.012
RVWTd	3.2	0.93	< 0.001	6.5	0.80	0.004
RV FAC	5.0	0.81	0.001	8.8	0.50	0.002
TAPSE	3.1	0.90	< 0.001	5.9	0.80	0.002
RV s'	2.8	0.97	< 0.001	2.9	0.95	< 0.001
RV MPI	7.8	0.88	< 0.001	12.3	0.64	0.002
RV SV	4.4	0.98	< 0.001	8.9	0.94	< 0.001
$RV\text{-}SL_{3seg}$	4.4	0.93	< 0.001	5.0	0.92	< 0.001
$RV\text{-}SrL_{3seg}$	6.1	0.95	< 0.001	9.3	0.89	< 0.001
$RV\text{-}SL_{6seg}$	5.2	0.90	< 0.001	7.2	0.85	< 0.001
$RV\text{-}SrL_{6seg}$	5.8	0.94	< 0.001	7.6	0.93	< 0.001

3seg, only right ventricular free wall analysis; 6seg, right ventricular global analysis; CI, confidence interval; CV, coefficient of variation; ICC, intra- or inter-class correlation coefficients; PA:Ao, pulmonary artery to aortic diameter ratio; RV FAC, right ventricular fractional area change; RV MPI, right ventricular myocardial performance index; RV s', tissue Doppler imaging-derived peak systolic myocardial velocity of lateral tricuspid annulus; RV SV, right ventricular stroke volume; RVEDA, end-diastolic right ventricular area; RVESA, end-systolic right ventricular area; RV-SL, right ventricular longitudinal strain; RV-SrL, right ventricular longitudinal strain rate; RVWTd, end-diastolic right ventricular wall thickness; TAPSE, tricuspid annular plane systolic excursion.

In this study, certain conventional echocardiographic indices, such as TAPSEn and RV MPI, did not significantly change with increased PAP in the acute phase, although these indices were significantly worse in the chronic phase of PH. Nonetheless, 2D-STE indices showed substantial changes in the acute phase as well as in the chronic phase of PH. Previous studies reported that these conventional echocardiographic indices are affected by angle- and load-dependent limitations (34–36). Furthermore, all the model dogs in our study had echocardiographic evidence of tricuspid valve and pulmonary valve regurgitation; therefore, these volume overloads may prevent the detection of RV dysfunction using conventional indices. In contrast, 2D-STE variables have been used to assess intrinsic RV myocardial function with angle-independency and the low effect of these loading conditions (10). Additionally, considering PH would induce full RV remodeling against RV pressure overload, assessment of the global right ventricular function based on 2D-STE indices may help detect precise RV myocardial function more sensitively than conventional indices. Therefore, 2D-STE indices can be used to detect changes in intrinsic RV systolic function, which cannot be detected using conventional indices.

In the acute phase, RV-SL was significantly reduced in the sPAP30 phase and gradually increased in the sPAP40 and sPAP50 phases. In the sPAP30 phase, all the dogs did not have RV remodeling; therefore, the acute rise in PAP might have induced the imbalance between RV contractility and RV pressure overload (i.e., RV arterial uncoupling caused by increased RV pressure overload). However, RV-SL gradually increased with PAP and RVWTd, which indicates RV adaptive remodeling. In human medicine, RV adaptation remodeling was induced in PH patients through various mechanisms such as neurological activation, inflammation, and altered bioenergetics (19, 37, 38). In this study, the RVWTd gradually increased with the rise in PAP during the process of creating the chronic PH model dogs. Therefore, our results indicate that 2D-STE indices may be highly sensitive to changes that reflect the adaptation in RV myocardial contractility.

There was a significant difference between the 2D-STE-derived RV systolic functional indices of the sPAP50 and the chronic phases, although there was no significant difference in the RV loading condition (sPAP was stable at 50 mmHg). In general, chronic RV pressure overload increases myocardial wall stress, which in turn increases RV wall thickness and contractility to maintain RV CO (6–9). However, the RV myocardial contractility may be unable to cope with the chronic, excessive pressure overload. Our results suggest that RV-SL may reflect the intrinsic RV myocardial contractility, which showed decompensation in the chronic phase. Additionally, myocardial fibrosis might have also affected the results. Several studies have reported the prevalence of RV myocardial fibrosis in patients with PH (39, 40). Furthermore, in human patients with severe heart failure, the 2D-STE-derived RV-SL was reported to have a strong correlation with RV myocardial fibrosis, which could induce RV maladaptive remodeling and subsequent RV myocardial dysfunction (41). Although we have not conducted histopathological examinations in all the model dogs, the changes in RV-SL may also be indicative of RV fibrosis and RV maladaptation with PH progression.

In this study, RV-SL changed more drastically in 3seg than in 6seg in the acute phase, although both indices were significantly decreased in the chronic phase. Considering the interventricular septum when evaluating RV function is a matter of controversy (14, 42). A previous study has reported that RV-SL in the RV free wall is more sensitive to mild RV pressure overload than that in the interventricular septum (14). Our results also suggest that 2D-STE indices in the RV free wall may be more sensitive to increased RV pressure overload than those in the interventricular septum in dogs with moderate RV pressure overload. However, through the current 2D-STE assessment, we could not distinguish between the interventricular septum function of the RV and left ventricular components. Our results may vary in dogs with moderate PH secondary to left heart disease, which might impair the septal left ventricular function. Further studies to assess the precise myocardial function of both ventricles in dogs with PH secondary to left heart disease are expected in the future.

Our study has several limitations. First, the results were obtained from dogs with PH that was experimentally induced by microsphere infusion, which may vary in actual clinical settings or dogs with PH. Additionally, our findings may not be applicable in dogs with PH because of other causes such as left heart disease owing to its different pathophysiology that can increase PAP. Further studies are warranted to evaluate the relationship between echocardiographic indices and invasive PAP in dogs with spontaneous PH. Second, two of the seven dogs were sedated using butorphanol tartrate and midazolam hydrochloride. However, sedation with these agents have minimal effect on cardiovascular function (43). Furthermore, in dogs that required sedation so that hemodynamic measurements could be taken and echocardiography could be performed, these agents were used throughout the study protocol. Thus, sedation would have had minimal effect on our results. Finally, we have evaluated only longitudinal RV strain and strain rate. RV circumferential function would also contribute to RV systolic function in addition to the longitudinal function (30, 44, 45).

In conclusion, our study found that 2D-STE-derived RV-SL was significantly decreased in the sPAP30 phase compared with that in the baseline phase; it gradually increased in the sPAP40 and sPAP50 phases compared with that in the sPAP30 phase and decreased in the chronic phase compared with the baseline and sPAP50 phases. These results suggest that this non-invasive echocardiographic variable may reflect the RV compensative mechanism against PH pathophysiology, which could not be detected by conventional echocardiographic indices for RV function.

DATA AVAILABILITY STATEMENT

The raw data supporting the conclusions of this article will be made available by the authors, without undue reservation.

ETHICS STATEMENT

The animal study was reviewed and approved by Ethical committee for laboratory animal use of the Nippon Veterinary and Life Science University.

AUTHOR CONTRIBUTIONS

YY performed the concept/design, data analysis/interpretation, drafting article, and critical revision of article. RS performed the concept/design, data analysis/interpretation, critical revision of article, and approved the article. HK performed the data analysis as the second observer. TT, HM, and HK performed data interpretation, critically revised the manuscript, and approved the article. All authors contributed to the article and approved the submitted version.

FUNDING

This work was partially supported by Japan Society for the Promotion of Science (JSPS) KAKENHI Grant Number 20K15667.

ACKNOWLEDGMENTS

The authors would like to express their deepest appreciation to Kana Yanagisawa for their technical assistance. This work was conducted at the Laboratory of Veterinary Internal Medicine, School of Veterinary Science, Faculty of Veterinary Medicine, Nippon Veterinary and Life Science University in Tokyo, Japan. Additionally, we would like to thank Editage (www.editage.com) for English language editing.

REFERENCES

1. Reinero C, Visser LC, Kellihan HB, Masseau I, Rozanski E, Clercx C, et al. ACVIM consensus statement guidelines for the diagnosis, classification, treatment, and monitoring of pulmonary hypertension in dogs. *J Vet Intern Med.* (2020) 34:549–73. doi: 10.1111/jvim.15725
2. Johnson L, Boon J, Orton EC. Clinical characteristics of 53 dogs with Doppler-derived evidence of pulmonary hypertension: 1992–1996. *J Vet Intern Med.* (1999) 13:440–7. doi: 10.1111/j.1939-1676.1999.tb01461.x
3. Borgarelli M, Abbott J, Braz-Ruivo L, Chiavegato D, Crosara S, Lamb K, et al. Prevalence and prognostic importance of pulmonary hypertension in dogs with myxomatous mitral valve disease. *J Vet Intern Med.* (2015) 29:569–74. doi: 10.1111/jvim.12564
4. Jaffey JA, Wiggen K, Leach SB, Masseau I, Girens RE, Reinero CR. Pulmonary hypertension secondary to respiratory disease and/or hypoxia in dogs: clinical features, diagnostic testing and survival. *Vet J.* (2019) 251:105347. doi: 10.1016/j.tvjl.2019.105347
5. Haddad F, Doyle R, Murphy DJ, Hunt SA. Right ventricular function in cardiovascular disease, part II: pathophysiology, clinical importance, and management of right ventricular failure. *Circulation.* (2008) 117:1717–31. doi: 10.1161/CIRCULATIONAHA.107.653584
6. Llucià-Valldeperas A, de Man FS, Bogaard HJ. Adaptation and maladaptation of the right ventricle in pulmonary vascular diseases. *Clin Chest Med.* (2021) 42:179–94. doi: 10.1016/j.ccm.2020.11.010
7. Ryan JJ, Huston J, Kutty S, Hatton ND, Bowman L, Tian L, et al. Right ventricular adaptation and failure in pulmonary arterial hypertension. *Can J Cardiol.* (2015) 31:391–406. doi: 10.1016/j.cjca.2015.01.023
8. Vonk Noordegraaf A, Westerhof BE, Westerhof N. The relationship between the right ventricle and its load in pulmonary hypertension. *J Am Coll Cardiol.* (2017) 69:236–43. doi: 10.1016/j.jacc.2016.10.047
9. Wauthy P, Pagnamenta A, Vassalli F, Naeije R, Brimioulle S. Right ventricular adaptation to pulmonary hypertension: an interspecies comparison. *Am J Physiol Circ Physiol.* (2004) 286:H1441–7. doi: 10.1152/ajpheart.00640.2003
10. Amundsen BH, Helle-Valle T, Edvardsen T, Torp H, Crosby J, Lyseggen E, et al. Noninvasive myocardial strain measurement by speckle tracking echocardiography: validation against sonomicrometry and tagged magnetic resonance imaging. *J Am Coll Cardiol.* (2006) 47:789–93. doi: 10.1016/j.jacc.2005.10.040
11. Potter E, Marwick TH. Assessment of left ventricular function by echocardiography: the case for routinely adding global longitudinal strain to ejection fraction. *JACC Cardiovasc Imaging.* (2018) 11:260–74. doi: 10.1016/j.jcmg.2017.11.017
12. Jamal F, Bergerot C, Argaud L, Loufouat J, Ovize M. Longitudinal strain quantitates regional right ventricular contractile function. *Am J Physiol Circ Physiol.* (2003) 285:H2842–7. doi: 10.1152/ajpheart.00218.2003
13. Akabane R, Shimano S, Sakatani A, Ogawa M, Nagakawa M, Miyakawa H, et al. Relationship between right heart echocardiographic parameters and invasive pulmonary artery pressures in canine models of chronic embolic pulmonary hypertension. *J Vet Med Sci.* (2019) 81:1485–91. doi: 10.1292/jvms.19-0350
14. Morita T, Nakamura K, Osuga T, Yokoyama N, Morishita K, Sasaki N, et al. Changes in right ventricular function assessed by echocardiography in dog models of mild RV pressure overload. *Echocardiography.* (2017) 34:1040–9. doi: 10.1111/echo.13560
15. Grubb T, Sager J, Gaynor JS, Montgomery E, Parker JA, Shafford H, et al. 2020 AAHA anesthesia and monitoring guidelines for dogs and cats. *J Am Anim Hosp Assoc.* (2020) 56:59–82. doi: 10.5326/JAAHA-MS-7055
16. Rothman A, Wiencek RG, Davidson S, Evans WN, Restrepo H, Sarukhanov V, et al. Challenges in the development of chronic pulmonary hypertension models in large animals. *Pulm Circ.* (2017) 7:156–66. doi: 10.1086/690099
17. Hori Y, Uchide T, Saitoh R, Thoei D, Uchida M, Yoshioka K, et al. Diagnostic utility of NT-proBNP and ANP in a canine model of chronic embolic pulmonary hypertension. *Vet J.* (2012) 194:215–21. doi: 10.1016/j.tvjl.2012.03.022
18. Visser LC, Scansen BA, Schober KE, Bonagura JD. Echocardiographic assessment of right ventricular systolic function in conscious healthy dogs: repeatability and reference intervals. *J Vet Cardiol.* (2015) 17:83–96. doi: 10.1016/j.jvc.2014.10.003
19. Rudski LG, Lai WW, Afilalo J, Hua L, Handschumacher MD, Chandrasekaran K, et al. Guidelines for the echocardiographic assessment of the right heart in adults: a report from the American Society of Echocardiography. Endorsed by the European Association of Echocardiography, a registered branch of the European Society of Cardiology, and the Canadian Society of Echocardiography. *J Am Soc Echocardiogr.* (2010) 23:685–713. doi: 10.1016/j.echo.2010.05.010
20. Gentile-Solomon JM, Abbott JA. Conventional echocardiographic assessment of the canine right heart: reference intervals and repeatability. *J Vet Cardiol.* (2016) 18:234–47. doi: 10.1016/j.jvc.2016.05.002
21. Visser LC, Im MK, Johnson LR, Stern JA. Diagnostic value of right pulmonary artery distensibility index in dogs with pulmonary hypertension: comparison with doppler echocardiographic estimates of pulmonary arterial pressure. *J Vet Intern Med.* (2016) 30:543–52. doi: 10.1111/jvim.13911
22. Visser LC, Scansen BA, Brown NV, Schober KE, Bonagura JD. Echocardiographic assessment of right ventricular systolic function in conscious healthy dogs following a single dose of pimobendan versus atenolol. *J Vet Cardiol.* (2015) 17:161–72. doi: 10.1016/j.jvc.2015.04.001
23. Yuchi Y, Suzuki R, Teshima T, Matsumoto H, Koyama H. Utility of tricuspid annular plane systolic excursion normalized by right ventricular size indices in dogs with postcapillary pulmonary hypertension. *J Vet Intern Med.* (2021) 35:107–19. doi: 10.1111/jvim.15984
24. Caivano D, Dickson D, Pariaut R, Stillman M, Rishniw M. Tricuspid annular plane systolic excursion-to-aortic ratio provides a bodyweight-independent measure of right ventricular systolic function in dogs. *J Vet Cardiol.* (2018) 20:79–91. doi: 10.1016/j.jvc.2018.01.005
25. Visser LC, Sintov DJ, Oldach MS. Evaluation of tricuspid annular plane systolic excursion measured by two-dimensional echocardiography in healthy dogs: repeatability, reference intervals, and comparison with M-mode assessment. *J Vet Cardiol.* (2018) 20:165–74. doi: 10.1016/j.jvc.2018.04.002
26. Lewis JF, Kuo LC, Nelson JG, Limacher MC, Quinones MA. Pulsed Doppler echocardiographic determination of stroke volume and cardiac output: clinical validation of two new methods using the apical window. *Circulation.* (1984) 70:425–31. doi: 10.1161/01.CIR.70.3.425
27. Lancellotti P, Moura L, Pierard LA, Agricola E, Popescu BA, Tribouilloy C, et al. European association of echocardiography recommendations for the assessment of valvular regurgitation. Part 2: mitral and tricuspid regurgitation (native valve disease). *Eur J Echocardiogr.* (2010) 11:307–32. doi: 10.1093/ejechocard/jeq031
28. Vezzosi T, Domenech O, Costa G, Marchesotti F, Venco L, Zini E, et al. Echocardiographic evaluation of the right ventricular dimension and systolic function in dogs with pulmonary hypertension. *J Vet Intern Med.* (2018) 32:1541–8. doi: 10.1111/jvim.15253
29. Suzuki R, Matsumoto H, Teshima T, Koyama H. Clinical assessment of systolic myocardial deformations in dogs with chronic mitral valve insufficiency using two-dimensional speckle-tracking echocardiography. *J Vet Cardiol.* (2013) 15:41–9. doi: 10.1016/j.jvc.2012.09.001

30. Suzuki R, Yuchi Y, Kanno H, Teshima T, Matsumoto H, Koyama H. Left and right myocardial functionality assessed by two-dimensional speckle-tracking echocardiography in cats with restrictive cardiomyopathy. *Animals.* (2021) 11:1578. doi: 10.3390/ani11061578
31. Suzuki R, Matsumoto H, Teshima T, Koyama H. Effect of age on myocardial function assessed by two-dimensional speckle-tracking echocardiography in healthy beagle dogs. *J Vet Cardiol.* (2013) 15:243–52. doi: 10.1016/j.jvc.2013.07.001
32. Suzuki R, Matsumoto H, Teshima T, Koyama H. Influence of heart rate on myocardial function using two-dimensional speckle-tracking echocardiography in healthy dogs. *J Vet Cardiol.* (2013) 15:139–46. doi: 10.1016/j.jvc.2012.12.004
33. Kanda Y. Investigation of the freely available easy-to-use software "EZR" for medical statistics. *Bone Marrow Transplant.* (2013) 48:452–8. doi: 10.1038/bmt.2012.244
34. Hsiao S-H, Lin S-K, Wang W-C, Yang S-H, Gin P-L, Liu C-P. Severe tricuspid regurgitation shows significant impact in the relationship among peak systolic tricuspid annular velocity, tricuspid annular plane systolic excursion, and right ventricular ejection fraction. *J Am Soc Echocardiogr.* (2006) 19:902–10. doi: 10.1016/j.echo.2006.01.014
35. Tidholm A, Höglund K, Häggström J, Ljungvall I. Diagnostic value of selected echocardiographic variables to identify pulmonary hypertension in dogs with myxomatous mitral valve disease. *J Vet Intern Med.* (2015) 29:1510–7. doi: 10.1111/jvim.13609
36. Morita T, Nakamura K, Osuga T, Yokoyama N, Morishita K, Sasaki N, et al. Effect of acute volume overload on echocardiographic indices of right ventricular function and dyssynchrony assessed by use of speckle tracking echocardiography in healthy dogs. *Am J Vet Res.* (2019) 80:51–60. doi: 10.2460/ajvr.80.1.51
37. Champion HC, Michelakis ED, Hassoun PM. Comprehensive invasive and non-invasive approach to the right ventricle-pulmonary circulation unit state of the art and clinical and research implications. *Circulation.* (2009) 120:992–1007. doi: 10.1161/CIRCULATIONAHA.106.674028
38. Benza RL, Miller DP, Gomberg-Maitland M, Frantz RP, Foreman AJ, Coffey CS, et al. Predicting survival in pulmonary arterial hypertension: insights from the registry to evaluate early and long-term pulmonary arterial hypertension disease management (REVEAL). *Circulation.* (2010) 122:164–72. doi: 10.1161/CIRCULATIONAHA.109.898122
39. Rain S, Handoko ML, Trip P, Gan CTJ, Westerhof N, Stienen GJ, et al. Right ventricular diastolic impairment in patients with pulmonary arterial hypertension. *Circulation.* (2013) 128:2016–25. doi: 10.1161/CIRCULATIONAHA.113.001873
40. Bogaard HJ, Natarajan R, Henderson SC, Long CS, Kraskauskas D, Smithson L, et al. Chronic pulmonary artery pressure elevation is insufficient to explain right heart failure. *Circulation.* (2009) 120:1951–60. doi: 10.1161/CIRCULATIONAHA.109.883843
41. Lisi M, Cameli M, Righini FM, Malandrino A, Tacchini D, Focardi M, et al. RV longitudinal deformation correlates with myocardial fibrosis in patients with end-stage heart failure. *JACC Cardiovasc Imaging.* (2015) 8:514–22. doi: 10.1016/j.jcmg.2014.12.026
42. Chetboul V, Damoiseaux C, Lefebvre HP, Concordet D, Desquilbet L, Gouni V, et al. Quantitative assessment of systolic and diastolic right ventricular function by echocardiography and speckle-tracking imaging: a prospective study in 104 dogs. *J Vet Sci.* (2018) 19:683–92. doi: 10.4142/jvs.2018.19.5.683
43. Kojima K, Nishimura R, Mutoh T, Takao K, Matsunaga S, Mochizuki M, et al. Comparison of cardiopulmonary effects of medetomidine-midazolam, acepromazine-butorphanol and midazolam-butorphanol in dogs. *J Vet Med Ser A Physiol Pathol Clin Med.* (1999) 46:353–9. doi: 10.1046/j.1439-0442.1999.00224.x
44. Vitarelli A, Terzano C. Do we have two hearts? New insights in right ventricular function supported by myocardial imaging echocardiography. *Hear Fail Rev.* (2010) 15:39–61. doi: 10.1007/s10741-009-9154-x
45. Caivano D, Rishniw M, Birettoni F, Petrescu VF, Porciello F. Transverse right ventricle strain and strain rate assessed by 2-dimensional speckle tracking echocardiography in dogs with pulmonary hypertension. *Vet Sci.* (2020) 7:1–10. doi: 10.3390/vetsci7010019

Conflict of Interest: HK received a grant from Toray Industries, Inc.

The remaining authors declare that the research was conducted in the absence of any commercial or financial relationships that could be construed as a potential conflict of interest.

frontiers in Veterinary Science

ORIGINAL RESEARCH
published: 16 September 2021
doi: 10.3389/fvets.2021.738898

Plasmatic Dimethylarginines in Dogs With Myxomatous Mitral Valve Disease

Carlotta Valente[1], Carlo Guglielmini[1], Marco Baron Toaldo[2†], Giovanni Romito[2], Carlo Artusi[3], Laura Brugnolo[3], Barbara Contiero[1] and Helen Poser[1]*

[1] *Department of Animal Medicine, Production and Health, University of Padua, Padua, Italy,* [2] *Department of Veterinary Medical Sciences, Alma Mater Studiorum–University of Bologna, Bologna, Italy,* [3] *Department of Laboratory Medicine, University-Hospital of Padua, Padua, Italy*

Plasmatic dimethylarginines, asymmetric dimethylarginine (ADMA) and symmetric dimethylarginine (SDMA) are considered biomarkers of endothelial and renal dysfunction, respectively, in humans. We hypothesize that plasmatic concentration of dimethylarginines in dogs with myxomatous mitral valve disease (MMVD) is influenced by heart disease stage. Eighty-five client-owned dogs with MMVD, including 39, 19, and 27 dogs in ACVIM stages B1, B2, and C+D, respectively, and a control group of 11 clinically healthy dogs were enrolled. A prospective, multicentric, case-control study was performed. Each dog underwent a complete clinical examination, arterial blood pressure measurement, thoracic radiography, six-lead standard electrocardiogram, transthoracic echocardiography, CBC, biochemical profile, and urinalysis. Plasmatic concentration of dimethylarginines was determined through high-performance liquid chromatography coupled with tandem mass spectrometry. Median ADMA was significantly increased in dogs of group C+D (2.5 μmol/L [2.1–3.0]) compared to those of group B1 (1.8 μmol/L [1.6–2.3]; $p < 0.001$) and healthy dogs (1.9 μmol/L [1.7–2.3]; $p = 0.02$). Median SDMA was significantly increased in dogs of group C+D (0.7 μmol/L [0.5–0.9]) compared to those of groups B1 (0.4 μmol/L [0.3–0.5]; $p < 0.001$), B2 (0.4 μmol/L [0.3–0.6]; $p < 0.01$), and the control group (0.4 μmol/L [0.35–0.45]; $p = 0.001$). In the final multivariable analysis, ADMA and SDMA were significantly associated with left atrium to aorta ratio ($p < 0.001$), and creatinine ($p < 0.001$), respectively. Increased plasmatic concentrations of dimethylarginines suggest a possible role as biomarkers of disease severity in dogs with decompensated MMVD.

Keywords: ADMA, canine, heart failure, SDMA, arginine, dimethylarginines

OPEN ACCESS

Edited by:
Zeki Yilmaz,
Faculty of Veterinary Medicine, Turkey

Reviewed by:
Sirilak Disatian Surachetpong,
Chulalongkorn University, Thailand
Domenico Caivano,
University of Perugia, Italy

****Correspondence:***
Carlotta Valente
carlotta.valente@unipd.it

†Current affiliation: Division of Cardiology, Clinic for Small Animal Internal Medicine, Vetsuisse Faculty, University of Zürich, Zürich, Switzerland

Specialty section:
This article was submitted to Comparative and Clinical Medicine, a section of the journal Frontiers in Veterinary Science

Received: *09 July 2021*
Accepted: *23 August 2021*
Published: *16 September 2021*

Citation:
Valente C, Guglielmini C, Baron Toaldo M, Romito G, Artusi C, Brugnolo L, Contiero B and Poser H (2021) Plasmatic Dimethylarginines in Dogs With Myxomatous Mitral Valve Disease. Front. Vet. Sci. 8:738898. doi: 10.3389/fvets.2021.738898

INTRODUCTION

Dimethylarginines (DMAs) are biological products derived by the methylation process of L-arginine. Among them, asymmetric dimethylarginine (ADMA) and its stereoisomer, symmetric dimethylarginine (SDMA), are the most frequently investigated as circulating biomarkers.

Despite their common origin, ADMA and SDMA have different clearance pathways, and consequently, are involved in different pathophysiological processes. Asymmetric dimethylarginine is transported to the kidneys, brain, and liver where it is mainly metabolized by dimethylarginine

dimethylaminohydrolase (1) and only a minimal portion is excreted by the kidneys, whereas SDMA is almost completely eliminated through renal excretion (2).

Asymmetric dimethylarginine acts as an endogenous nitric oxide synthase (NOS) inhibitor, impairing nitric oxide (NO) production (3), which is involved in the homeostasis of vascular tone and blood pressure (4). The L-arginine/ADMA ratio has been studied as an index of NO bioavailability and this ratio seems to be reduced in humans with endothelial dysfunction (5). On the contrary, SDMA is not a direct inhibitor of NO production, but competing with L-arginine cellular uptake, it contributes to reducing NOS activity. Symmetric dimethylarginine is mainly considered a marker of renal damage (6), whereas ADMA is considered a biomarker of endothelial dysfunction (5, 7–10). High levels of both ADMA and SDMA are considered risk factors for cardiovascular and renal morbidity and mortality in humans (11).

Myxomatous mitral valve disease (MMVD) is the most common acquired cardiac disease in dogs and can eventually lead to congestive heart failure (CHF). The American College of Veterinary Internal Medicine (ACVIM) has classified MMVD into four main stages of severity based on clinical, radiographic and echocardiographic parameters (12). Symmetric dimethylarginine has been validated both in dogs and cats as a reliable, early and specific biomarker of renal damage, but little information is available about the role of DMAs in canine cardiovascular diseases (13). Increased SDMA concentration has been described in dogs with MMVD according to disease severity, leading to the hypothesis that impaired cardiac function might consequently alter renal activity (14), whereas ADMA has previously been studied in healthy dogs and in dogs with MMVD in the preclinical stages of disease (15, 16). Understanding the role of DMAs in dogs with cardiac disease can be helpful in recognizing potential risk factors. Furthermore, evaluation of DMAs can be an adjunctive and non-invasive diagnostic tool for the identification of early impaired cardiac and/or renal function in these animals. The aim of this study was to evaluate if plasmatic DMA concentrations in dogs with MMVD are influenced by heart disease stage. We hypothesized that plasmatic levels of ADMA and SDMA increase according to the progression of MMVD and that the L-arginine/ADMA ratio decreases in the most advanced stage of disease.

MATERIALS AND METHODS

Study Design and Animals

The protocol of this prospective, multicentric, case-control study was approved by the University of Padua Animal Welfare Ethics Committee (Authorization number 26/2017).

Dogs were prospectively enrolled from September 2017 to September 2019 at the Veterinary Teaching Hospital of the University of Padua and the University of Bologna. All animals were recruited among external or internal cardiological referral cases or dogs evaluated for a health status check-up. After written informed consent was signed by the dog's owner, each animal underwent a complete physical examination, indirect measurement of arterial systemic pressure through high definition oscillometry (VET HDO Monitor MD PRO-it), six-lead standard electrocardiography (Cardioline Touch ECG, Cardioline s.p.a., Trento Italy), survey thoracic radiography, echocardiographic examination, including real-time 2D, M-mode and echo-Doppler evaluation, and blood and urine sampling for CBC and serum biochemistry profile. Urinalysis, including determination of urinary protein to creatinine ratio and urine specific gravity (USG) was also performed.

Small- and medium-sized dogs with body weight (BW) $<$ 20 kg, aged over seven years, with a diagnosis of MMVD, and absence of other heart or systemic diseases were enrolled. The severity of MMVD was defined according to the ACVIM guidelines (12). In particular, asymptomatic dogs without radiographic or echocardiographic evidence of cardiac remodeling were considered as stage B1; dogs were considered as stage B2 if diagnostic imaging evidenced cardiac remodeling (i.e., cardiomegaly with left atrial and ventricular enlargement). Symptomatic dogs in which at least one episode of pulmonary edema and/or pleural effusion due to CHF had occurred were considered as stage C; symptomatic dogs with end-stage disease and refractory to standard cardiac treatment were considered as stage D. Due to the few animals classified in stage D of MMVD, these dogs were merged with those in stage C for statistical evaluation (group C+D) (12).

Dogs referred to the cardiology units for general screening or pre-anesthetic evaluation for surgery (i.e., orthopedic or neutering surgery), without any clinical, echocardiographic, and laboratory signs of cardiovascular or systemic diseases were enrolled as the control group.

Cardiac Imaging

Right lateral and dorsoventral or ventrodorsal radiographic views of the thorax were obtained and the vertebral heart score was calculated from the lateral view as previously described (17).

The transthoracic echocardiographic examination was performed by experienced operators (CG, HP, MBT) in awake animals from the right and left parasternal windows using standard views (18). Commercially available ultrasound units (CX50, Philips, Eindhoven, Netherlands and iE33, Philips Healthcare, Monza, Italy), equipped with multi-frequency phased array transducers, were employed with continuous ECG monitoring.

Left ventricle measurements, including the internal diameter of the left ventricle in diastole and systole (LVIDd and LVIDs, respectively) were obtained from the right parasternal window, short-axis view at the level of *chordae tendinae* using the 2D guided M-mode. The internal diameters of the left ventricle were indexed to the BW using the formula: normalized LVIDd (LVIDd-N) = LVIDd/[$BW^{0.294}$] and normalized LVIDs (LVIDs-N) = LVIDs/[$BW^{0.315}$] (19). Left ventricular enlargement was considered for values of LVIDd-N $\geq$ 1.7. The left atrium (LA) and aortic diameter (Ao) were measured from the right parasternal window using a short-axis view at the level of the aortic root with the 2D method and measurements taken at early diastole.

From these variables, the left atrium to aortic root ratio (LA/Ao) was then calculated and LA enlargement was considered for a LA/Ao $\geq$ 1.6 (20–22). From the left parasternal window, apical four-chamber view, early and late diastolic trans-mitral (MV E and MV A, respectively) and trans-tricuspid (TV E and TV A, respectively) peak diastolic velocities were obtained using pulsed-wave Doppler, placing the sample volume on the ventricular side at the tip of the mitral or tricuspid valve's leaflets, respectively. When systolic regurgitant blood flow was observed on color-flow mapping of the tricuspid valve, tricuspid regurgitation (TR) peak velocity was recorded, trying to adjust the interrogation beam as parallel as possible to the regurgitant jet. A value of TR peak velocity $\geq$ to 3.4 m/s (corresponding to a systolic pressure gradient $\geq$ 46 mmHg using the modified Bernoulli equation) was used to diagnose pulmonary hypertension in dogs without obstruction of the right ventricular outflow (23). Pulsed-wave tissue Doppler imaging was studied from the left apical four-chamber view, with the sample gate positioned on the lateral and septal mitral annulus, and, after optimizing the alignment of the ultrasound with right ventricle free wall, on the lateral tricuspid annulus. For each position, we considered measurements of the peak velocity of early diastolic lateral and septal mitral annular motion (LatMV E' and SepMV E', respectively) and of the peak velocity of early diastolic lateral tricuspid annular motion (TV E').

Each echocardiographic variable was measured in triplicate, using the average value for the subsequent statistical analysis.

Laboratory Analysis

Complete blood count and serum biochemical analyses were performed at the laboratories of Veterinary Teaching Hospital of the University of Padua and the University of Bologna within 24 h of blood collection, and urinalysis within 4 h of urine sampling, with dogs fasted for 12 h beforehand. The hematologic parameters were measured using automated analyzers (Advia 120, Hematology System, Siemens, Italy; Advia 2120, Siemens Healthcare Diagnostics, Erlangen, Germany). The biochemical variables and urinary protein to creatinine ratio were evaluated using other automated analyzers (BT1500, Biotecnica, Roma, Italy; AU 480, Beckman Coulter-Olympus, Brea, California, USA). Normal and pathological internal quality controls were performed daily for both analyzers, whereas external control quality was performed once a month.

Urine physical and chemical examinations were performed using a commercial urinalysis stick (DIRUI A10). Then, the USG was determined using a refractometer. Finally, after centrifugation, the urinary sediment was examined.

Blood used for hematological analysis was collected in vacutainer tubes containing K3-EDTA. They were centrifuged at 3,000 rpm for 10 min, then about 0.5 ml of plasma was separated and stored at −20 °C for successive DMA analyses. Plasmatic levels of ADMA, SDMA, and L-arginine were measured simultaneously at the laboratory of University-Hospital of Padua using high-performance liquid chromatography coupled with tandem mass spectrometry (Agilent 1200 Series LC system coupled with an Agilent 6430 triple quadrupole, Palo Alto, CA, USA), as previously described (24, 25). Quantification of N-terminal propeptide of B-type natriuretic peptide (NT-proBNP) was obtained from plasmatic samples by a referring laboratory (IDEXX Laboratories, Leipzig, Germany), through the Cardiopet® NT-proBNP method.

Statistical Analysis

A preliminary analysis was conducted to calculate the minimum sample size necessary to obtain significant results. In particular, the determination of sample size was based on the studies of Nabity et al. (13) and Pedersen et al. (16). Considering a power of the statistical test equal to 80% and a type I error equal to 5%, 11 dogs for each group were adequate to check a standardized difference of 1.27 and 1.30 for SDMA and ADMA, respectively.

The statistical analysis was performed with commercially available statistical software (SAS®, 9.2 SAS Institute Inc; XLStat Addinsoft (2021) – XLSTAT statistical and data analysis solution, Paris, France; and MedCalc Statistical Software, version 19.3.1 – MedCalc Software Ltd., Ostend, Belgium).

Normal distribution of data was assessed using the Shapiro–Wilk's test. As the variables were not normally distributed, the differences among groups were analyzed using a non-parametric approach (Kruskal–Wallis test). *Post hoc* pairwise comparisons among levels were tested using the Steel–Dwass–Critchlow–Fligner procedure.

Differences in categorical variables, expressed as count data, were tested using the Chi-squared test. The association between clinical, laboratory, and echocardiographic variables with DMAs and L-arginine/ADMA were studied using the Spearman's rank correlation index. The variables showing the most significant correlations were successively evaluated in a multivariable model, to assess their effect on DMAs and L-arginine/ADMA.

Data are expressed as median and interquartile range. An overall $p < 0.05$ was considered as statistically significant, whereas a $p < 0.001$ was set for Spearman's correlations.

RESULTS

Study Population

Ninety-six dogs met the inclusion criteria, including 11 (11.5%) control dogs and 85 (88.5%) dogs with MMVD at different stages. Of all enrolled dogs, 49 (51%) were mongrels, followed by nine (9.3%) Cavalier King Charles Spaniels, four (4.1%) Jack Russell Terriers, and four (4.1%) Miniature Pinschers. All less represented breeds are reported in **Table 1**. Forty-four (45.8%) dogs were females and 52 (54.2%) males. The median (interquartile range) age was 11 years (9–14 years) and the median BW was 9.1 kg (6.7–12.1 kg). Dogs in the control group were younger compared to those of group C+D ($p = 0.014$).

Among dogs with MMVD, 39 (41%), 19 (20%), and 27 (28%) were classified as B1, B2, and C+D, respectively. Seventy-six dogs (79%) with MMVD had TR, of which 11 (14%) were considered affected by pulmonary hypertension. Among dogs with pulmonary hypertension, one (2.5%), four (21%), and six (22%) were in groups B1, B2, and C+D, respectively. Forty-three (50.5%) dogs with MMVD were receiving some cardiovascular treatment at the time of enrollment (**Table 1**).

TABLE 1 | Clinical parameters of the 96 dogs included in the study.

Parameter	Control	B1	B2	C+D	Overall *p*-value
N. of dogs (%)	11 (11)	39 (41)	19 (20)	27 (28)	
Age (Y)	9 (7–12)	11 (8–13)	12 (11–14)	12 (10–14) *	0.01
BW (Kg)	9 (7.2–17.5)	10.5 (8–13.6)	7.3 (5.4–10.9)	9 (7.5–13.8)	0.23
Sex M/F	3/8	22/17	12/7	15/12	0.27
Breed (N.)	Mongrel (4), Miniature Pinscher (2), Australian Shepherd, Beagle, WHWT, English Bulldog, Pug (1)	Mongrel (18), CKCS (6), Dachshund (2), Jack Russell Terrier (2) English Setter (2), Maltese, Fox Terrier, Russian Toy, Yorkshire Terrier, Miniature Pinscher, Miniature Schnauzer, Spitz, Cocker Spaniel, Pug (1)	Mongrel (10), CKCS (3), Pomeranian Fox, Miniature Schnauzer, Miniature Pinscher, Bolognese, Shih-Tzu, Greyhound (1)	Mongrel (17), Jack Russell Terrier (2), Yorkshire Terrier, Beagle, Bolognese, Border Collie, Shih-Tzu, Maltese, Epagneul Breton, English Setter (1)	0.41
PH (%)	0 (0)	1 (2.5)	4 (21)	6 (22)	0.05
Cardiovascular treatment, N. (%)	0 (0)	8 (20)	12 (63)**	26 (96)**,***	<0.001
Furosemide, N. (%) [doses range] mg/kg	0 (0)	5 (13) [0.5–5.0]	4 (21) [0.6–4.0]	23 (88) [0.6–9.0]	
Benazepril, N. (%) [doses range] mg/kg	0 (0)	7 (18) [0.2–0.8]	5 (26) [0.16–0.5]	20 (74) [0.25–1.1]	
Spironolactone, N. (%) [doses range] mg/kg	0 (0)	1 (3) [2.3]	0 (0)	6 (22) [1.0–3.0]	
Pimobendan, N. (%) [doses range] mg/kg	0 (0)	2 (5) [0.5–0.6]	9 (47) [0.4–0.8]	19 (70) [0.1–0.8]	

Data are presented as median and interquartile range.

N., number of dogs; BW, bodyweight; PH, pulmonary hypertension; H, clinically healthy dogs; B1, dogs with myxomatous mitral valve disease (MMVD) belonging to B1 stage (American College of Veterinary Internal Medicine (ACVIM) guidelines); B2, dogs with MMVD belonging to B2 stage (ACVIM guidelines); C+D, dogs with MMVD belonging to C and D stage (ACVIM guidelines); M/F, male/female; CKCS, Cavalier King Charles Spaniel; PH, pulmonary hypertension; WHWT, West Highland White Terrier.

$p < 0.05$ in comparison with H.

**$p < 0.001$ in comparison with B1.*

***$p < 0.001$ in comparison with B2.*

Laboratory and Cardiac Parameters

The results of laboratory analyses are shown in **Table 2**. The median of blood urea nitrogen (BUN) and creatinine was higher in dogs of group C+D (65 mg/dl [50–116] and 1.4 mg/dl [1.1–1.6], respectively) compared to that of dogs of group B1 (36 mg/dl [32–51] and 1.0 mg/dl [0.8–1.1], respectively; $p < 0.001$ for both comparisons). The median of BUN was also higher in dogs of group C+D compared to that of control dogs (43 mg/dl [26–50]; $p < 0.01$) and dogs of group B2 (50 mg/dl [35–58.36]; $p = 0.04$). The median serum phosphorus was higher in dogs of group C+D (3.9 mg/dl [3.4–5.1]) compared to that of dogs of group B1 (3.4 mg/dl [3.0–4.2]; $p = 0.02$). The median USG was lower in dogs of group C+D (1,014 [1,012–1,017.5]) compared to that of dogs of groups H (1,029 [1,020–1,044]; $p < 0.01$), B1 (1,026 [1,018–1,043]; $p = 0.02$), and B2 (1,028 [1,018–1,038]; $p < 0.01$).

The median SDMA was higher in dogs of group C+D (0.7 μmol/L [0.5–0.9]) compared to that of dogs of groups B1 (0.4 μmol/L [0.3–0.5]; $p < 0.001$), B2 (0.4 μmol/L [0.3–0.6]; $p < 0.01$), and clinically healthy dogs (0.4 μmol/L [0.35–0.45]; $p = 0.001$). The median ADMA was higher in dogs of group C+D (2.5 μmol/L [2.1–3.0]) compared to that of dogs of group B1 (1.8 μmol/L [1.6–2.3]; $p < 0.001$) and control group (1.9 μmol/L [1.7–2.3]; $p = 0.02$), but not to that of group B2 (2.0 μmol/L [1.6–2.4]; $p = 0.05$). No difference was found for median L-arginine among dogs of the different groups (overall $p = 0.59$). On the contrary, the median L-arginine/ADMA was lower in dogs of group C+D (41.7 [27.6–46.0]) compared to that of dogs of groups B1 (50.9 [44.2–68.9]; $p < 0.001$) and B2 (51.9 [39.4–65.9]; $p = 0.03$), but not to that of the control group (47.2 [37.1–63.0]; $p = 0.172$).

The median NT-proBNP was higher in dogs of groups B2 (1423 pmol/L [798–3,984]) and C+D (4,062 pmol/L [2,169–5,482]) compared to that of dogs of control group (372 pmol/L [249–529]; $p < 0.01$ and $p < 0.001$, respectively) and group B1 (434.5 pmol/L [342.5–584.5]; $p = 0.001$ and $p < 0.001$, respectively).

According to the progressive nature of MMVD, radiographic and echocardiographic parameters of cardiac remodeling and dysfunction progressively changed among groups, according to disease severity (**Supplementary Table 1**).

Both SDMA and ADMA were positively correlated with BUN ($r = 0.472$ and $r = 0.391$; $p < 0.001$ for both correlations) and creatinine ($r = 0.604$ and $r = 0.462$; $p < 0.001$ for both correlations).

Symmetric dimethylarginine was also positively correlated with age ($r = 0.426$; $p < 0.001$) and NT-proBNP ($r = 0.489$; $p < 0.001$). L-arginine/ADMA was negatively correlated with NT-proBNP ($r = -0.414$; $p < 0.001$), BUN ($r = -0.438$; $p < 0.001$),

TABLE 2 | Clinical pathology parameters of 11 clinically healthy dogs (Control) and 85 dogs with myxomatous mitral valve disease grouped in different disease stages according to ACVIM guidelines.

Variable	Control N. = 11	B1 N. = 39	B2 N. = 19	C+D N. = 27	Overall *p*-value
BUN (mg/dl)	43 (26–50)	36 (32–51)	50 (35–58.36)	65 (50–116)$^{**,\circ\circ,\#}$	**<0.001**
Total protein (g/L)	72.9 (70.0–78.9)	71.8 (66.8–76.2)	69.9 (66.6–71.7)	72.5 (60.4–81.1)	0.52
Albumin (g/L)	30.7 (28.4–31.7)	31.1 (29.6–32.4)	29.4 (27.3–33.7)	28.9 (26.8–33.5)	0.13
Creatinine (mg/dl)	1.0 (1.0–1.2)	1.0 (0.8–1.1)	1.1 (0.8–1.5)	1.4 (1.1–1.6)$^{\circ\circ}$	**<0.001**
Cholesterol (mg/dl)	272 (214–299)	236 (195–279)	210.5 (164–231)	211 (172–269)	0.10
Triglycerides (mg/dl)	74 (48–139)	62.5 (48–88)	53.5 (35–68)	69.5 (44.5–79)	0.20
Calcium (mg/dl)	10.5 (10.0–10.7)	10.2 (9.7–10.6)	10.1 (9.6–10.3)	10.3 (9.6–10.8)	0.28
Phosphorus (mg/dl)	4.0 (3.7–5.5)	3.4 (3.0–4.2)	3.6 (2.8–4.0)	3.9 (3.4–5.1)$^{\circ}$	**0.02**
Na^+ (mEq/L)	147.4 (144.2–153.6)	148 (144.5–151.3)	148.8 (143.2–150)	147.4 (144.9–152)	0.95
K^+ (mEq/L)	4.9 (4.3-5.1)	4.6 (4.4-4.7)	4.6 (4.2-4.9)	4.3 (4.0-4.6)	0.09
USG	1,029 (1,020–1,044)	1,026 (1,018–1,043)	1,028 (1,018–1,038)	1,014 (1,012–1,017.5)$^{**,\circ,\#\#}$	**0.002**
PU/CU	0.1 (0.02–0.1)	0.1 (0.1–0.3)	0.2 (0.1–0.4)	0.1 (0.1–0.3)	0.23
RBC ($10^6/\mu l$)	7.3 (6.7–7.7)	7.0 (6.4–7.5)	6.8 (6.1–7.7)	7.3 (6.1–8.0)	0.61
WBC ($10^3/\mu l$)	8.4 (6.0–9.9)	8.0 (7.3–9.3)	9.1 (7.3–12.6)	14.5 (9.6–22.5)$^{**,\circ\circ}$	**<0.001**
NT-proBNP (pmol/L)	372 (249–529)	434.5 (342.5–584.5)	1,423 (798–3,984) $^{**,\circ\circ}$	4,062 (2,169–5,482)$^{***,\circ\circ}$	**<0.001**
SDMA (μmol/L)	0.4 (0.35–0.45)	0.4 (0.3–0.5)	0.4 (0.3–0.6)	0.7 (0.5–0.9)$^{**,\circ\circ,\#\#}$	**<0.001**
ADMA (μmol/L)	1.9 (1.7–2.3)	1.8 (1.6–2.3)	2.0 (1.6–2.4)	2.5 (2.1–3.0)$^{*,\circ\circ}$	**<0.001**
L-Arg (μmol/L)	95.1 (76.4–127.3)	105.8 (85.7–126.5)	124.3 (86.6–143.8)	103 (73.1–138.5)	0.59
L-Arg/ADMA	47.2 (37.1–63.0)	50.9 (44.2–68.9)	51.9 (39.4–65.9)	41.7 (27.6–46.0)$^{\circ\circ,\#}$	**<0.001**

Data are presented as median and interquartile range.
Significant overall P values are reported in bold.
N., number of dogs; ADMA, asymmetric dimethylarginine; BUN, blood urea nitrogen; L-Arg, L-arginine; L-Arg/ADMA, L-arginine to ADMA ratio; NT-proBNP, N-terminal prohormone of brain natriuretic peptide; RBC, red blood cell; PU/CU, urinary protein to creatinine ratio; SDMA, symmetric dimethylarginine; WBC, white blood cell; USG, urine specific gravity.
$^*p < 0.05$ in comparison with H.
$^{**}p < 0.01$ in comparison with H.
$^{***}p < 0.001$ in comparison with H.
$^\circ p < 0.05$ in comparison with B1.
$^{\circ\circ}$ $p < 0.001$ in comparison with B1.
$^\#$ $p < 0.05$ in comparison with B2.
$^{\#\#}$ $p < 0.01$ in comparison with B2.

and creatinine ($r = -0.457$; $p < 0.001$) (**Table 3**). Symmetric dimethylarginine and ADMA were also positively correlated with the echocardiographic variables LA/Ao ($r = 0.449$ and $r = 0.424$; $p < 0.001$ for both correlations), lateral MV E/E' ($r = 0.410$ and $r = 0.522$; $p = 0.001$ and $p < 0.001$, respectively), and septal MV E/E' ($r = 0.5$ and $r = 0.478$; $p < 0.001$ and $p < 0.001$, respectively) (**Table 4**).

In the final multivariable analysis, considering the effect of both creatinine and LA/Ao on DMAs and the L-arginine/ADMA, ADMA was significantly and positively associated with the LA/Ao ($R^2 = 0.18$; $p < 0.001$) and SDMA with creatinine ($R^2 = 0.27$; $p < 0.001$) whereas L-arginine/ADMA was nearly significantly and negatively associated with creatinine ($p = 0.001$) (**Table 5**).

DISCUSSION

This study showed an increase of plasmatic DMA's concentration associated with the more advanced stage of MMVD. Indeed, both SDMA and ADMA were higher in dogs with decompensated heart disease (group C+D) when compared to dogs in the preclinical stages of valvular disease and to dogs in the control group. On the contrary, the L-arginine/ADMA was lower in dogs with decompensated MMVD when compared to those with compensated disease. Both ADMA and SDMA were positively correlated with BUN and creatinine, and with the echocardiographic parameters, LA/Ao and both lateral and septal MV E/E'. Finally, in the multivariable analysis evaluating the effect of an echocardiographic (i.e., LA/Ao) and renal (i.e., creatinine) variable, ADMA was more associated with the LA/Ao than creatinine, whereas the SDMA and L-arginine/ADMA showed the opposite result. These findings are similar to those of previous studies showing an increase of ADMA in dogs with experimentally induced CHF (26) but not in animals in the preclinical stages of naturally occurring MMVD (16). However, Cunningham et al. showed that in dogs with naturally occurring CHF, ADMA did not increase if compared to healthy dogs (27). The difference between our results and this latter study is probably due to different sample size of dogs enrolled, methods of classification of MMVD severity (ACVIM guidelines vs. International Small Animal Cardiac Health Council classification), and finally, to the inclusion of either dogs with both MMVD or dilated cardiomyopathy.

TABLE 3 | Spearman's ranks correlations index between symmetric dimethylarginine (SDMA), asymmetric dimethylarginine (ADMA), L-arginine, L-arginine/ADMA and demographic and clinical pathology parameters obtained from 11 control dogs and 85 dogs with myxomatous mitral valve disease at different disease stages.

Parameter	SDMA		ADMA		L-arginine		L-arginine/ADMA	
	r	*P*	*r*	*P*	*r*	*P*	*r*	*P*
Age	0.426	**<0.001**	0.300	0.002	−0.106	0.30	−0.328	0.001
BW	0.103	0.32	0.220	0.03	0.385	**<0.001**	0.142	0.17
BUN	0.472	**<0.001**	0.391	**<0.001**	0.120	0.24	−0.438	**<0.001**
Total protein	0.044	0.67	0.026	0.80	−0.046	0.65	−0.029	0.77
Albumin	−0.241	0.02	−0.123	0.23	0.106	0.30	0.238	0.02
Creatinine	0.604	**<0.001**	0.462	**<0.001**	−0.094	0.36	−0.457	**<0.001**
Cholesterol	−0.019	0.85	−0.002	0.97	−0.077	0.45	−0.076	0.46
Triglycerides	0.049	0.67	0.100	0.38	0.121	0.29	0.095	0.41
Calcium	0.120	0.24	0.152	0.14	−0.001	0.02	−0.133	0.20
Phosphorus	0.099	0.33	0.207	0.04	0.190	0.06	−0.024	0.82
Na^+	0.155	0.14	0.173	0.10	−0.071	0.50	−0.182	0.08
K^+	0.022	0.83	0.061	0.56	0.268	0.01	0.129	0.22
USG	−0.360	0.002	−0.392	0.001	0.001	0.98	0.333	0.005
PU/CU	−0.146	0.23	−0.084	0.49	0.083	0.49	0.071	0.56
RBC	0.068	0.50	0.146	0.15	0.128	0.21	0.037	0.72
WBC	0.281	0.005	0.199	0.05	−0.016	0.87	−0.187	0.07
NT-proBNP	0.489	**<0.001**	0.336	0.008	−0.070	0.59	−0.414	**<0.001**

Significant overall P values are reported in bold. ADMA, asymmetric dimethylarginine; BUN, blood urea nitrogen; BW, body weight; NT-proBNP, N-terminal prohormone of brain natriuretic peptide; PU/CU, urinary protein to creatinine ratio; RBC, red blood cell; SDMA, symmetric dimethylarginine; WBC, white blood cell; USG, urine specific gravity.

TABLE 4 | Spearman's ranks correlations index between symmetric dimethylarginine (SDMA), asymmetric dimethylarginine (ADMA), L-arginine, L-arginine/ADMA and radiographic and echocardiographic parameters obtained from 11 control dogs and 85 dogs with myxomatous mitral valve disease at different diseases stages.

Parameter	SDMA		ADMA		L-arginine		L-arginine/ADMA	
	r	*P*	*r*	*P*	*r*	*P*	*r*	*P*
VHS	0.284	0.03	0.365	0.004	0.330	0.01	−0.087	0.50
LA/Ao	0.449	**<0.001**	0.424	**<0.001**	0.083	0.42	−0.294	0.004
LVIDd	0.266	0.009	0.347	**<0.001**	0.305	0.003	−0.038	0.71
LVIDd-N	0.252	0.01	0.267	0.009	0.083	0.43	−0.159	0.12
LVIDs	0.011	0.91	0.138	0.18	0.330	0.001	0.139	0.18
LVIDs-N	0.011	0.91	0.105	0.31	0.169	0.103	0.020	0.84
FS (%)	0.350	<0.001	0.250	0.02	−0.145	0.17	−0.308	0.003
MV E	0.366	<0.001	0.339	<0.001	0.035	0.73	−0.266	0.009
MV A	0.043	0.68	0.078	0.45	0.001	0.99	−0.097	0.36
MV E/A	0.244	0.02	0.213	0.04	0.010	0.92	−0.145	0.17
TV E	0.107	0.40	0.046	0.72	−0.158	0.21	−0.138	0.27
TV A	−0.058	0.66	−0.089	0.49	−0.153	0.24	−0.027	0.83
TV E/A	0.042	0.75	−0.011	0.92	−0.014	0.91	−0.040	0.76
TR Vmax	0.301	0.01	0.175	0.15	0.052	0.67	−0.048	0.69
LatMV E/E'	0.410	**0.001**	0.522	**<0.001**	0.263	0.05	−0.196	0.14
SepMV E/E'	0.500	**<0.001**	0.478	**<0.001**	0.030	0.82	−0.324	0.01
TV E/E'	−0.131	0.35	−0.240	0.08	−0.149	0.29	−0.023	0.87

Significant overall P values are reported in bold. VHS, vertebral heart score; LA/Ao, left atrium to aortic root diameter ratio; LVIDd, Left ventricular internal diameter in diastole; LVIDd-N, Left ventricular internal diameter in diastole normalized for body weight; LVIDs, Left ventricular internal diameter in systole; LVIDs-N, Left ventricular internal diameter in systole normalized for body weight; FS, fractional shortening; MV E, mitral valve early diastolic velocity; MV A, mitral valve late diastolic velocity; TV E, tricuspidal valve early diastolic velocity; TV A, tricuspidal valve late diastolic velocity; TR Vmax, tricuspid regurgitation peak velocity; LatMV E', peak velocity of early diastolic lateral mitral annular motion; SepMV E', peak velocity of early diastolic septal mitral annular motion; TV E', peak velocity of early diastolic lateral tricuspid annular motion.

TABLE 5 | Final multivariable analysis for asymmetric dimethylarginine (ADMA), symmetric dimethylarginine (SDMA) and L-arginine/ADMA as response variables and LA/Ao and creatinine as explanatory variables.

	LA/Ao		Creatinine		
Variables	**RCE ± SE**	***P***	**RCE ± SE**	***P***	R^2
ADMA	0.383 ± 0.104	<0.001	0.286 ± 0.184	0.12	0.18
SDMA	0.113 ± 0.042	<0.01	0.307 ± 0.074	<0.001	0.27
L-arginine/ADMA	−5.040 ± 2.816	0.08	−15.988 ± 4.992	0.001	0.16

Regression coefficients estimates, their standard errors and the determination coefficient of the model (R^2) were reported.
ADMA, asymmetric dimethylarginine; LA/Ao, left atrium to aortic root ratio; RCE, regression coefficient estimate; SDMA, symmetric dimethylarginine; SE, standard error.

It has been shown that in canine myocardial cells the enzymatic activity of dimethylarginine dimethylaminohydrolase, which partly contributes to ADMA accumulation, is reduced in the failing heart (28). Furthermore, ADMA can also be excreted through the kidneys; thus, renal damage might be responsible for ADMA accumulation (29). In humans, the "cardiorenal syndrome" is a well-known pathophysiological mechanism where decreased renal function is the consequence of reduced cardiac output (30). In dogs with decompensated MMVD, the increase of BUN is a common finding, partly due to diuretic treatment used to control clinical signs of CHF, namely prerenal azotemia. However, primary renal damage or renal dysfunction secondary to a cardiac disorder cannot be completely excluded in these animals (31–33). In humans, the presence of chronic kidney disease has been associated with increased ADMA concentration (34). The positive correlation we found between creatinine and ADMA in dogs with MMVD suggests that a reduced renal function can also have an effect on ADMA in the dog. However, results of the multivariable analysis, that evaluated the combined effect of variables of both cardiac and renal function, showed that ADMA is influenced by the LA/Ao, an index of cardiac remodeling due to MMVD, rather than by renal function. Other studies are needed to confirm if ADMA might be related to renal damage in dogs with kidney disease and if it could be predictive of a negative cardiovascular outcome, as demonstrated in humans (35).

In the present study, SDMA was higher in dogs with decompensated MMVD, whereas no difference was found in asymptomatic dogs (i.e., stages B1 and B2). This finding confirms the results of a previous prospective study in which SDMA was correlated with cardiac disease severity and with echocardiographic parameters of left atrio-ventricular dilation (14). Conversely, two other retrospective studies failed to demonstrate a correlation between SDMA and MMVD progression (36, 37). The discrepancy between our study and these latter studies can be explained by differences in study design and laboratory analytical method used to determine SDMA. Our study had a prospective design and we used high-performance liquid chromatography coupled with tandem mass spectrometry, considered a reliable diagnostic tool for measuring DMAs (38), whereas SDMA concentrations were measured through high-throughput immunoassay in previous studies (36, 37). Symmetric dimethylarginine was also positively correlated with laboratory (i.e., NT-proBNP) and echocardiographic (i.e., LA/Ao and lateral and septal MV E/E') indices of cardiac wall stress, remodeling, and dysfunction. In humans, SDMA is correlated with E/E' in patients with chronic CHF and it has been suggested that a prolonged NOS inhibition enhanced myocardial fibrotic processes, potentially modifying myocardial function (39, 40). Previous studies suggested that NT-proBNP is more likely associated with cardiac damage rather than renal injury in both humans and dogs with chronic kidney disease (41, 42). High SDMA concentrations in our dogs with decompensated MMVD were associated with renal function, as confirmed by increased BUN, creatinine, and phosphorus, and decreased USG. However, we cannot discriminate if renal dysfunction was caused by primary renal disease, impaired cardiac function, cardiovascular treatment, or a combination of these causes. The results of this study suggest that cardiorenal syndrome, in particular cardiovascular renal disorders (43), can develop in dogs with decompensated MMVD, whereas the absence of significant increases of BUN, creatinine, and SDMA in dogs with compensated MMVD likely exclude a cardiorenal syndrome in these animals. Thus, our findings confirm that SDMA is a biomarker of renal damage, but it is also likely influenced by heart disease.

The L-arginine/ADMA was significantly lower in dogs with decompensated MMVD compared to those of group B1 and clinically healthy controls. This finding is in contrast with the results of a previous study in which no significant difference was found for L-arginine/ADMA in 43 Cavalier King Charles Spaniels with MMVD at various stages, classified according to a mitral regurgitation quantitative score (44). However, that study found decreased flow mediated dilation, a reference diagnostic method to identify endothelial dysfunction in humans (45). Different results from this study and that of Moesgaard et al. (44) are likely due to differences in number and type of enrolled dogs, various breeds vs. a unique breed, and method of MMVD classification. The L-arginine/ADMA ratio is considered an index of NO bioavailability and, in humans, it is reduced in patients with endothelial dysfunction (46). Endothelial dysfunction can develop early and become progressively severe in both humans and dogs with heart disease (46, 47), but few studies have specifically evaluated endothelial dysfunction in dogs with MMVD (44, 47). The reduced L-arginine/ADMA observed in dogs of this study confirms the presence of endothelial dysfunction in animals with decompensated MMVD. This biomarker was negatively correlated with NT-proBNP and the renal parameters, BUN and creatinine. Renal dysfunction induces an increase of ADMA concentration leading to a decrease of the L-arginine/ADMA, more evident in the advanced stages of MMVD. The association between NT-proBNP and the L-arginine/ADMA has been studied in humans with CHF and it has been correlated with impaired NO production in those patients with endothelial dysfunction (48). Based on the results

of our final multivariable analysis, renal dysfunction likely has a greater influence on this parameter compared to heart disease in dogs with MMVD, but further studies are needed to confirm this hypothesis.

One limitation of this study is the smaller sample size of clinically healthy dogs compared to the other groups of dogs, but it was considered appropriate according to our preliminary statistical analysis. Moreover, this group of dogs had a lower median age compared to that of dogs in the more advanced stage of MMVD. Based on a previous study, ADMA could be influenced by breed (15). Specifically, in that study, Pointers showed increased concentrations of ADMA compared to Cairn Terriers and Cavalier King Charles Spaniels. However, it should also be noted that ADMA concentrations were evaluated exclusively in healthy dogs and only in the three aforesaid breeds. Of note, no Pointer was included in our study. Therefore, further data are needed to conclusively clarify a potential breed effect on ADMA concentration.

The presence of renal dysfunction was based on different established laboratory parameters, namely BUN, creatinine, and USG; however, evaluation of the glomerular filtration rate, the standard reference method to evaluate renal dysfunction, was not used. Finally, a cardiovascular treatment effect could not be excluded. However, cardiovascular drugs used for CHF treatment (i.e., diuretics, ACE-I, and nitrovasodilators) did not show any influence on ADMA concentrations in humans (49).

In dogs, diuretic therapy has been shown to impair renal function, leading to an increase of renal parameters. Two studies obtained contrasting results regarding the effect of therapies on SDMA concentrations in dogs with MMVD (36, 37). In the study of Savarese et al. no therapies effect has been shown (36), whereas in the other study increasing doses of furosemide seemed to be associated with an increase of SDMA concentrations. However, the combined analysis of therapy effect with MMVD ACVIM stage did not show any significant result (37). Cardiovascular therapy effect on SDMA in dogs with MMVD is still unclear and, so far, it is not possible to discriminate if the variation of SDMA concentrations is more influenced by cardiovascular drugs effect on glomerular filtration rate, or by the cardiac disease itself. Furthermore, some dogs were referred cases and, occasionally, they were already receiving several different cardiovascular treatments from the referring veterinarian that were not always in agreement with the ACVIM guidelines. Thus, further investigations considering a more standardized dog's population are needed. Finally, the dogs included in the study did not receive a standardized diet, thus an effect of the diet composition on the plasmatic concentration of DMAs cannot be excluded.

CONCLUSION

The results of this study showed an increase of ADMA and SDMA and a reduction of the L-arginine/ADMA in dogs in the more advanced stage of MMVD. Asymmetric dimethylarginine can be considered a biomarker of cardiac and endothelial dysfunction in dogs with decompensated MMVD. However, an impaired renal function might contribute for its increase in these animals. At the same time, SDMA is mainly dependent on renal function but the presence of advanced valvular disease can also influence its concentration.

DATA AVAILABILITY STATEMENT

The raw data supporting the conclusions of this article will be made available by the authors, without undue reservation.

ETHICS STATEMENT

The animal study was reviewed and approved by the University of Padua Animal Welfare Ethics Committee (authorization number 26/2017). Written informed consent was obtained from the owners for the participation of their animals in this study.

AUTHOR CONTRIBUTIONS

CG and HP: Conceptualization. BC: formal analysis. CV, CG, MBT, GR, CA, LB, and HP: investigation and data collection. CV: writing-original draft preparation. CV, CG, MBT, GR, CA, LB, BC, and HP: writing-review and editing. All authors contributed to the article and approved the submitted version.

FUNDING

This work was supported by a grant of University of Padua, Italy, to Dr. Poser (SID Year: 2017- Protocol number: BIRD173881).

ACKNOWLEDGMENTS

Authors acknowledge Dr. Tamara Badon and Dr. Silvia Bedin for their valuable technical support. Presented in part as an oral presentation at the 73th Congress of the Italian Society of Veterinary Science, Olbia, Italy, 19th-22nd June 2019.

SUPPLEMENTARY MATERIAL

The Supplementary Material for this article can be found online at: https://www.frontiersin.org/articles/10.3389/fvets.2021.738898/full#supplementary-material

REFERENCES

1. Ogawa T, Kimoto M, Sasaoka K. Purification and properties of a new enzyme, NG,NG-dimethylarginine dimethylaminohydrolase, from rat kidney. *J Biol Chem.* (1989) 264:10205–9. doi: 10.1016/S0021-9258(18)81786-0

2. Nijveldt RJ, Van Leeuwen PA, Van Guldener C, Stehouwer CD, Rauwerda JA, Teerlink T. Net renal extraction of asymmetrical (ADMA) and symmetrical (SDMA) dimethylarginine in fasting humans. *Nephrol Dial Transplant.* (2002) 17:1999–2002. doi: 10.1093/ndt/17.11.1999

3. Vallance P, Leone A, Calver A, Collier J, Moncada S. Endogenous dimethylarginine as an inhibitor of nitric oxide synthesis. *J Cardiovasc Pharmacol*. (1992) 20:S60–62. doi: 10.1097/00005344-199204002-00018
4. Tousoulis D, Kampoli AM, Tentolouris C, Papageorgiou N, Stefanadis C. The role of nitric oxide on endothelial function. *Curr Vasc Pharmacol.* (2012) 10:4–18. doi: 10.2174/157016112798829760
5. Böger RH, Bode-Böger SM, Szuba A, Tsao PS, Chan JR, Tangphao O, et al. Asymmetric dimethylarginine (ADMA): a novel risk factor for endothelial dysfunction: its role in hypercholesterolemia. *Circulation.* (1998) 98:1842–7. doi: 10.1161/01.cir.98.18.1842
6. Kielstein JT, Salpeter SR, Bode-Boeger SM, Cooke JP, Fliser D. Symmetric dimethylarginine (SDMA) as endogenous marker of renal function–a meta-analysis. *Nephrol Dial Transplant.* (2006) 21:2446–51. doi: 10.1093/ndt/gfl292
7. Zoccali C, Bode-Böger S, Mallamaci F, Benedetto F, Tripepi G, Malatino L, et al. Plasma concentration of asymmetrical dimethylarginine and mortality in patients with end-stage renal disease: a prospective study. *Lancet.* (2001) 358:2113–7. doi: 10.1016/s0140-6736(01)07217-8
8. Surdacki A, Nowicki M, Sandmann J, Tsikas D, Boeger RH, Bode-Boeger SM, et al. Reduced urinary excretion of nitric oxide metabolites and increased plasma levels of asymmetric dimethylarginine in men with essential hypertension. *J Cardiovasc Pharmacol.* (1999) 33:652–8. doi: 10.1097/00005344-199904000-00020
9. Abbasi F, Asagmi T, Cooke JP, Lamendola C, McLaughlin T, Reaven GM, et al. Plasma concentrations of asymmetric dimethylarginine are increased in patients with type 2 diabetes mellitus. *Am J Cardiol.* (2001) 88:1201–3. doi: 10.1016/s0002-9149(01)02063-x
10. Lundman P, Eriksson MJ, Stühlinger M, Cooke JP, Hamsten A, Tornvall P. Mild-to-moderate hypertriglyceridemia in young men is associated with endothelial dysfunction and increased plasma concentrations of asymmetric dimethylarginine. *J Am Coll Cardiol.* (2001) 38:111–6. doi: 10.1016/s0735-1097(01)01318-3
11. Jarzebska N, Mangoni AA, Martens-Lobenhoffer J, Bode-Böger SM, Rodionov RN. The second life of methylarginines as cardiovascular targets. *Int J Mol Sci.* (2019) 20:4592. doi: 10.3390/ijms20184592
12. Keene BW, Atkins CE, Bonagura JD, Fox PR, Häggström J, Fuentes VL, et al. ACVIM consensus guidelines for the diagnosis and treatment of myxomatous mitral valve disease in dogs. *J Vet Intern Med.* (2019) 33:1127–40. doi: 10.1111/jvim.15488
13. Nabity MB, Lees GE, Boggess MM, Yerramilli M, Obare E, Yerramilli M, et al. Symmetric Dimethylarginine Assay Validation, Stability, and Evaluation as a Marker for the Early Detection of Chronic Kidney Disease in Dogs. *J Vet Intern Med.* (2015) 29:1036–44. doi: 10.1111/jvim.12835
14. Choi BS, Moon HS, Seo SH, Hyun C. Evaluation of serum cystatin-C and symmetric dimethylarginine concentrations in dogs with heart failure from chronic mitral valvular insufficiency. *J Vet Med Sci.* (2017) 79:41–6. doi: 10.1292/jvms.16-0188
15. Moesgaard SG, Holte AV, Mogensen T, Mølbak J, Kristensen AT, Jensen AL, et al. Effects of breed, gender, exercise and white-coat effect on markers of endothelial function in dogs. *Res Vet Sci.* (2007) 82:409–15. doi: 10.1016/j.rvsc.2006.09.003
16. Pedersen LG, Tarnow I, Olsen LH, Teerlink T, Pedersen HD. Body size, but neither age nor asymptomatic mitral regurgitation, influences plasma concentrations of dimethylarginines in dogs. *Res Vet Sci.* (2006) 80:336–42. doi: 10.1016/j.rvsc.2005.07.005
17. Buchanan JW, Bücheler J. Vertebral scale system to measure canine heart size in radiographs. *J Am Vet Med Assoc.* (1995) 206:194–9.
18. Thomas WP, Gaber CE, Jacobs GJ, Kaplan PM, Lombard CW, Moise NS, et al. Recommendations for standards in transthoracic two-dimensional echocardiography in the dog and cat. Echocardiography committee of the specialty of cardiology, american college of veterinary internal medicine. *J Vet Intern Med.* (1993) 7:247–52. doi: 10.1111/j.1939-1676.1993.tb01015.x
19. Cornell CC, Kittleson MD, Della Torre P, Häggström J, Lombard CW, Pedersen HD, et al. Allometric scaling of M-mode cardiac measurements in normal adult dogs. *J Vet Intern Med.* (2004) 18:311–21. doi: 10.1892/0891-6640(2004)18<311:asomcm>2
20. Rishniw M, Erb HN. Evaluation of four 2-dimensional echocardiographic methods of assessing left atrial size in dogs. *J Vet Intern Med.* (2000) 14:429–35. doi: 10.1892/0891-6640(2000)014<0429:eofemo>2.3.co;2
21. Hansson K, Häggström J, Kvart C, Lord P. Left atrial to aortic root indices using two-dimensional and M- mode echocardiography in cavalier King Charles spaniels with and without left atrial enlargement. *Vet Radiol Ultrasound.* (2002) 43:568–75. doi: 10.1111/j.1740-8261.2002.tb01051.x
22. Rishniw M, Caivano D, Dickson D, Vatne L, Harris J, Matos JN. Two-dimensional echocardiographic left- atrial-to-aortic ratio in healthy adult dogs: a reexamination of reference intervals. *J Vet Cardiol.* (2019) 26:29–38. doi: 10.1016/j.jvc.2019.11.001
23. Reinero C, Visser LC, Kellihan HB, Masseau I, Rozanski E, Clercx C, et al. ACVIM consensus statement guidelines for the diagnosis, classification, treatment, and monitoring of pulmonary hypertension in dogs. *J Vet Intern Med.* (2020) 34:549–73. doi: 10.1111/jvim.15725
24. Ivanova M, Artusi C, Boffa GM, Zaninotto M, Plebani M, HPLC. determination of plasma dimethylarginines: method validation and preliminary clinical application. *Clin Chim Acta.* (2010) 411:1632–163. doi: 10.1016/j.cca.2010.06.001
25. Gervasoni J, Bonelli F, Zuppi C, Zappacosta B, Mordente A, Calvani R, et al. Determination of asymmetric dimethyl arginine in human serum by liquid chromatography-tandem mass spectrometry: clinical application in hypertensive subjects. *Clin Chem Lab Med.* (2011) 49:2109–15. doi: 10.1515/CCLM.2011.691
26. Ohnishi M, Wada A, Tsutamoto T, Fujii M, Matsumoto T, Yamamoto T, et al. Endothelin stimulates an endogenous nitric oxide synthase inhibitor, asymmetric dimethylarginine, in experimental heart failure. *Clin Sci.* (2002) 103:S241–4. doi: 10.1042/CS103S241S
27. Cunningham SM, Rush JE, Freeman LM. Systemic inflammation and endothelial dysfunction in dogs with congestive heart failure. *J Vet Intern Med.* (2012) 26:547–57. doi: 10.1111/j.1939-1676.2012.00923.x
28. Chen Y, Li Y, Zhang P, Traverse JH, Hou M, Xu X, et al. Dimethylarginine dimethylaminohydrolase and endothelial dysfunction in failing hearts. *Am J Physiol Heart Circ Physiol.* (2005) 289:2212–9. doi: 10.1152/ajpheart.00224.2005
29. Vallance P, Leone A, Calver A, Collier J, Moncada S. Accumulation of an endogenous inhibitor of nitric oxide synthesis in chronic renal failure. *Lancet.* (1992) 339:572–5. doi: 10.1016/0140-6736(92)90865-z
30. Ronco C, Haapio M, House AA, Anavekar N, Bellomo R. Cardiorenal syndrome. *J Am Coll Cardiol.* (2008) 52:1527–39. doi: 10.1016/j.jacc.2008.07.051
31. Guglielmini C, Poser H, Pria AD, Drigo M, Mazzotta E, Berlanda M, et al. Red blood cell distribution width in dogs with chronic degenerative valvular disease. *J Am Vet Med Assoc.* (2013) 243:858–62. doi: 10.2460/javma.243.6.858
32. Nicolle AP, Chetboul V, Allerheiligen T, Pouchelon JL, Gouni V, Tessier-Vetzel D, et al. Azotemia and glomerular filtration rate in dogs with chronic valvular disease. *J Vet Intern Med.* (2007) 21:943–9. doi: 10.1892/0891-6640(2007)21[943:aagfri]2.0.co;2
33. Martinelli E, Locatelli C, Bassis S, Crosara S, Paltrinieri S, Scarpa P, et al. Preliminary investigation of cardiovascular–renal disorders in dogs with chronic mitral valve disease. *J Vet Intern Med.* (2016) 30:1612–8. doi: 10.1111/jvim.14524
34. Schwedhelm E, Böger RH. The role of asymmetric and symmetric dimethylarginines in renal disease. *Nat Rev Nephrol.* (2011) 7:275–85. doi: 10.1038/nrneph.2011.31
35. Liu X, Xu X, Shang R, Chen Y. Asymmetric dimethylarginine (ADMA) as an important risk factor for the increased cardiovascular diseases and heart failure in chronic kidney disease. *Nitric oxide.* (2018) 78:113–20. doi: 10.1016/j.niox.2018.06.004
36. Savarese A, Probo M, Locatelli C, Zanzani SA, Gazzonis AL, Papa M, et al. Reliability of symmetric dimethylarginine in dogs with myxomatous mitral valve disease as kidney biomarker. *Open Vet J.* (2018) 8:318–24. doi: 10.4314/ovj.v8i3.11
37. Valente C, Guglielmini C, Domenech O, Contiero B, Zini E, Poser H. Symmetric dimethylarginine in dogs with myxomatous mitral valve disease at various stages of disease severity. *PLoS ONE.* (2020) 15:e0238440. doi: 10.1371/journal.pone.0238440
38. Teerlink T, Nijveldt RJ, de Jong S, van Leeuwen PA. Determination of arginine, asymmetric dimethylarginine, and symmetric dimethylarginine in human plasma and other biological samples

by high-performance liquid chromatography. *Anal Biochem.* (2002) 303:131–7. doi: 10.1006/abio.2001.5575
39. Paulus WJ, Vantrimpont PJ, Shah AM. Acute effects of nitric oxide on left ventricular relaxation and diastolic distensibility in humans. Assessment by bicoronary sodium nitroprusside infusion. *Circulation.* (1994) 89:2070–8. doi: 10.1161/01.cir.89.5.2070
40. Tang WH, Tong W, Shrestha K, Wang Z, Levison BS, Delfraino B, et al. Differential effects of arginine methylation on diastolic dysfunction and disease progression in patients with chronic systolic heart failure. *Eur Heart J.* (2008) 29:2506–251. doi: 10.1093/eurheartj/ehn360
41. Manzano-Fernández S, Januzzi JL, Boronat-García M, Pastor P, Albaladejo-Otòn MD, Garrido IP, et al. Impact of kidney dysfunction on plasma and urinary N-terminal pro-B-type natriuretic peptide in patients with acute heart failure. *Congest Heart Fail.* (2010) 16:214–20. doi: 10.1111/j.1751-7133.2010.00153.x
42. Pelander L, Häggström J, Ley CJ, Ljungvall I. Cardiac troponin I and amino-terminal pro B-Type natriuretic peptide in dogs with stable chronic kidney disease. *J Vet Intern Med.* (2017) 31:805–13. doi: 10.1111/jvim.14703
43. Pouchelon JL, Atkins CE, Bussadori C, Oyama MA, Vaden SL, Bonagura JD, et al. Cardiovascular-renal axis disorders in the domestic dog and cat: a veterinary consensus statement. *J Small Anim Pract.* (2015) 56:537–52. doi: 10.1111/jsap.12387
44. Moesgaard SG, Klostergaard C, Zois NE, Teerlink T, Molin M, Falk T, et al. Flow-mediated vasodilation measurements in Cavalier King Charles Spaniels with increasing severity of myxomatous mitral valve disease. *J Vet Intern Med.* (2012) 26:61–8. doi: 10.1111/j.1939-1676.2011.00846.x
45. Corretti MC, Anderson TJ, Benjamin EJ, Celermajer D, Charbonneau F, Creager MA, et al. Guidelines for the ultrasound assessment of endothelial-dependent flow-mediated vasodilation of the brachial artery: a report of the International Brachial Artery Reactivity Task Force. *J Am Coll Cardiol.* (2002) 39:257–65. doi: 10.1016/s0735-1097(01)01746-6
46. Bank AJ, Lee PC, Kubo SH. Endothelial dysfunction in patients with heart failure: relationship to disease severity. *J Card Fail.* (2000) 6:29–36. doi: 10.1016/s1071-9164(00)00009-9
47. Pedersen HD, Schütt T, Søndergaard R, Qvortrup K, Olsen LH, Kristensen AT. Decreased plasma concentration of nitric oxide metabolites in dogs with untreated mitral regurgitation. *J Vet Intern Med.* (2003) 17:178–18. doi: 10.1111/j.1939-1676.2003.tb02431.x
48. Seljeflot I, Nilsson BB, Westheim AS, Bratseth V, Arnesen H. The L-arginine-asymmetric dimethylarginine ratio is strongly related to the severity of chronic heart failure. No effects of exercise training. *J Card Fail.* (2011) 17:135–42. doi: 10.1016/j.cardfail.2010.09.003
49. Usui M, Matsuoka H, Miyazaki H, Ueda S, Okuda S, Imaizumi T. Increased endogenous nitric oxide synthase inhibitor in patients with congestive heart failure. *Life Sci.* (1998) 62:2425–30. doi: 10.1016/s0024-3205(98)00225-2

Conflict of Interest: The authors declare that the research was conducted in the absence of any commercial or financial relationships that could be construed as a potential conflict of interest.

Publisher's Note: All claims expressed in this article are solely those of the authors and do not necessarily represent those of their affiliated organizations, or those of the publisher, the editors and the reviewers. Any product that may be evaluated in this article, or claim that may be made by its manufacturer, is not guaranteed or endorsed by the publisher.

frontiers in Veterinary Science

ORIGINAL RESEARCH
published: 11 October 2021
doi: 10.3389/fvets.2021.729929

Identification and Characterization of Circulating MicroRNAs as Novel Biomarkers in Dogs With Heart Diseases

*Woong-Bin Ro, Min-Hee Kang, Doo-Won Song, Heyong-Seok Kim, Ga-Won Lee and Hee-Myung Park**

Department of Veterinary Internal Medicine, College of Veterinary Medicine, Konkuk University, Seoul, South Korea

Background: Previous studies in humans have confirmed dysregulations of circulating microRNAs (miRNAs) in patients with various cardiovascular diseases. However, studies on circulating miRNAs in dogs with various heart diseases are limited in number. This study aimed to identify significantly dysregulated circulating miRNAs and characterize them as novel biomarkers in dogs with heart diseases.

Materials and Methods: Circulating levels of 11 miRNAs were investigated in serum samples of 82 dogs (72 with heart diseases and 10 healthy dogs) using quantitative reverse transcription-polymerase chain reaction. The results were correlated to clinical data including echocardiographic results and N-terminal pro B-type natriuretic peptide (NT-proBNP) levels.

Results: Upregulation of cfa-miR-130b was observed in dogs with myxomatous mitral valve degeneration (MMVD) stage B, patent ductus arteriosus, and pulmonic stenosis. In dogs with MMVD stage B, cfa-miR-130b was upregulated and correlated with clinical indices. In receiver operating characteristic (ROC) analysis, cfa-miR-130b accurately distinguished dogs with diseases from healthy dogs. We also observed that cfa-miR-375 and cfa-let-7b were upregulated in dogs with concentric cardiac hypertrophy. The cfa-miR-375 was correlated with concentric hypertrophy indices and was an accurate indicator of concentric hypertrophy in ROC analysis.

Conclusions: The miRNAs identified in this study may be used as novel biomarkers and possible candidates for therapeutic targets in various canine heart diseases.

Keywords: microRNA, circulating, dog, canine, heart disease, cardiac hypertrophy, novel biomarker, therapeutic target

OPEN ACCESS

Edited by:
Zeki Yilmaz,
Faculty of Veterinary Medicine, Turkey

Reviewed by:
Anusak Kijtawornrat,
Chulalongkorn University, Thailand
Yadong Zheng,
Zhejiang Agriculture and Forestry University, China

****Correspondence:***
Hee-Myung Park
parkhee@konkuk.ac.kr

Specialty section:
This article was submitted to Comparative and Clinical Medicine, a section of the journal Frontiers in Veterinary Science

Received: *24 June 2021*
Accepted: *07 September 2021*
Published: *11 October 2021*

Citation:
Ro W-B, Kang M-H, Song D-W, Kim H-S, Lee G-W and Park H-M (2021) Identification and Characterization of Circulating MicroRNAs as Novel Biomarkers in Dogs With Heart Diseases. Front. Vet. Sci. 8:729929. doi: 10.3389/fvets.2021.729929

INTRODUCTION

MicroRNAs (miRNA) are small, non-coding single-stranded RNAs consisting of 19–24 nucleotides, which form complementary pairs with target mRNAs to inhibit and regulate their expression through translation inhibition or degradation (1). Previous studies have shown that miRNAs are involved in cardiac development and play crucial roles in pathological processes of cardiovascular diseases (2, 3). In humans, altered expressions of miRNAs were reported in various heart diseases

(4–6), and circulating miRNAs are increasingly investigated as novel biomarkers in heart diseases because of its stability in peripheral blood (7). In addition, since cardiac hypertrophy is one of the most important pathological response in heart diseases, miRNAs related to cardiac hypertrophy are considered as promising therapeutic targets for various cardiovascular diseases (8, 9).

However, little is known about expressions and role of circulating miRNAs in dogs with naturally occurring heart diseases. To date, several studies have reported dysregulation of circulating miRNAs in dogs with myxomatous mitral valve degeneration (MMVD) (10–13), and no significant change of circulating miRNAs was reported in a previous study in dogs with dilated cardiomyopathy (DCM) (14). However, circulating miRNAs in heart diseases other than MMVD and DCM, such as patent ductus arteriosus (PDA) and pulmonic stenosis (PS), have not been studied in dogs. Moreover, there have been no studies in dogs that have evaluated and characterized the dysregulated miRNAs as novel biomarkers or candidate for therapeutic targets through further analysis with clinical data.

This study aimed to identify significantly dysregulated circulating miRNAs and evaluate them as novel biomarkers in dogs with various heart diseases, and also investigate and characterize circulating miRNAs associated with specific cardiac hypertrophy type.

MATERIALS AND METHODS

Study Design

This study is a retrospective study. In this study, serum levels of 11 candidate miRNAs associated with cardiac hypertrophy in a previous study in dogs (cfa-miR-130b, cfa-miR-346, cfa-let-7b, cfa-miR-30c, cfa-miR-30d, cfa-miR-19b, cfa-miR-425, cfa-let-7g, cfa-miR-151, cfa-miR-375, and cfa-miR-505) were investigated in dogs with various heart diseases using quantitative reverse transcription-polymerase chain reaction (qRT-PCR) (15). The results of qRT-PCR and clinical data including medical records, echocardiographic results, and N-terminal pro B-type natriuretic peptide (NT-proBNP) levels were analyzed together. Bioinformatics analysis was performed on miRNAs with significant results to identify functions and pathways of the target genes.

To investigate different factors related to expression of miRNAs, the dogs included in this study were sub-grouped by two different classifications, classification by disease type and classification by cardiac hypertrophy type, and each classification was analyzed independently (**Figure 1**).

Sample Collection

Stored serum samples of 10 healthy dogs from a previous study were utilized in this study. The previous study was conducted under the supervision of Korea Institute for Advancement of Technology (KIAT) for Regional Specialized Industry Development Program (R&D, R0006046) and approved by KBNP Institutional Animal Care and Use Committee (KBNP 18-01-01). All healthy dogs were confirmed to be healthy in physical examination, complete blood count, serum chemistry, and urinalysis. Stored serum samples of 72 dogs with heart diseases were also retrospectively collected from the Veterinary Medical Teaching Hospital of Konkuk University between July 2014 and January 2019. Informed owner consent was obtained.

The inclusion criteria for dogs with heart diseases were as follows: (1) acquired or congenital heart diseases or (2) cardiac hypertrophy by non-cardiac cause, such as hyperadrenocorticism (HAC). Exclusion criteria were systemic disorders other than HAC. Dogs with heart diseases and concurrent HAC were included in the study because HAC is known to induce cardiac hypertrophy in dogs (16). The diagnoses of MMVD, patent ductus arteriosus (PDA), pulmonic stenosis (PS), and HAC followed the proposed guidelines in dogs, as previously described (17–20). Dogs with MMVD were classified according to the American College of Veterinary Internal Medicine (ACVIM) consensus guidelines as follows (20): stage B included MMVD dogs that had not yet developed clinical signs due to heart failure [stage B1 had no cardiac remodeling or had remodeling not enough to meet the criteria for stage B2, while stage B2 had cardiac enlargement to meet the criteria of murmur intensity $\geq$ 3/6; ratio of left atrial to aortic diameter (LA/Ao) $\geq$ 1.7; normalized value of end-diastolic LV internal dimension (LVIDdN) $\geq$ 1.7; vertebral heart score (VHS) $>$ 10.5], stage C included dogs with present or past clinical signs due to heart failure caused by MMVD, and stage D included dogs with end-stage MMVD that were refractory to standard treatment.

Case Classification

In the classification by disease type, dogs were classified by their diagnosis of heart disease to identify the changes of miRNA in various heart diseases. Dogs with concurrent HAC, those with more than two congenital heart diseases (e.g., tetralogy of Fallot), or those not diagnosed with heart disease were excluded from this classification.

In the classification by cardiac hypertrophy type, dogs were classified into eccentric hypertrophy or concentric hypertrophy groups. Eccentric hypertrophy group was defined as dogs with volume overload heart diseases (e.g., MMVD and PDA) with evidence of increased left ventricle (LV) or left atrium (LA) cavity: LA/Ao $>$ 1.13 or LVIDdN $>$ 1.73 or normalized value of end-systolic LV internal dimension (LVIDsN) $>$ 1.14 (21, 22). Concentric hypertrophy group was defined as dogs with pressure overload heart diseases (e.g., PS and tetralogy of Fallot), or dogs with concentric hypertrophy by non-cardiac cause (e.g., hypertension, HAC) (16, 23, 24) with evidence of increased LV wall thickness: normalized value of end-diastolic interventricular septal thickness (IVSdN) $>$ 0.52 or normalized value of end-diastolic LV free wall thickness (LVPWdN) $>$ 0.53 (22).

Clinical Data and NT-proBNP Measurement

Clinical data including breed, age, sex, body surface area (BSA), heart rate (HR), blood pressure, and cardiovascular medication history were retrieved from medical records. Serum concentration of NT-proBNP was measured by enzyme-linked immunosorbent assay (IDEXX Laboratories Inc., Westbrook, ME, USA).

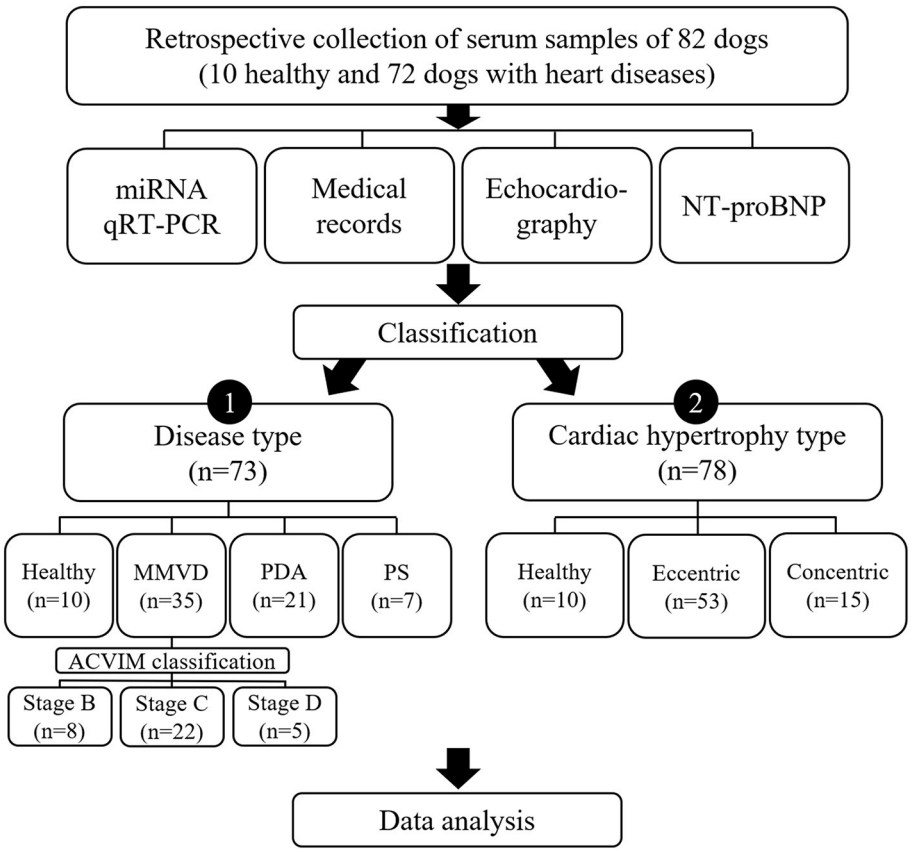

FIGURE 1 | Study design. Results of qRT-PCR on 11 miRNAs, medical records, echocardiography, and NT-proBNP measurement in 82 dogs were analyzed in this study. To investigate different factors related to expression of miRNAs, the dogs included in this study were sub-grouped by two different classifications, classification by disease type and classification by cardiac hypertrophy type, and each classification was analyzed independently. ACVIM, American College of Veterinary Internal Medicine; miRNA, microRNA; MMVD, myxomatous mitral valve degeneration; NT-proBNP, N-terminal pro B-type natriuretic peptide; PDA, patent ductus arteriosus; PS, pulmonic stenosis; qRT-PCR, quantitative reverse transcription-polymerase chain reaction.

Echocardiographic Evaluation

Echocardiographic data were obtained from previous medical records. Examinations were performed on conscious unsedated dogs. Standard two-dimensional, spectral, and tissue Doppler echocardiographic examinations were performed in the left and right lateral recumbency with continuous monitoring of electrocardiography (ECG). A high-quality echocardiograph (EPIQ 7 ultrasound system, Philips Medical Systems, Andover, MA, USA) was used.

M-mode measurements of LV were acquired at the chordae tendineae level from the standard right parasternal short axis view. These measurements included IVSd, LVPWd, LVIDs, LVIDd, and fractional shortening (FS). The LV measurements were normalized using body weight (IVSdN, LVPWdN, LVIDsN, and LVIDdN) according to the results of a previous study on regression analysis (22). LV hypertrophy was evaluated by the normalized measurements based on the 95% prediction interval for normal range (22). Calculations of LV volumes (end-diastolic and end-systolic volumes) and ejection fraction (EF) were derived from Teichholz's formula. The end-diastolic volume index (EDVI) and end-systolic volume index (ESVI) were calculated as the following formula: EDVI or ESVI = (end-diastolic volume or end-systolic volume)/BSA. The LA/Ao was calculated from the right parasternal short axis view by using B-mode. Relative wall thickness (RWT) was calculated as an indicator of LV hypertrophy. RWT was measured as the following formula: RWT = (IVSd + LVPWd)/LVIDd (23). The LV mass (LVM) as well as LV mass index (LVMI) were calculated for additional assessment of LV remodeling. The LVM was calculated as the following formula: LVM (g) = $0.8 \times (1.04 \times (\text{LVIDd} + \text{LVPWd} + \text{IVSd})^3 - (\text{LVIDd})^3) + 0.6$. The LVMI was calculated as the following formula: LVMI = LVM/BSA (23). Trans-mitral flow was obtained by pulsed-wave Doppler from the left apical four-chamber view to measure the peak velocities of early diastolic wave (E) and late diastolic wave (A). The mitral annular motion velocity of the interventricular septum was obtained from the left apical four-chamber view by pulsed wave tissue Doppler. The peak velocity of the mitral annular motion in systole (S′), early diastole (E′), and late diastole (A′) were measured and the E/E' ratio was calculated. Pulmonary hypertension was tentatively diagnosed when peak tricuspid regurgitation flow gradient was confirmed to be 30–50

mmHg (mild), 50–75 mmHg (moderate), or more than 75 mmHg (severe) (25–27).

RNA Preparation

RNA was extracted from serum samples using the miRNeasy Serum/Plasma Kit (Qiagen, Hilden, Germany) according to the manufacturer's protocol. Briefly, 1 ml of QIAzol Lysis Reagent was mixed with 200 μl of serum. Following incubation at room temperature (RT) for 5 min, 3.5 μl of cel-miR-39 working solution (1.6×10^8 copies/μl) was added as an exogenous spike-in to the lysate. RNA precipitation was carried out with 900 μl of 100% ethanol and 200 μl of chloroform in two separate steps. Subsequently, 700 μl of the sample was added to the RNeasy MinElute spin column and was centrifuged at 11,000 *g* and RT for 15 s. This was followed by washing of the columns with 500 μl of RPE buffer and 700 μl of RWT, centrifugation at 11,000 *g* and RT for 15 s, and precipitation of RNA with 500 μl of 80% ethanol, consecutively. RNAs were eluted from the columns with 14 μl of RNase-free water.

RNA quantity and integrity were evaluated with nanodrop 1000 Spectrophotometer (Thermo Scientific, Madison, WI, USA), Quant-IT microRNA assay kit by QuantusTM Fluorometer (Promega, Madison, WI, USA), and Agilent 2100 Bioanalyzer (Agilent Technologies, Palo Alto, CA, USA). No samples were excluded by low RNA quality.

Quantitative Reverse Transcription-Polymerase Chain Reaction of miRNAs

Extracted RNA (5 μl) was used for cDNA synthesis using miScript II RT Kit (Qiagen), miScript Reverse Transcriptase Mix, 5× miScript HiSpec Buffer, and 10 × miScript Nucleics Mix. The primers used in this study are shown in **Supplementary Table 1**. The mixture was incubated for 60 min at 37°C and 5 min at 95°C to inactivate the miScript Reverse transcriptase mix and placed on ice. The cDNA was diluted in RNase-free water (10 μl of cDNA obtained above was mixed with 40 μl of water). The diluted cDNA (5 μl) was preamplified using miScript PreAmp PCR Kit (Qiagen), miScript PreAMP Primer Mix, 5× miScript PreAMP Buffer, HotstarTaq DNA Polymerase, and miScript PreAMP Universal Primer. Cycling conditions were 95°C for 15 min and 12 cycles of 94°C for 30 s and 60°C for 3 min on an ABI 9700 Thermal Cycler (Thermo Fisher Scientific, Waltham, MA, USA). The PreAmp Product was diluted in RNase-free water (25 μl of cDNA mixed with 475 μl of water).

miScript miRNA PCR array enabled and SYBR Green-based real-time PCR analysis was carried out using QuantStudio 12k Flex PCR system (Applied Biosystems, Darmstadt, Germany). In a 20 μl reaction, 1 μl of preamplified product was mixed with 5 μl of 2× QuantiTect SYBR Green PCR Master Mix, 1 μl of 10× miScript Universal Primer, and 1 μl of 10× miScript Primer Assay. qRT-PCR was performed at 95°C for 15 min; 40 cycles of 94°C for 15 s; 55°C for 30 s; and 70°C for 30 s.

The qRT-PCR assays were done in triplicate with exogenous synthetic spiked-in miRNA across all the samples. Mean threshold cycles (Ct) for the synthetic miRNA and all samples were calculated. Seven endogenous and exogenous genes (SNORD61, SNORD68, SNORD95, SNORD72, SNORD96A, RNU6_2, and cel-miR-39) were selected as candidates for reference gene. In order to select the most suitable gene for internal reference, statistical analysis was performed using NormFinder software (28). According to the statistical algorithm, small nuclear RNA SNORD61 was selected as the most stabilized internal reference miRNA to normalize the cDNA levels of the samples. The Ct values obtained for each miRNA were normalized to the respective SNORD61 Ct value to obtain normalized Ct (ΔCt) values, which were subsequently used for statistical analysis. The $\Delta\Delta$Ct method was used to calculate fold change (FC) ($2^{-\Delta\Delta Ct}$) relative to the healthy group.

Statistical Analysis

The ΔCt values were used for statistical analysis. All data were expressed as mean ± standard deviation. Normal distribution assumption was confirmed using the Kolmogorov-Smirnov test and Anderson-Darling test. For normally distributed values, ordinary one-way ANOVA with Dunnett's multiple comparisons test was used for comparison of each group with the healthy group, and Pearson's correlation was performed to evaluate correlation between miRNA levels and clinical variables. For variables without normal distribution, Kruskal–Wallis test with Dunn's multiple comparisons test and Spearman's correlation were used. Receiver-operating characteristic (ROC) curves were performed to evaluate miRNAs as indicators of diseases. In the correlation test and ROC curve analysis, the log2-transformed FC values were used for relative miRNA expressions. Statistical analysis was performed by using the Prism 9 software (GraphPad Software, San Diego, CA, USA) and the SPSS 25.0 software (SPSS, Inc., Chicago, IL). A $p < 0.05$ indicated statistical significance. Unsupervised hierarchical clustering of miRNAs was conducted by MultiExperiment Viewer (MeV) software version 4.9.0.

RESULTS

Classification by Disease Type

The classification by disease type included 73 dogs consisting of 10 healthy dogs, 35 dogs with MMVD, 21 dogs with PDA, and seven dogs with PS. In the MMVD group, one dog was in stage B1, seven dogs were in stage B2, 22 dogs were in stage C, and five dogs were in stage D based on the ACVIM consensus guideline. The clinical characteristics, breed distribution, and cardiovascular medication history of dogs included in this classification are shown in **Table 1** and **Supplementary Tables 2, 3**, respectively.

Circulating miRNA Expression According to Disease Type

The overall expression profiles of 11 miRNAs in each disease group and hierarchical clustering of miRNAs with similar expressions are shown in **Figure 2**.

Compared with the healthy group, cfa-miR-151 was upregulated in the PDA group (FC = 9.00, $p < 0.001$); cfa-miR-30c was upregulated in the PDA group (FC = 6.53, $p = 0.005$) and PS group (FC = 8.88, $p = 0.032$); cfa-miR-130b was

TABLE 1 | Clinical characteristics of dogs included in the classification by disease type.

Variables	Healthy ($n = 10$)	MMVD ($n = 35$)	PDA ($n = 21$)	PS ($n = 7$)	p
Age, years	2.55 ± 0.46	11.72 ± 2.43[a]	3.52 ± 2.40[b]	2.26 ± 1.85[b]	<0.0001
Male, *n* (%)	10 (100)	22 (63)	3 (14)	5 (71)	
BSA, m^2	0.49 ± 0.02	0.26 ± 0.08[a]	0.24 ± 0.11[a]	0.33 ± 0.10	<0.0001
Heart rate, bpm	132 ± 12	151 ± 23	146 ± 19	131 ± 23	0.023
Systolic BP, mmHg	128 ± 8	142 ± 13[a]	134 ± 17	136 ± 11	0.014
Diastolic BP, mmHg	79 ± 4	96 ± 15[a]	87 ± 22	99 ± 10	0.005
Pulmonary hypertension, *n* (%)	0 (0)	25 (71)	3 (14)	7 (100)	
Mild	0	10	0	0	
Moderate	0	9	1	0	
Severe	0	6	2	7	
NTproBNP, pmol/L	439 ± 159	2,939 ± 2,611[a]	2,581 ± 3,379[a]	1,759 ± 1,583	<0.001
Echocardiography					
LA/Ao	1.18 ± 0.07	1.79 ± 0.47[a]	1.51 ± 0.34[a]	1.31 ± 0.05[b]	<0.0001
EDVI	79.63 ± 11.02	96.00 ± 45.93	130.00 ± 96.87	28.30 ± 15.64[b,c]	0.001
ESVI	24.00 ± 4.22	13.92 ± 11.03	45.94 ± 51.63[b]	7.00 ± 7.92[a,c]	<0.001
IVSdN	0.44 ± 0.07	0.45 ± 0.14	0.44 ± 0.13	0.60 ± 0.07[a,b,c]	0.011
LVIDdN	1.58 ± 0.10	1.63 ± 0.43	1.86 ± 0.56	1.02 ± 0.24[b,c]	0.001
LVIDsN	0.94 ± 0.08	0.72 ± 0.25	1.12 ± 0.51[b]	0.54 ± 0.22[a,c]	<0.001
RWT	0.49 ± 0.09	0.52 ± 0.18	0.48 ± 0.22	1.08 ± 0.43[a,b,c]	0.001
Symptomatic, *n*	0	27	21	7	
ACVIM stage, *n*					
B	NA	8	NA	NA	
C	NA	22	NA	NA	
D	NA	5	NA	NA	

ACVIM, American College of Veterinary Internal Medicine; BP, blood pressure; BSA, body surface area; EDVI, end-diastolic volume index; ESVI, end-systolic volume index; IVSdN, normalized value of end-diastolic interventricular septal thickness; LA/Ao, ratio of left atrium to aorta; LVIDdN, normalized value of end-diastolic left ventricular internal dimension; LVIDsN, normalized value of end-systolic left ventricular internal dimension; MMVD, myxomatous mitral valve degeneration; NA, not applicable; NT-proBNP, N-terminal pro B-type natriuretic peptide; PDA, patent ductus arteriosus; PS, pulmonic stenosis; RWT, relative wall thickness.
Continuous variables were expressed as means ± standard deviations.
[a]$p < 0.05$ compared with the Healthy group, [b]$p < 0.05$ compared with the MMVD group, [c]$p < 0.05$ compared with the PDA group in the post-hoc comparison.

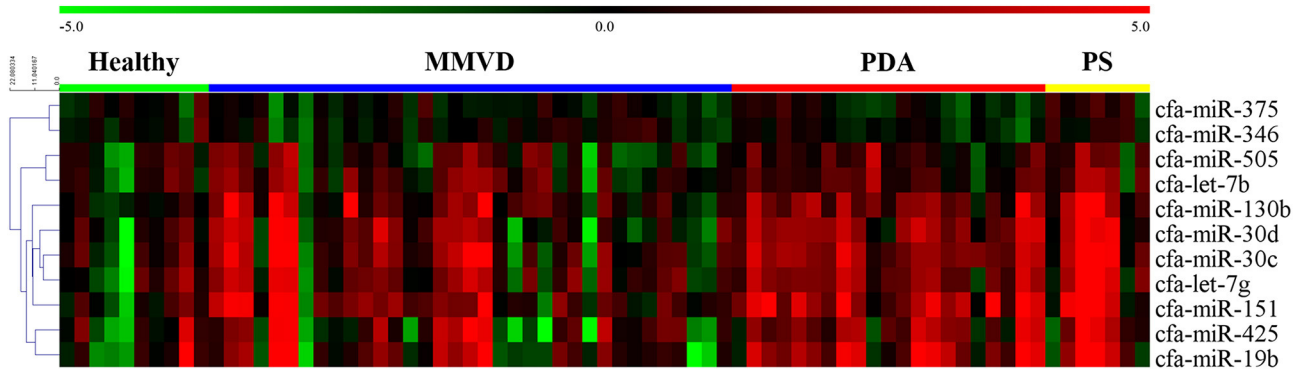

FIGURE 2 | Heat map of overall miRNA expression according to disease type. Sample species shown at the top and the miRNA species shown on the right. Unsupervised average link hierarchical clustering of miRNAs with similar expressions using the Euclidean distance measure. Red indicates relatively high expression of miRNA, and green indicates low expression of miRNA. MMVD, myxomatous mitral valve degeneration; PDA, patent ductus arteriosus; PS, pulmonic stenosis.

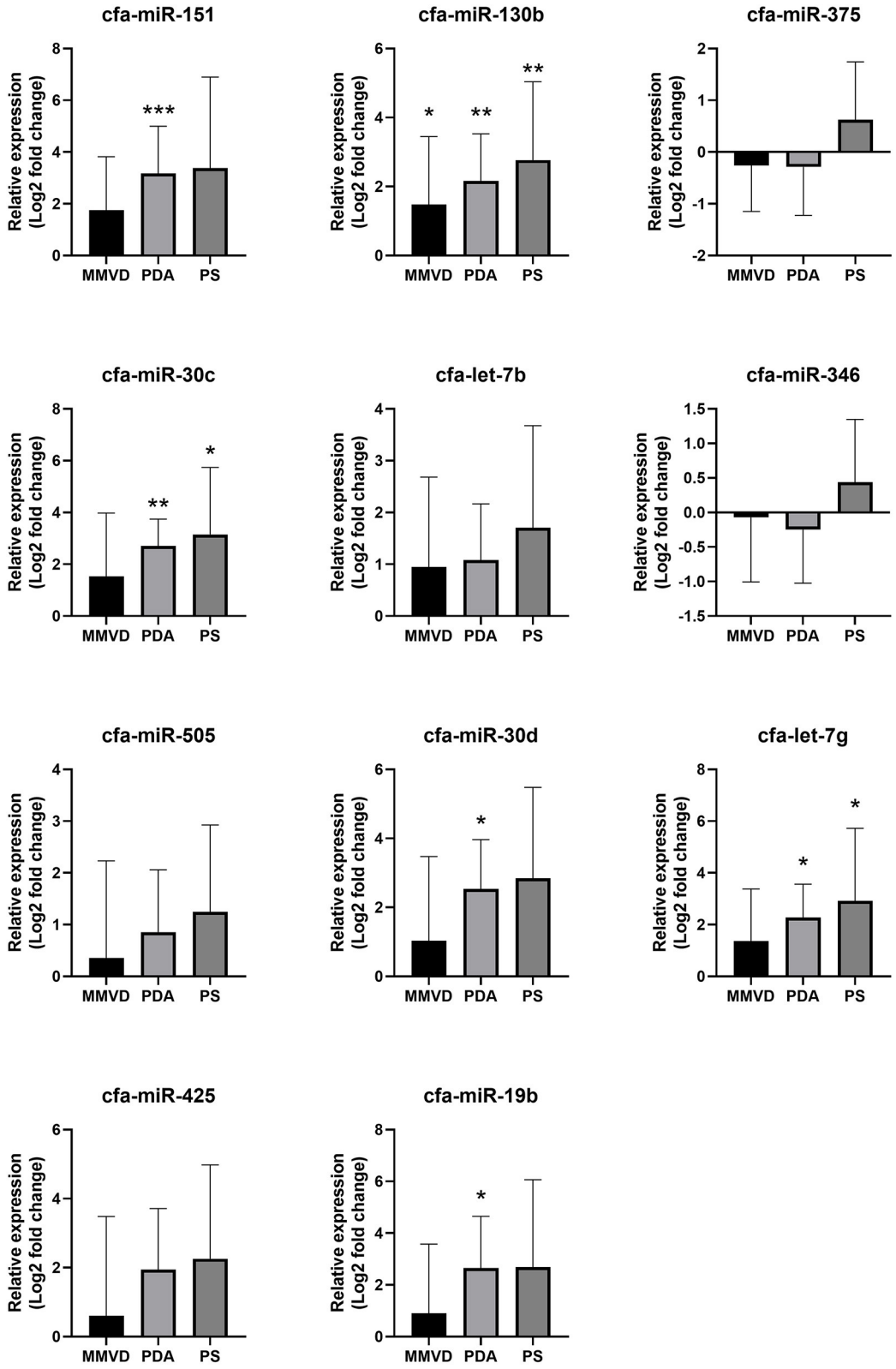

FIGURE 3 | Relative expressions of circulating miRNAs according to disease type. Data were presented as log2 transformed fold change relative to the healthy group (mean and standard deviation). MMVD, myxomatous mitral valve degeneration; PDA, patent ductus arteriosus; PS, pulmonic stenosis. *$p < 0.05$, **$p < 0.01$, ***$p < 0.001$ in Kruskal–Wallis test, p-value adjusted by Dunn's multiple comparison test.

upregulated in the MMVD group (FC = 2.79, $p = 0.047$), PDA group (FC = 4.48, $p = 0.001$), and PS group (FC = 6.81, $p = 0.009$); cfa-let-7g was upregulated in the PDA group (FC = 4.83, $p = 0.001$) and PS group (FC = 7.55, $p = 0.034$); cfa-miR-30d was upregulated in the PDA group (FC = 5.81, $p = 0.014$); and cfa-miR-19b was upregulated in the PDA group (FC = 6.27, $p = 0.018$). The relative expressions of miRNAs in each group compared with the healthy group are shown in **Figure 3**.

Based on these results, cfa-miR-130b was selected as a candidate for promising common biomarker in various heart diseases.

Expression Profile of cfa-miR-130b in MMVD According to the ACVIM Stage

Although cfa-miR-130b was significantly upregulated in all three disease groups, some low expressions of cfa-miR-130b in MMVD group were observed in the heat map analysis (**Figure 2**). Therefore, cfa-miR-130b expression according to ACVIM stage was investigated to determine whether it changes according to the disease progression. As a result, cfa-miR-130b was significantly upregulated in stage B ($n = 8$) while no statistical difference from the healthy group was observed in stage C ($n = 22$) and stage D ($n = 5$) (**Figure 4**).

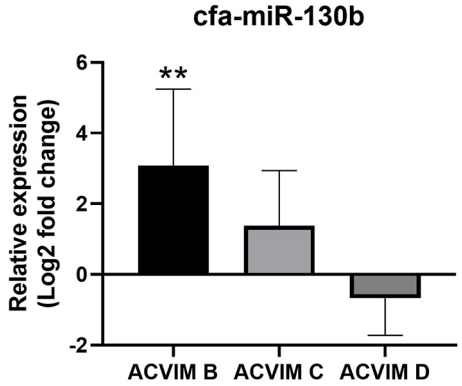

FIGURE 4 | Relative expression of cfa-miR-130b in MMVD group according to ACVIM stage. Data were presented as log2 transformed fold change relative to the healthy group (mean and standard deviation). The cfa-miR-130b was significantly upregulated in stage B while no statistical difference from healthy group was observed in stage C and D. $^{**}p < 0.01$, p-value adjusted by Dunn's multiple comparison test. Only dogs in the MMVD group were assigned the ACVIM stage in this study.

Correlation of cfa-miR-130b Level With Clinical Data

The correlation between cfa-miR-130b level and clinical data including medical records, echocardiographic results, and NT-proBNP level was investigated in groups that showed significant dysregulation of cfa-miR-130b compared with the healthy group (MMVD, MMVD stage B, PDA, and PS groups) (**Supplementary Table 4**). In the MMVD group, mild negative correlation between cfa-miR-130b and age ($r = -0.352$, $p = 0.038$) was observed. In the MMVD stage B group, cfa-miR-130b showed strong positive correlation ($r > 0.7$) with HR ($r = 0.755$, $p = 0.031$), NT-proBNP ($r = 0.786$, $p = 0.021$), and LA/Ao ratio ($r = 0.719$, $p = 0.045$).

ROC Analysis for cfa-miR-130b

To evaluate cfa-miR-130b as a biomarker for various heart diseases, receiver operating characteristic (ROC) curves were analyzed in the groups, which showed significant dysregulation of cfa-miR-130b compared with the healthy group. Accordingly, ROC curves for cfa-miR-130b and NT-proBNP were generated to discriminate dogs with MMVD, MMVD stage B, PDA, and PS from healthy dogs (**Figure 5**). In all groups, cfa-miR-130b showed optimal area under the curve (AUC > 0.7). In MMVD stage B, PDA, and PS groups, cfa-miR-130b was more accurate than NT-proBNP for discriminating dogs with heart diseases from healthy dogs.

Classification by Cardiac Hypertrophy Type

The classification by cardiac hypertrophy type included 78 dogs consisting of 10 healthy dogs, 53 dogs with eccentric cardiac hypertrophy, and 15 dogs with concentric cardiac hypertrophy. The clinical characteristics of dogs included in this classification are shown in **Table 2**.

Circulating miRNA Expression According to Cardiac Hypertrophy Type

The expression heat map and hierarchical clustering of 11 miRNAs according to cardiac hypertrophy type are shown in **Figure 6**.

Compared with the healthy group, cfa-miR-130b was upregulated in both the eccentric hypertrophy group (FC = 3.10, $p = 0.014$) and the concentric hypertrophy group (FC = 5.39, $p = 0.002$), cfa-miR-151 was upregulated in the eccentric hypertrophy group (FC = 4.44, $p = 0.020$), cfa-let-7b was upregulated in the concentric hypertrophy group (FC = 3.27, $p = 0.020$), and cfa-miR-375 was upregulated in the concentric hypertrophy group (FC = 1.90, $p = 0.038$). The relative expressions of miRNAs in each group compared with the healthy group are shown in **Figure 7**.

Based on these results, cfa-miR-375 and cfa-let-7b were selected for further analysis to identify specific association with concentric cardiac hypertrophy.

Correlation of cfa-miR-375 and cfa-let-7b Level With Clinical Data

The correlations between selected miRNAs and various clinical indices were analyzed in dogs with heart diseases (**Supplementary Table 5**). Significant positive correlations were observed between cfa-miR-375 and LV concentric hypertrophy indices, LVPWdN ($r = 0.236$, $p = 0.046$) and RWT ($r = 0.290$, $p = 0.014$).

ROC Analysis for cfa-miR-375 and cfa-let-7b

ROC curves for cfa-miR-375 and cfa-let-7b were generated to evaluate discriminatory power for distinguishing dogs with concentric cardiac hypertrophy from dogs without concentric cardiac hypertrophy, which included healthy and eccentric cardiac hypertrophy groups (**Figure 8**). Both cfa-miR-375 and

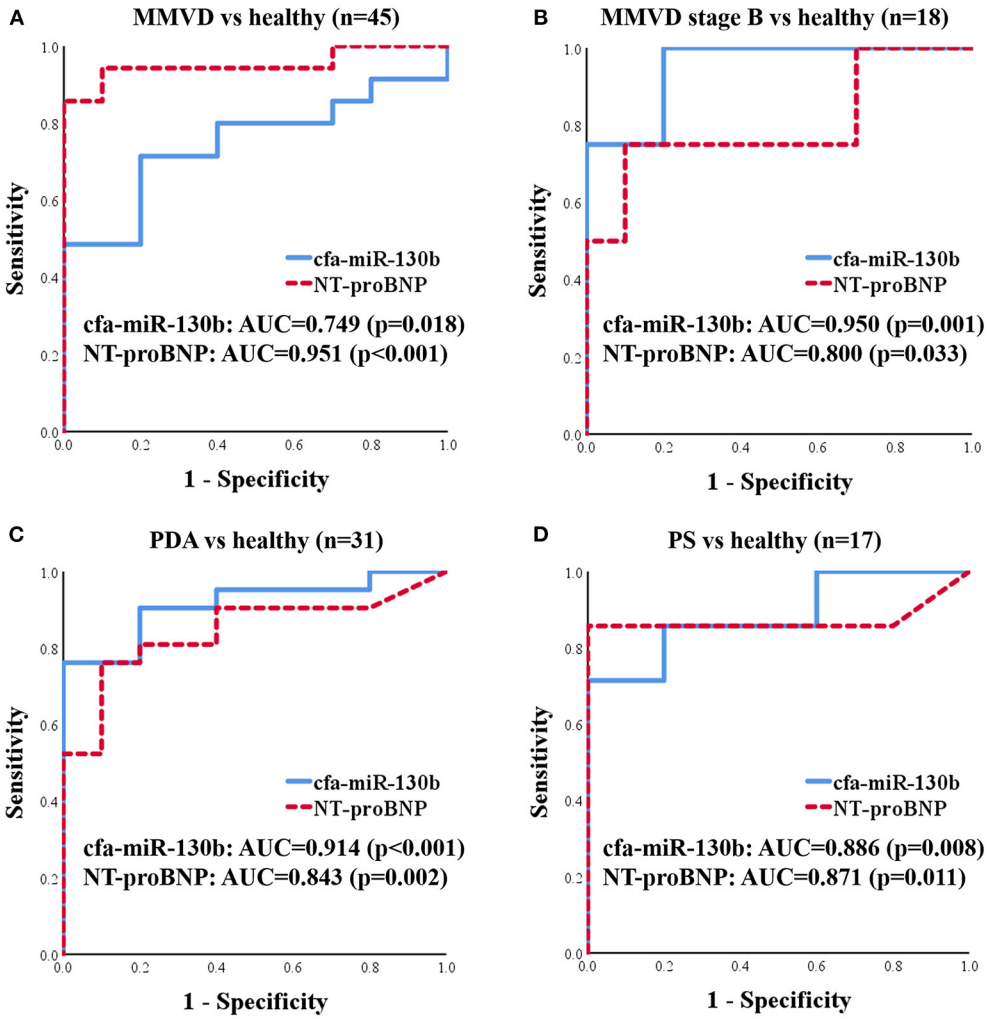

FIGURE 5 | ROC curves for cfa-miR-130b and NT-proBNP to discriminate dogs with MMVD ($n = 35$) **(A)**, MMVD stage B ($n = 8$) **(B)**, PDA ($n = 21$) **(C)**, and PS ($n = 7$) **(D)** from healthy dogs ($n = 10$). AUC, area under curve; MMVD, myxomatous mitral valve degeneration; NT-proBNP, N-terminal pro B-type natriuretic peptide; PDA, patent ductus arteriosus; PS, pulmonic stenosis.

cfa-let-7b were able to distinguish dogs with concentric hypertrophy from dogs without concentric hypertrophy. In particular, cfa-miR-375 was an accurate indicator associated with concentric cardiac hypertrophy (AUC = 0.816).

DISCUSSION

In this study, cfa-miR-130b showed several characteristics as a novel biomarker for various heart diseases. First, upregulation of cfa-miR-130b was detected in MMVD stage B, PDA, and PS groups, which indicates its wide range of applicability as a common biomarker in various heart diseases. Secondly, significant upregulation of cfa-miR-130b was observed in dogs with MMVD stage B, which indicates its suitability as an early diagnostic biomarker. Thirdly, the level of cfa-miR-130b was significantly correlated with HR, NT-proBNP, and LA/Ao in dogs with MMVD stage B, which shows that cfa-miR-130b may be able to represent cardiac status in dogs with early-stage MMVD. Fourthly, in ROC analysis, cfa-miR-130b showed higher sensitivity and specificity than NT-proBNP in MMVD stage B, PDA, and PS groups. However, since no significant changes of cfa-miR-130b level were observed in advanced stages of MMVD (stage C and D), NT-proBNP was a more accurate biomarker than cfa-miR-130b when analyzed in the entire MMVD group. Based on these results, cfa-miR-130b is considered to be a useful biomarker for early detection and monitoring of various heart diseases, and may be more valuable when used in combination with NT-proBNP.

Since cfa-miR-130b was commonly upregulated in various heart diseases regardless of the type of disease or type of cardiac hypertrophy, it may be related to common physiological or pathological changes that can be induced by various heart diseases. In addition, significant upregulation of cfa-miR-130b in MMVD stage B, an early asymptomatic disease

TABLE 2 | Clinical characteristics of dogs included in the classification by cardiac hypertrophy type.

Variables	Healthy ($n = 10$)	Eccentric hypertrophy ($n = 53$)	Concentric hypertrophy ($n = 15$)	p
Age, years	2.55 ± 0.46	9.00 ± 4.54[a]	6.49 ± 5.22	<0.001
Male, *n* (%)	10 (100)	24 (45)	8 (53)	
BSA, m^2	0.49 ± 0.02	0.25 ± 0.09[a]	0.31 ± 0.12[a]	<0.0001
Heart rate, bpm	132 ± 12	149 ± 21	138 ± 33	0.056
Systolic BP, mmHg	128 ± 8	139 ± 14	135 ± 19	0.072
Diastolic BP, mmHg	79 ± 4	92 ± 16[a]	96 ± 16[a]	0.021
Pulmonary hypertension, *n* (%)	0 (0)	26 (49)	12 (80)	
Mild	0	10	2	
Moderate	0	10	0	
Severe	0	6	10	
NTproBNP, pmol/L	439 ± 159	2,836 ± 2,923[a]	2,216 ± 2,555	0.038
Echocardiography				
LA/Ao	1.18 ± 0.07	1.70 ± 0.44[a]	1.30 ± 0.15[b]	<0.0001
EDVI	79.63 ± 11.02	113.30 ± 71.96	34.09 ± 31.21[b]	<0.001
ESVI	24.00 ± 4.22	27.42 ± 36.80	8.63 ± 9.67	0.123
IVSdN	0.44 ± 0.07	0.43 ± 0.14	0.63 ± 0.11[a,b]	<0.0001
LVPWdN	0.43 ± 0.07	0.43 ± 0.10	0.55 ± 0.15[a,b]	<0.001
LVIDdN	1.58 ± 0.10	1.74 ± 0.49	1.13 ± 0.40[a,b]	<0.0001
LVIDsN	0.94 ± 0.08	0.89 ± 0.41	0.57 ± 0.26[a,b]	0.010
RWT	0.49 ± 0.09	0.49 ± 0.17	1.09 ± 0.50[a,b]	<0.0001
Diagnosis	Healthy ($n = 10$)	MMVD ($n = 35$) PDA ($n = 18$)	PS ($n = 7$) MMVD-HAC ($n = 4$) CH-NCC ($n = 3$) TOF ($n = 1$)	

BP, blood pressure; BSA, body surface area; CH-NCC, concentric hypertrophy by non-cardiac cause; EDVI, end-diastolic volume index; ESVI, end-systolic volume index; IVSdN, normalized value of end-diastolic interventricular septal thickness; LA/Ao, ratio of left atrium to aorta; LVIDdN, normalized value of end-diastolic left ventricular internal dimension; LVIDsN, normalized value of end-systolic left ventricular internal dimension; LVPWdN, normalized value of end-diastolic left ventricular free wall thickness; MMVD, myxomatous mitral valve degeneration; MMVD-HAC, myxomatous mitral valve degeneration with concurrent hyperadrenocorticism; NT-proBNP, N-terminal pro B-type natriuretic peptide; PDA, patent ductus arteriosus; PS, pulmonic stenosis; RWT; relative wall thickness; TOF, tetralogy of Fallot.

Continuous variables were expressed as means ± standard deviations.

[a]$p < 0.05$ compared with the Healthy group, [b]$p < 0.05$ compared with the Eccentric hypertrophy group in the post-hoc comparison.

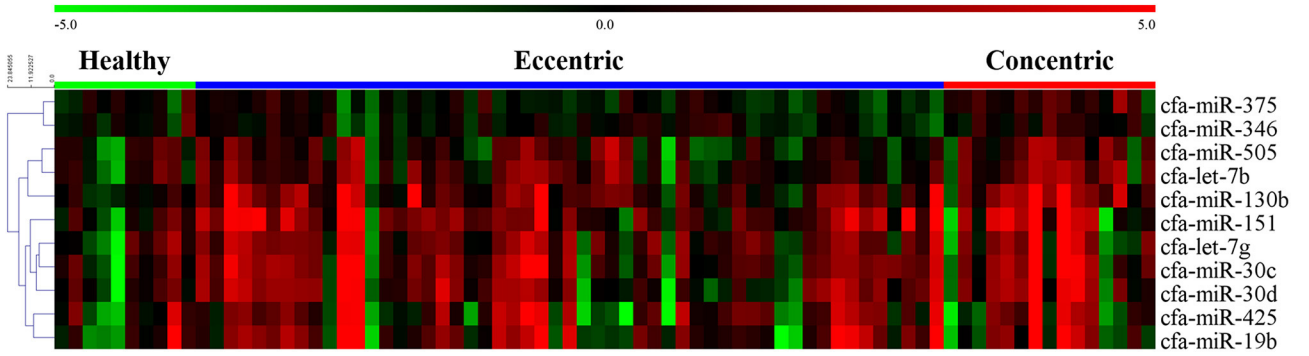

FIGURE 6 | Heat map of overall miRNA expression according to cardiac hypertrophy type. Sample species shown at the top and the miRNA species shown on the right. Unsupervised average link hierarchical clustering of miRNAs with similar expressions using the Euclidean distance measure. Red indicates relatively high expression of miRNA, and green indicates low expression of miRNA.

state, suggests that the expression of cfa-miR-130b may be associated with early gene response to cardiac stress, which is required for subsequent cardiac hypertrophy, fibrosis, and eventual development of heart failure (29). However, the specific target genes and pathways of cfa-miR-130b were not identified in this study, which remains to be clarified in future studies in dogs.

In a previous study in rats with induced myocardial infarction (30), peroxisome proliferator-activated receptor γ (PPAR-γ) was verified to be the target of miR-130b, and expression of miR-130b was associated with NFκB-mediated cardiac inflammation and TGF-β1-mediated cardiac fibrosis. Similar to this result, a prior study in humans reported that circulating miR-130b regulated expression of PPAR-γ and was related to development

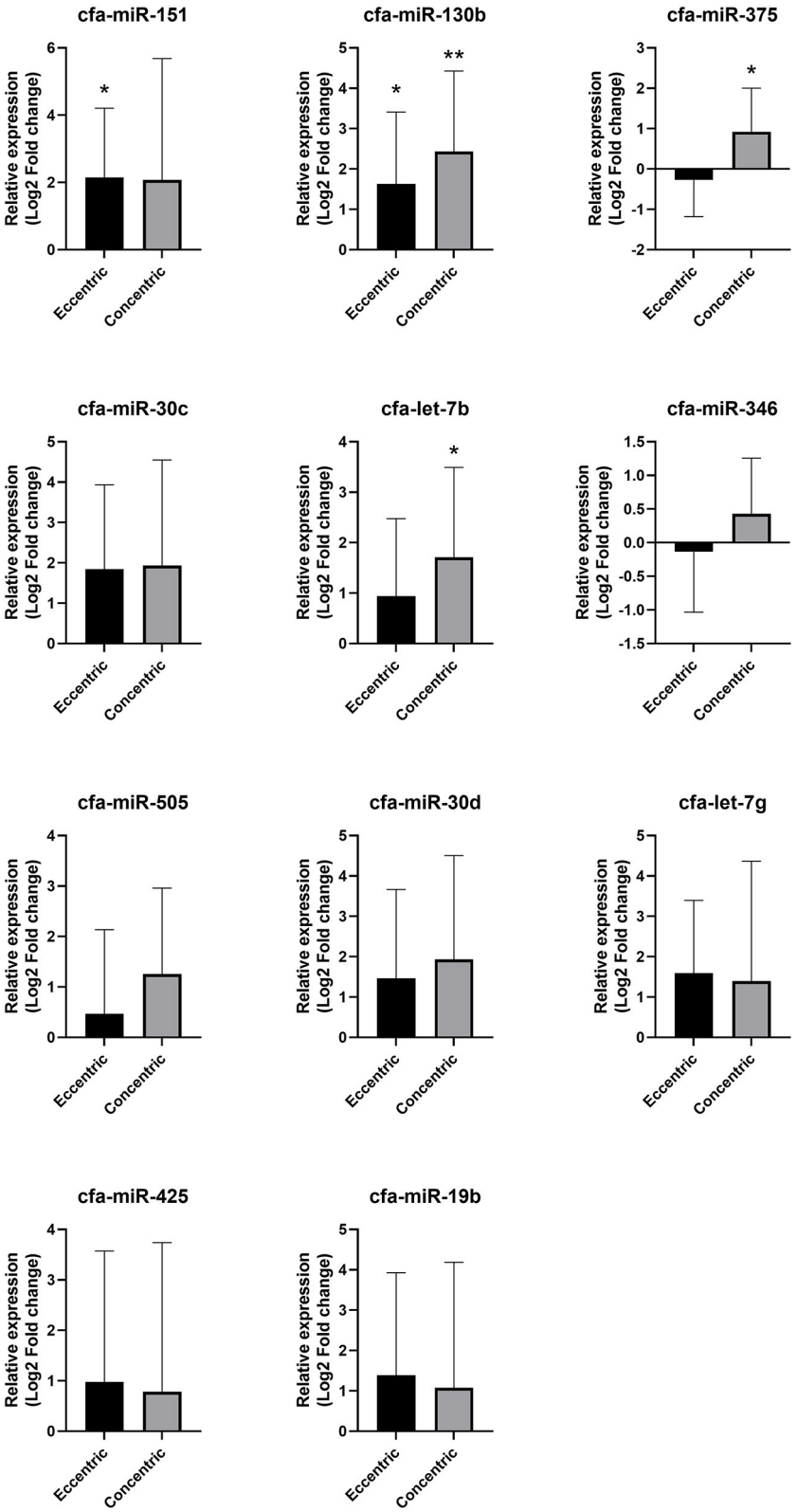

FIGURE 7 | Relative expressions of circulating miRNAs according to cardiac hypertrophy type. Data were presented as log2 transformed fold change relative to the healthy group (mean and standard deviation). $*p < 0.05$, $**p < 0.01$ in one-way ANOVA among healthy, eccentric hypertrophy, and concentric hypertrophy groups, *p*-value adjusted by Dunnett's multiple comparison test.

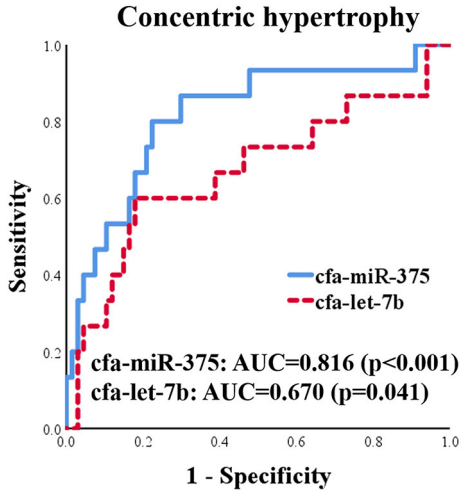

FIGURE 8 | ROC curves for cfa-miR-375 and cfa-let-7b to distinguish dogs with concentric cardiac hypertrophy from dogs without concentric cardiac hypertrophy.

of coronary artery disease (31). Meanwhile, miR-130b was also reported to be upregulated in response to hypoxic condition and regulated target gene DDX6 to increase hypoxia-inducible factor 1-alpha, which is a key factor in protection against myocardial ischemic injury (32, 33). Despite the fact that most miRNAs and their targets are known to be highly conserved across different species, conserved miRNAs can exhibit different expression levels or target regulation in different species (34). In addition, it is known that one miRNA can regulate several target genes and have various functions in different conditions (35). Therefore, the target genes and specific pathways of cfa-miR-130b in heart diseases should be identified and validated in further studies in dogs.

In the present study, the upregulation of cfa-miR-130b level was observed only in the MMVD stage B group. Therefore, cfa-miR-130b is considered not to be a reliable biomarker for the entire MMVD group. Similarly, in a previous study in dogs (13), cfa-miR-30b was significantly dysregulated only in MMVD stage B dogs when compared with healthy dogs, although the reason was not discussed in that study. This was an interesting finding, but the reason for the significant dysregulation only in MMVD stage B group is difficult to clarify in this study. The largely different medication history between stage B vs. stage C and D (**Supplementary Table 3**) may be considered as one of the possible reasons. Further controlled studies are expected to clarify and explain the findings of this study.

Meanwhile, although cfa-miR-375 and cfa-let-7b were significantly associated with concentric cardiac hypertrophy, cfa-let-7b alone seems to be less specific for concentric cardiac hypertrophy than cfa-miR-375. In ROC and correlation analysis, the specificity of cfa-let-7b was lower than that of cfa-miR-375, and no correlation was observed between cfa-let-7b and concentric cardiac hypertrophy indices. In addition, in a previous study (11), cfa-let-7b was upregulated in dogs with MMVD. Therefore, based on the results of the previous and present studies (11), cfa-let-7b is thought to be associated with both eccentric and concentric cardiac hypertrophy in dogs. The reason why significant dysregulation of cfa-let-7b was not observed in MMVD or eccentric hypertrophy group in the present study may be the relatively low sensitivity of cfa-let-7b in heart diseases or the insufficient number of samples in this study.

A previous study in mice reported that let-7b was upregulated by thioredoxin 1 (Trx1) in angiotensin-II (AT-II)-induced cardiac hypertrophy and inhibited AT-II by targeting cyclin D2 (36). The upregulation of Trx1 and downregulation of angiotensinogen, which is a precursor of AT-II, were also reported in mitral valves of MMVD dogs, suggesting that there may be a similar pathway involving cfa-let-7b (11). However, the direct target genes and pathways of cfa-let-7b are not identified in dogs yet.

In contrast to cfa-let-7b, cfa-miR-375 seems to be more specifically related to concentric cardiac hypertrophy based on the results of ROC and correlation analysis in this study. In previous human studies, miR-375 was upregulated in patients with concentric cardiac hypertrophy (37) and downregulated in patients with eccentric cardiac hypertrophy (heart failure with reduced ejection fraction) (38). These expression patterns of miR-375 from human studies are similar to those observed in cfa-miR-375 in this study, although no statistical significance was observed in the eccentric cardiac hypertrophy group. Further research is required to verify the expression and specific role of cfa-miR-375 in dogs with different types of cardiac hypertrophy.

In previous studies in mice (39, 40), inhibition of miR-375 by interleukin-10 administration or anti-miR-375 therapy enhanced cardiac recovery and reduced inflammatory response after myocardial infarction by activation of the PDK-1-AKT pathway. In another study (41), upregulation of miR-375 in P19 cell resulted in inhibition of cell proliferation, increased cell apoptosis, and disruption of cardiomyocyte differentiation through Notch signaling pathway. On the other hand, a contrasting result was also reported in a prior study in humans (42), in which downregulation of miR-375 was observed in myocardial infarction patients and overexpression of miR-375 by mimic-miR-375 prevented hypoxia/reoxygenation-induced cardiac injury by upregulating Nemo-like kinase (NLK) gene.

This study has several limitations. First, the age, breed, sex, and BSA of the healthy dogs could not be matched with the dogs with heart diseases. In this study, only young male beagle dogs were included in the healthy group because those samples were the only available samples that were definitely confirmed to be healthy in our sample archive. Since miRNAs are known to be associated with various physical conditions and diseases (43), and very little is known in dogs, we tried to use samples from definitely healthy dogs without any disease. In previous studies in humans (44–48), several miRNAs have been reported to be associated with age, sex, and racial difference. However, the relationship between those factors and the miRNAs investigated in this study has not been identified in dogs. In this study, negative correlation between age and cfa-miR-130b was observed in the MMVD group. This finding could not be confirmed in healthy dogs because only young dogs were included in the

healthy group. In addition, it is difficult to elucidate the cause of this correlation because factors that could affect miRNA expression in the MMVD group such as severity of disease and use of medication were not controlled in this study. Regarding the sex, there were no significant differences between male and female in MMVD stage B, PDA, and PS groups in which cfa-miR-130b showed a significant upregulation (data not shown). However, this also should be investigated in healthy dogs. Therefore, further controlled studies are needed to clarify the association between miRNA expression and age, as well as breed, sex, and BSA.

Secondly, since only one dog with MMVD was in stage B1, the data between stage B1 and B2 could not be compared properly. If the miRNA expressions can differentiate dogs with stage B2 from B1, it will be beneficial for both early diagnosis and treatment of MMVD in dogs. In addition, seven dogs were included in the PS group in this study, which was a relatively small number compared with other groups. Further large-scale studies are expected in the future. Moreover, in order to verify the target genes and potential mechanisms of the miRNAs identified in this study, and to apply them as therapeutic agents, further follow-up studies with miRNA mimics or miRNA inhibitors (anti-miRs) are necessary in dogs with heart diseases (6).

To our knowledge, this is the first study to investigate circulating miRNAs in dogs with various heart diseases to identify and characterize them as novel biomarkers and possible therapeutic targets, according to the disease type and cardiac hypertrophy type. The miRNAs identified in this study may be used as promising novel biomarkers and candidates for therapeutic targets in various canine heart diseases. The results of this study are expected to provide basis for further studies and accelerate the application of new diagnostic and therapeutic approaches for dogs with heart diseases.

DATA AVAILABILITY STATEMENT

The original contributions presented in the study are included in the article/**Supplementary Material**, further inquiries can be directed to the corresponding author.

ETHICS STATEMENT

Ethical review and approval was not required for the animal study because informed consent was obtained from the owner for sample collection of client-owned dog. Stored serum samples of healthy dogs from a previous study were utilized in this study. The previous study was conducted under the supervision of Korea Institute for Advancement of Technology (KIAT) for Regional Specialized Industry Development Program (R&D, R0006046) and approved by KBNP Institutional Animal Care and Use Committee (KBNP 18-01-01).

AUTHOR CONTRIBUTIONS

W-BR, M-HK, and H-MP conceived and designed the study. W-BR, D-WS, H-SK, and G-WL participated in sample and data collection. W-BR and D-WS curated the data and carried out the research. W-BR, M-HK, D-WS, and H-MP analyzed the data. W-BR wrote the manuscript. All authors have read and approved the final manuscript.

ACKNOWLEDGMENTS

This manuscript included a portion of a dissertation submitted by W-BR to the Department of Veterinary Medicine and the Graduate School of Konkuk University in partial fulfillment of the requirements for the degree of Doctor of Philosophy Veterinary Medicine. The authors thank the members of our internal medicine laboratory for their support in collection of serum samples used in this study.

SUPPLEMENTARY MATERIAL

The Supplementary Material for this article can be found online at: https://www.frontiersin.org/articles/10.3389/fvets.2021.729929/full#supplementary-material

REFERENCES

1. Bartel DP. MicroRNAs: genomics, biogenesis, mechanism, and function. *Cell.* (2004) 116:281–97. doi: 10.1016/S0092-8674(04)00045-5
2. Cai B, Pan Z, Lu Y. The roles of microRNAs in heart diseases: a novel important regulator. *Curr Med Chem.* (2010) 17:407–11. doi: 10.2174/092986710790226129
3. Thum T, Catalucci D, Bauersachs J. MicroRNAs: novel regulators in cardiac development and disease. *Cardiovasc Res.* (2008) 79:562–70. doi: 10.1093/cvr/cvn137
4. Oury C, Servais L, Bouznad N, Hego A, Nchimi A, Lancellotti P. MicroRNAs in valvular heart diseases: potential role as markers and actors of valvular and cardiac remodeling. *Int J Mol Sci.* (2016) 17:1120. doi: 10.3390/ijms17071120
5. Ikeda S, Kong SW, Lu J, Bisping E, Zhang H, Allen PD, et al. Altered microRNA expression in human heart disease. *Physiol Genomics.* (2007) 31:367–73. doi: 10.1152/physiolgenomics.00144.2007
6. Zhou S-s, Jin J-p, Wang J-q, Zhang Z-g, Freedman JH, Zheng Y, et al. miRNAS in cardiovascular diseases: potential biomarkers, therapeutic targets and challenges. *Acta Pharmacol Sin.* (2018) 39:1073. doi: 10.1038/aps.2018.30
7. Xu J, Zhao J, Evan G, Xiao C, Cheng Y, Xiao J. Circulating microRNAs: novel biomarkers for cardiovascular diseases. *J Mol Med.* (2012) 90:865–75. doi: 10.1007/s00109-011-0840-5
8. Chen C, Ponnusamy M, Liu C, Gao J, Wang K, Li P. MicroRNA as a therapeutic target in cardiac remodeling. *BioMed Res Int.* (2017) 2017. doi: 10.1155/2017/1278436
9. Cheng Y, Ji R, Yue J, Yang J, Liu X, Chen H, et al. MicroRNAs are aberrantly expressed in hypertrophic heart: do they play a role in cardiac hypertrophy? *Am J Pathol.* (2007) 170:1831–40. doi: 10.2353/ajpath.2007.061170
10. Yang VK, Loughran KA, Meola DM, Juhr CM, Thane KE, Davis AM, et al. Circulating exosome microRNA associated with heart failure secondary to myxomatous mitral valve disease in a naturally occurring canine model. *J Extracellular Vesicles.* (2017) 6:1350088. doi: 10.1080/20013078.2017.1350088
11. Li Q, Freeman L, Rush J, Laflamme D. Expression profiling of circulating microRNAs in canine myxomatous mitral valve disease. *Int J Mol Sci.* (2015) 16:14098–108. doi: 10.3390/ijms160614098
12. Jung S, Bohan A. Genome-wide sequencing and quantification of circulating microRNAs for dogs with congestive heart failure secondary to myxomatous mitral valve degeneration. *Am J Vet Res.* (2018) 79:163–9. doi: 10.2460/ajvr.79.2.163

13. Hulanicka M, Garncarz M, Parzeniecka-Jaworska M, Jank M. Plasma miRNAs as potential biomarkers of chronic degenerative valvular disease in Dachshunds. *BMC Vet Res.* (2014) 10:205. doi: 10.1186/s12917-014-0205-8
14. Steudemann C, Bauersachs S, Weber K, Wess G. Detection and comparison of microRNA expression in the serum of Doberman Pinschers with dilated cardiomyopathy and healthy controls. *BMC Vet Res.* (2013) 9:12. doi: 10.1186/1746-6148-9-12
15. Ro W-b. Identification and characterization of circulating microRNAs as novel biomarkers and therapeutic targets in dogs with heart diseases [Dissertation for Degree of Doctor]: Konkuk University (2020).
16. Takano H, Kokubu A, Sugimoto K, Sunahara H, Aoki T, Fijii Y. Left ventricular structural and functional abnormalities in dogs with hyperadrenocorticism. *J Vet Cardiol.* (2015) 17:173–81. doi: 10.1016/j.jvc.2015.07.002
17. Bussadori C, Amberger C, Le Bobinnec G, Lombard CW. Guidelines for the echocardiographic studies of suspected subaortic and pulmonic stenosis. *J Vet Cardiol.* (2000) 2:15–22. doi: 10.1016/s1760-2734(06)70007-8
18. Schneider M, Hildebrandt N, Schweigl T, Wehner M. Transthoracic echocardiographic measurement of patent ductus arteriosus in dogs. *J Vet Intern Med.* (2007) 21:251–7. doi: 10.1111/j.1939-1676.2007.tb02957.x
19. Peterson ME. Diagnosis of hyperadrenocorticism in dogs. *Clin Tech Small Anim Pract.* (2007) 22:2–11. doi: 10.1053/j.ctsap.2007.02.007
20. Keene BW, Atkins CE, Bonagura JD, Fox PR, Häggström J, Fuentes VL, et al. ACVIM consensus guidelines for the diagnosis and treatment of myxomatous mitral valve disease in dogs. *J Vet Intern Med.* (2019) 33:1127–40. doi: 10.1111/jvim.15488
21. Chetboul V, Sampedrano CC, Concordet D, Tissier R, Lamour T, Ginesta J, et al. Use of quantitative two-dimensional color tissue Doppler imaging for assessment of left ventricular radial and longitudinal myocardial velocities in dogs. *Am J Vet Res.* (2005) 66:953–61. doi: 10.2460/ajvr.2005.66.953
22. Cornell CC, Kittleson MD, Torre PD, Häggström J, Lombard CW, Pedersen HD, et al. Allometric scaling of M-mode cardiac measurements in normal adult dogs. *J Vet Intern Med.* (2004) 18:311–21. doi: 10.1111/j.1939-1676.2004.tb02551.x
23. Foppa M, Duncan BB, Rohde LE. Echocardiography-based left ventricular mass estimation. How should we define hypertrophy? *Cardiovasc Ultrasound.* (2005) 3:17. doi: 10.1186/1476-7120-3-17
24. Mehlman E, Bright J, Jeckel K, Porsche C, Veeramachaneni D, Frye M. Echocardiographic evidence of left ventricular hypertrophy in obese dogs. *J Vet Intern Med.* (2013) 27:62–8. doi: 10.1111/jvim.12018
25. Kellum HB, Stepien RL. Sildenafil citrate therapy in 22 dogs with pulmonary hypertension. *J Vet Intern Med.* (2007) 21:1258–64. doi: 10.1111/j.1939-1676.2007.tb01947.x
26. Johnson L, Boon J, Orton EC. Clinical characteristics of 53 dogs with Doppler-derived evidence of pulmonary hypertension: 1992–1996. *J Vet Intern Med.* (1999) 13:440–7. doi: 10.1111/j.1939-1676.1999.tb01461.x
27. Schober KE, Baade H. Doppler echocardiographic prediction of pulmonary hypertension in West Highland white terriers with chronic pulmonary disease. *J Vet Intern Med.* (2006) 20:912–20. doi: 10.1111/j.1939-1676.2006.tb01805.x
28. Andersen CL, Jensen JL, Ørntoft TF. Normalization of real-time quantitative reverse transcription-PCR data: a model-based variance estimation approach to identify genes suited for normalization, applied to bladder and colon cancer data sets. *Cancer Res.* (2004) 64:5245–50. doi: 10.1158/0008-5472.CAN-04-0496
29. Van Rooij E, Sutherland LB Qi X, Richardson JA, Hill J, Olson EN. Control of stress-dependent cardiac growth and gene expression by a microRNA. *Science.* (2007) 316:575–9. doi: 10.1126/science.1139089
30. Chu X, Wang Y, Pang L, Huang J, Sun X, Chen X. miR-130 aggravates acute myocardial infarction-induced myocardial injury by targeting PPAR-γ. *J Cell Biochem.* (2018) 119:7235–44. doi: 10.1002/jcb.26903
31. Yuan Y, Peng W, Liu Y, Xu Z. Circulating miR-130 and its target PPAR-γ may be potential biomarkers in patients of coronary artery disease with type 2 diabetes mellitus. *Molecular genetics & genomic medicine.* (2019) 7:e909. doi: 10.1002/mgg3.909
32. Saito K, Kondo E, Matsushita M. MicroRNA 130 family regulates the hypoxia response signal through the P-body protein DDX6. *Nucleic Acids Res.* (2011) 39:6086–99. doi: 10.1093/nar/gkr194
33. Eckle T, Köhler D, Lehmann R, El Kasmi KC, Eltzschig HK. Hypoxia-inducible factor-1 is central to cardioprotection. *Circulation.* (2008) 118:166–75. doi: 10.1161/CIRCULATIONAHA.107.758516
34. Ha M, Pang M, Agarwal V, Chen ZJ. Interspecies regulation of microRNAs and their targets. Biochimica et Biophysica Acta (BBA)-Gene Regulatory. *Mechanisms.* (2008) 1779:735–42. doi: 10.1016/j.bbagrm.2008.03.004
35. Hashimoto Y, Akiyama Y, Yuasa Y. Multiple-to-multiple relationships between microRNAs and target genes in gastric cancer. *PLoS ONE.* (2013) 8:e62589. doi: 10.1371/journal.pone.0062589
36. Yang Y, Ago T, Zhai P, Abdellatif M, Sadoshima J. Thioredoxin 1 negatively regulates angiotensin II–induced cardiac hypertrophy through upregulation of miR-98/let-7. *Circ Res.* (2011) 108:305–13. doi: 10.1161/CIRCRESAHA.110.228437
37. Akat KM, Moore-McGriff DV, Morozov P, Brown M, Gogakos T, Da Rosa JC, et al. Comparative RNA-sequencing analysis of myocardial and circulating small RNAs in human heart failure and their utility as biomarkers. *Proc Nat Acad Sci.* (2014) 111:11151–6. doi: 10.1073/pnas.1401724111
38. Watson CJ, Gupta SK, O'Connell E, Thum S, Glezeva N, Fendrich J, et al. MicroRNA signatures differentiate preserved from reduced ejection fraction heart failure. *Eur J Heart Fail.* (2015) 17:405–15. doi: 10.1002/ejhf.244
39. Garikipati VNS, Krishnamurthy P, Verma SK, Khan M, Abramova T, Mackie AR, et al. Negative regulation of miR-375 by interleukin-10 enhances bone marrow-derived progenitor cell-mediated myocardial repair and function after myocardial infarction. *Stem Cells.* (2015) 33:3519–29. doi: 10.1002/stem.2121
40. Garikipati VN, Verma SK, Jolardarashi D, Cheng Z, Ibetti J, Cimini M, et al. Therapeutic inhibition of miR-375 attenuates post-myocardial infarction inflammatory response and left ventricular dysfunction via PDK-1-AKT signalling axis. *Cardiovasc Res.* (2017) 113:938–49. doi: 10.1093/cvr/cvx052
41. Wang L, Song G, Liu M, Chen B, Chen Y, Shen Y, et al. MicroRNA-375 overexpression influences P19 cell proliferation, apoptosis and differentiation through the Notch signaling pathway. *Int J Mol Med.* (2016) 37:47–55. doi: 10.3892/ijmm.2015.2399
42. Sheikh A, Sayed M. Overexpression of miR-375 protects cardiomyocyte injury following hypoxic-reoxygenation injury. *Oxid Med Cell Longev.* (2020) 2020. doi: 10.1155/2020/7164069
43. Ardekani AM, Naeini MM. The role of microRNAs in human diseases. *Avicenna J Med Biotechnol.* (2010) 2:161.
44. Florijn BW, Bijkerk R, van der Veer EP, van Zonneveld AJ. Gender and cardiovascular disease: are sex-biased microRNA networks a driving force behind heart failure with preserved ejection fraction in women? *Cardiovasc Res.* (2018) 114:210–25. doi: 10.1093/cvr/cvx223
45. Sharma S, Eghbali M. Influence of sex differences on microRNA gene regulation in disease. *Biol Sex Differ.* (2014) 5:1–8. doi: 10.1186/2042-6410-5-3
46. Hooten NN, Fitzpatrick M. Wood 3rd WH, De S, Ejiogu N, Zhang Y, et al. Age-related changes in microRNA levels in serum. *Aging (Albany N Y).* (2013) 5:725. doi: 10.18632/aging.100603
47. Hooten NN, Abdelmohsen K, Gorospe M, Ejiogu N, Zonderman AB, Evans MK. microRNA expression patterns reveal differential expression of target genes with age. *PLoS ONE.* (2010) 5:e10724. doi: 10.1371/journal.pone.0010724
48. Dluzen DF, Hooten NN, Zhang Y, Kim Y, Glover FE, Tajuddin SM, et al. Racial differences in microRNA and gene expression in hypertensive women. *Sci Rep.* (2016) 6:1–14. doi: 10.1038/srep35815

Conflict of Interest: The authors declare that the research was conducted in the absence of any commercial or financial relationships that could be construed as a potential conflict of interest.

Publisher's Note: All claims expressed in this article are solely those of the authors and do not necessarily represent those of their affiliated organizations, or those of the publisher, the editors and the reviewers. Any product that may be evaluated in this article, or claim that may be made by its manufacturer, is not guaranteed or endorsed by the publisher.

frontiers in Veterinary Science

ORIGINAL RESEARCH
published: 08 November 2021
doi: 10.3389/fvets.2021.771408

Analysis of the Serum Peptidomics Profile for Cats With Sarcomeric Gene Mutation and Hypertrophic Cardiomyopathy

*Pratch Sukumolanan[1], Narumon Phanakrop[2], Siriwan Thaisakun[3], Sittiruk Roytrakul[3] and Soontaree Petchdee[4]**

[1] Veterinary Clinical Studies Program, Faculty of Veterinary Medicine, Graduated School, Kasetsart University, Nakorn Pathom, Thailand, [2] Functional Ingredients and Food Innovation Research Group, National Center for Genetic Engineering and Biotechnology, National Science and Technology Development Agency, Pathum Thani, Thailand, [3] Proteomics Research Laboratory, National Center for Genetic Engineering and Biotechnology, National Science and Technology Development Agency, Pathum Thani, Thailand, [4] Department of Large Animal and Wildlife Clinical Sciences, Faculty of Veterinary Medicine, Kasetsart University, Nakorn Pathom, Thailand

OPEN ACCESS

Edited by:
Zeki Yilmaz,
Faculty of Veterinary Medicine, Turkey

Reviewed by:
Meric Kocaturk,
Uludag University, Turkey
Carlos Fernando Agudelo,
University of Veterinary and Pharmaceutical Sciences Brno, Czechia

***Correspondence:**
Soontaree Petchdee
fvetstr@ku.ac.th

Specialty section:
This article was submitted to Comparative and Clinical Medicine, a section of the journal Frontiers in Veterinary Science

Received: 06 September 2021
Accepted: 11 October 2021
Published: 08 November 2021

Citation:
Sukumolanan P, Phanakrop N, Thaisakun S, Roytrakul S and Petchdee S (2021) Analysis of the Serum Peptidomics Profile for Cats With Sarcomeric Gene Mutation and Hypertrophic Cardiomyopathy. Front. Vet. Sci. 8:771408. doi: 10.3389/fvets.2021.771408

Background: Hypertrophic cardiomyopathy (HCM) has a complex phenotype that is partly explained by genetic variants related to this disease. The serum peptidome profile is a promising approach to define clinically relevant biomarkers. This study aimed to classify peptide patterns in serum samples between cats with sarcomeric gene mutations and normal cats.

Materials and Methods: In the total serum samples from 31 cats, several essential proteins were identified by peptidomics analysis. The 5,946 peptides were differentially expressed in cats with sarcomeric gene mutations compared with cats without mutations.

Results: Our results demonstrated characteristic protein expression in control cats, Maine Coon cats, and Maine Coon cats with gene mutations. In cats with gene mutations, peptide expression profiling showed an association with three peptides, Cytochrome 3a132 (CYP3A132), forkhead box O1 (FOXO1), and ArfGAP, with GTPase domains, ankyrin repeats, and PH domain 2 (AGAP2).

Discussion: The serum peptidome of cats with mutations might provide supporting evidence for the dysregulation of metabolic and structural proteins. Genetic and peptidomics investigations may help elucidate the phenotypic variability of HCM and treatment targets to reduce morbidity and mortality of HCM in cats.

Keywords: feline, hypertrophic cardiomyopathy, myocardial disease, peptidomics analysis, echocardiography

INTRODUCTION

Myocardial disease is the most common genetic heart problem in cats, especially in Maine Coon, Ragdoll, and Persian cats. Hypertrophic cardiomyopathy (HCM) is one of the most common genetic heart problems in cats. HCM is a myocardial disease caused by dominant mutations in genes encoding cardiac sarcomere protein. Many gene polymorphisms, such as MYBPC3-A31P

and A74T, have been detected in Maine Coon cats or cats crossbred with Maine Coon cats (1–4). HCM can be characterized by an increase in left ventricular myocardial mass. However, other causes of cardiac hypertrophy, such as hyperthyroidism, systemic hypertension, and aortic stenosis, are the primary differential diagnosis for this disease (5–7).

The complex and dynamic pathophysiological mechanisms surrounding cardiac hypertrophy have focused on many investigations seeking therapeutic strategies (8). Additional studies may involve understanding the risk factors for cardiovascular disease. Many studies have investigated the pathway that plays critical roles in mediating cardiac hypertrophy (9–12). The mechanisms for the effect of testosterone on muscle hypertrophy are not entirely understood. It is known that free testosterone concentrations increase in response to cardiac muscle hypertrophy (13). Previous studies have suggested that testosterone-induced cardiomyocyte hypertrophy is accompanied by increased glucose uptake and glycolysis. In addition, testosterone increased AMPK phosphorylation, which is the crucial pathway in the development of eccentric hypertrophy (14).

Peptide analysis is being increasingly used to identify the protein changes accompanying changes in clinical appearance. Two-dimensional gel electrophoresis coupled with mass spectrometry offers a key advantage of profiling proteins in biological samples. Alterations in the proteome profile determined using two-dimensional gel electrophoresis in conjunction with matrix-assisted laser desorption ionization-time of flight (MALDI-TOF) mass spectrometry may explain the mechanistic pathways and identify novel potential biomarkers for the diagnosis and prognosis of HCM in cats. The proteomic data may contribute to understanding the pathogenesis of myocardial remodeling, and the proteins found may be candidate biomarkers for the diagnosis and prognosis of HCM in cats.

The purpose of this study is to provide important information on clinical presentation, protein expression, and genes associated with feline HCM. The detection of HCM with a normal phenotype in the early stage may provide an advantage for the treatment strategies, prognosis, and prevention of HCM in the clinic.

MATERIALS AND METHODS

Animals

This study design is a case-control study. The study protocol was approved by the Ethics Committee, Kasetsart University (ACKU-62-VET-059), and written informed consent from the owners. Thirty-one cats, 17 domestic shorthair cats, and 14 Maine Coon cats were enrolled in this study. The cat underwent a complete physical examination to evaluate the general condition. A complete blood count and serum biochemistry profile were performed for each cat. The cardiovascular system is evaluated by echocardiographic analysis. B-mode and M-mode echocardiography were used to define the left ventricular structure. The thickening of left ventricular wall at diastole phase which more than 6 mm indicated left ventricular hypertrophy (15). Echocardiography images have demonstrated left ventricular hypertrophy, the dynamic obstruction of the left ventricular outflow tract, which are common findings in HCM cats, as shown in **Figure 1**.

DNA Sequencing

DNA amplification was performed to detect MYBPC3-A31P and A74T. The PCR product was extracted and purified with FavorPrep GEL/PCR Purification Kit, Taiwan. The purified PCR product was stored at −20°C. The Sanger sequencing method was performed to detect the PCR product's nucleotide with a specific forward and reverse primer. MYBPC3-A31P and A74T polymorphism was detected using Bioedit program and ApE (A plasmid Editor) program.

Analysis of Peptide Patterns by MALDI-TOF MS

The protein concentration in serum was determined by the Lowry method (16). The absorbance at 750 nm (OD750) was measured, and the protein concentration was calculated using the standard curve, plotted between OD750 on Y-axis and BSA concentration (g/ml) on X-axis. The peptides from serum were acidified with 0.1% trifluoroacetic acid to the final concentration of 0.1 mg/ml. The peptides were mixed with MALDI matrix solution (10 mg sinapinic acid in 1 ml of 50% acetonitrile containing 0.1% trifluoroacetic acid), directly spotted onto MALDI target (MTP 384 ground steel, Bruker Daltonik, GmbH), and allowed to dry at room temperature. Maldi-TOF MS spectra were collected using Ultraflex III TOF/TOF (Bruker Daltonik, GmbH) in a positive linear mode with a mass range of 2,000–15,000 Da. Five hundred shots were accumulated with a 50 Hz laser for each sample. MS spectra were analyzed by using flexAnalysis and ClinproTool software (Bruker Daltonik, GmbH), including fingerprint spectra, pseudo-gel view, and principal component analysis (PCA). ACTH fragment 18–39 (human), Insulin oxidized B chain (bovine), Insulin (bovine), Cytochrome C (equine), and Apomyoglobin (equine) were used as external protein calibrations.

Peptidomics Analysis by LC-MS

Peptide solutions were analyzed using an HCTultra PTM Discovery System (Bruker Daltonics Ltd., Germany.) coupled to an UltiMate 3000 LC System (Dionex Ltd., U.K.). Peptides were separated on a nanocolumn (PepSwift monolithic column 100 μm i.d. × 50 mm). Eluent A was 0.1% formic acid, and eluent B was 80% acetonitrile in water containing 0.1% formic acid. Peptide separation was achieved with a linear gradient from 10 to 70% B for 13 min at a flow rate of 300 nl/min, including a regeneration step at 90% B and an equilibration step at 10% B. One run took 20 min. Peptide fragment mass spectra were acquired in data-dependent AutoMS (2) mode with a scan range of 300–1,500 m/z, three averages, and up to 5 precursor ions selected from the MS scan 50–3,000 m/z.

For peptides quantitation, DeCyder MS Differential Analysis software (DeCyderMS, GE Healthcare) was used (17, 18). Acquired LC-MS raw data were converted, and the PepDetect module was used for automated peptide detection, charge

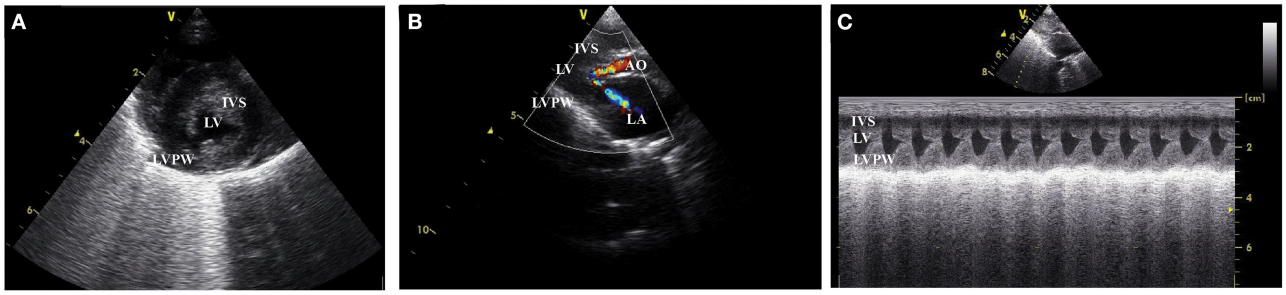

FIGURE 1 | Left ventricular wall of HCM cat visualized by two dimensional echocardiography in the **(A)** short axis view, **(B)** color flow doppler in long axis view, and **(C)** the motion mode (M mode) in long axis view. IVS, interventricular septum; LVPW, left ventricular proximal wall; LV, left ventricle; LA, left atrium; AO, aorta.

state assignments, and quantitation based on the peptide ions signal intensities in MS mode. The analyzed MS/MS data from DeCyderMS were submitted for a database search using the Mascot software (Matrix Science, London, UK) (19). The data were searched against the NCBI database for protein identification. Database interrogation was; taxonomy (Canis lupus amilaris); enzyme (trypsin); variable modifications (carbamidomethyl, oxidation of methionine residues); mass values (monoisotopic); protein mass (unrestricted); peptide mass tolerance (1.2 Da); fragment mass tolerance (± 0.6 Da), peptide charge state (1+, 2+, and 3+) and max missed cleavages. The maximum value of each group was used to determine the presence or absence of each identified protein.

Data normalization and quantification of the changes in peptide abundance between the control and Maine Coon cats were performed and visualized using MultiExperiment Viewer (Mev) software version 4.6.1 (20). Briefly, peptide intensities from the LC-MS analyses were transformed and normalized using a mean central tendency procedure.

Statistical Analysis

Data are presented as mean ± standard error of the mean (SEM). The normal distribution of data sets were conducted and then analyzed using one-way analysis of variance (ANOVA), a $P < 0.05$ was considered statistically significant.

RESULTS

Cats in the control group had the higher trend of age than the Maine Coon group (5.01 vs. 1.97 years, $P = 0.065$). In addition, there were significant differences by sex and weight between cats in the control and Maine Coon group. General characteristics and echocardiographic parameters for all cats are reported in **Table 1**. Blood profiles and serum biochemistry are reported in **Table 2**. Serum biochemistry (BUN/creatinine ratio) showed a statistically significant increase in control groups than cats in the Maine Coon group ($P = 0.032$). However, the levels of other biochemical profiles such as creatinine and blood urea nitrogen were not significantly different between groups. In addition, the blood profiles such as red blood cell count and hematocrit are not different in the control group vs. the Maine Coon group.

TABLE 1 | Characteristics and echocardiographic variables of cats.

Parameters (Mean ± SEM)	Control group	Maine Coon group	Reference value
Age in years	5.01 ± 1.40	1.97 ± 0.40	$P = 0.065$
Weight (kg)	4.08 ± 0.30**	5.72 ± 0.27**	$P < 0.001$
Male (number [%])	6/17 [35 %]	8/14 [55 %]	–
LA/AO ratio	1.48 ± 0.05	1.50 ± 0.12	0.97–1.39
IVSd (cm)	0.58 ± 0.02	0.60 ± 0.03	0.347–0.621
LVPWd (cm)	0.56 ± 0.03	0.71 ± 0.05	0.343–0.634
LVIDd (cm)	1.21 ± 0.09	1.58 ± 0.08	1.076–1.883
IVSs (cm)	0.63 ± 0.02	0.73 ± 0.03	0.571–1.022
LVPWs (cm)	0.64 ± 0.03	0.78 ± 0.05	0.578–0.989
LVIDs (cm)	0.82 ± 0.07	1.02 ± 0.08	0.495–1.103
Fractional shortening (%)	42.50 ± 1.70	37.90 ± 3.00	39.9–64.3

Values showed as mean ± SEM, $^{**}P < 0.001$.

TABLE 2 | Serum biochemistry, red blood cell count, and hematocrit in all cats and each groups ($^{*}P < 0.05$).

Parameters Mean ± SEM	Overall population	Control group	Maine Coon group	Reference value
BUN (mg%)	36.44 ± 7.16	42.93 ± 11.67	24.28 ± 3.79	15–34
Creatinine (mg%)	2.01 ± 0.29	2.23 ± 0.47	1.61 ± 0.18	<2.0
BUN/Creatinine ratio	17.16 ± 0.99	18.48 ± 1.51*	14.68 ± 0.73*	7–37
HGB (gm%)	11.22 ± 0.60	11.21 ± 0.81	11.25 ± 0.91	10–15
PCV (%)	33.94 ± 1.71	34.79 ± 2.38	32.15 ± 2.44	30–45
RBC ($\times 10^6$/ul)	7.42 ± 0.43	7.27 ± 0.64	7.74 ± 0.54	5–10
WBC	13.88 ± 1.06	13.27 ± 1.66	15.18 ± 0.90	5.5–19.0

Analysis of the association between Maine Coon cats and genotype at A31P and A74T mutation was performed. Results showed significant differences between 78.57% ($n = 11$) and 21.43% ($n = 3$) genotypes for the homozygous wildtype and heterozygous mutation, respectively (**Figure 2**).

Three-dimension component analysis showed distinct clusters among the sarcomeric gene mutation, non-mutation cats, and

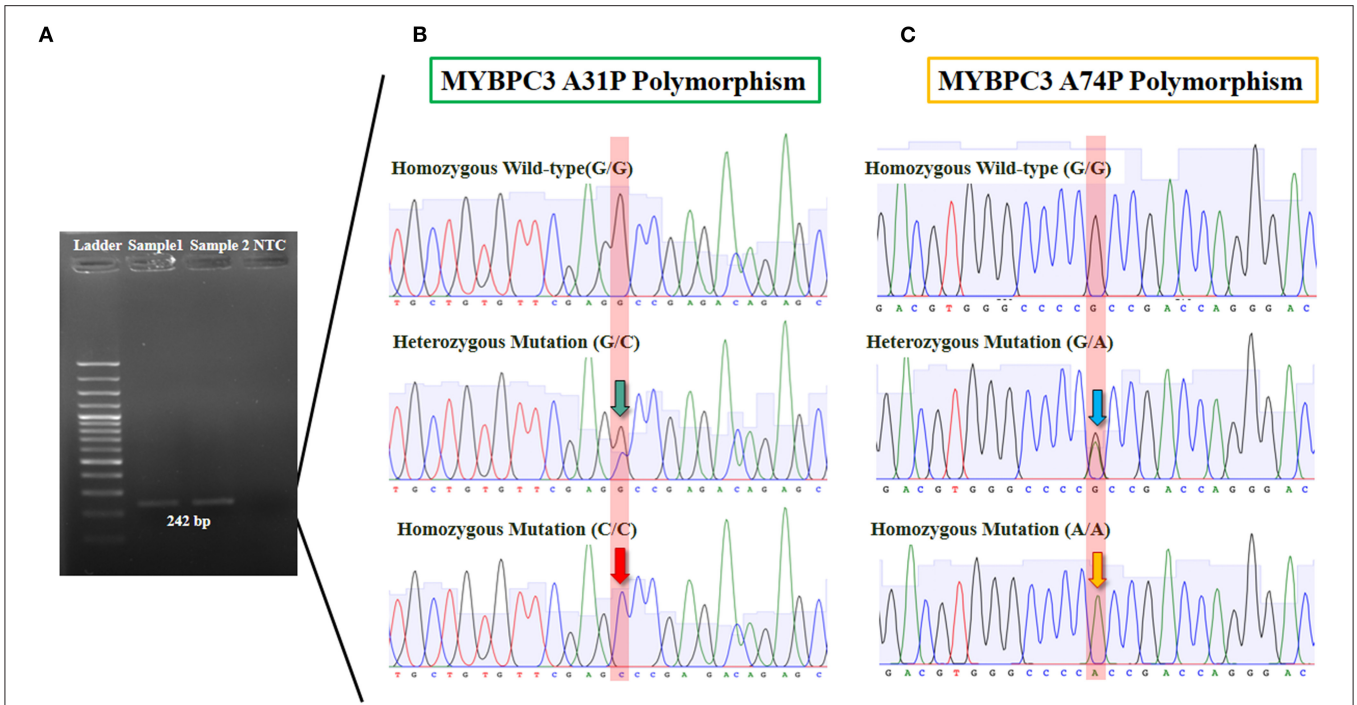

FIGURE 2 | The results of MYBPC3-A31P and A74T polymorphism from genotyping by sequencing. **(A)** Gel electrophoresis was represented 242 bp of target DNA of MYBPC3 gene in lane 2 and 3. **(B)** The sanger sequencing result of MYBPC3-A31P was showed in three group including homozygous wild-type (G/G), heterozygous mutation (G/C), and homozygous mutation (C/C). The green arrow pointed 2 peaks of guanine and cytosine and the red arrow pointed of only cytosine. **(C)** MYBPC3-A74T sequencing result was showed in three group including homozygous wild-type (G/G), heterozygous mutation (G/A), and homozygous mutation (A/A). The blue arrow pointed 2 peaks of guanine and alanine while the yellow arrow represented one peak of alanine.

normal control groups. All 31 replicates from each pooled serum sample group exhibited a distinguished cluster from the others, indicating a distinctive peptide profile in each group and demonstrating the uniformity and homogeneity of data within the groups as showed in **Figure 3**. In the present study, peptidomics analysis showed a total of 5,946 peptides differentially expressed between groups (**Figure 4**). STITCH version 5.0 was used to determine the protein names and interactions. Results showed that eight peptides were found to be up-regulated in the Maine Coon group including, IQ motif and Sec7 domain 2 (IQSEC2), zinc finger NFX1-type containing 1 (ZNFX1), discs large (Drosophila) homolog-associated protein 1 (DLGAP1), CTS telomere maintenance complex component 1 (CTC1), opiate receptor-like 1 (OPRL1), aryl hydrocarbon receptor nuclear translocator-like (ARNTL), nudix (nucleoside diphosphate linked moiety X)-type motif 16 (NUDT16), and KH domain containing RNA binding signal transduction associated 2 (KHDRBS2). In addition, three peptides were up-regulated in the Maine Coon group with sarcomeric gene mutation containing, cytochrome 3a132 (CYP3A132), forkhead box O1 (FOXO1), and ArfGAP with GTPase domain, ankyrin repeat and PH domain 2 (AGAP2).

The proteins were identified using Gene Ontology Annotation Database. The expression of hepatic markers such as CYP3a132 was investigated in the present study, CYP3a132 has been reported to associate with liver disease in domestic cats (21). In addition, gene mutation cats were associated with specific antioxidant defense changes in a distinct functional group of proteins. The different expression peptides were from a wide range of functional classes and included proteins involved in signal transduction, such as FOXO1. Transcription factor FOXO1 plays an essential role in glucose metabolism, cell cycle progression, apoptosis, and differentiation (22).

Moreover, AGAP2 was another peptide that expressed in the gene mutation Maine Coon cats. AGAP2 seems to be involved in TGFβ1 signaling that could contribute to the progression of hepatic fibrosis, suggesting AGAP2 as a potential new molecular target for liver fibrogenesis (23). Moreover, the peptides of gene mutation in cats were associated with testosterone, analgesic, anticonvulsant, and anticancer drugs, as shown in **Figure 4**. Verification of expressed protein sequences by LC-MS, the peptides mass peaks were compared among groups (**Figure 5**).

DISCUSSION

In this study, the differential peptidomic profiles expressed in Maine Coon cats compared to control cats may provide complementary tools for detecting and evaluating hypertrophic cardiomyopathy. Results showed the protein and drug interaction networks of proteins that dominate in sarcomeric gene mutation cats (**Figure 4B**). Since diseases are often a consequence of multiple changes in the same pathway or protein

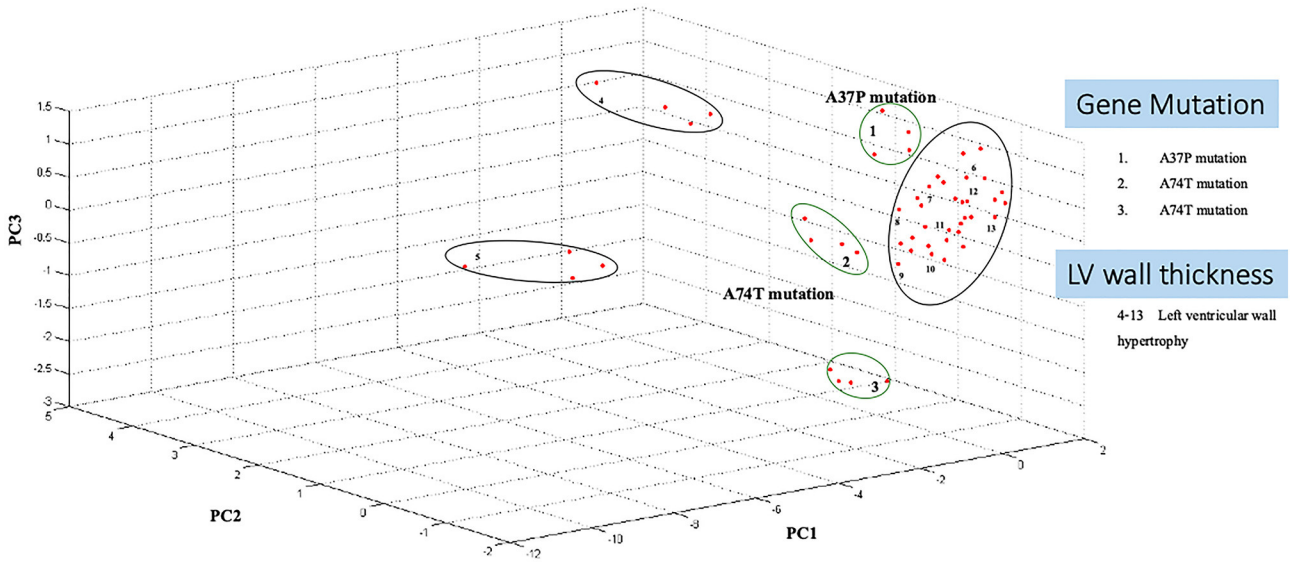

FIGURE 3 | Principal component analysis shows Maine Coon cats samples segregate from control cats. A three-dimensional scatterplot plot of non-gene mutation, gene mutation (A31P and A74T), and left ventricular wall hypertrophy cats (LV wall Thickening).

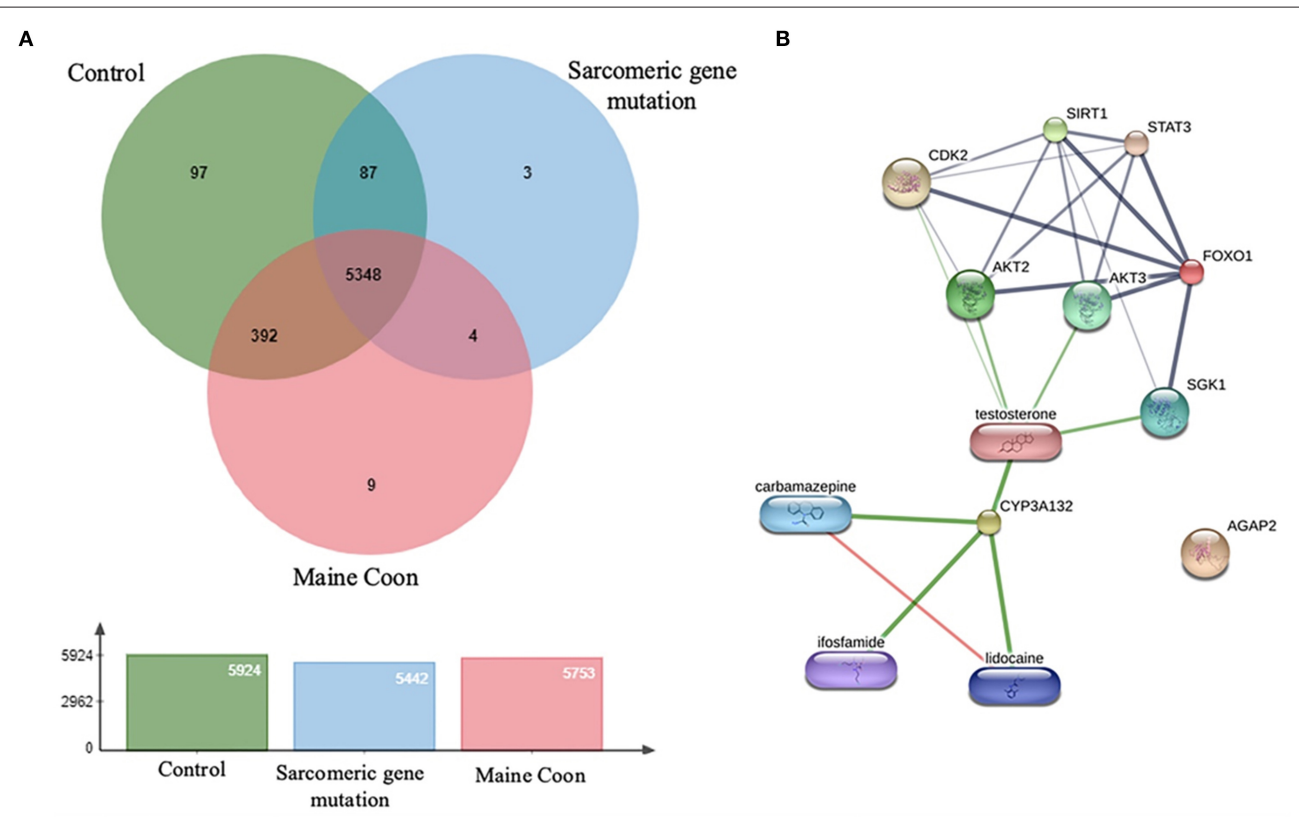

FIGURE 4 | (A) The diagram represents overlap among protein types with 5,946 identified proteins. **(B)** Protein and drug interaction networks of proteins dominate in sarcomeric gene mutation cats.

complex, the role of proteins in biological systems can be understood with the function of the targeted small molecules or drugs. Chemicals or drugs in the interaction network predicted by STITCH can lead to a better understanding of the potential function of the interacting protein partners. Among the expressed peptides, three peptides were increased in Maine Coon

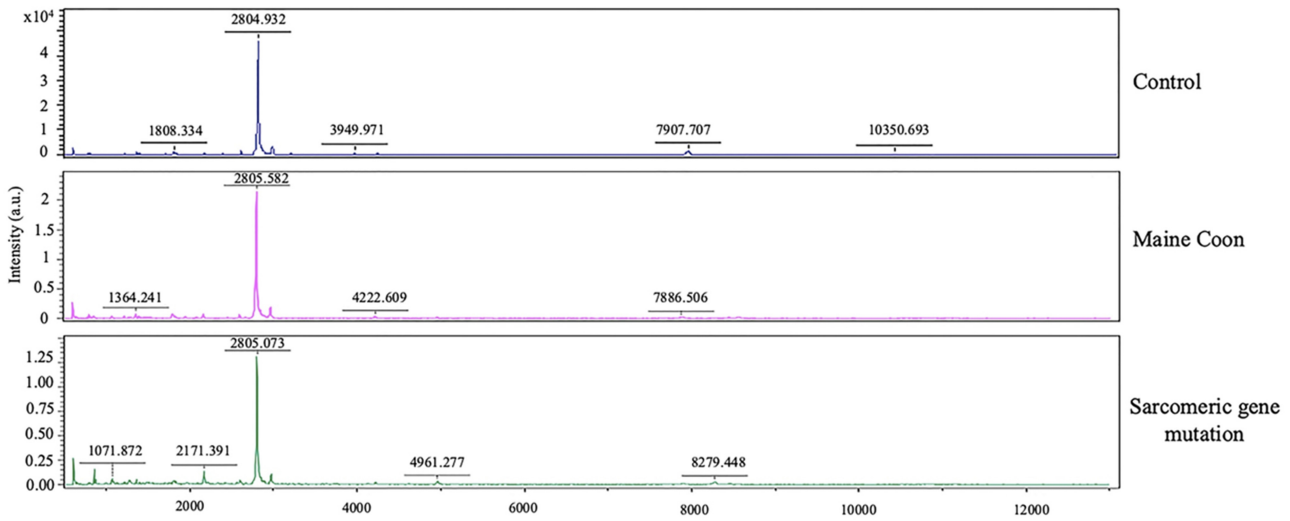

FIGURE 5 | Protein identification by MALDI-TOF analysis. Mass spectrometry of the protein isolated from the 2D gels of protein extracts of cat serum in domestic shorthair cats (Control), Maine Coon cat, and Maine Coon with sarcomeric gene mutation cats.

cats with sarcomeric gene mutations compared to nonmutated cats. The findings in our study are consistent with previously reported findings that the proteins involved in glucogenesis and oxidative phosphorylation are closely related to cardiac hypertrophy. The proteins identified in the cat with sarcomeric gene mutations included FOXO1 and CYP3A132. These proteins have an important role in several conditions associated with testosterone and glucose metabolic control. Testosterone has been reported to stimulate glucose metabolism by activating AMP-activated protein kinase (AMPK) and androgen receptor (AR) signaling, which are critical for induction of cardiomyocyte hypertrophy. Our results suggest that inhibiting AMPK and AR may help block glycolysis and cardiomyocyte hypertrophy, similar to the findings in previous reports (14). However, further studies should be performed to confirm this result.

FOXO1 is a transcription factor that modulates cell apoptosis and cell differentiation (24). It has been reported that TGFβ1 regulates the overexpression of FOXO1 as a consequence of inducing cardiac myoblast differentiation to myofibroblasts (25). Thus, FOXO1 may be related to the pathway of cardiac fibrosis and cardiac hypertrophy in Maine Coon cats with sarcomeric protein mutations. Similar to the findings in chronic intermittent hypoxia, FOXO1 induces upregulated expression of an apoptosis-related gene (Bim) and caspase 9, leading to cardiac hypertrophy in obstructive sleep apnea syndrome (26). Furthermore, this finding agrees with previous research showing that the regulation of FOXO1 is correlated with apoptosis-related genes such as Bcl-2 and Bim (27). A report in 2020 revealed that FOXO1 knockdown or deletion reduces cardiac hypertrophy caused by pressure overload (28).

AGAP2 is a GTPase-activating protein associated with numerous signaling pathways, including cell survival, cellular migration, and cell apoptosis. Evidence has shown that AGAP2 regulates profibrotic properties in liver fibrosis *via* TGFβ1. In addition, elevated AGAP2 acts as a pathological factor of cancer and liver fibrosis (29). According to the results in this study, AGAP2 might be correlated with cardiac fibrosis and hypertrophy in Maine Coon cats with HCM. However, reports linking AGAP2 with cardiac hypertrophy in cats still require further confirmation.

CYP3A132 belongs to the cytochrome P450 3A (CYP3A) family and is normally expressed in the liver (21). A previous study reported that CYP3A132 could be used as a marker for liver fibrosis. CYP3A132 has been found in domestic cats and is related to biotransformation and therapeutic drug metabolism, including that of calcium channel blockers, benzodiazepines, and immunosuppressant drugs (21). Moreover, subclinical liver fibrosis is associated with a history of atrial fibrillation, heart failure, and congestive heart disease (30). CYP3A132 was expressed in Maine Coon cats with sarcomeric gene mutations compared with nonmutated cats. Therefore, CYP3A132 may be used as a marker to detect cardiac hypertrophy in cats. However, further studies are warranted to determine the relationship between these peptides and HCM in cats.

According to the crucial serum biochemistry, thyroxine hormone concentration and feline NT-proBNP plasma concentration should use as a screening tool for cats with subclinical hypertrophic cardiomyopathy (HCM). These factors can influence the inclusion criteria in our study. Unfortunately, in this study, these factors were not measured, which is our study's limitation. However, our study used transthoracic echocardiography to measure left ventricular wall thickness is considered the reliable criteria in classifying HCM as recommended in the ACVIM guidelines (31).

CONCLUSION

The MYBPC3-A31P and A74T mutations had a high frequency in Maine Coon cats. A mutation was associated with the

hypertrophic cardiomyopathy phenotype. Peptidomic testing of Maine Coon cats will be a helpful tool for identifying carriers of the mutated gene for myocardial disease in cats. The results from this study may provide important information on clinical presentation, protein expression, and a gene associated with feline HCM.

DATA AVAILABILITY STATEMENT

The original contributions presented in the study are included in the article/supplementary materials, further inquiries can be directed to the corresponding author/s.

ETHICS STATEMENT

The animal study was reviewed and approved by the Animal Care Committee of Kasetsart University, Approval Number ACKU-62-VET-059. Written informed consent was obtained from the owners for the participation of their animals in this study.

AUTHOR CONTRIBUTIONS

SP and PS wrote the original manuscript and prepared figures. SR, ST, NP, and SP analyzed and interpreted the data regarding the serum peptidomics profiles. PS performed the PCR and DNA sequencing. SP was a major contributor in writing the manuscript. All authors read and approved the final version of the manuscript.

FUNDING

This research project was supported by National Research Council of Thailand (NRCT): NRCT5-RGJ63002-035.

ACKNOWLEDGMENTS

The authors are grateful to Kasetsart University Veterinary Teaching Hospital, Faculty of Veterinary Medicine, Kasetsart University, for providing facilities for the study.

REFERENCES

1. Fries R, Heaney AM, Meurs KM. Prevalence of the myosin-binding protein C mutation in Maine Coon cats. *J Vet Intern Med.* (2008) 22:893–6. doi: 10.1111/j.1939-1676.2008.0113.x
2. Mary J, Chetboul V, Sampedrano CC, Abitbol M, Gouni V, Trehiou-Sechi E, et al. Prevalence of the MYBPC3-A31P mutation in a large European feline population and association with hypertrophic cardiomyopathy in the Maine Coon breed. *J Vet Cardiol.* (2010) 12:155–61. doi: 10.1016/j.jvc.2010.06.004
3. Wess G, Schinner C, Weber K, Küchenhoff H, Hartmann K. Association of A31P and A74T polymorphisms in the myosin binding protein C3 gene and hypertrophic cardiomyopathy in Maine Coon and other breed cats. *J Vet Intern Med.* (2010) 24:527–32. doi: 10.1111/j.1939-1676.2010.0514.x
4. Longeri M, Ferrari P, Knafelz P, Mezzelani A, Marabotti A, Milanesi L, et al. Myosin-binding protein C DNA variants in domestic cats (A31P, A74T, R820W) and their association with hypertrophic cardiomyopathy. *J Vet Intern Med.* (2013) 27:275–85. doi: 10.1111/jvim.12031
5. Häggström J, Fuentes VL, Wess G. Screening for hypertrophic cardiomyopathy in cats. *J Vet Cardiol.* (2015) 17:S134–S49. doi: 10.1016/j.jvc.2015.07.003
6. Kitamura Y, Mise N, Mori Y, Suzuki Y, Ohashi T, Tada-Oikawa S, et al. Proteomic identification of the proteins related to cigarette smoke-induced cardiac hypertrophy in spontaneously hypertensive rats. *Sci Rep.* (2020) 10:1–12. doi: 10.1038/s41598-020-75429-3
7. Said S, Hernandez GT. The link between chronic kidney disease and cardiovascular disease. *J Nephropathol.* (2014) 3:99–104. doi: 10.12860/jnp.2014.19
8. Wang J, Choi H, Chung NC, Cao Q, Ng DCM, Mirza B, et al. Integrated dissection of cysteine oxidative post-translational modification proteome during cardiac hypertrophy. *J Proteome Res.* (2018) 17:4243–57. doi: 10.1021/acs.jproteome.8b00372
9. Lau E, Cao Q, Lam MPY, Wang J, Ng DCM, Bleakley BJ, et al. Integrated omics dissection of proteome dynamics during cardiac remodeling. *Nat Commun.* (2018) 9:1–14. doi: 10.1038/s41467-017-02467-3
10. Gomes AV, Kazmierczak K, Cheah JX, Gilda JE, Yuan CC, Zhou Z, et al. Proteomic analysis of physiological versus pathological cardiac remodeling in animal models expressing mutations in myosin essential light chains. *J Muscle Res Cell Motil.* (2015) 36:447–61. doi: 10.1007/s10974-015-9434-0
11. Li Z, Liu N, Zhang LS, Gong K, Cai Y, Gao W, et al. Proteomic profiling reveals comprehensive insights into adrenergic receptor-mediated hypertrophy in neonatal rat cardiomyocytes. *Proteomics Clin Appl.* (2009) 3:1407–21. doi: 10.1002/prca.200900029
12. Troncoso MF, Pavez M, Wilson C, Lagos D, Duran J, Ramos S, et al. Testosterone activates glucose metabolism through AMPK and androgen signaling in cardiomyocyte hypertrophy. *Biol Res.* (2021) 54:1–16. doi: 10.1186/s40659-021-00328-4
13. Kraemer RR, Hollander DB, Reeves GV, Francois M, Ramadan ZG, Meeker B, et al. Similar hormonal responses to concentric and eccentric muscle actions using relative loading. *Eur J Appl Physiol.* (2006) 96:551–7. doi: 10.1007/s00421-005-0094-4
14. Zhang W, Elimban V, Nijjar MS, Gupta SK, Dhalla NS. Role of mitogen-activated protein kinase in cardiac hypertrophy and heart failure. *Exp Clin Cardiol.* (2003) 8:173–83.
15. Fox PR, Liu SK, Maron BJ. Echocardiographic assessment of spontaneously occurring feline hypertrophic cardiomyopathy: an animal model of human disease. *Circulation.* (1995) 92:2645–51. doi: 10.1161/01.CIR.92.9.2645
16. Lowry OH, Rosebrough NJ, Farr AL, Randall RJ. Protein measurement with the Folin phenol reagent. *J Biol Chem.* (1951) 193:265–75. doi: 10.1016/S0021-9258(19)52451-6
17. Johansson C, Samskog J, Sundström L, Wadensten H, Björkesten L, Flensburg J. Differential expression analysis of *Escherichia coli* proteins using a novel software for relative quantitation of LC-MS/MS data. *Proteomics.* (2006) 6:4475–85. doi: 10.1002/pmic.200500921
18. Thorsell A, Portelius E, Blennow K, Westman-Brinkmalm A. Evaluation of sample fractionation using micro-scale liquid-phase isoelectric focusing on mass spectrometric identification and quantitation of proteins in a SILAC experiment. *Rapid Commun Mass Spectrom.* (2007) 21:771–8. doi: 10.1002/rcm.2898
19. Perkins DN, Pappin DJ, Creasy DM, Cottrell JS. Probability-based protein identification by searching sequence databases using mass spectrometry data. *Electrophoresis.* (1999) 20:3551–67. doi: 10.1002/(SICI)1522-2683(19991201)20:18<3551::AID-ELPS3551>3.0.CO;2-2
20. Howe E, Holton K, Nair S, Schlauch D, Sinha R, Quackenbush J. MEV: Multiexperiment viewer. In: Ochs M, Casagrande J, Davuluri R, editors. *Biomedical Informatics for Cancer Research.* Boston, MAL Springer (2010). p. 267–77.
21. Honda K, Komatsu T, Koyama F, Kubota A, Kawakami K, Asakura H, et al. Expression of two novel cytochrome P450 3A131 and 3A132 in liver and small intestine of domestic cats. *J Vet Med Sci.* (2011) 73:1489–92. doi: 10.1292/jvms.11-0098
22. Xing YQ, Li A, Yang Y, Li XX, Zhang LN, Guo HC. The regulation of FOXO1 and its role in disease progression. *Life Sci.* (2018) 193:124–31. doi: 10.1016/j.lfs.2017.11.030

23. Navarro-Corcuera A, López-Zabalza MJ, Martínez-Irujo JJ, Álvarez-Sola G, Ávila MA, Iraburu MJ, et al. Role of AGAP2 in the profibrogenic effects induced by TGFβ in LX-2 hepatic stellate cells. *Biochim Biophys Acta Mol Cell Res.* (2019) 1866:673–85. doi: 10.1016/j.bbamcr.2019.01.008
24. Ronnebaum SM, Patterson C. The FoxO family in cardiac function and dysfunction. *Annu. Rev. Physiol.* (2010) 72:81–94. doi: 10.1146/annurev-physiol-021909-135931
25. Vivar R, Humeres C, Muñoz C, Boza P, Bolivar S, Tapia F, et al. FoxO1 mediates TGF-beta1-dependent cardiac myofibroblast differentiation. *Biophys Acta Mol Cell Res.* (2016) 1863:128–38. doi: 10.1016/j.bbamcr.2015.10.019
26. Li G, Jin M, He Y, Ren J, Zhang M, Chen Y, et al. Fork head box class o1 (foxo1) activates BIM expression to mediate cardiac apoptosis in chronic intermittent hypoxia-induced cardiac hypertrophy. *Med Sci Mon Int Med J Exp Clin Res.* (2017) 23:3603. doi: 10.12659/MSM.905210
27. Yu W, Chen C, Cheng J. The role and molecular mechanism of FoxO1 in mediating cardiac hypertrophy. *ESC Heart Fail.* (2020) 7:3497–504. doi: 10.1002/ehf2.13065
28. Pfleger J, Coleman RC, Ibetti J, Roy R, Kyriazis ID, Gao E, et al. Genomic binding patterns of forkhead box protein o1 reveal its unique role in cardiac hypertrophy. *Circulation.* (2020) 142:882–98. doi: 10.1161/CIRCULATIONAHA.120.046356
29. Navarro-Corcuera A, Ansorena E, Montiel-Duarte C, Iraburu MJ. AGAP2: modulating TGFβ1-signaling in the regulation of liver fibrosis. *Int J Mol Sci.* (2020) 21:1400. doi: 10.3390/ijms21041400
30. Ostovaneh MR, Ambale-Venkatesh B, Fuji T, Bakhshi H, Shah R, Murthy VL, et al. Association of liver fibrosis with cardiovascular diseases in the general population: the multi-ethnic study of atherosclerosis (MESA). *Circ Cardiovasc Imaging.* (2018) 11:e007241. doi: 10.1161/CIRCIMAGING.117.007241
31. Fuentes VL, Abbott J, Chetboul V, Côté E, Fox PR, Häggström J, et al. ACVIM consensus statement guidelines for the classification, diagnosis, and management of cardiomyopathies in cats. *J Vet Intern Med.* (2020) 34:1062–77. doi: 10.1111/jvim.15745

Conflict of Interest: The authors declare that the research was conducted in the absence of any commercial or financial relationships that could be construed as a potential conflict of interest.

Publisher's Note: All claims expressed in this article are solely those of the authors and do not necessarily represent those of their affiliated organizations, or those of the publisher, the editors and the reviewers. Any product that may be evaluated in this article, or claim that may be made by its manufacturer, is not guaranteed or endorsed by the publisher.

frontiers in Veterinary Science

ORIGINAL RESEARCH
published: 15 November 2021
doi: 10.3389/fvets.2021.771244

Detection of Congestive Heart Failure and Myocardial Dysfunction in Cats With Cardiomyopathy by Using Two-Dimensional Speckle-Tracking Echocardiography

Ryohei Suzuki†, Takahiro Saito*†, Yunosuke Yuchi, Haruka Kanno, Takahiro Teshima, Hirotaka Matsumoto and Hidekazu Koyama*

Laboratory of Veterinary Internal Medicine, School of Veterinary Medicine, Faculty of Veterinary Science, Nippon Veterinary and Life Science University, Musashino, Japan

OPEN ACCESS

Edited by:
Zeki Yilmaz,
Faculty of Veterinary Medicine, Turkey

Reviewed by:
Luis Gustavo Cal Pereyra,
Universidad de la República, Uruguay
Domenico Caivano,
University of Perugia, Italy

***Correspondence:**
Ryohei Suzuki
ryoheisuzuki0130@gmail.com

†These authors have contributed equally to this work and share first authorship

Specialty section:
This article was submitted to Comparative and Clinical Medicine, a section of the journal Frontiers in Veterinary Science

Received: *06 September 2021*
Accepted: *25 October 2021*
Published: *15 November 2021*

Citation:
Suzuki R, Saito T, Yuchi Y, Kanno H, Teshima T, Matsumoto H and Koyama H (2021) Detection of Congestive Heart Failure and Myocardial Dysfunction in Cats With Cardiomyopathy by Using Two-Dimensional Speckle-Tracking Echocardiography. Front. Vet. Sci. 8:771244. doi: 10.3389/fvets.2021.771244

Congestive heart failure (CHF) is a life-threatening condition in cats with cardiomyopathy. We hypothesized that myocardial dysfunction may induce progression to CHF pathophysiology in cats with cardiomyopathy. However, no previous studies have evaluated the involvement of myocardial dysfunction in cats with CHF. In this study, we aimed to evaluate the relationship between CHF and myocardial function assessed using two-dimensional speckle-tracking echocardiography (2D-STE). Sixteen client-owned healthy cats and 32 cats with cardiomyopathy were enrolled in this study. Cats were classified into three groups: healthy cats, cardiomyopathy without CHF (CM group), and cardiomyopathy with CHF (CHF group). Left ventricular (LV) longitudinal and circumferential strains (SL and SC, respectively), and right ventricular (RV) SL were measured using 2D-STE. Logistic regression analysis was performed to assess the relationship between CHF and echocardiographic variables, including 2D-STE. Results comparing the healthy cats and CM vs. CHF groups showed that increased left atrial to aortic diameter ratio and decreased LV apical SC were significantly associated with the existence of CHF (odds ratio [95% confidence interval]: 1.40 [1.16–1.78] and 1.59 [1.06–2.36], respectively). Results comparing the CM vs. CHF group showed that increased end-diastolic RV internal dimension and decreased RV SL were significantly associated with the existence of CHF (odds ratio: 1.07 [1.00–1.13] and 1.34 [1.07–1.68], respectively). Left atrial enlargement and depressed LV apical myocardial function may be useful tools for predicting the progression to CHF in cats. Furthermore, RV enlargement and dysfunction may lead to the onset of CHF in asymptomatic cats with cardiomyopathy.

Keywords: cat, feline, heart, hypertrophic cardiomyopathy, myocardial function, restrictive cardiomyopathy, right heart function, strain

INTRODUCTION

Congestive heart failure (CHF) is a life-threatening condition in cats with heart disease (1). In veterinary medicine, hypertrophic cardiomyopathy (HCM) and restrictive cardiomyopathy (RCM) are common heart diseases that progress to CHF in cats (2). Both diseases are thought to be primarily caused by myocardial lesions, and may involve deterioration of myocardial function. We hypothesized that myocardial dysfunction may lead to increased left ventricular (LV) filling pressure and thereby induce progression to CHF pathophysiology. However, no previous studies have evaluated the involvement of myocardial dysfunction in cats with CHF.

Currently, some echocardiographic parameters have been used to evaluate disease progression in cats with cardiomyopathy, as well as to detect CHF pathophysiology (1, 3–5). However, most conventional echocardiographic parameters may be affected by loading conditions, heart rate, and technical limitations (such as Doppler angle limitation), which may inhibit the early detection of CHF (5). Recently, two-dimensional speckle-tracking echocardiography (2D-STE) has enabled the quantitative assessment of intrinsic myocardial function, and has been reported for myocardial assessment in feline patients (6–12). However, no previous studies have evaluated the relationship between variables of myocardial function using the 2D-STE and CHF. We consider that the 2D-STE technique may provide detailed myocardial functional parameters, and that these novel variables may be useful for detecting CHF in the early stage.

In this study, we hypothesized that 2D-STE-determined myocardial function would be associated with the presence of CHF. We aimed to evaluate the relationship between the existence of CHF and myocardial function assessed by 2D-STE in cats with cardiomyopathy, with and without CHF.

MATERIALS AND METHODS

This was a hypothesis-driven, prospective, cross-sectional clinical study. All procedures in this study followed the Guidelines for University Hospital Animal Care of Nippon Veterinary and Life Science University in Japan, and were approved by the ethical committee of our institute (approval number: R2-4).

Abbreviations: 2D-STE, two-dimensional speckle tracking echocardiography; AP, apical level of the left ventricle; AUC, area under the receiver operating characteristic curve; A-wave, peak velocity of the late diastolic wave; CHF, congestive heart failure; Cis, confidence intervals; E/A, E-wave to A-wave ratio; E/e', trans-mitral E-wave velocity to early diastolic myocardial velocity of the septal mitral annulus ratio; e', early diastolic myocardial velocity of the septal mitral annulus; E-wave, peak velocity of the early diastolic wave; FS, fractional shortening; HCM, hypertrophic cardiomyopathy; LA/Ao, left atrium to aortic diameter ratio; LV, left ventricular; LVIDd, end-diastolic LV internal diameter; MV, mitral valve level of the left ventricle; PM, papillary muscle level of the left ventricle; RCM, restrictive cardiomyopathy; ROC, receiver operating characteristic; RV, right ventricular; RV e', early-diastolic myocardial velocity of the lateral tricuspid annulus; RV s', systolic myocardial velocity of the lateral tricuspid annulus;RVFWd, end-diastolic RV free wall thickness; RVIDd, end-diastolic right ventricular internal dimension; s', systolic myocardial velocity of the septal mitral annulus; SC, circumferential strain; SL, longitudinal strain; TAPSE, tricuspid annulus plane systolic excursion.

Animals

Forty-eight client-owned cats (with cardiomyopathy: $n = 32$; healthy cats: $n = 16$). All cats underwent complete physical examination, electrocardiography, thoracic radiography, blood pressure measurement, and transthoracic echocardiography. Cats were classified into three groups: healthy cats, cardiomyopathy without CHF (CM group), and cardiomyopathy with CHF (CHF group). The healthy cats included cats with no abnormal findings as assessed by the aforementioned examinations. None of the cats were on medication or had a history of clinical signs of heart disease. The CM group included cats clinically diagnosed with HCM or RCM. We diagnosed HCM with echocardiographic evidence of LV hypertrophy and the absence of other diseases known to cause LV hypertrophy. Echocardiographic LV hypertrophy was judged if the LV wall thickness at end-diastole was 6 mm or more, as measured on B-mode echocardiography. LV thickness was measured from the short-axis view, and the mean values of the thickest segment obtained in three consecutive cardiac cycles were used (12). We diagnosed RCM with echocardiographic evidence of left atrial or bi-atrial enlargement and a prominent endomyocardial scar that bridges the interventricular septum and LV free wall. Left atrial enlargement was defined as a left atrial to aortic diameter ratio (LA/Ao) greater than 1.5, obtained from the right parasternal short-axis view, using B-mode echocardiography (13). Right atrial enlargement was judged on the right parasternal long-axis view according to previously published allometric scaling reference intervals (14). Endomyocardial scar findings were macroscopically assessed by B-mode echocardiography. A restricted pattern of LV inflow in cats with RCM was not required because the fusion of E and A waves may prevent detection.

To exclude other forms of feline cardiomyopathy (2), we checked for normal or near-normal LV systolic function, according to previously published allometric scaling reference intervals (15). We excluded cats that had systolic blood pressure >160 mmHg (non-invasive oscillometric method), or systemic or other cardiovascular diseases, including dehydration and myocarditis.

The CHF group included cats that had at least one echocardiographic or radiographic finding providing evidence of left heart failure, such as pulmonary edema, pleural effusion, and the associated clinical signs. Cats with tricuspid regurgitation >2.7 m/s were diagnosed as having pulmonary hypertension (5, 11).

Echocardiography

Standard 2D and Doppler examinations were performed by a single trained investigator (RS) using a Vivid E95 echocardiography scanner (GE Healthcare) and a 12S transducer (GE Healthcare). Lead II ECG was recorded simultaneously and was displayed on the images. All echocardiographic data were obtained from at least five consecutive cardiac cycles in sinus rhythm in non-sedated cats that were manually restrained in the right and left lateral recumbent positions. Echocardiographic images were analyzed by a single observer (HK) on a separate day from the examination, using an offline workstation (EchoPAC PC, Version 204, GE Healthcare). LA/Ao,

end-diastolic interventricular septal thickness, end-diastolic LV free-wall thickness, end-diastolic LV internal diameter (LVIDd), end-systolic LV internal diameter, and fractional shortening (FS) were measured from the right parasternal short-axis view at the level of the chordae tendineae level. Trans-mitral inflow was obtained from the left apical four-chamber view using the pulsed wave Doppler method, and the peak velocity of the early diastolic wave (E-wave) and peak velocity of the late diastolic wave (A-wave) were measured. The E-wave to A-wave ratio (E/A) was also evaluated. In cats whose E and A waves were fused, these values were not used. The end-diastolic right ventricular (RV) internal dimension (RVIDd), end-diastolic RV free wall thickness (RVFWd), and tricuspid annulus plane systolic excursion (TAPSE) were measured using B-mode echocardiography from the left apical four-chamber view modified for right heart measurement (14, 15). The right atrial diameter was measured using the B-mode echocardiography from the mid-point of the interatrial septum to the right atrial lateral wall in the cranial–caudal plane and parallel to the tricuspid valve annulus at end-systole (15). The acceleration-time-to-ejection-time ratio of the pulmonary artery was also calculated from the right parasternal short-axis view of the LV (3). Systolic and early diastolic myocardial velocity of the septal mitral annulus (s' and e', respectively) and the lateral tricuspid annulus (RV s' and RV e', respectively) were obtained by pulsed wave, based on the tissue Doppler method, from the left apical four-chamber view and the left apical four-chamber view modified for right heart measurement (16). Trans-mitral E-wave velocity to early diastolic myocardial velocity of the septal mitral annulus ratio (E/e') was also evaluated. For all analyses, the mean values of three consecutive cardiac cycles from high-quality images were used.

Two-Dimensional Speckle Tracking Echocardiography

High-quality images for 2D-STE analysis were carefully obtained by the same investigator (RS) using the same echocardiographic system and the same transducer. To evaluate LV myocardial deformations, a right parasternal short-axis view of the left ventricle at the papillary muscles, mitral valve, and apical level of the left ventricle (PM, MV and AP, respectively) and a left apical four-chamber view were obtained in this study. A left apical four-chamber view modified for right heart measurement was also obtained to analyze the right myocardial deformations (11). We measured the peak global strain in the longitudinal and circumferential directions (SL and SC, respectively), which were measured at both ventricles (LV-SL and RV-SL, respectively) (11). For RV deformations, we assessed only the RV lateral wall segments. SC was measured at the papillary muscle, mitral valve, and apical levels of the left ventricle (SC-PM, SC-MV, and SC-AP, respectively) (9, 17). The observer variability of 2D-STE analysis in our laboratory has been described in our previous studies (6, 8, 9, 11). All 2D-STE analyses were performed on a separate day from the examination by a single trained observer (HK) using an offline EchoPAC workstation. The outline of the feline 2D-STE analysis has been described previously (6–9, 12). The mean values of the measurements from three consecutive cardiac cycles from high-quality images were used in all analyses.

Statistical Analysis

Data are reported as median and interquartile range. Statistical analyses were performed using commercially available software (R 2.8.1; https://www.r-project.org/). The normality of the data distribution was tested using the Shapiro–Wilk test. Continuous variables were compared among groups using one-way analysis of variance or the Kruskal–Wallis test, whichever was appropriate. When a statistically significant difference was detected among the three groups, multiple comparisons were performed using the Steel–Dwass test or Tukey's *post-hoc* test. Logistic regression analysis was used to evaluate the relationship between the existence of CHF and echocardiographic indices (healthy cats + CM vs. CHF group, CM vs. CHF group). Variables with $P < 0.15$ in the univariate models, were included in the multivariate models. Receiver operating characteristic (ROC) curve analysis was performed to assess the diagnostic accuracy of each variable, to detect the presence of CHF. The area under the ROC curve (AUC) was used as a summary measure for diagnostic accuracy and was reported with 95% confidence intervals (CIs). Diagnostic cutoffs for each variable were chosen based on the highest of various combinations of sensitivity and specificity, using Youden's index (18). Multivariable ROC analysis was performed using the variables that were significant ($P < 0.05$) in the univariate ROC analysis to identify the combination of variables that best detected the presence of CHF. The AUC was reported with 95% CIs, and was considered to have high accuracy if it was > 0.9, moderate accuracy if it was 0.7–0.9, and low accuracy if it was 0.5–0.7. For this purpose, different submodels were tested against the full model by taking one submodel at a time as a reference model. The significance level was set at $P < 0.05$.

RESULTS

Demographic Data

The demographic data and results of the physical examinations are summarized in **Table 1**. The CM group included 18 HCM cats and one RCM cat, and there were no cats with pulmonary hypertension. The CHF group included four HCM cats and nine RCM cats, and there were four cats with pulmonary hypertension ($P < 0.01$).

Echocardiography

Echocardiographic variables are summarized in **Table 2**. FS was significantly lower in the CM and CHF groups than in the healthy cats ($P < 0.05$). E/e' was significantly higher in the CM and CHF groups than in the healthy cats ($P < 0.05$). LA/Ao, E/A, right atrial diameter, RVIDd, and RVFWd were significantly higher in the CHF group than in the healthy cats ($P < 0.05$). TAPSE and RV s' were significantly decreased in the CHF group as compared to the healthy cats ($P < 0.05$). LA/Ao, LVIDd, and E/A were significantly higher in the CHF group than in the CM group ($P < 0.05$). TAPSE was significantly lower in the CHF group than in the CM group ($P < 0.05$).

TABLE 1 | Clinical characteristics in cats with cardiomyopathy and healthy controls.

Variables	Healthy cats ($n = 16$)	CM ($n = 19$)	CHF ($n = 13$)
Age (month)	65 (29–139)	48 (34–76)	97 (46–133)
Sex (male/female)	9/7	12/7	8/5
Body weight (kg)	4.2 (3.6–4.9)	3.9 (3.4–4.2)	4.6 (4.1–5.5)
Heart rate (bpm)	198 (176–225)	170 (158–199)	209 (184–233)
Diagnosis		HCM = 18 RCM = 1	HCM = 4 RCM = 9
CHF (present/past)	0/0	0/0	8/4
Pulmonary hypertension	0 (0%)	0 (0%)	4 (31%)

CM, cardiomyopathy; CHF, congestive heart failure. Continuous variables were displayed as median (interquartile range).

TABLE 2 | Results of conventional echocardiographic indices in cats with cardiomyopathy and healthy controls.

Variables	Healthy cats ($n = 16$)	CM ($n = 19$)	CHF ($n = 13$)
LA/Ao	1.4 (1.2–1.5)	1.5 (1.1–1.5)	2.2 (1.8–3.0) *†
LVIDd (mm)	14.2 (13.6–15.6)	13.3 (12.6–14.8)	16.2 (13.7–17.5)†
FS (%)	49.8 (41.3–53.0)	41.0 (37.1–43.4)*	37.3 (27.9–52.0)*
E/A	0.8 (0.8–1.2)	0.9 (0.7–1.2)	3.4 (2.5–3.8)*†
E/e'	7.9 (7.3–10.1)	14.4 (10.7–19.7)*	12.7 (11.7–17.4)*
RAD (mm)	9.2 (8.4–10.8)	10.6 (8.1–11.9)	10.8 (10.2–13.4)*
RVIDd (mm)	5.7 (4.7–6.4)	4.7 (3.6–6.6)	7.7 (5.6–9.9)*†
RVFWd (mm)	1.7 (1.6–2.0)	2.0 (1.8–2.2)	2.3 (2.1–2.5)*
TAPSE (mm)	9.4 (7.8–11.1)	8.2 (7.6–9.5)	6.6 (5.5–8.2)*†
RV s' (cm/s)	10.5 (8.6–13.2)	9.4 (8.2–11.0)	7.9 (6.2–9.7)*

*CM, cardiomyopathy; CHF, congestive heart failure; LA/Ao, left atrial-to-aortic diameter ratio; LVIDd, end-diastolic LV internal diameter; FS, fractional shortening; E/A, peak velocity of the early diastolic wave-to-peak velocity of the late diastolic wave ratio; E/e', peak velocity of the early diastolic wave-to-early diastolic myocardial velocity of the septal mitral annulus ratio; RAD, right atrial diameter; RVIDd, end-diastolic right ventricular internal dimension; RVFWd, end-diastolic right ventricular free wall thickness; TAPSE, tricuspid annulus plane systolic excursion; RV s', systolic myocardial velocity of the lateral tricuspid annulus. Continuous variables were displayed as median (interquartile range). *The value is significantly different from the healthy cats ($P < 0.05$). † The value is significantly different from that of cardiomyopathy group ($P < 0.05$).*

Two-Dimensional Speckle Tracking Echocardiography

The results of the 2D-STE variables are summarized in **Table 3** and **Figure 1**. LV-SL (**Figure 1A**) and LV-SC AP (**Figure 1E**) were significantly decreased in the CM and CHF groups as compared to the healthy cats ($P < 0.05$). LV-SC PM (**Figure 1C**) was significantly lower in the CM group than in the healthy cats ($P < 0.05$). RV-SL (**Figure 1B**) was significantly decreased in the healthy cats and CM groups as compared to that in the CHF group ($P < 0.05$).

Logistic Regression Analysis

The significant variables in the logistic regression analysis are summarized in **Table 3**. Logistic regression analysis in the healthy cats + CM vs. CHF group showed a significant difference in terms LA/Ao, RVIDd, LV-SC AP, and RV-SL in univariate analysis ($P < 0.01$). LA/Ao and LV-SC AP also showed significant differences in multivariate analysis ($P < 0.01$ and $P = 0.02$, respectively). Logistic regression analysis in the CM vs. CHF group showed a significant difference in LVIDd, RVIDd, LV-SC AP, and RV-SL in univariate analysis ($P = 0.02$, $P = 0.01$, $P = 0.03$, and $P < 0.01$, respectively). RVIDd and RV-SL also showed significant differences in multivariate analysis ($P = 0.01$).

TABLE 3 | Significant variables in the logistic regression analysis.

Variables	Univariate analysis		Multivariate analysis	
	Odds ratio (95%CI)	*P*	Odds ratio (95%CI)	*P*
Healthy cats + CM vs CHF				
LA/Ao	1.44 (1.16–1.78)	<0.01	1.40 (1.12–1.75)	<0.01
RVIDd	1.06 (1.02–1.10)	<0.01		
LV-SC AP	1.44 (1.13–1.83)	<0.01	1.59 (1.06–2.36)	0.02
RV-SL	2.80 (1.44–5.43)	<0.01		
CM vs CHF				
LVIDd	1.06 (1.01–1.12)	0.02		
RVIDd	1.05 (1.01–1.09)	0.01	1.07 (1.00–1.13)	0.01
LV-SC AP	1.30 (1.02–1.65)	0.03		
RV-SL	2.24 (1.16–4.35)	<0.01	1.34 (1.07–1.68)	0.01

CM, cardiomyopathy; CHF, congestive heart failure; CI, confidence interval; LA/Ao, left atrial-to-aortic diameter ratio; RVIDd, end-diastolic right ventricular internal dimension; LV-SC AP, peak global strain in the circumferential direction at the level of the apical levels of the left ventricle; RV-SL, peak global strain in the longitudinal direction of the right ventricle; LVIDd, end-diastolic LV internal diameter; RVIDd, end-diastolic right ventricular internal dimension. Continuous variables were displayed as median (interquartile range).

The results obtained by using the ROC curve for variables that were significant in the logistic regression analysis are summarized in **Table 4**. In the healthy cats + CM vs. CHF group showed high AUC, sensitivity, and specificity in LA/Ao, RVIDd, LV-SC AP, and RV-SL. The ROC curve for the CM vs. CHF group showed a significantly high AUC, sensitivity, and specificity for LVIDd, RVIDd, LV-SC AP, and RV-SL.

DISCUSSION

Our study demonstrated that some echocardiographic parameters, including myocardial strain assessed by 2D-STE, are useful for detecting CHF in cats. Specifically, LA/Ao and LV-SC AP derived by 2D-STE may be associated with the progression of CHF in apparently healthy cats. Furthermore, RVIDd and RV-SL derived by 2D-STE might lead to CHF onset in asymptomatic cats with cardiomyopathy. The ROC curves revealed that these parameters had a high AUC with sufficient sensitivity and specificity. We concluded that evaluation of 2D-STE-derived myocardial strain in addition to conventional parameters showed a significant association with the existence of CHF in cats and may be useful tools for the early detection of CHF in these cats.

In this study, left atrial enlargement measured by LA/Ao was significantly higher in the CHF group and performed well in supporting the diagnosis of CHF. Our results agreed with those of previous studies that have reported that LA/Ao is a

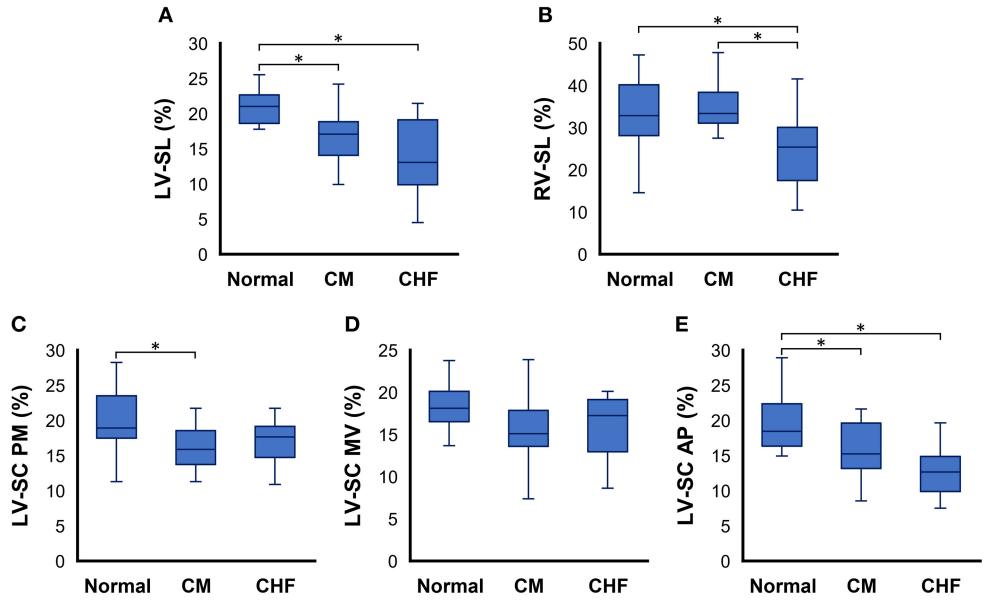

FIGURE 1 | Box and whisker plots of two-dimensional speckle tracking echocardiography indices in cats with cardiomyopathy. **(A)** left ventricular longitudinal strain (LV-SL), **(B)** right ventricular longitudinal strain (RV-SL), **(C)** left ventricular circumferential strain (LV-SC) at the papillary muscles level of the left ventricle (PM), **(D)** LV-SC at the mitral valve level of the left ventricle (MV), and (E) LV-SC at the apical level of the left ventricle AP, respectively. *The value is significantly different between groups ($P < 0.05$).

significant predictor and prognostic indicator of the development of CHF in cats (4, 19, 20). Left atrial enlargement is currently considered a morphophysiological expression of LV diastolic dysfunction, with increasing left atrial size corresponding to progressively worse LV diastolic function and atrial hypertension (21, 22). The higher LA/Ao values observed in the CHF groups in this study reflect diastolic dysfunction that is attributable to cardiomyopathy and increased left atrial pressure, due to congestion pathophysiology. Left atrial enlargement measured by LA/Ao will continue to be a simple and readily available echocardiographic finding that determines the severity of the increase in left atrial pressure and supports the clinical diagnosis of left-sided CHF.

In addition to the left atrium parameter, LV myocardial circumferential strain measured by LV-SC AP was lower in the CHF group than in the CM group. In addition, logistic regression analysis comparing healthy cats + CM vs. CHF revealed that LA enlargement and depressed LV apical myocardial function may be associated with the progression to CHF in apparently healthy cats. Circumferential deformations play an important role in cardiac pump function in humans and dogs with various heart diseases (23–25), and LV myocardial contractions that are impaired in the longitudinal direction are compensated for by circumferential shortening in subclinical patients with cardiovascular risk factors (26). Previous studies on cats have demonstrated that longitudinal strain had already deteriorated in the early stages of cardiomyopathy in cats (11, 12), and circumferential deformations differ according to myocardial compensation. In our results, circumferential deformations differed among LV levels (AP, PM, MV). Apical deformation was lower in cats with cardiomyopathy. Apical deformations have been reported as a major factor in torsion and relaxation of the entire left ventricle (9) thus, early myocardial dysfunction may occur at the apical level of circumferential deformations. The depressed LV-SC AP variables observed in this study may reflect myocardial dysfunction in decompensated patients and may lead to CHF development in these cats. In addition to LA enlargement,

TABLE 4 | Results of receiver operating characteristic curves of the significant variables in the logistic regression analysis.

Variables	AUC (95%CI)	Cutoff	Sensitivity	Specificity
Healthy cats + CM vs. CHF				
LA/Ao	0.87 (0.71–1.00)	2.07	0.77	1.00
RVIDd	0.78 (0.61–0.96)	6.62	0.77	0.80
LV-SC AP	0.84 (0.72–0.97)	15.16	0.92	0.74
RV-SL	0.86 (0.72–1.00)	24.09	0.77	0.91
CM vs. CHF				
LVIDd	0.74 (0.56–0.95)	16.2	0.54	1.00
RVIDd	0.80 (0.63–0.96)	6.85	0.69	0.84
LV-SC AP	0.76 (0.59–0.93)	15.16	0.92	0.58
RV-SL	0.86 (0.71–1.00)	24.09	0.77	0.90

CM, cardiomyopathy; CHF, congestive heart failure; AUC, area under the curve; CI, confidence interval; LA/Ao, left atrial-to-aortic diameter ratio; RVIDd, end-diastolic right ventricular internal dimension; LV-SC AP, peak global strain in the circumferential direction at the apical level of the left ventricle; RV-SL, peak global strain in the longitudinal direction of the right ventricle; LVIDd, end-diastolic LV internal diameter; RVIDd, end-diastolic right ventricular internal dimension.

decreased LV-SC AP may be a useful tool for detecting CHF in cats.

In the present study, significant findings were also observed in RV echocardiographic indices. Furthermore, a comparison between the CM and CHF groups revealed that RV enlargement and dysfunction might lead to CHF onset in asymptomatic cats with cardiomyopathy. In humans, RV assessment has been shown to have a clinically relevant impact on predicting clinical status and outcome in a variety of cardiovascular diseases (27–31). In veterinary medicine, RV dysfunction has been shown to be a prognostic factor in dogs with arrhythmogenic RV cardiomyopathy and myxomatous mitral valve disease (32, 33). In the present study, RV-SL measured by 2D-STE, which may allow for a more detailed evaluation of myocardial function, showed no significant change in the CM group, but was decreased in the CHF group as compared with the healthy cats. Previous reports have shown no significant differences in RV-SL between asymptomatic HCM cats and healthy cats (10), which was in agreement with our study. The results of cats with CHF suggest that more extensive cardiomyopathy-associated lesions may develop in the right as well as in the left ventricle, and/or that pulmonary hypertension due to pulmonary venous congestion might affect RV function, particularly in cats with advanced stages of heart failure (i.e., CHF condition). A previous case report on RCM demonstrated that RV-SL decreased with the progression of the clinical course of RCM, although it did not decrease in the early stage of this disease (34). Additionally, it has also been reported that, in human HCM patients, a decrease in RV-SL is associated with the development of CHF (35). Therefore, our results suggest that RV dysfunction might occur in cats with CHF and that decreased RV-SL may be a predictor of CHF development in cats with cardiomyopathy.

In this study, RV dilatation, as assessed by RVIDd, showed a significant association with the presence of CHF. We previously described the RV adaptation mechanism during the progression of pulmonary hypertension, which would induce RV dilatation to maintain cardiac output (36). Only cats with CHF showed significant RV dysfunction and dilatation in our study population, suggesting that the RV adaptation mechanism might be decompensated in these cats. Therefore, our results suggest that RV dilatation, as assessed by RVIDd, as well as decreased RV-SL might provide additional information for CHF development in cats with cardiomyopathy.

This study had several limitations. First, because it was a non-invasive clinical investigation, we had no access to histopathological findings to make a definitive diagnosis and assess myocardial histopathological alterations. Second, we could not consider the influence of medication on the values assessed by 2D-STE. Because cats with CHF showed signs of heart failure, some cats had received drugs that could affect myocardial performance prior to examination. However, medication-controlled cats in the CHF group had the worst myocardial function in this study. Third, the small number of cats in our study may have influenced the statistical power and limited extrapolation of our findings to larger populations. Fourth, recent study has reported that the ratio of pulmonary veins to pulmonary artery might be useful for the detection of cats with CHF (37). Unfortunately, we could not have evaluated the variable due to the lack of appropriate echocardiographic data to measure the variables in this study. The relationship between the variables and the presence of CHF should be compared in the future. Finally, this was a cross-sectional study and included cases with different types of cardiomyopathy and pulmonary hypertension. These confounding factors may influence interpretation of our results.

In conclusion, logistic regression analysis comparing healthy cats + CM vs. CHF revealed that left atrial enlargement and depressed LV apical myocardial function may be associated with the progression from subclinical patients to CHF. Furthermore, a comparison between the CM and CHF groups revealed that RV enlargement and dysfunction might lead to CHF onset in asymptomatic cats with cardiomyopathy. Additionally, the receiver operating characteristic curves revealed that LA/Ao, RVIDd, and 2D-STE-derived apical LV-SC and RV-SL had a high AUC in ROC curve analysis, with sufficient sensitivity and specificity for indicating the presence of CHF. Thus, 2D-STE-derived myocardial strain showed a significant association with the existence of CHF in cats and may therefore be a useful tool for the early detection of CHF in cats with cardiomyopathy. Nevertheless, further studies with larger sample sizes are required to verify our findings.

DATA AVAILABILITY STATEMENT

The raw data supporting the conclusions of this article will be made available by the authors, without undue reservation.

ETHICS STATEMENT

The animal study was reviewed and approved by Ethical Committee for Laboratory Animal Use of the Nippon Veterinary and Life Science University. Written informed consent was obtained from the owners for the participation of their animals in this study.

AUTHOR CONTRIBUTIONS

RS and TS performed the concept/design, data acquisition, interpretation, critical revision of the article, and drafting the article. YY and HKa performed the data acquisition and data analysis, and summarized the clinical data. TT, HM, and HKo performed data acquisition and interpretation, and provided the academic direction. All authors have read the final version of this paper and approved submission.

FUNDING

This work was partially supported by the Japan Society for the Promotion of Science (JSPS), Grant Number 20K15667.

ACKNOWLEDGMENTS

This work was conducted at the Laboratory of Veterinary Internal Medicine, School of Veterinary Science, Faculty of Veterinary Medicine, Nippon Veterinary and Life Science University in Tokyo, Japan. We would also like to thank Editage (www.editage.com) for English language editing.

REFERENCES

1. Rohrbaugh MN, Schober KE, Rhinehart JD, Bonagura JD, Habing A, Yildiz V. Detection of congestive heart failure by Doppler echocardiography in cats with hypertrophic cardiomyopathy. *J Vet Intern Med.* (2020) 34:1091–101. doi: 10.1111/jvim.15777
2. Luis Fuentes V, Abbott J, Chetboul V, Côté E, Fox PR, Häggström J, et al. ACVIM consensus statement guidelines for the classification, diagnosis, and management of cardiomyopathies in cats. *J Vet Intern Med.* (2020) 34:1062–1077. doi: 10.1111/jvim.15745
3. Vezzosi T, Schober KE. Doppler-derived echocardiographic evidence of pulmonary hypertension in cats with left-sided congestive heart failure. *J Vet Cardiol.* (2019) 23:58–68. doi: 10.1016/j.jvc.2019.01.007
4. Duler L, Scollan KF, LeBlanc NL. Left atrial size and volume in cats with primary cardiomyopathy with and without congestive heart failure. *J Vet Cardiol.* (2019) 24:36–47. doi: 10.1016/j.jvc.2019.04.003
5. Fox PR, Keene BW, Lamb K, Schober KA, Chetboul V, Luis Fuentes V, et al. International collaborative study to assess cardiovascular risk and evaluate long-term health in cats with preclinical hypertrophic cardiomyopathy and apparently healthy cats: the REVEAL study. *J Vet Intern Med.* (2018) 32:930–43. doi: 10.1111/jvim.15285
6. Suzuki R, Mochizuki Y, Yoshimatsu H, Teshima T, Matsumoto H, Koyama H. Determination of multidirectional myocardial deformations in cats with hypertrophic cardiomyopathy by using two-dimensional speckle-tracking echocardiography. *J Feline Med Surg.* (2017) 19:1283–9. doi: 10.1177/1098612X17691896
7. Suzuki R, Mochizuki Y, Yoshimatsu H, Niina A, Teshima T, Matsumoto H, et al. Early detection of myocardial dysfunction using two-dimensional speckle tracking echocardiography in a young cat with hypertrophic cardiomyopathy. *J Feline Med Surg Open Reports.* (2018) 4:205511691875621. doi: 10.1177/2055116918756219
8. Suzuki R, Mochizuki Y, Yoshimatsu H, Niina A, Teshima T, Matsumoto H, et al. Layer-specific myocardial function in asymptomatic cats with obstructive hypertrophic cardiomyopathy assessed using 2-dimensional speckle-tracking echocardiography. *J Vet Intern Med.* (2019) 33:37–45. doi: 10.1111/jvim.15339
9. Suzuki R, Mochizuki Y, Yoshimatsu H, Ohkusa T, Teshima T, Matsumoto H, et al. Myocardial torsional deformations in cats with hypertrophic cardiomyopathy using two-dimensional speckle-tracking echocardiography. *J Vet Cardiol.* (2016) 18:350–7. doi: 10.1016/j.jvc.2016.06.004
10. Spalla I, Boswood A, Connolly DJ, Luis Fuentes V. Speckle tracking echocardiography in cats with preclinical hypertrophic cardiomyopathy. *J Vet Intern Med.* (2019) 33:1232–41. doi: 10.1111/jvim.15495
11. Suzuki R, Yuchi Y, Kanno H, Teshima T, Matsumoto H, Koyama H. Left and right myocardial functionality assessed by two-dimensional speckle-tracking echocardiography in cats with restrictive cardiomyopathy. *Animals.* (2021) 11:1578. doi: 10.3390/ani11061578
12. Suzuki R, Mochizuki Y, Yuchi Y, Yasumura Y, Saito T, Teshima T, et al. Assessment of myocardial function in obstructive hypertrophic cardiomyopathy cats with and without response to medical treatment by carvedilol. *BMC Vet Res.* (2019) 15:1–8. doi: 10.1186/s12917-019-2141-0
13. Abbott JA, Maclean HN. Two-dimensional echocardiographic assessment of the feline left atrium jonathan. *J Vet Intern Med.* (2006) 20:111–9. doi: 10.1111/j.1939-1676.2006.tb02830.x
14. Schober KE, Savino SI, Yildiz V. Right ventricular involvement in feline hypertrophic cardiomyopathy. *J Vet Cardiol.* (2016) 18:297–309. doi: 10.1016/j.jvc.2016.08.001
15. Visser LC, Sloan CQ, Stern JA. Echocardiographic assessment of right ventricular size and function in cats with hypertrophic cardiomyopathy. *J Vet Intern Med.* (2017) 31:668–77. doi: 10.1111/jvim.14688
16. Heckman JJ, Pinto R, Savelyev PA. Pulsed tissue doppler imaging in normal cats and cats with hypertrophic cardiomyopathy. *Angew Chemie Int.* (1967) 6:951–2
17. Suzuki R, Matsumoto H, Teshima T, Koyama H. Noninvasive clinical assessment of systolic torsional motions by two-dimensional speckle-tracking echocardiography in dogs with myxomatous mitral valve disease. *J Vet Intern Med.* (2013) 27:69–75. doi: 10.1111/jvim.12024
18. Schober KE, Hart TM, Stern JA, Li X, Samii VF, Zekas LJ, et al. Detection of congestive heart failure in dogs by doppler echocardiography. *J Vet Intern Med.* (2010) 24:1358–1368. doi: 10.1111/j.1939-1676.2010.0592.x
19. Chetboul V, Passavin P, Trehiou-Sechi E, Gouni V, Poissonnier C, Pouchelon JL, et al. Clinical, epidemiological and echocardiographic features and prognostic factors in cats with restrictive cardiomyopathy: a retrospective study of 92 cases (2001-2015). *J Vet Intern Med.* (2019) 33:1222–31. doi: 10.1111/jvim.15464
20. Linney CJ, Dukes-Mcewan J, Stephenson HM, López-Alvarez J, Fonfara S. Left atrial size, atrial function and left ventricular diastolic function in cats with hypertrophic cardiomyopathy. *J Small Anim Pract.* (2014) 55:198–206. doi: 10.1111/jsap.12186
21. Tsang TS, Barnes ME, Gersh BJ, Bailey KR, Seward JB. Left atrial volume as a morphophysiologic expression of left ventricular diastolic dysfunction and relation to cardiovascular risk burden *Am J Cardiol.* (2002) 90:1284–9. doi: 10.1016/S0002-9149(02)02864-3
22. Bauer F, Shiota T, White RD, Lever HM, Qin JX, Drinko J, et al. Determinant of left atrial dilation in patients with hypertrophic cardiomyopathy: a real-time 3-dimensional echocardiographic study. *J Am Soc Echocardiogr.* (2004) 17:968–975. doi: 10.1016/j.echo.2004.05.018
23. Wang J, Khoury DS, Yue Y, Torre-Amione G, Nagueh SF. Preserved left ventricular twist and circumferential deformation, but depressed longitudinal and radial deformation in patients with diastolic heart failure. *Eur Heart J.* (2008) 29:1283–9. doi: 10.1093/eurheartj/ehn141
24. Mizuguchi Y, Oishi Y, Miyoshi H, Iuchi A, Nagase N, Oki T. Concentric left ventricular hypertrophy brings deterioration of systolic longitudinal, circumferential, and radial myocardial deformation in hypertensive patients with preserved left ventricular pump function. *J Cardiol.* (2010) 55:23–33. doi: 10.1016/j.jjcc.2009.07.006
25. Suzuki R, Matsumoto H, Teshima T, Koyama H. Clinical assessment of systolic myocardial deformations in dogs with chronic mitral valve insufficiency using two-dimensional speckle-tracking echocardiography. *J Vet Cardiol.* (2013) 15:41–9. doi: 10.1016/j.jvc.2012.09.001
26. Mizuguchi Y, Oishi Y, Miyoshi H, Iuchi A, Nagase N, Oki T. The functional role of longitudinal, circumferential, and radial myocardial deformation for regulating the early impairment of left ventricular contraction and relaxation in patients with cardiovascular risk factors: a study with two-dimensional strain imaging. *J Am Soc Echocardiogr.* (2008) 21:1138–44. doi: 10.1016/j.echo.2008.07.016
27. Finocchiaro G, Knowles JW, Pavlovic A, Perez M, Magavern E, Sinagra G, et al. Prevalence and clinical correlates of right ventricular dysfunction in patients with hypertrophic cardiomyopathy. *Am J Cardiol.* (2014) 113:361–7. doi: 10.1016/j.amjcard.2013.09.045
28. Haddad F, Doyle R, Murphy DJ, Hunt SA. Right ventricular function in cardiovascular disease, part II: pathophysiology, clinical importance, and management of right ventricular failure. *Circulation.* (2008) 117:1717–31. doi: 10.1161/CIRCULATIONAHA.107.653584
29. Le Tourneau T, Deswarte G, Lamblin N, Foucher-Hossein C, Fayad G, Richardson M, et al. Right ventricular systolic function in organic mitral regurgitation impact of biventricular impairment. *Circulation.* (2013) 127:1597–608. doi: 10.1161/CIRCULATIONAHA.112.000999
30. Meluzin J, Spinarová L, Hude P, Krejcí J, Kincl V, Panovský R, et al. Prognostic importance of various echocardiographic right ventricular

functional parameters in patients with symptomatic heart failure. *J Am Soc Echocardiogr.* (2005) 18:435–44. doi: 10.1016/j.echo.2005.02.004
31. De Groote P, Millaire A, Foucher-Hossein C, Nugue O, Marchandise X, Ducloux G, et al. Right ventricular ejection fraction is an independent predictor of survival in patients with moderate heart failure. *J Am Coll Cardiol.* (1998) 32:948–54. doi: 10.1016/S0735-1097(98)00337-4
32. Kaye BM, Borgeat K, Mõtsküla PF, Luis Fuentes V, Connolly DJ. Association of tricuspid annular plane systolic excursion with survival time in boxer dogs with ventricular arrhythmias. *J Vet Intern Med.* (2015) 29:582–8. doi: 10.1111/jvim.12572
33. Nakamura K, Morita T, Osuga T, Morishita K, Sasaki N, Ohta H, et al. Prognostic value of right ventricular tei index in dogs with myxomatous mitral valvular heart disease. *J Vet Intern Med.* (2016) 30:69–75. doi: 10.1111/jvim.13820
34. Saito T, Suzuki R, Yuchi Y, Teshima T, Matsumoto H, Koyama H. Early detection of myocardial dysfunction in a cat that gradually progressed to endomyocardial form of restrictive cardiomyopathy. *BMC Vet Res.* (2021) 17:274. doi: 10.1186/s12917-021-02987-7
35. Hiemstra YL, Debonnaire P, Bootsma M, Schalij MJ, Bax JJ, Delgado V, et al. Prevalence and Prognostic Implications of Right Ventricular Dysfunction in Patients With Hypertrophic Cardiomyopathy. *Am J Cardiol.* (2019) 124:604–12. doi: 10.1016/j.amjcard.2019.05.021
36. Yuchi Y, Suzuki R, Kanno H, Teshima T, Matsumoto H, Koyama H. Right ventricular myocardial adaptation assessed by two-dimensional speckle tracking echocardiography in canine models of chronic pulmonary hypertension. *Front Vet Sci.* (2021) 8:727155. doi: 10.3389/fvets.2021.727155
37. Patata V, Caivano D, Porciello F, Rishniw M, Domenech O, Marchesotti F, et al. Pulmonary vein to pulmonary artery ratio in healthy and cardiomyopathic cats. *J Vet Cardiol.* (2020) 27:23–33. doi: 10.1016/j.jvc.2019.12.001

Conflict of Interest: The authors declare that the research was conducted in the absence of any commercial or financial relationships that could be construed as a potential conflict of interest.

Publisher's Note: All claims expressed in this article are solely those of the authors and do not necessarily represent those of their affiliated organizations, or those of the publisher, the editors and the reviewers. Any product that may be evaluated in this article, or claim that may be made by its manufacturer, is not guaranteed or endorsed by the publisher.

frontiers in Veterinary Science

ORIGINAL RESEARCH
published: 02 December 2021
doi: 10.3389/fvets.2021.773035

Measurement of Pulmonary Artery Wave Reflection Before and After Mitral Valvuloplasty in Canine Patients With Pulmonary Hypertension Caused by Myxomatous Mitral Valve Disease

Tomohiko Yoshida[1,2]*, *Kazumi Shimada*[2], *Lina Hamabe*[2], *Tsuyoshi Uchide*[2], *Ryou Tanaka*[2] *and Katsuhiro Matsuura*[1,2]*

[1] Veterinary Centers of America (VCA) Japan Shiraishi Animal Hospital, Saitama, Japan, [2] Department of Veterinary Surgery, Tokyo University of Agriculture and Technology, Fuchu, Japan

OPEN ACCESS

Edited by:
Micaela Sgorbini,
University of Pisa, Italy

Reviewed by:
Matheus Matioli Mantovani,
Federal University of Uberlandia, Brazil
Ryohei Suzuki,
Nippon Veterinary and Life Science University, Japan

***Correspondence:**
Katsuhiro Matsuura
k.matsuura.vet@gmail.com
Tomohiko Yoshida
tomohiko7731-yoshida@yahoo.co.jp

Specialty section:
This article was submitted to Comparative and Clinical Medicine, a section of the journal Frontiers in Veterinary Science

Received: 09 September 2021
Accepted: 05 November 2021
Published: 02 December 2021

Citation:
Yoshida T, Shimada K, Hamabe L, Uchide T, Tanaka R and Matsuura K (2021) Measurement of Pulmonary Artery Wave Reflection Before and After Mitral Valvuloplasty in Canine Patients With Pulmonary Hypertension Caused by Myxomatous Mitral Valve Disease. Front. Vet. Sci. 8:773035. doi: 10.3389/fvets.2021.773035

Background: Pulmonary arterial wave reflection provides novel information about pulmonary artery hemodynamics in pulmonary hypertension (PH). PH is common in dogs with myxomatous mitral valve disease (MMVD), though research examining the relationship between pulmonary arterial wave reflection and MMVD with PH is lacking.

Hypothesis/Objective: This study investigated conventional echocardiographic parameters and pulmonary artery wave reflection parameters before and after mitral valvuloplasty in canine patients with PH due to MMVD. The parameters were backward pressure (Pb), forward pressure (Pf), and the reflection coefficient calculated as the ratio of peak Pb to peak Pf (RC).

Animals: The study subjects were 10 client-owned dogs receiving mitral valvuloplasty for MMVD with PH.

Methods: Conventional echocardiographic parameters and pulmonary artery wave reflection parameters were measured before and after mitral valvuloplasty. The relationships between pulmonary artery wave reflection parameters and echocardiographic parameters, estimation of pulmonary artery systolic pressure, and right atrium pressure (RAP) gained by catheter in mitral valvuloplasty were also investigated. Post-operative echocardiography and the measurement of pulmonary arterial wave reflection were performed 2 weeks after mitral valvuloplasty.

Results: The parameters of normalized left ventricular internal diameter at end-diastole (LVIDDN), E velocity, and the estimation of pulmonary artery systolic pressure were significantly reduced post-operatively compared with baseline measurements ($p < 0.05$). Post-operative Pb decreased significantly compared with pre-operative measurements (8.8 ± 5.9 to 5.0 ± 3.2 mmHg, $p = 0.037$) as did RC (0.37 ± 0.15 to 0.22 ± 0.11, $p < 0.01$). A statistically significant positive correlation existed between wave reflection parameters and RAP, an estimation of pulmonary artery systolic pressure.

Conclusions: Results demonstrate that mitral valvuloplasty can be used to treat secondary PH caused by MMVD, resulting in the improvement of post-operative echocardiographic and wave reflection parameters and a decrease in the right afterload. In some patients, some degree of vascular admittance mismatch persisted, despite the improvement of left atrial pressure. This may be indicative of residual pulmonary arterial disease, which may continue to adversely affect interactions between the right ventricle and the vasculature.

Keywords: mitral valvuloplasty, pulmonary artery wave reflection, wave separation analysis, pulmonary hypertension, non-invasive methods of measurement

INTRODUCTION

Myxomatous mitral valve degeneration (MMVD) is the most common heart disease in dogs, with severe MMVD causing congestive heart failure, resulting in death within a year (1, 2). Medical treatment has been shown to improve the clinical conditions and prolong the lifespan of dogs with congestive heart failure, as demonstrated in several clinical trials and studies in recent years (3). As medical treatment for MMVD with cardiovascular drugs is palliative, however, MMVD is progressive and the prognosis is poor (2). In addition, persistent increasing left atrial pressure can cause pulmonary hypertension (PH) (4, 5). PH generated from left heart failure is classified into either reactive post-capillary-PH [pulmonary vascular resistance (PVR) $\geq$2.5 wood units (WU), and transpulmonary pressure gradient (TPPG) $>$12 mmHg] and passive post-capillary-PH (PVR $\geq$2.5 WU and TPPG $\leq$12 mmHg) (6–8). Reactive post-capillary-PH is caused by a chronic increase in pulmonary artery pressure, which involves physiologically active substances such as Endothelin-1, and the remodeling of pulmonary artery blood vessels (9, 10). Reactive post-capillary-PH is considered to have a poor prognosis; despite improvements in left atrial pressure through surgery and drug therapy, pulmonary artery pressure is not improved (10–13). Thus, it is very important to detect reactive post-capillary-PH. In human medicine, surgical mitral valvuloplasty (MVP) and valve replacement are performed to radically treat PH caused by left heart failure (14–18). In small animal medicine, MVP is often selected in consideration of the need for permanent antithrombotic therapy and biocompatibility (19). Although the treatment results of mitral valve reconstruction have improved, the prognosis after MVP is poor in cases with reactive post-capillary-PH in which remodeling occurs in the pulmonary artery. Therefore, assessing the pathophysiology of pulmonary hypertension is very important. In recent years, several studies have reported that pulmonary arterial wave reflection may provide additional information about right ventricular afterload and can be a useful indicator in assessing the pathophysiology of pulmonary hypertension (20, 21). Pulmonary artery wave reflection occurs when the forward blood flow out the right ventricle is reflected by the pulmonary arterial tree, generating a backward wave (22, 23). The method of estimating the magnitude of pulmonary artery wave reflection is to separate pulmonary artery pulse pressure into its forward and backward components by wave separation analysis (24, 25). This analysis requires measurements of both pressure and flow velocity waveforms simultaneously (20, 25). A previous paper proposed that measuring pulmonary artery wave reflection can be carried out non-invasively by estimating the pulmonary artery pulse pressure from tricuspid regurgitation (TR) velocity and evaluating the pattern of flow profile at the right ventricular outflow tract (RVOT). In addition, the pulmonary artery wave reflection gained by Doppler echocardiography also can be related to the prognosis of PH in a small animal clinical environment (26).

This study evaluated the change in pulmonary artery wave reflection before and after MVP in canine patients with PH due to MMVD. In addition, we investigated the relationship between the pulmonary artery wave reflection and cases with residual post-operative PH by measuring pulmonary artery wave reflection before and after MVP in patients with PH due to MMVD.

Abbreviations: AcT, acceleration time; ACVIM, American college of veterinary internal medicine; AO, aortic; BSA, body surface area; CTEPH, chronic thromboembolic pulmonary hypertension; ET, ejection time; LVIDDN, normalized left ventricular internal diameter at end-diastole; MMVD, myxomatous mitral valve disease; MPA, main pulmonary artery; MVP, mitral valvuloplasty; LVIDd, left ventricular internal dimension in diastole; P, pressure; PAH, pulmonary artery hypertension; PAP, pulmonary artery pressure; Pb, backward pressure; Pf, forward pressure; PH, pulmonary hypertension; PVR, pulmonary vascular resistance; RAA index, right atrial area index; RAP, right atrium pressure; RC, reflection coefficient; ROC, receiver-operating characteristic; RVEDA index, right ventricular end-diastolic area index; RVOT, right ventricular outflow tract; SD, standard deviation; TR, tricuspid valve regurgitation; U, velocity; WRI, wave reflection indices.

MATERIALS AND METHODS

Animals

The study was carried out at a private clinic (SHIRAISHI Animal Hospital, Saitama, Japan) between August 2019 and April 2021. The subjects were 10 client-owned dogs receiving MVP exclusively for MMVD with suspected PH due to left heart disease. Permission for this study was granted by SHIRAISHI Animal Hospital Animal Care and Use Committee (protocol number R2-062). Before subject enrollment, written, informed client consent was obtained. All cases were classified with American College of Veterinary Internal Medicine (ACVIM) stage C or D, as determined through comprehensive evaluation including medical history and records, physical examination, hematology, serum biochemistry, diagnostic

electrocardiography, radiography, and echocardiography. MVP with cardiopulmonary bypass was performed in all cases.

The definitive diagnosis of PH requires right heart catheterization (RHC). However, given RHC is difficult to apply in small animals. Therefore, PH were suspected if a maximal TR velocity of ≥3.4 m/s was observed, based on ACVIM consensus, and if the dogs presented with PH-related clinical signs. PH was also suspected if a maximal TR velocity of ≥2.9 m/s was observed via Doppler echocardiographic assessment, or if other echocardiographic findings suggestive of PH were found in dogs with PH-related clinical signs. Other echocardiographic findings were defined as the flattening of the interventricular septum, especially systolic flattening, pulmonary artery enlargement, or systolic notching of the Doppler RV outflow profile (6). Clinical signs considered potentially related to PH included: syncope without another identifiable cause; respiratory distress at rest; activity or exercise terminating in respiratory distress; abdominal distention due to ascites; tachypnea at rest; increased respiratory effort at rest; prolonged post-exercise or post-activity tachypnea; and cyanotic or pale mucous membranes (6). If the patient included above criteria after surgery, we judged the patient to be persistent PH.

The main causes of precapillary (heartworm disease, pulmonary embolism, chronic respiratory diseases, etc.) were excluded using blood examination, ultrasonogram, thorax radiography as much as possible without hemodynamic examination by catheter.

Study Protocol

Conventional echocardiographic parameters and pulmonary artery wave reflection parameters were measured before and after MVP. The relationships between pulmonary artery wave reflection parameters and echocardiographic parameters, right atrium pressure (RAP) gained by catheter, and pulmonary artery systolic pressure gained by echo-Doppler were also investigated. Echocardiography and measurement of pulmonary artery wave reflection were performed 2 weeks after MVP.

Principles Underlying the Echo-Doppler Method of Assessing Pulmonary Artery Wave Reflection

Pulmonary artery wave reflection can be obtained by simultaneously measuring pulmonary artery pressure and flow velocity. Previous research, however, reported that wave reflection as measured by Doppler echocardiography correlated with wave reflection measured by catheter, indicating that wave reflection can also be measured in this manner. The pulmonary artery wave reflection was calculated by measuring the TR flow and RVOT using Doppler echocardiography by the same method as in the previous paper (26). The method of calculating pulmonary artery wave reflection from Doppler echocardiography is briefly described; pulmonary artery wave reflection can be analyzed based on the concept of wave intensity analysis, which determines the origin, type, and timing of traveling waves in circulation by combining measurements of pressure (P) and velocity (U) (27). This allows the wave to be separated into forward-traveling and backward-traveling components (24, 27, 28). Wave speed, which represents the local elastic properties of the artery, can be calculated by the P-U loop method (29). This takes advantage of the water hammer equation for the relationship between P and U under conditions with no wave reflection.

$$c = (dP / dU) / \rho \quad (1)$$

where dP is the temporal change in P, dU is the temporal change in U, ρ is the blood density (1,050 kg/m^3), and c is the wave speed. Pressure attributed to forward-traveling (forward pressure; Pf) and backward-traveling (backward pressure; Pb) waves can be separated using Equations (2) and (3). Backward-traveling waves indicate pulmonary artery wave reflection.

$$dPf = (dP + \rho c\, dU) / 2 \quad (2)$$

$$dPb = (dP - \rho c\, dU) / 2 \quad (3)$$

where dPf is the temporal change in Pf and dPb is the temporal change in Pb. Pf and Pb can then be determined as the total sum of these differences.

$$Pf = \Sigma dPf \quad (4)$$

$$Pb = \Sigma dPb \quad (5)$$

The non-invasive method proposed for the assessment of pulmonary artery wave reflection adopts echo-Doppler-derived P and U values rather than direct measurements. The P waveform is estimated from a continuous-wave Doppler tracing of TR, using the simplified Bernoulli equation. Once the right atrial pressure was assumed to be constant, the temporal change in P (dP) could be calculated using only the instantaneous pressure gradient of TR. In contrast, the U waveform was obtained by measuring flow at the right ventricular RV outflow tract (RVOT), using pulsed-wave Doppler. The calculations were performed throughout the ejection period. Wave separation analysis is performed on the pulse pressure and flow velocity waveforms by synchronizing waveforms of TR flow and RVOT flow using electrocardiogram. This analysis resulted in the determination of three wave reflection indices: Pb, Pf, and the reflection coefficient (RC), which was calculated as peak Pb/peak Pf. These waveforms were smoothened using a Savitzky–Golay filter and then ensemble-averaged over three cardiac cycles with reference to the R wave on the electrocardiogram. The calculations were performed using an in-house program code, written in MATLAB (MathWorks 2019b, Massachusetts, USA).

Echocardiography

The echocardiographic assessment was carried out while the subject was maintained in lateral recumbency and examined under standard conditions, using an Aplio^{TM} 300 with a sector probe of five MHz (Canon medical system, Tokyo, Japan). Analysis of pulmonary artery wave reflection was also performed by same echocardiography machine. Three consecutive heartbeats were recorded at the end of the expiratory phase. To evaluate structural and functional changes during

the course of reverse remodeling of the left atrium and the left ventricle, combined conventional echocardiography protocol including Two-dimensional, M-mode, Doppler blood flow, and tissue Doppler imaging techniques from the right and left parasternal long- and short-axes views were carried out (30, 31). The following parameters were measured at each time interval: normalized left ventricular internal dimension in diastole (LVIDDN); the ratio of the left atrial dimension to the aortic annulus dimension (LA/Ao); fractional shortening (FS); early diastolic mitral inflow (E) velocity; the ratio of peak velocity of early diastolic transmitral flow to peak velocity of late diastolic transmitral flow (E:A); systolic ($S^{'}$), early diastolic ($E^{'}$), and late diastolic ($A^{'}$) wave signals as measured by Tissue Doppler imaging at septum (sep) and left ventricular lateral (lat) wall, respectively. LVIDDN was calculated from the left ventricular internal dimension in diastole (LVIDd) and the bodyweight was measured concurrently by an established allometric formula (30). TR velocity, obtained by continuous-wave Doppler, was measured from the view that allowed the clearest envelope of the TR velocity and maximum speed (6). The flattening of the interventricular septum was identified on M-mode images from the right parasternal short-axis view (32). The RVOT and main pulmonary artery-to-aortic root diameter ratio (MPA:AO) were measured from the standard right parasternal short-axis view (2, 33). RVOT flow was assessed with pulse-wave Doppler and obtained by placing the sample volume (2 mm) centrally between the opened pulmonary valve leaflets. Ejection time (ET), acceleration time (AcT), and AcT:ET ratio were assessed using RVOT flow profiles as follows. The AcT was measured as the time between the onset of the Doppler flow signal to the peak flow velocity. ET was measured from the onset of the Doppler RVOT signal to the end of the signal, and the AcT:ET ratio was calculated (33, 34). In all dogs, the echocardiographic characterization of the RA and RV were obtained from the left apical 4-chamber view optimized for the right heart. The right atrial area (RAA) was measured by planimetry at the end of the ventricular systole tracing from the lateral aspect of the tricuspid annulus to the septal aspect, excluding the area between the leaflets and annulus, following the RA endocardium, and excluding the caudal vena cava, cranial vena cava, and RA appendage. The RAA index was calculated as RAA divided by body surface area (BSA). Right ventricular end-diastolic area index (RVEDA) was measured by planimetry at the end of ventricular diastole, tracing from the lateral aspect of the tricuspid annulus to the septal aspect, excluding the area of the annulus and trabecular structures, following the RV endocardium. The RVEDA index was calculated as the ratio of RVEDA and BSA. The BSA was calculated as following equation.

$$\text{BSA} = 0.101 \times \text{body weight (kg)}^{2/3}$$

The end-diastolic MPA diameter was measured just below the closed pulmonary valve, with the aortic diameter being measured from the same view, and through this the MPA:AO ratio was calculated. Pulmonary artery systolic pressure (sPAP) was estimated by applying the simplified Bernoulli equation to a continuous-wave Doppler tracing of TR flow and adding a term of right atrial pressure as below.

$$\text{Estimated sPAP} = 4 \times (\text{TR velocity})2 + \text{RAP}$$

The RAP was measured at the time of MVP invasively.

Surgical Procedure

Atropine (Atropine Sulfate injection; Mitsubishi Tanabe Pharma Corporation, Osaka, Japan, 0.05 mg/kg, SC), fentanyl (Fentanyl Citrate; Daiichi Sankyo Company, Limited, Tokyo, Japan, 5 μg/kg, IV), and midazolam hydrochloride (Dormicum; Astellas Pharma Inc., Tokyo, Japan, 0.2 mg/kg, IV), were administered pre-operatively. Anesthesia was induced with propofol 1% (Propofol Mylan; Mylan Seiyaku, Tokyo, Japan, 6 mg/kg bolus, IV) and maintained with 1–2 vol% of isoflurane (Isoflurane for Animal Use; Intervet, Osaka, Japan) in 100% oxygen.

The patient was placed in right lateral recumbency. The right femoral artery and vein were cannulated for measurement of atrial pressure (RAP). After patients were heparinized at a dose of 400 U/kg, the left carotid artery and jugular vein were cannulated for cardiopulmonary bypass (CPB). activated clotting time was used for determining the anticoagulant effect of heparin. Cardiac arrest was achieved by aortic clamping followed by the administration of cardioplegia from an aortic root cannula. MVP was performed as previously described. In brief, the left atrium was approached through a fifth intercostal thoracotomy and left auricle incision. The MVP is consisted of artificial chordae tendineae reconstruction and mitral annuloplasty, using expanded polytetrafluoroethylene. After the closure of the left atrium, the aorta was unclamped and sinus rhythm was restored. Patients were weaned from CPB after conducting modified ultrafiltration and confirming the stability of the hemodynamic system. A constant-rate infusion of protamine 4 mg/kg was administered for 30 min through the cephalic vein. The activated clotting time was measured after the end of the protamine infusion. After confirming that the protamine was antagonized, the chest was closed according to the standard method, and the crotch and cervical arteries and veins were anastomosed to finish the operation.

Statistical Analysis

Continuous data are expressed as the mean ± standard deviation (SD). Categorical data are expressed as a number and percentage. The level of significance was set to $p < 0.05$. The normal distribution of the data was evaluated using a Kolmogorov–Smirnov test. The assumption of homogeneity of variances was determined by Bartlett's test. For normally distributed parameters, differences between groups were analyzed using a paired *t*-test. For non-parametric statistics, differences between groups were analyzed using a Wilcoxon matched-pairs signed-rank test. Spearman's correlation coefficients and multivariate linear regression analysis were used to assess the relationship between the pulmonary artery wave reflection parameters and echocardiographic parameters, and the hemodynamic parameters gained by catheter. Statistical analyses were performed using GraphPad Prism 8.0 (GraphPad Software, San Diego, California, USA).

TABLE 1 | Conventional echocardiography parameters before and after mitral valvuloplasty.

Conventional echo parameter	Pre-operative	Post-operative	*P*-value
LVIDd, mm	34.6 ± 5.1	23.6 ± 4.05	<0.01
LVIDDN	2.27 ± 0.26	1.52 ± 0.19	<0.01
LA/Ao	2.33 ± 0.28	1.52 ± 0.18	<0.01
FS (%)	49.4 ± 6.2	32.6 ± 6.1	<0.01
E velocity, cm/s	139.3 ± 24.2	77.98 ± 13.3	<0.01
E:A	1.5 ± 0.42	0.77 ± 0.22	<0.01
E′ sep, cm/s	8.6 ± 2.6	5.3 ± 1.67	0.04
A′ sep, cm/s	6.9 ± 0.73	5.5 ± 2.28	0.08
E:E′ sep, cm/s	17.2 ± 4.6	16.8 ± 6.23	0.7
E′ lat, cm/s	8.7 ± 1.6	5.47 ± 1.07	<0.01
A′ lat, cm/s	7.9 ± 2.7	4.9 ± 1.55	<0.01
E:E′ lat, cm/s	16.8 ± 6	15.03 ± 3.13	0.56
RVOT velocity, cm/s	78.6 ± 19.1	106 ± 19.1	0.04
AcT:ET	0.4 ± 0.09	0.52 ± 0.05	0.16
MPA:Ao	1.02 ± 0.13	1.01 ± 0.1	0.39
TR velocity, m/sec	3.79 ± 0.49	2.81 ± 0.39	<0.01
RAA index	7.7 ± 3.5	6.6 ± 1.7	0.69
RVEDA index	10.0 ± 3.5	8.9 ± 3.1	0.37

Data are expressed as means ±. P-values represent significant statistical differences between pre-operative and post-operative echo parameters.
A′, late diastolic wave signal as measured by Tissue Doppler imaging; E velocity, early diastolic mitral inflow velocity; E′, early diastolic wave signal as measured by Tissue Doppler imaging; E:A, the ratio of peak velocity of early diastolic transmitral flow to peak velocity of late diastolic transmitral flow; FS, fractional shortening; LA/Ao, the ratio of the left atrial dimension to the aortic annulus dimension; lat, mitral annulus at the left ventricular lateral wall; LVIDd, left ventricular internal dimension in diastole; LVIDDN, normalized left ventricular internal dimension in diastole; MPA/AO, main pulmonary artery/aorta; RAA index, right atrial area index; RVEDA index, right ventricular end-diastolic area index; RVOT, right ventricular outflow tract; S′, systolic wave signal as measured by Tissue Doppler imaging; sep, mitral annulus at the septal wall; TR, tricuspid regurgitation.

RESULTS

Study Population

A total of 10 dogs were the subject of this study, aged 9.6 ± 2.3 years old (range 7−14 years), and with a bodyweight of 4.6 ± 2.1 kg (range 2.4−10 kg). Breeds were Cavalier King Charles spaniel ($n = 1$), Chihuahua ($n = 4$), Maltese ($n = 1$), miniature dachshund ($n = 1$), mixed-breed ($n = 2$), Shiba Inu ($n = 1$). In accordance with the ACVIM classifications scheme, seven and three dogs were diagnosed with stage C and D ACVIM, respectively. When first diagnosed, 30% of patients had syncope, 20% of patients had ascites and/or pleural effusion. In addition, 20% of PH cases presented with septal flattening, and 30% had a notch in the pulmonary artery waveform at the initial visit. Before surgery, pimobendan and a diuretic drug had been prescribed in all dogs and sildenafil had been prescribed in only one dog. All canine subjects were discharged post-operatively within 2 weeks and in medication affecting hemodynamics (diuretics, inotropes, etc.) were discontinued. However, after hospitalization, two cases were prescribed sildenafil 0.5 mg/kg BID (sildenafil: Camber Pharmaceuticals, Inc., New Jersey, USA) due to presenting symptoms and echocardiography findings associated with PH. Two dogs with persistent PH after MVP presented with the flattening of the interventricular septum, however, TR was mild (TR velocity 3.0 m/s in both PH patient).

Conventional Echocardiographic Parameters Before and After MVP

Conventional echocardiographic data before and after MVP are summarized in **Table 1**. Compared with baseline measurements, the following were significantly reduced ($p < 0.05$) post-operatively: LVIDd, LVIDDN, LA/Ao, FS, E velocity, E′ sep, E′ lat, A′ lat, RVOT, and TR velocity. Echocardiography revealed a

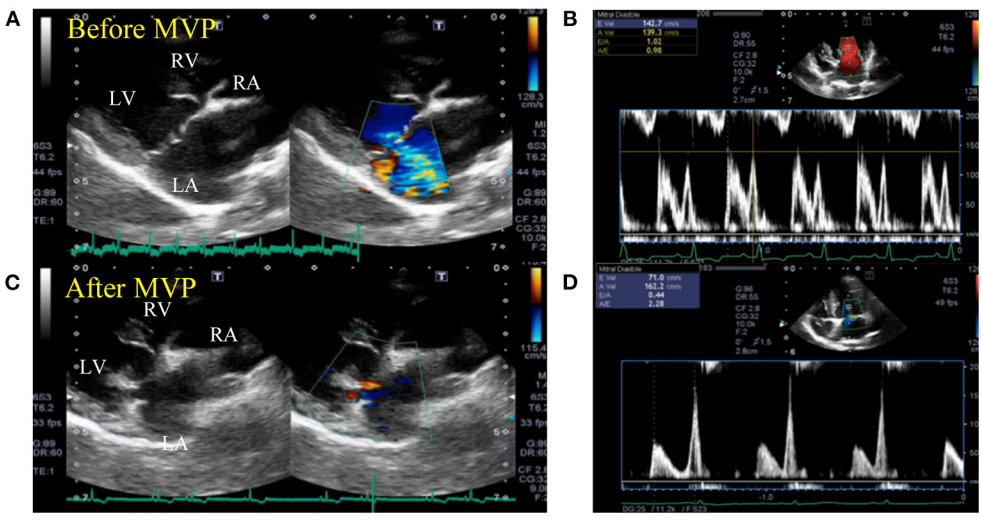

FIGURE 1 | Representative echocardiogram images before and after mitral valvuloplasty. Two-dimensional echocardiography at the long-axis LV inflow view showing the enlarged left ventricle and atrium chamber **(A)** and elevated mitral inflow velocity **(B)** before mitral valvuloplasty. The cardiac functional parameters were greatly restored, with reduced left ventricular and atrium lumen size **(C)** and mitral inflow velocities **(D)** after mitral valvuloplasty. LA, left atrium; LV, left ventricle; RA, right atrium; RV, right ventricle.

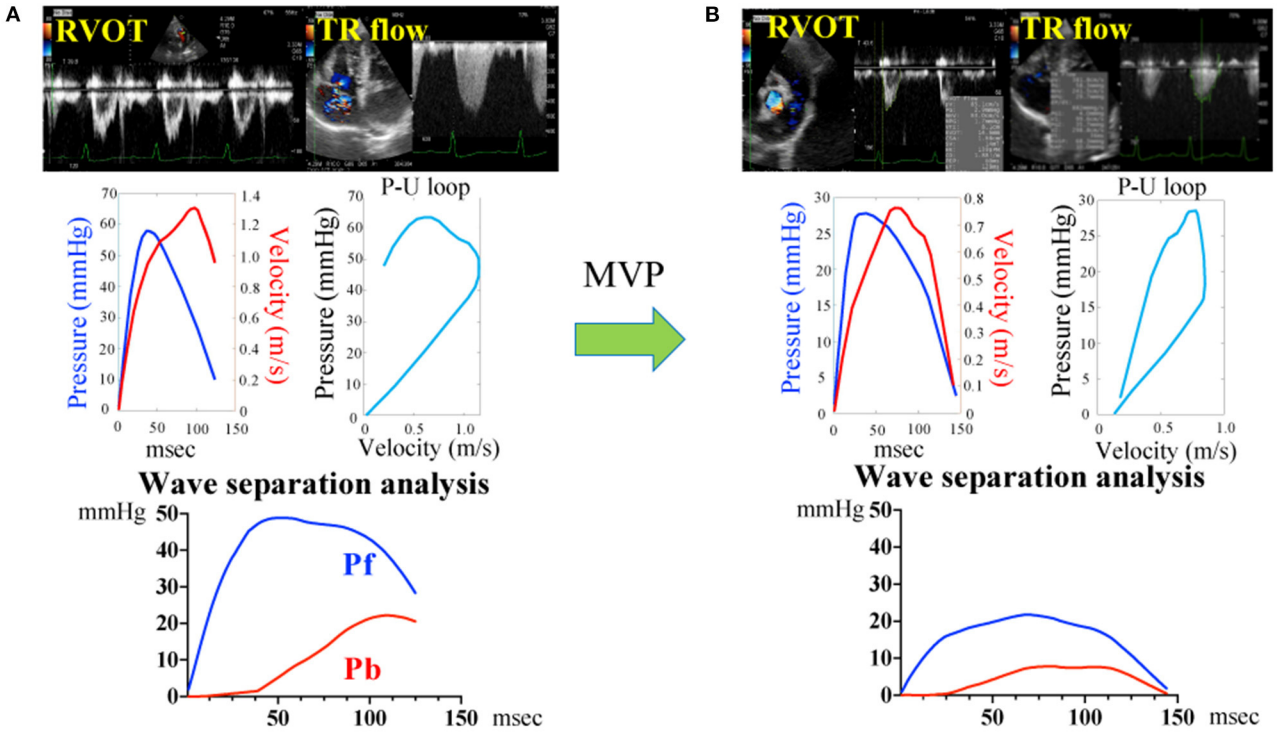

FIGURE 2 | Pulmonary artery wave reflection measured by representative original trace using Doppler echocardiography before **(A)** and after **(B)** mitral valvuloplasty. Pressure (P) information was gained from the TR flow using the Bernoulli equation and the flow velocity (U) information was gained from the RVOT. Determination of the P-V loop from P and U. Pulmonary artery wave reflection parameters were gained by wave separation analysis. Pf, forward pressure; Pb, backward pressure; P-U loop, pressure-flow loop; RVOT, right ventricular outflow tract; TR, tricuspid valve regurgitation flow.

TABLE 2 | Wave reflection parameters before and after mitral valvuloplasty.

Wave reflection parameter	Pre-operative	Post-operative	*P*-value
Forward pressure (Pf), mmHg	23.6 ± 11.7	21.0 ± 6.4	0.77
Backward pressure (Pb), mmHg	8.8 ± 5.9	5.0 ± 3.2	0.037
Reflection coefficient (RC = Pb:Pf)	0.37 ± 0.15	0.22 ± 0.11	<0.01

Data are expressed as means ±. P-values represent significant statistical differences between pre-operative and post-operative wave reflection parameters. Pb, backward pressure; RC, reflection coefficient.

reduction in the left-sided chamber size and stable mild mitral regurgitation after MVP in all dogs (**Figure 1**).

Pulmonary Artery Wave Reflection Parameters Before and After MVP

Figure 2 and **Table 2** show the representative assessment method of pulmonary artery wave reflection, and pulmonary artery wave reflection parameters before and after MVP. Post-operative Pb and RC decreased significantly compared with pre-operative measurements (**Table 2**, Pb decreased from 8.8 ± 5.9 to 5.0 ± 3.2 mmHg, $p = 0.037$; RC also decreased from 0.37 ± 0.15 to 0.22 ± 0.11, $p < 0.01$).

Figure 3 represents the individual change in pulmonary artery wave reflection parameters and TR velocity, RAA index, RVEDA index for each dog before and after MVP. The red dots represent the two dogs in which PH remained after MVP surgery. When looking at the individual change in pulmonary artery wave reflection parameters for each dog, Pb and RC were significantly decreased after MVP in almost all dogs. However, two dogs in which PH persisted after MVP (red dots) had higher Pb (12.1 and 9.34 mmHg) and RC (0.49 and 0.32) compared with the other dogs (black dots). On the other hand, TR and RAA index, RVEDA index of these two dogs were not so high compared with the other dogs.

Correlation Between the Pulmonary Artery Wave Reflection Parameter, Echocardiographic Parameters, and RAP

Table 3 summarizes the correlation results between the pulmonary artery wave reflection parameters and hemodynamic parameters, and echocardiographic parameters before MVP. There was no correlation between Pf, RC and RAP, Estimated sPAP (**Table 3** and **Figures 4A,D,F**, Pf vs. RAP, $r = 0.5$, $p = 0.22$; Pf vs. Estimated sPAP, $r = 0.58$, $p = 0.08$; RC vs. Estimated sPAP, $r = 0.2$, $p = 0.58$). On the other hands, there was a statistically significant positive correlation between 676 Pb, RC, and RAP, Estimated sPAP (**Table 3** and **Figures 4B,C,E**, Pb vs. RAP, $r = 0.76$, $p = 0.014$; Pb vs. Estimated sPAP, $r = 0.76$, $p = 0.014$; RC vs. RAP, $r = 0.68$, $p = 0.03$). RAP and Estimated sPAP measured during surgery were 11 ± 2.8 mmHg and 69.5 ± 18.73 mmHg.

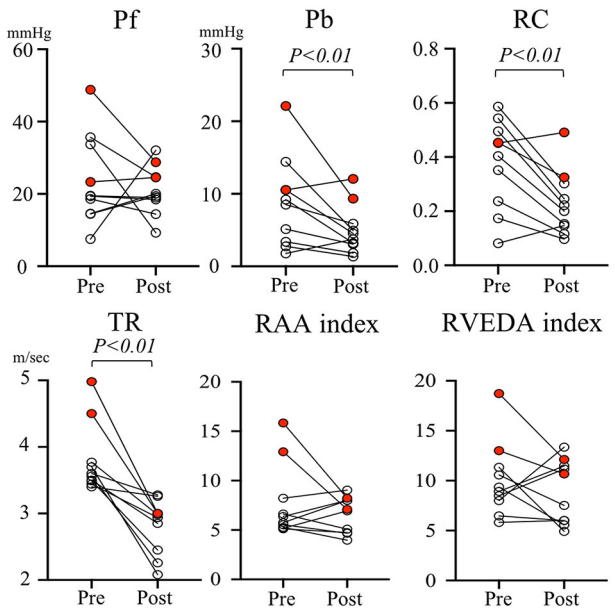

FIGURE 3 | Individual change in pulmonary artery wave reflection parameters and tricuspid valve regurgitation velocity and right atrial area index, right ventricular end-diastolic area index for each dog before and after mitral valvuloplasty. The red dots represent the two dogs in which PH remains after MVP surgery. Pb, backward pressure; Pf, forward pressure; RAA index, right atrial area index; RC, reflection coefficient which is calculated as the ratio of peak Pb to peak Pf; RVEDA index, right ventricular end-diastolic area index; TR, tricuspid valve regurgitation.

No significant correlation was identified between pulmonary artery wave reflection parameters and other echocardiographic parameters (**Table 3**).

The Effect of Pulmonary Artery Wave Reflection Parameters on Hemodynamic and Echocardiographic Parameters

Result of linear regression analysis of the parameters of pulmonary artery wave reflection, hemodynamic parameters are shown in **Table 4**. There was a significant effect of Pb on RAP, and Estimated sPAP (Pb vs. RAP, $R^2 = 0.54$, $p = 0.015$; Pb vs. Estimated sPAP, $R^2 = 0.44$, $p = 0.036$; RC vs. RAP), respectively. RC demonstrated significant effect on RAP and Estimated sPAP ($R^2 = 0.46$, $p = 0.03$; RC vs. Estimated sPAP, $R^2 = 0.042$, $p = 0.57$). Pb and RC did not significantly affect other parameters.

DISCUSSION

This study investigated both conventional echocardiographic parameters and pulmonary artery wave reflection parameters before and after MVP in patients with PH due to MMVD. Results indicated pulmonary artery wave reflection was closely related to PH that persisted despite treatment.

In recent years, cardiac surgery techniques in the small animal field have made great strides and MVP has contributed significantly to lowering left atrial pressure by improving mitral regurgitation caused by MMVD (35–37). Reduction of left atrial pressure by MVP is one of the treatments for secondary PH caused by MMVD, as a persistent increase in left atrial pressure induces PH (38, 39). MVP could be an effective treatment for MMVD with PH due to decreasing the following parameters after surgery: LVIDDN; LA/Ao; E velocity; E′ sep; E′ lat; TR velocity and wave reflection. In two cases, higher wave reflection was observed both before and after MVP, with the RC diminished only slightly following MVP in one dog, however, RC increased slightly in the other one. This finding suggests that despite improving the left atrial pressure caused by left heart failure after MVP, the remodeling of pulmonary artery vascular caused reactive PH in some patient. This may be indicative of residual pulmonary arterial disease, which may continue to adversely affect interactions between the right ventricle and the vasculature.

Pulmonary artery wave reflection occurs when the forward flow out of the right ventricle is reflected by the pulmonary arterial tree, generating a backward wave. Pulmonary artery wave reflection can be detected by measuring pulmonary artery flow and pressure simultaneously using wave intensity analysis. In particular, wave reflection is enhanced when the energy transmission property changes between the proximal and distal vasculature due to vascular remodeling, arteriosclerosis, or thrombus (20, 24, 40). Pulmonary artery wave reflection can potentially provide novel information regarding pulmonary hemodynamics to supplement traditional methods used to evaluate PH, such as PAP and PVR, which are the most common hemodynamic measurements used to evaluate its progression (20, 41, 42). Wave reflection is not typically applied in the small animal clinical setting as this requires catheterization. In this study, we could measure wave reflection non-invasively in MMVD cases with PH, as in recent years, wave

TABLE 3 | Correlation analysis between pulmonary artery wave reflection parameters and hemodynamic and echocardiographic parameters.

	Pb		RC	
	R	***P*-value**	***R***	***P*-value**
RAP	0.76*	0.014	0.68*	0.03
Estimated sPAP	0.66*	0.035	0.32	0.12
RVOT velocity	0.017	0.96	−0.2	0.59
E velocity	0.1	0.77	−0.03	0.94
LVIDDN	−0.42	0.22	0.15	0.67
E:e′ sep	0.41	0.23	0.2	0.59
E:e′ lat	−0.05	0.88	−0.24	0.5
TR velocity	0.6	0.07	0.1	0.78
RAA index	0.61	0.06	0.19	0.6
RVEDA index	0.33	0.35	0.18	0.6

E velocity, early diastolic mitral inflow velocity; e′, early diastolic wave signal as measured by Tissue Doppler imaging; lat, mitral annulus at the left ventricular lateral wall; LVIDDN, normalized left ventricular internal dimension in diastole; Pb, backward pressure; RAA index, right atrial area index; RC, reflection coefficient; RVEDA index, right ventricular end-diastolic area index; RVOT, right ventricular outflow tract; RAP, right atrial pressure; Estimated sPAP, estimated systolic pulmonary arterial pressure; sep, mitral annulus at the septal wall; TR velocity, tricuspid regurgitation flow velocity.
*$p < 0.05$.

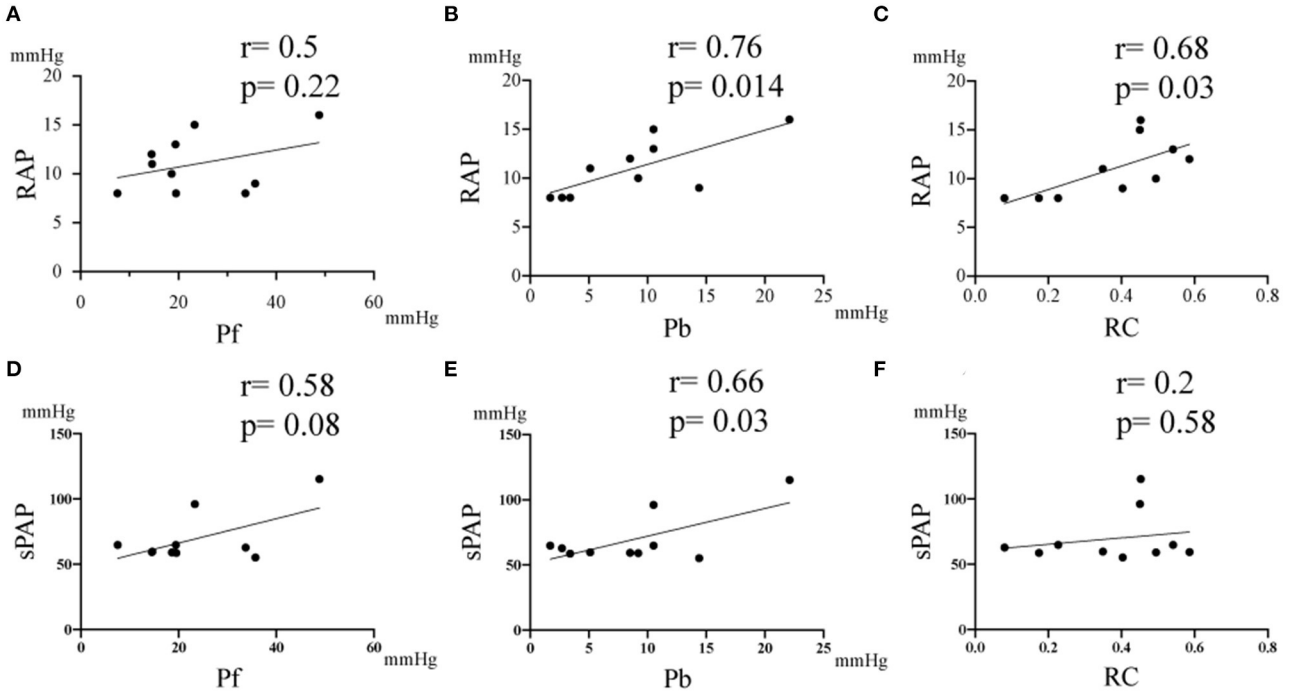

FIGURE 4 | Correlation between the pulmonary artery wave reflection parameter and right atrium pressure (RAP), and estimated systolic pulmonary artery pressure (sPAP). **(A)** Correlation between RAP vs Pf. **(B)** Correlation between RAP vs Pb. **(C)** Correlation between RAP vs RC. **(D)** Correlation between sPAP vs Pf. **(E)** Correlation between Estimated sPAP vs Pb. **(F)** Correlation between Estimated sPAP vs RC. RC, reflection coefficient which is calculated as the ratio of peak Pb to peak Pf; Pb, backward pressure; Pf, forward pressure; r, the correlation coefficient.

TABLE 4 | The effect of pulmonary artery wave reflection parameters on hemodynamic and echocardiographic parameters.

	Pb		RC	
	R^2	*P*-value	R^2	*P*-value
RAP	0.54*	0.015	0.46*	0.03
Estimated sPAP	0.44*	0.036	0.042	0.57
RVOT velocity	0.0003	0.96	0.04	0.59
E velocity	0.011	0.77	0.0007	0.94
LVIDDN	0.18	0.23	0.023	0.67
E:e′ sep	0.17	0.24	0.039	0.59
E:e′ lat	0.003	0.88	0.058	0.5
TR velocity	0.36	0.065	0.01	0.78
RAA index	0.374	0.06	0.03	0.06
RVEDA index	0.10	0.36	0.03	0.61

E velocity, early diastolic mitral inflow velocity; e′, early diastolic wave signal as measured by Tissue Doppler imaging; lat, mitral annulus at the left ventricular lateral wall; LVIDDN, normalized left ventricular internal dimension in diastole; Pb, backward pressure; RAA index, right atrial area index; RC, reflection coefficient; RVEDA index, right ventricular end-diastolic area index; RVOT, right ventricular outflow tract; RAP, right atrial pressure; Estimated sPAP, estimated systolic pulmonary arterial pressure; sep, mitral annulus at the septal wall; TR velocity, tricuspid regurgitation flow velocity.
*$p < 0.05$.

reflection has been calculated non-invasively through Doppler echocardiography (26).

In eight out of 10 cases, the post-operative Pb and RC decreased significantly compared with pre-operative measurements. This was attributed to the decrease in pulmonary arterial pressure and the pulmonary vascular resistance, through improving the pulmonary vein pressure by MVP. However, the Pb and RC of two cases in which pulmonary hypertension remained after MVP had higher Pb and RC than the other eight cases, suggesting that the wave reflection did not improve. It could be that the two cases may have already progressed to reactive post-capillary-PH, due to remodeling of the pulmonary artery. Therefore, we suggest that pulmonary hypertension remained and the wave reflection was a high value, despite the pulmonary vein pressure decreasing after MVP. Two dogs with persistent PH after MVP presented with flattened interventricular septum despite mild TR flow velocity (TR velocity 3.0 m/s in both PH patient). Although the measurement of estimated pulmonary artery systolic pressure using TR is often used as a screening tool for the diagnosis and severity of PH, the accuracy of this method has been questioned because it is affected by right ventricular dysfunction and technical errors (43, 44). Thus, it may not be possible to detect the presence of persistent PH simply by measuring the TR flow velocity. This study also indicated that measurement of the RAA index and RVEDA index couldn't detect the presence of persistent PH. Since the RAA index and RVEDA index are affected by changes in left ventricular volume, size of right heart is not always associated with severity of PH. On the other hand, analysis of pulmonary artery wave reflection could help detection of persistent PH.

Su et al. previously demonstrated that in patients with chronic thromboembolic pulmonary hypertension, both a large wave reflection and symptoms related to PH remained and were not improved despite pulmonary endarterectomy being performed (45). Despite successful surgery, the sustained and potentially irreversible impact of vascular remodeling could contribute to persistent vascular admittance mismatching. Persistent vascular admittance mismatching leads to higher wave reflection. Therefore, we concluded that it is useful to measure pulmonary artery wave reflection in PH due to MMVD before and after MVP, since pulmonary artery wave reflection, as determined by wave intensity analysis, may provide additional information about assessing pulmonary hemodynamics. Interestingly, Pb correlates with right atrial pressure and systolic pulmonary artery pressure, suggesting that wave reflection may be an indicator of congestion of the right heart and right ventricular afterload. On the other hand, RC represents the ratio of wave reflection pressure to forward wave pressure. It has been reported that RC is an index of right ventricular function and right ventricular afterload, indicating that it may not simply correlate with pulmonary arterial pressure (20, 26). Thus, caution is required in interpreting this result.

In conclusion, both before and after MVP in PH patients with left heart failure, high wave reflection was observed. The magnitude of wave reflection diminished in almost all patients after MVP. From the results, we conclude that MVP is one of the treatment methods for secondary PH due to MMVD. Through this method post-operative echocardiographic and wave reflection parameters can improve and the right afterload can be reduced. In some patients, however, despite improving the left atrial pressure due to left heart failure after MVP, some degree of vascular admittance mismatch persisted. This may be indicative of residual pulmonary arterial disease, which may continue to adversely affect interactions between the right ventricle and the vasculature.

LIMITATIONS

In this study, the number of PH due to MMVD cases was small; therefore, additional studies should be performed. PH may not have been accurately evaluated, given pulmonary vascular resistance and pulmonary artery wedge pressure—the gold standards for evaluating the hemodynamic assessment of PH—were not measured using a catheter. The value of the pulmonary artery wave reflection may differ from that measured by a catheter since the measurement method is by non-invasive Doppler echocardiography. In this non-invasive method using echocardiography, since pressure and flow velocity profile are gained at different timing, pulmonary arterial wave reflection may be affected by situation of examined dogs (exciting level) and respiration timing. In clinical cases, measuring the pulmonary artery wave reflection in cases that do not exhibit TR can be difficult, as can the evaluation of wave reflection in cases that present with severe arrhythmia. Right ventricular function (TAPSE, tricuspid annular plane systolic excursion; RV-STE, right ventricular speckle tracking, etc.) wasn't measured in this study. However, we think the indicator of right ventricular function cannot be evaluated correctly after surgery. After MVP, heart function decreases temporarily due to invasive open-heart surgery. In addition, cardiac contractility decreases ostensibly due to reducing the volume loading by improved mitral regurgitation. Therefore, relationship between pulmonary arterial wave reflection and right ventricular function are unclear. In the future, it is necessary to investigate the relationship between wave reflection and the right ventricular function.

The scale of this study was small and that limits being able to affirm that the technique has been validated completely. More animal research and subsequent research in humans are necessary to clinically apply this novel indicator.

DATA AVAILABILITY STATEMENT

The raw data supporting the conclusions of this article will be made available by the authors, without undue reservation.

ETHICS STATEMENT

The animal study was reviewed and approved by Shiraishi Animal Hospital Animal Care and Use Committee (protocol number R2-062). Written informed consent was obtained from the owners for the participation of their animals in this study.

AUTHOR CONTRIBUTIONS

TY and KM designed the study and prepared original draft. KS acquired and analyzed the data. LH interpreted the results and critically reviewed the results. RT and TU edited the manuscript and approved the final version of the manuscript. All authors contributed to the article and approved the submitted version.

ACKNOWLEDGMENTS

The authors would like to thank Tokuhisa Uejima from the Cardiovascular Institute, Tokyo, Japan for his expertise with programing in MATLAB (MathWorks 2019b, Massachusetts, USA).

REFERENCES

1. Buchanan J. Chronic valvular disease (endocardiosis) in dogs. *Adv Vet Sci Comp Med.* (1977) 21:75–106.
2. Serres F, Chetboul V, Tissier R, Sampedrano CC, Gouni V, Nicolle AP, et al. Chordae tendineae rupture in dogs with degenerative mitral valve disease: prevalence, survival, and prognostic factors (114 cases, 2001–2006). *J Vet Int Med.* (2007) 21:258–64. doi: 10.1892/0891-6640(2007)21[258:CTRIDW]2.0.CO;2
3. Boswood A, Gordon S, Häggström J, Wess G, Stepien R, Oyama M, et al. Longitudinal analysis of quality of life, clinical, radiographic, echocardiographic, and laboratory variables in dogs with preclinical

myxomatous mitral valve disease receiving pimobendan or placebo: the EPIC study. *J Vet Int Med.* (2018) 32:72–85. doi: 10.1111/jvim.14885
4. Borgarelli M, Abbott J, Braz-Ruivo L, Chiavegato D, Crosara S, Lamb K, et al. Prevalence and prognostic importance of pulmonary hypertension in dogs with myxomatous mitral valve disease. *J Vet Int Med.* (2015) 29:569–74. doi: 10.1111/jvim.12564
5. Tidholm A, Höglund K, Häggström J, Ljungvall I. Diagnostic value of selected echocardiographic variables to identify pulmonary hypertension in dogs with myxomatous mitral valve disease. *J Vet Int Med.* (2015) 29:1510–7. doi: 10.1111/jvim.13609
6. Reinero C, Visser LC, Kellihan HB, Masseau I, Rozanski E, Clercx C, et al. ACVIM consensus statement guidelines for the diagnosis, classification, treatment, and monitoring of pulmonary hypertension in dogs. *J Vet Int Med.* (2020) 34:549–73. doi: 10.1111/jvim.15725
7. Galiè N, Humbert M, Vachiery J-L, Gibbs S, Lang I, Torbicki A, et al. 2015 ESC/ERS guidelines for the diagnosis and treatment of pulmonary hypertension: the joint task force for the diagnosis and treatment of pulmonary hypertension of the European Society of Cardiology (ESC) and the European Respiratory Society (ERS): endorsed by: Association for European Paediatric and Congenital Cardiology (AEPC), International Society for Heart and Lung Transplantation (ISHLT). *Eur Heart J.* (2016) 37:67–119. doi: 10.1093/eurheartj/ehv317
8. Pfeuffer-Jovic E, Weiner S, Wilkens H, Schmitt D, Frantz S, Held M. Impact of the new definition of pulmonary hypertension according to world symposium of pulmonary hypertension 2018 on diagnosis of post-capillary pulmonary hypertension. *Int J Cardiol.* (2021) 335:105–10. doi: 10.1016/j.ijcard.2021.04.006
9. Fukumoto S, Hanazono K, Miyasho T, Endo Y, Kadosawa T, Iwano H, et al. Serum big endothelin-1 as a clinical marker for cardiopulmonary and neoplastic diseases in dogs. *Life Sci.* (2014) 118:329–32. doi: 10.1016/j.lfs.2014.01.002
10. Tatebe S, Fukumoto Y, Sugimura K, Miyamichi-Yamamoto S, Aoki T, Miura Y, et al. Clinical significance of reactive post-capillary pulmonary hypertension in patients with left heart disease. *Circ J.* (2012) 76:1235–44. doi: 10.1253/circj.CJ-11-1288
11. Gerges M, Gerges C, Pistritto A-M, Lang MB, Trip P, Jakowitsch J, et al. Pulmonary hypertension in heart failure. Epidemiology, right ventricular function, and survival. *Am J Respir Crit Care Med.* (2015) 192:1234–46. doi: 10.1164/rccm.201503-0529OC
12. Vevecka AH, Uerban M, Jurcut R, Ginghină C. Reactive pulmonary hypertension in left heart disease "post-capillary PH with a pre-capillary component". *Romanian J Cardiol.* (2015) 25:147–52.
13. Ibe T, Wada H, Sakakura K, Ugata Y, Maki H, Yamamoto K, et al. Combined pre-and post-capillary pulmonary hypertension: the clinical implications for patients with heart failure. *PLoS ONE.* (2021) 16:e0247987. doi: 10.1371/journal.pone.0247987
14. Enriquez-Sarano M, Akins CW, Vahanian A. Mitral regurgitation. *Lancet.* (2009) 373:1382–94. doi: 10.1016/S0140-6736(09)60692-9
15. Walls MC, Cimino N, Bolling SF, Bach DS. Persistent pulmonary hypertension after mitral valve surgery: does surgical procedure affect outcome? *J Heart Valve Dis.* (2008) 17:1–9.
16. Paşaoglu I, Demircin M, Dogan R, Ozmen F, Ersoy U, Böke E, et al. Mitral valve surgery in the presence of pulmonary hypertension. *Jpn Heart J.* (1992) 33:179–84. doi: 10.1536/ihj.33.179
17. Murashita T, Okada Y, Kanemitsu H, Fukunaga N, Konishi Y, Nakamura K, et al. The impact of preoperative and postoperative pulmonary hypertension on long-term surgical outcome after mitral valve repair for degenerative mitral regurgitation. *Ann Thorac Cardiovasc Surg.* (2015) 21:53–8. doi: 10.5761/atcs.oa.13-00364
18. Jegaden O, Rossi R, Delahaye F, Montagna P, Delaye J, Delahaye JP, et al. Mitral valve replacement in severe pulmonary hypertension. Long-term results. *Archives des Maladies du Coeur et des Vaisseaux.* (1991) 84:1297–301.
19. Uechi M. Mitral valve repair in dogs. *J Vet Cardiol.* (2012) 14:185–92. doi: 10.1016/j.jvc.2012.01.004
20. Su J, Manisty C, Parker KH, Simonsen U, Nielsen-Kudsk JE, Mellemkjaer S, et al. Wave intensity analysis provides novel insights into pulmonary arterial hypertension and chronic thromboembolic pulmonary hypertension. *J Am Heart Assoc.* (2017) 6:e006679. doi: 10.1161/JAHA.117.006679
21. Castelain V, Hervé P, Lecarpentier Y, Duroux P, Simonneau G, Chemla D. Pulmonary artery pulse pressure and wave reflection in chronic pulmonary thromboembolism and primary pulmonary hypertension. *J Am Coll Cardiol.* (2001) 37:1085–92. doi: 10.1016/S0735-1097(00)01212-2
22. Jones CJ, Sugawara M, Kondoh Y, Uchida K, Parker KH. Compression and expansion wavefront travel in canine ascending aortic flow: wave intensity analysis. *Heart Vessels.* (2002) 16:91–8. doi: 10.1007/s003800200002
23. Parker KH, Jones C. Forward and backward running waves in the arteries: analysis using the method of characteristics. *J Biomech Eng.* (1990) 112(3):322–6. doi: 10.1115/1.2891191
24. Hollander EH, Wang J-J, Dobson GM, Parker KH, Tyberg JV. Negative wave reflections in pulmonary arteries. *Am J Physiol Heart Circ Physiol.* (2001) 281:895–H902. doi: 10.1152/ajpheart.2001.281.2.H895
25. Fukumitsu M, Kawada T, Shimizu S, Turner MJ, Uemura K, Sugimachi M. Wave reflection correlates with pulmonary vascular wall thickening in rats with pulmonary arterial hypertension. *Int J Cardiol.* (2017) 249:396–401. doi: 10.1016/j.ijcard.2017.09.024
26. Yoshida T, Matsuura K, Seijirow G, Uemura A, Yilmaz Z, Tanaka R. Non-invasive assessment of pulmonary artery wave reflection in dogs with suspected pulmonary hypertension. *Front Vet Sci.* (2021) 8:659194. doi: 10.3389/fvets.2021.659194
27. Westerhof N, Sipkema P, Bos GVD, Elzinga G. Forward and backward waves in the arterial system. *Cardiovasc Res.* (1972) 6:648–56. doi: 10.1093/cvr/6.6.648
28. Li JK-J. Time domain resolution of forward and reflected waves in the aorta. *IEEE Transac Biomed Eng.* (1986) 33:783–5. doi: 10.1109/TBME.1986.325903
29. Khir A, O'brien A, Gibbs J, Parker K. Determination of wave speed and wave separation in the arteries. *J Biomech.* (2001) 34:1145–55. doi: 10.1016/S0021-9290(01)00076-8
30. Cornell CC, Kittleson MD, Torre PD, Häggström J, Lombard CW, Pedersen HD, et al. Allometric scaling of M-mode cardiac measurements in normal adult dogs. *J Vet Int Med.* (2004) 18:311–21. doi: 10.1111/j.1939-1676.2004.tb02551.x
31. Boon JA. *Veterinary Echocardiography*. Fort Collins: John Wiley & Sons (2011).
32. Pyle RL, Abbott J, MacLean H. Pulmonary hypertension and cardiovascular sequelae in 54 dogs. *Intern J Appl Res Vet Med.* (2004) 2:99–109.
33. Visser LC, Im M, Johnson LR, Stern JA. Diagnostic value of right pulmonary artery distensibility index in dogs with pulmonary hypertension: comparison with Doppler echocardiographic estimates of pulmonary arterial pressure. *J Vet Int Med.* (2016) 30:543–52. doi: 10.1111/jvim.13911
34. Serres F, Chetboul V, Gouni V, Tissier R, Sampedrano CC, Pouchelon JL. Diagnostic value of echo-Doppler and tissue Doppler imaging in dogs with pulmonary arterial hypertension. *J Vet Int Med.* (2007) 21:1280–9. doi: 10.1111/j.1939-1676.2007.tb01950.x
35. Kanemoto I, Taguchi D, Yokoyama S, Mizuno M, Suzuki H, Kanamoto T. Open heart surgery with deep hypothermia and cardiopulmonary bypass in small and toy dogs. *Vet Surg.* (2010) 39:674–9. doi: 10.1111/j.1532-950X.2010.00687.x
36. Kanemoto I, Mihara K, Sato K. Open-heart techniques and mitral valve plasty for mitral regurgitation in toy-and small-breed dogs: a review. *Open Vet J.* (2021) 11:14–26. doi: 10.4314/ovj.v11i1.4
37. Uechi M, Mizukoshi T, Mizuno T, Mizuno M, Harada K, Ebisawa T, et al. Mitral valve repair under cardiopulmonary bypass in small-breed dogs: 48 cases (2006–2009). *J Am Vet Med Assoc.* (2012) 240:1194–201. doi: 10.2460/javma.240.10.1194
38. Ward C, Hancock B. Extreme pulmonary hypertension caused by mitral valve disease. Natural history and results of surgery. *Heart.* (1975) 37:74–8. doi: 10.1136/hrt.37.1.74

39. Zener JC, Hancock EW, Shumway NE, Harrison DC. Regression of extreme pulmonary hypertension after mitral valve surgery. *Am J Cardiol.* (1972) 30:820–6. doi: 10.1016/0002-9149(72)90005-7
40. Bouwmeester JC, Belenkie I, Shrive NG, Tyberg JV. Wave reflections in the pulmonary arteries analysed with the reservoir–wave model. *J Physiol.* (2014) 592:3053–62. doi: 10.1113/jphysiol.2014.273094
41. Quail MA, Knight DS, Steeden JA, Taelman L, Moledina S, Taylor AM, et al. Noninvasive pulmonary artery wave intensity analysis in pulmonary hypertension. *Am J Physiol Heart Circ Physiol.* (2015) 308:1603–H11. doi: 10.1152/ajpheart.00480.2014
42. Su J, Hughes AD, Simonsen U, Howard LS. Nitric oxide attenuates arterial pulse wave reflection in a vasodilator responding pulmonary arterial hypertension patient. *Circ Cardiovasc Interv.* (2018) 11:e006242. doi: 10.1161/CIRCINTERVENTIONS.117.006242
43. Fisher MR, Forfia PR, Chamera E, Housten-Harris T, Champion HC, Girgis RE, et al. Accuracy of Doppler echocardiography in the hemodynamic assessment of pulmonary hypertension. *Am J Respir Crit Care Med.* (2009) 179:615–21. doi: 10.1164/rccm.200811-1691OC
44. Mutlak D, Aronson D, Lessick J, Reisner SA, Dabbah S, Agmon, et al. Functional tricuspid regurgitation in patients with pulmonary hypertension: is pulmonary artery pressure the only determinant of regurgitation severity? *Chest.* (2009) 135:115–21. doi: 10.1378/chest.08-0277
45. Su J, Hughes AD, Simonsen U, Nielsen-Kudsk JE, Parker KH, Howard LS, et al. Impact of pulmonary endarterectomy on pulmonary arterial wave propagation and reservoir function. *Am J Physiol Heart Circ Physiol.* (2019) 317:505–H16. doi: 10.1152/ajpheart.00181.2019

Conflict of Interest: The authors declare that the research was conducted in the absence of any commercial or financial relationships that could be construed as a potential conflict of interest.

Publisher's Note: All claims expressed in this article are solely those of the authors and do not necessarily represent those of their affiliated organizations, or those of the publisher, the editors and the reviewers. Any product that may be evaluated in this article, or claim that may be made by its manufacturer, is not guaranteed or endorsed by the publisher.

frontiers in Veterinary Science

ORIGINAL RESEARCH
published: 20 January 2022
doi: 10.3389/fvets.2021.789137

Assessment of Right Ventricular Function, Blood Lactate Levels, and Serum Peptidomics Profiles Associated With Mitral Valve Disease in Dogs

Soontaree Petchdee, Mona Yalong, Methawee Kaewnet, Burasarin Ithisariyanont and Tanawat Padawong*

Department of Large Animal and Wildlife Clinical Sciences, Faculty of Veterinary Medicine, Kasetsart University, Bangkok, Thailand

OPEN ACCESS

Edited by:
Zeki Yilmaz,
Faculty of Veterinary Medicine, Turkey

Reviewed by:
Jean-Claude Desfontis,
Oniris, Ecole Nationale Vétérinaire Agroalimentaire et de l'Alimentation, France
Mitsuhiro Isaka,
Rakuno Gakuen University, Japan

****Correspondence:***
Soontaree Petchdee
fvetstr@ku.ac.th

Specialty section:
This article was submitted to Comparative and Clinical Medicine, a section of the journal Frontiers in Veterinary Science

Received: *04 October 2021*
Accepted: *10 December 2021*
Published: *20 January 2022*

Citation:
Petchdee S, Yalong M, Kaewnet M, Ithisariyanont B and Padawong T (2022) Assessment of Right Ventricular Function, Blood Lactate Levels, and Serum Peptidomics Profiles Associated With Mitral Valve Disease in Dogs. Front. Vet. Sci. 8:789137. doi: 10.3389/fvets.2021.789137

Background: Degenerative mitral valve disease is a common heart problem in dogs. The aims are to evaluate the relationships between right and left ventricular function, and blood lactate concentrations, assess prognostic contribution, and investigate whether serum peptidomics profile could reveal markers or determine the stage in dogs with valve degeneration.

Materials and Methods: Ninety-three dogs were evaluated in this study. Thirty-nine dogs' serum was collected and analyzed using matrix-assisted laser desorption/ionization-time of flight mass spectrometry. The Kaplan–Meier curve was used to predict the outcomes of mitral valve disease. Follow-up was obtained by a questionnaire or telephone to determine a survival time.

Results: The BUN/creatinine ratio, vertebral heart score, and left atrium/aorta ratio were the independent predictors of cardiac mortality. Right ventricular systolic dysfunction was found in 50% of dogs with mitral valve disease. Dogs with right ventricular dysfunction had a significantly higher incidence of lower fractional shortening and larger right ventricular dimensions. The occurrence of right-sided dysfunction is proportionate to age and the degree of left ventricular dysfunction. High blood lactate concentrations were investigated in dogs with mitral valve disease stage C compared with stage B. The peptides such as mitogen-activated protein kinase, kallikrein, and tenascin-C appeared in the heart disease progression group.

Conclusion: Right-hearted function assessment, blood lactate levels, and peptidomics analysis may help early detection and prognosis of this disease in dogs. Peptidomics profiles from this study demonstrate the possibility for prognosis indicators of heart valve degeneration.

Keywords: canine, echocardiography, heart failure, lactate, peptide profile

INTRODUCTION

Left-sided congestive heart failure is commonly associated with mitral valve degeneration and is a significant heart problem in dogs (1, 2). Left ventricular function plays a vital role in evaluating dogs with congestive heart failure, while the right ventricle function has been less studied (3). The American College of Veterinary Internal Medicine (ACVIM) consensus statement has been used to classify dogs to determine the severity of this disease. Dogs have been classified into stages A, B, C, and D (4, 5). High blood lactate concentrations are frequently observed in dogs with abnormal thoracic radiographs such as cardiomegaly and pulmonary parenchyma (6). Dogs with degenerative mitral valve disease often have impaired renal function. Renal dysfunction is the critical determinant of cardiac compensation and disease progression (7).

Right ventricular function is an essential determinant of a human's clinical status with chronic heart failure (8). The right ventricle is commonly affected by cardiac diseases such as tricuspid dysplasia and dilated cardiomyopathy. Previous studies suggested a close relationship between right and left ventricle dysfunction. However, the right-sided functional assessment remains challenging due to the right heart anatomy (9–11). Echocardiographic measurement is a non-invasive method for heart function assessment. Echocardiographic imaging of dogs with left-sided congestive heart failure has been associated with adverse cardiovascular outcomes such as reduced cardiac output and decreased contraction function (12, 13). Right-hearted dysfunction has been verified in many human cardiac diseases, and clinical evaluation of right-sided heart function has also been reported in animals (14–16). Many parameters, such as right ventricle fractional area change (FAC), myocardial velocity of the lateral tricuspid annulus (S′), and tricuspid annular plane systolic excursion (TAPSE), are correlated well-with the right heart function.

Proteome analysis is a novel tool for exploring the changes in protein composition, and proteomics network analysis has been widely used to identify protein biomarkers in many diseases (17). It has shown that circulating proteins associated with heart failure can identify the stage increased across the heart failure process (18). A previous study identified phosphorylation of p38 mitogen-activated protein kinase (p 38 MAPK) and suggested linking p38 to inflammation, cell cycle, apoptotic process, and cell differentiation. In addition, the signaling mediated by the MAPK pathway may play a role in cardiac injury and remodeling (19). Many studies reported that the use of protein infusions such as kallikrein could improve cardiac function and reduce cardiomyocyte apoptosis and reduce inflammatory cell accumulation in the heart after myocardial ischemia (20, 21). Tenascin-C (TN-C) was also another peptide found in the serum of heart failure patients and suggested using it to predict ventricular remodeling and poor prognosis (22). The proteomic network assessment might be allowed in the evaluation of therapeutic targets for valvular heart diseases.

The present study aimed to assess the prognostic information about valvular heart disease in dogs, examine the echocardiographic alterations, assess the right ventricular function associated with mitral valve disease, determine the blood lactate concentrations, and MS-based identification of proteins and protein interacting in the mitral valve degeneration dogs.

TABLE 1 | Characteristics and echocardiographic variables in 93 dogs.

Parameters	Mean ± SEM
ACVIM classification [number (%)]	
Stage B	65.6
Stage C	34.4
VHS	11.54 ± 1.43
LA/AO ratio	1.59 ± 0.05
EDV (ml)	40.75 ± 3.19
ESV (ml)	17.35 ± 1.83
LVIDd (cm)	3.04 ± 0.10
LVIDs (cm)	2.05 ± 0.09
E deceleration time (ms)	107.37 ± 3.29
FS (%)	28.07 ± 0.94
RV parameters	
RV basal diameter (cm)	1.22 ± 0.05
RV mid diameter (cm)	0.93 ± 0.04
RV longitudinal diameter (cm)	2.27 ± 0.09
FAC (%)	29.86 ± 1.44
TAPSE (cm)	1.22 ± 0.06
TR [number (%)]	
Mild	60
Moderate	40

VHS, vertebral heart score; LA/AO ratio, left atrium/aorta ratio; EDV, end-diastolic volume; ESV, end-systolic volume; LVIDd, left ventricular internal diameter during diastole; LVIDs, left ventricular internal diameter during systole; FS, fractional shortening; RV, right ventricle; FAC, fractional area change; TAPSE, tricuspid annular plane systolic excursion; TR, tricuspid regurgitation. Data are shown as mean ± SEM.

MATERIALS AND METHODS

Animals

This study was performed in clinical cases at Kasetsart University Veterinary Teaching Hospital Kamphaeng Saen from January 2019 to April 2020 (**Table 1**). The follow-up was obtained by a questionnaire or telephone to determine a survival time. The Ethics Committee approved all procedures in the study for Animal Experiments, Kasetsart University. The owners provided informed consent before enrollment. Ninety-three dogs with mitral valve degeneration were recruited into the study. The breeds included Poodle, Shih Tzu, Pomeranian, and Crossbreed; body weight ranged from 2 to 20 kg. All dogs had normal or unremarkable hematology and chemistry before enrollment and had not previously received oral positive inotropic agents. Each dog showed cardiac murmur and abnormal cardiac dimension from chest radiography. The owners provided informed consent before enrollment. Dogs demonstrated evidence of the clinical signs of stages B and C according to the ACVIM classification system. The MMVD B1 group included 24 dogs, and stage B2 (37 dogs), dogs affected by MMVD stage B1 and B2 with no clinical signs of congestive heart failure (asymptomatic). No

radiographic evidence of congestive heart failure and no evidence of pulmonary edema were detected, but there was sufficient hemodynamic change to cause echocardiographic evidence of left atrial dilatation with an LA/AO ratio >1.6 in stage B2. The MMVD C group included 32 dogs affected by MMVD with echocardiographic evidence of mitral valve leaflet thickening and regurgitation. Dogs in stage C showed clinical signs of congestive heart failure identified by clinical examination and radiographic evidence of pulmonary edema. The survival information was examined from telephone calls and analyzed as the time between the first visit for echocardiographic recording and the date of death.

Blood Samples

Blood samples were obtained from a cephalic vein, and the blood lactate concentration was measured with a blood lactate analyzer (blood lactate test meter; XPER Technology, Taiwan) before the echocardiography examination. **Figure 1** shows the lactate values (mmol/L) of dogs in group 1 and group 2.

Echocardiographic Examination

Dogs underwent transthoracic echocardiography [General Electric (GE) Medical System, vivid5s, Germany] to diagnose and observe disease progression. The measurement was performed when the dog was on lateral recumbence with no sedation. Echocardiographic images were captured and evaluated offline by only one sonographer. Left and right ventricular dimension and function were calculated from two-dimensional and M-mode images. The cardiac parameters were measured during diastole and systole, such as interventricular septum thickness during diastole (IVSd), interventricular septum thickness during systole (IVSs), left ventricular internal diameter during diastole (LVIDd), left ventricular internal diameter during systole (LVIDs), left ventricular proximal wall thickness during diastole (LVPWd), and left ventricular proximal wall thickness during systole (LVPWs). The diameter of the left atrium (LA) and aortic root (AO) ratio (LA/AO) were assessed at the level of the aorta when the aortic valves were closed during diastole.

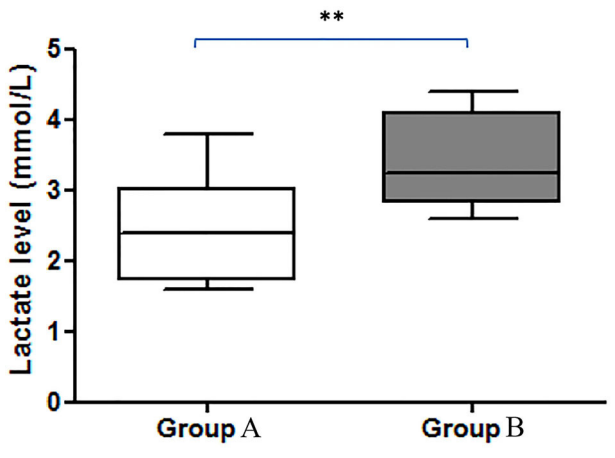

FIGURE 1 | Comparison of the blood lactate levels (mmol/L) between groups. There was a significant difference between the increase in lactate in group A and group B (**$p < 0.01$). Group A included dogs with normal right ventricular function, and group B included dogs with impaired right ventricular function.

Right ventricular dimensions were measured at end-diastole using the left apical 4-chamber view. Three sites are commonly used to determine the right ventricle size: (1) the basal distance measurement, (2) the mid-right ventricular measurement, and (3) the base to apex measurement, as shown in **Figure 2**. The right ventricular systolic function can be quantified using the fractional area change (FAC) of the right ventricle, which can be done on the apical 4-chamber view, as shown in **Figure 3**.

Tricuspid annular plane systolic excursion (TAPSE) was evaluated by placing the M mode cursor through the tricuspid valve in the apical 4-chamber view, as shown in **Figure 4**.

Dogs were divided into two groups according to the presence of impaired right ventricular systolic function, which was defined as the presence of FAC <30%. Group A included dogs with normal right ventricular function, and group B included dogs with impaired right ventricular function.

Analysis of Peptide Pattern by MALDI-TOF MS

The protein concentration in serum was determined by the Lowry method (23). The absorbance at 750 nm (OD750) was measured, and the protein concentration was calculated using the standard curve, plotted between OD750 on Y-axis and BSA concentration (g/ml) on X-axis. The peptides from serum were acidified with 0.1% trifluoroacetic acid to the final concentration of 0.1 mg/ml. The peptides were mixed with MALDI matrix solution (10 mg sinapinic acid in 1 ml of 50% acetonitrile containing 0.1% trifluoroacetic acid), directly spotted onto MALDI target (MTP 384 ground steel; Bruker Daltonik, GmbH), and dried at room temperature. Maldi-TOF MS spectra were collected using Ultraflex III TOF/TOF (Bruker Daltonik, GmbH) in a positive linear mode with a mass range of 2,000–15,000 Da. Five hundred shots were accumulated with a 50-Hz laser, and MS spectra were analyzed using flexAnalysis combination with ClinproTool software (Bruker Daltonik, GmbH), including fingerprint spectra, pseudo-gel view, and principal component analysis (PCA). The protein was calibrated using ACTH fragment 18–39 (human), Insulin oxidized B chain (bovine), Insulin (bovine), Cytochrome C (equine), and Apomyoglobin (equine). Data normalization and quantification of the changes in peptide abundance between the control and Maine Coon cats were performed and visualized using MultiExperiment Viewer (Mev) software version 4.6.1 (20). Briefly, peptide intensities from the LC-MS analyses were transformed and normalized using a mean central tendency procedure.

Statistical Analysis

Paired *t*-test model was used to estimate and compare the parameters between two groups. Statistical analysis was performed using commercially available software (GraphPad Software Inc., USA). A value of $p < 0.05$ was considered statistically significant. The continuous variable showed a mean ± SEM. The survival analysis was analyzed using the Kaplan–Meier survival curve.

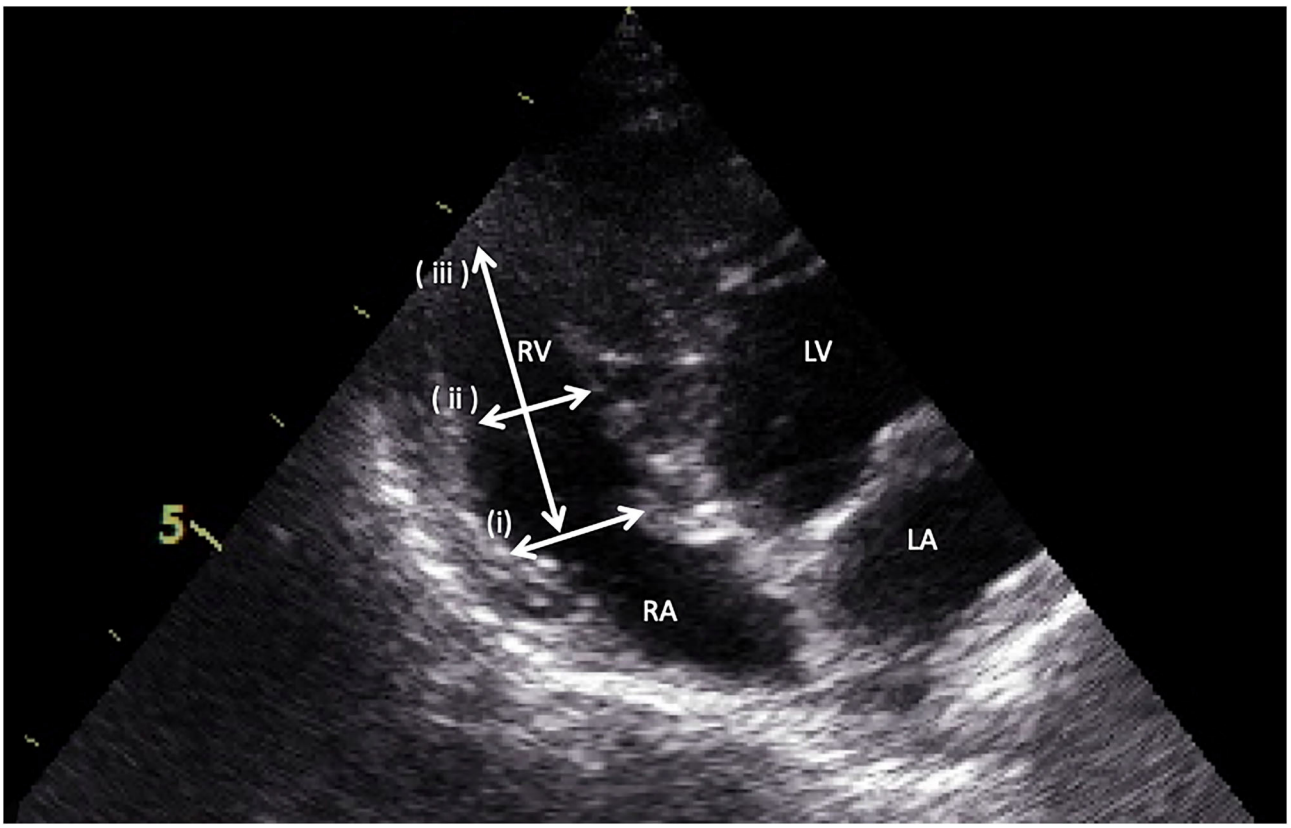

FIGURE 2 | Measurement of right ventricular dimensions by the apical four-chamber view. (i) the basal distance measurement, (ii) the mid-right ventricular measurement, and (iii) the base to apex measurement.

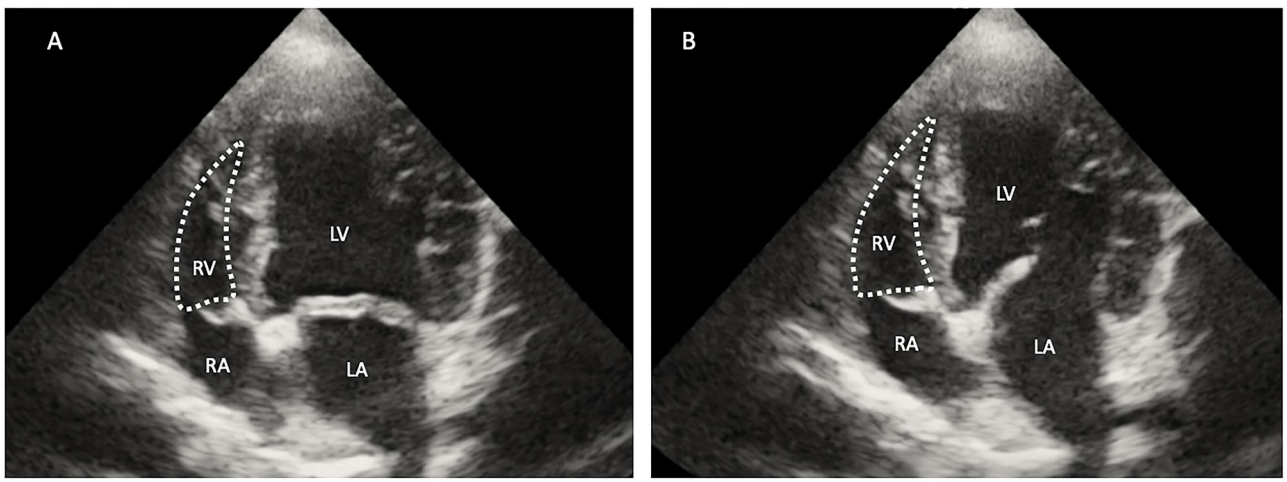

FIGURE 3 | Two-dimensional echocardiographic image of the right ventricular area (RV) during systole **(A)** and diastole **(B)**. The right fractional area change (FAC) was calculated using the formula [(RV diastole – RV systole)/RV diastole] ×100. RA, right atrium; RV, right ventricle; LV, left ventricle; LA, left atrium.

RESULTS

There were 93 dogs; at the end of the follow-up, 34 dogs had died due to their cardiac problems, and 59 dogs remained alive. The association between variable parameters and survival is shown in **Figure 5**. Kaplan–Meier curve shows the survival duration between group A and group B; **Figure 5i** displays the survival curve of MMVD patients with stage B and stage C.

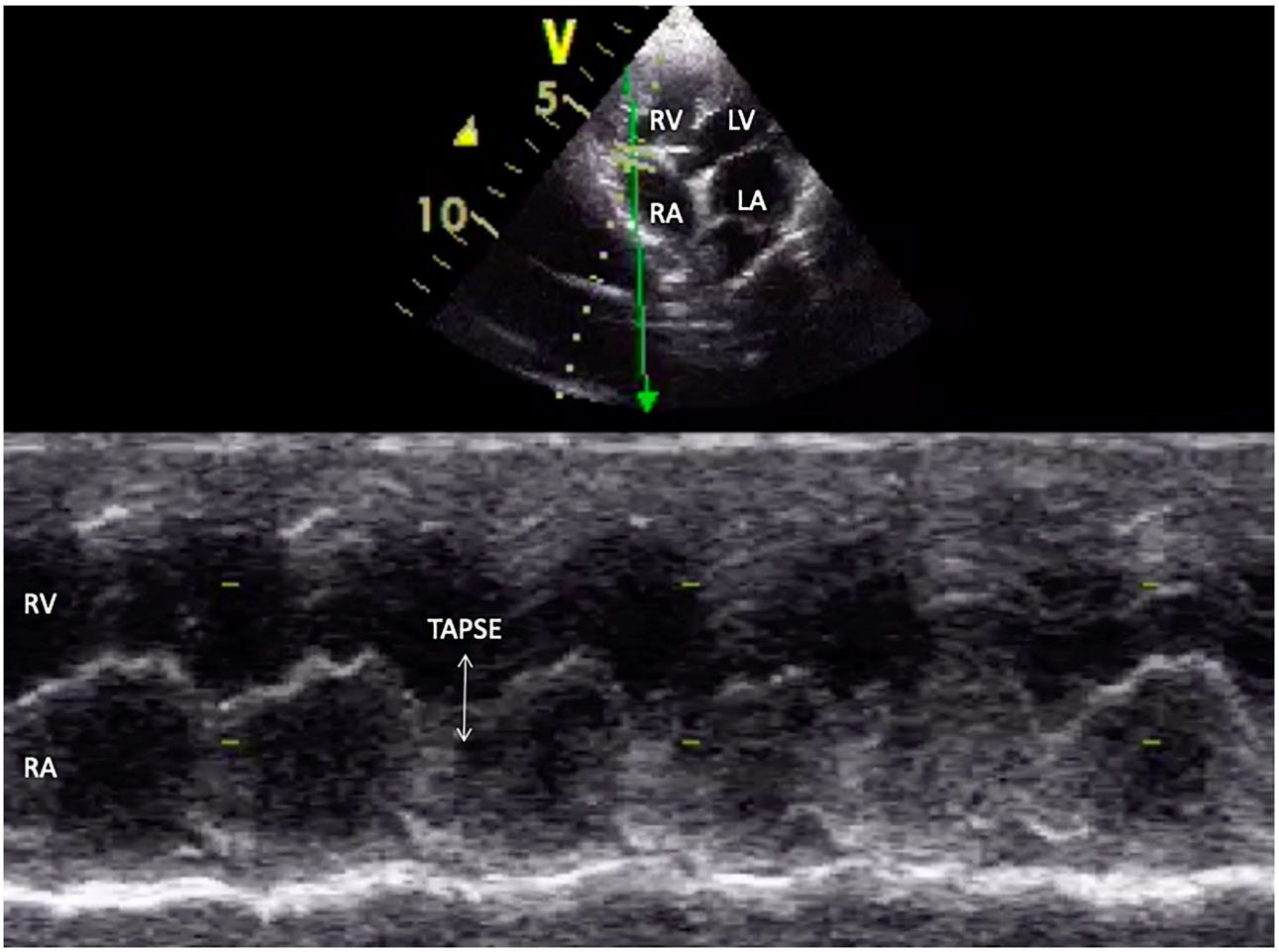

FIGURE 4 | M-mode echocardiographic image of tricuspid annular plane systolic excursion (TAPSE) in appearance (white arrow). RA, right atrium; RV, right ventricle; LV, left ventricle; LA, left atrium.

The cumulative probability of percent survival showed in MMVD patient stage B was 91.23, 82.54, 69.84, 53.40, and 37.38% for 1 to 5 years, respectively. In contrast, that of the patient in stage C was 96.87% and maintained at 83.51% for 2 and 3 years, and 74.23 and 30.13% for 4 and 5 years, respectively. The parameters such as vertebral heart score (VHS), left atrial and aorta diameter ratio (LA/AO), and quality of life score (QOL) had higher percent survival in group B than dogs in group A at 1 year after MMVD was diagnosed (**Figures 5ii,iv,v**) Hyperlactatemia (lactate concentration >2.5 mmol/L) was observed in 64% of dogs with mitral valve degeneration. Lactate concentrations were 2.90 ± 0.26 mmol/L in group A and 3.40 ± 0.23 mmol/L in group B dogs. There was a significant difference between the two groups. Dogs in group B had significantly higher ages (**Table 2**). However, no significant difference was found between the two groups regarding the left ventricular dimension and volume. The echocardiographic analysis revealed no statistically significant difference between the left ventricular end-diastolic and systolic volumes.

However, group B had a significantly higher incidence of left atrial and left ventricle dilation (**Table 3**). Group B showed significantly large right ventricular dimensions at the basal level and a worse degree of tricuspid regurgitation (TR) and lower fractional area change and TAPSE (**Table 4**). Right ventricular function in dogs with left-sided congestive heart failure is different between the stages of congestive heart failure. Dogs in ACVIM stage C showed decreased right ventricular systolic function as estimated by the decreased fractional area change and TAPSE relative to a previous study (12).

In the present study, we aimed to examine the peptide complement of the serum isolated from control dogs (group A) and dogs with impaired right ventricular function (group B). For preliminary comparison of the expression levels of the peptide's profiles, peptide mass fingerprint (**Figure 6**) was used, and LC/MS analyzed the specific peptide sequences. The control groups (group A) and group B (dogs with impaired right ventricular function) were identified with a detection range of 1,000–20,000 Da. **Figure 6** shows the identification of peptide mass and expected proteins. A mass spectral peak of peptide

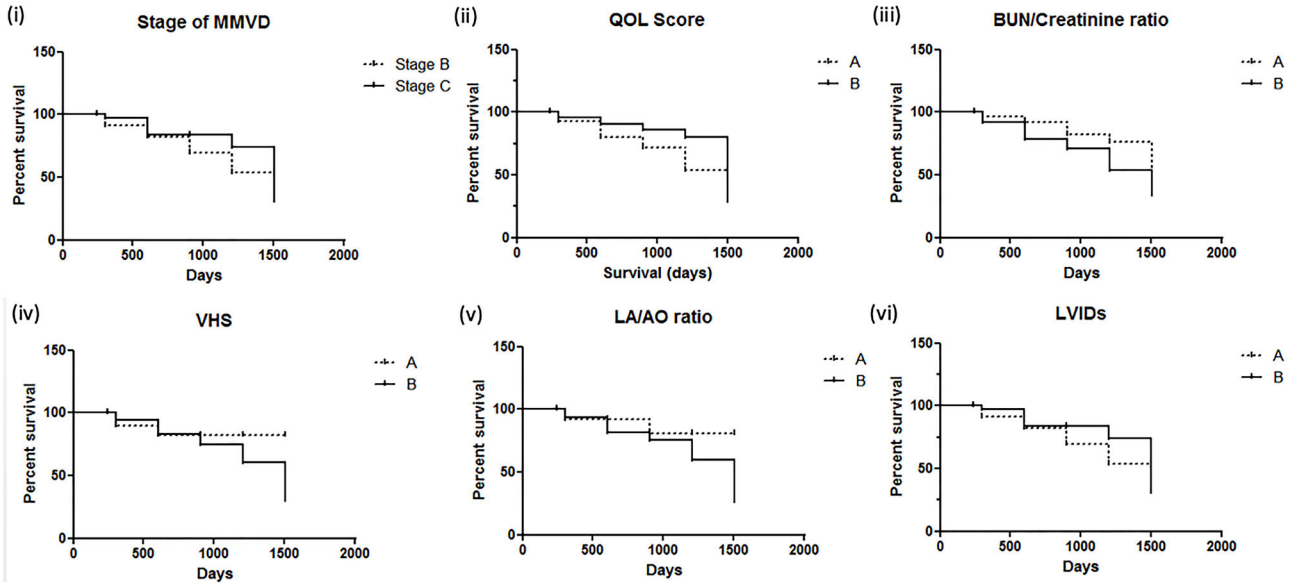

FIGURE 5 | Kaplan–Meier survival curves for dogs with mitral valve degeneration. **(i)** Stage of MMVD (myxomatous mitral valve degeneration); **(ii)** QOL score, quality of life score (A = QOL score <3, B = QOL score >3); **(iii)** BUN/creatinine ratio (A = BUN/creatinine <20, B = BUN/creatinine >20); **(iv)** VHS, vertebral heart score (A = VHS <10.5, B = VHS >10.5); **(v)** LA/AO ratio, left atrium/aorta ratio (A = LA/AO <1.60, B = LA/AO >1.60); **(vi)** LVIDs, left ventricular internal diameter during systole (A = LVIDs<2.0, B = LVIDs>2.0). Group A included dogs with normal right ventricular function, and group B included dogs with impaired right ventricular function.

TABLE 2 | Characteristics variables for two groups (*$p < 0.05$).

Parameters	Group A	Group B
Age in years	10.2 ± 0.82*	12.49 ± 0.63*
Male (%)	28	30

Group A included dogs with normal right ventricular function, and group B included dogs with impaired right ventricular function.

TABLE 3 | Echocardiography evaluation for two groups regarding left ventricular echocardiographic findings.

Parameters	Group A	Group B	*P*-value
Stage B (%)	40%	8%	–
Stage C (%)	18%	34%	–
LA/AO ratio	1.59 ± 0.05	1.95 ± 0.09	0.0007
LVIDd (cm)	2.72 ± 0.20	3.12 ± 0.14	NS
LVIDs (cm)	1.94 ± 0.18	2.31 ± 0.11	0.0826
EDV (ml)	33.96 ± 5.83	41.54 ± 4.34	NS
ESV (ml)	14.0 ± 3.70	20.41 ± 2.27	NS
E deceleration time (ms)	125.38 ± 2.61	90.08 ± 3.33	0.0001
FS (%)	32.0 ± 1.37	25.88 ± 0.75	0.0002

Group A included dogs with normal right ventricular function, and group B included dogs with impaired right ventricular function.

in our study showed that peptide fragments such as mitogen-activated protein kinase (MAPK), kallikrein related peptidase (KLK), and tenascin-C (TN-C) appeared in the heart disease progression group (group B).

TABLE 4 | Comparison between the two groups regarding right ventricular echocardiographic parameters.

Parameters	Group A	Group B	*P*-value
RV basal diameter (cm)	1.10 ± 0.06	1.32 ± 0.08	0.0302
RV mid diameter (cm)	0.90 ± 0.05	0.95 ± 0.07	NS
RV long diameter (cm)	2.18 ± 0.10	2.35 ± 0.16	NS
FAC (%)	37.05 ± 1.56	22.38 ± 1.21	0.0001
TAPSE (cm)	1.31 ± 0.07	1.09 ± 0.07	0.0286
TR [number (%)]			
Mild	80	36	–
Moderate	20	64	–

Group A included dogs with normal right ventricular function, and group B included dogs with impaired right ventricular function.

DISCUSSION

This study's objective was to assess the prognostic information about valvular heart disease in dogs and investigate the right ventricular systolic function and blood lactate concentration. Dogs with clinical signs of congestive heart failure can be controlled, and they can live longer with better life quality by the appropriate medical treatment. Previous studies have reported the association with survival of echocardiographic variables such as left atrium and aorta ratio (LA/AO ratio), left ventricular internal diameter (LVID), and mitral E velocity. Our study also showed that heart size had an essential predictive value; left atrium dimension and vertebral heart score are associated with decreased survival in patients with degenerative mitral valve

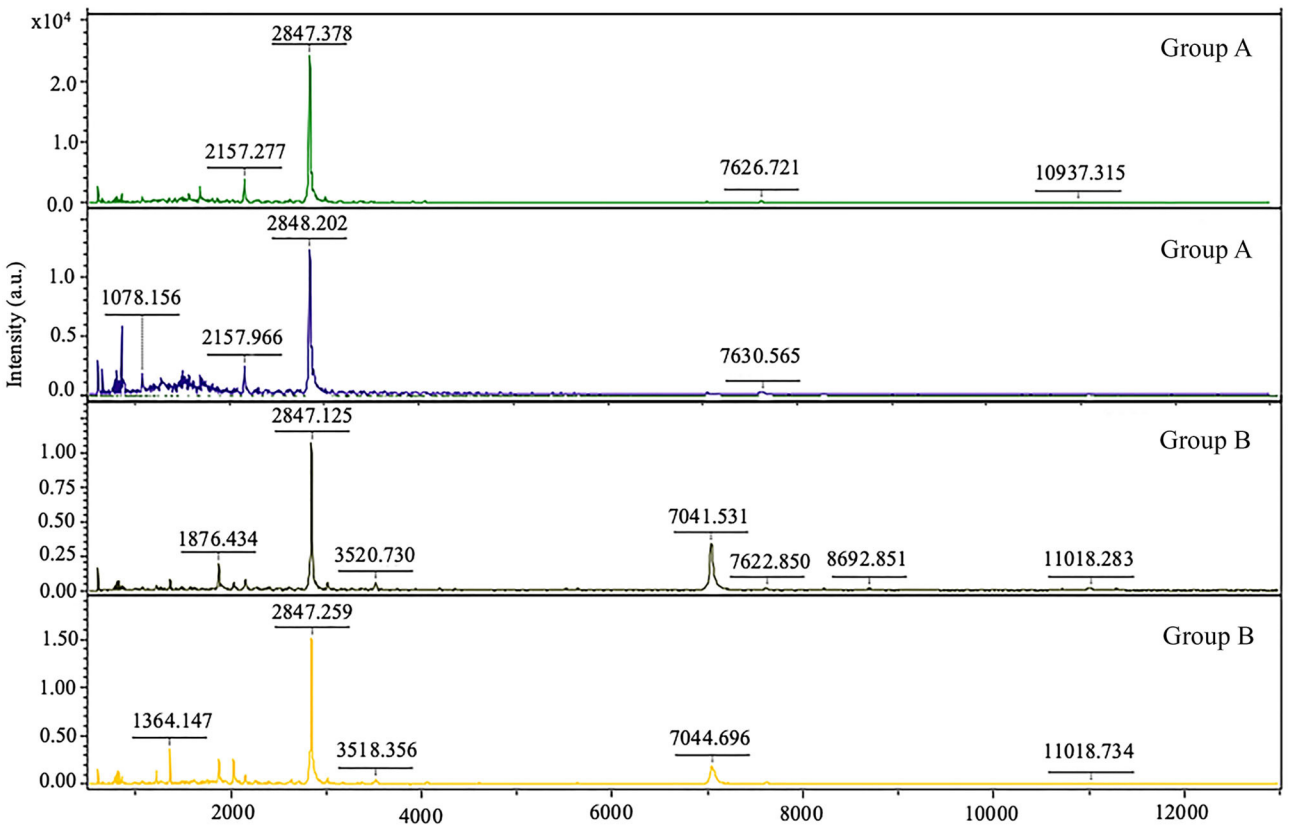

FIGURE 6 | Peptide mass fingerprint of dogs with normal right ventricular function (group A) and dogs with impaired right ventricular function (group B).

disease. However, the stage of mitral valve degeneration, systolic left ventricular internal diameter (LVIDs), and quality of life score were not indicators for survival predictors in our sample population. In addition, the percent survival in variables such as VHS, LA/AO ratio, and QOL was better in group B. Patients in group B contain more dogs in stage C, which had been treated with therapeutic drugs such as pimobendan, diuretic, and angiotensin-converting enzyme inhibitor. The results suggested that early treatment of MMVD patients in early stage B may improve the percent survival, which is similar to the ACVIM guideline (5).

The previous study reported the proteome expression in heart failure patients associated with the inflammation response and oxidative stress (19, 22), similar to our present study. The inflammation network response to mitral degeneration included the presentation of mitogen-activated protein 3 kinases (MAP3K), kallikrein related peptide (KLK), and tenascin C (TNC). Our data provided preliminary information on proteins in dogs with mitral valve degeneration. In addition, the peptidomics profiles may provide a potential independent marker for the detection of mitral valve disease progression. However, protein expression in our study was expressed not only on the heart but many pathological conditions, such as renal diseases, cancer, tissue injury, and inflammation. Thus, extending validation of the protein source may confirm the use of this protein for the prognostic and follow-up marker in the future.

Renal dysfunction can use as a neuro-humoral change in heart disease. Our study showed that the BUN/creatinine ratio impacts the predictive value of degenerative mitral valve disease in dogs. Dogs with mitral valve degeneration ACVIM stage C had higher blood lactate concentrations than dogs in stage B2. Although dogs in groups A and B were not found to have significant differences in the lactate values, the previous studies showed a significant difference between active vs. non-active subjects (24). Thus, it is essential to measure a dog's lactate values with similar physical activity before echocardiography.

This study suggested that the right and left ventricular functions are functionally related to each other. Right ventricular systolic dysfunction was relatively common in dogs with left-sided congestive heart failure, as 50% of the dogs in this study had right ventricular systolic dysfunction. Dogs with right ventricular systolic dysfunction had significant left atrium dilation. A worse ACVIM stage of congestive heart failure than dogs without right ventricular dysfunction was observed, as 34% of dogs in group B had ACVIM stage C, but 18% had it in group A. The current study demonstrated that less TAPSE was associated with left-sided systolic and diastolic dysfunction. The E deceleration time was significantly shorter in dogs with right ventricular dysfunction. An explanation for right heart dysfunction could be that the

alterations in preload and afterload that occur secondarily to left-sided congestive heart failure may alter the right heart function described earlier (25, 26).

In discordance with the present study, dogs with right heart systolic dysfunction had no significant difference in end-systolic and end-diastolic dimensions or left ventricular internal diameter. Right ventricular imaging was considered a limitation of the present study. Right ventricular imaging in dogs with congestive heart failure is challenging due to the cardiac remodeling that could affect the echocardiographic measurement. Cardiovascular magnetic resonance imaging is recommended as the standard gold technique for the right-side assessment due to the complexity of the right-side heart anatomy.

CONCLUSION

Dogs with mitral valve degeneration can have a mild increase in blood lactate values. In addition, dogs with right ventricular systolic dysfunction defined as FAC <30% and TAPSE <110 mm showed a significantly larger RV dimension at the basal level and a significantly worse degree of tricuspid regurgitation. Right ventricular dysfunction in degenerative mitral valve disease is common and is independent of left ventricular volume but is proportional to left contraction impairment. Peptidomics analysis results in this study suggested that these proteins may represent novel biomarkers of the disease progression in dogs with mitral valve degeneration. Our results in this present study will help in the detection and prognosis of mitral valve disease in dogs.

DATA AVAILABILITY STATEMENT

The datasets presented in this study can be found in online repositories. The names of the repository/repositories and accession number(s) can be found below: https://www.uniprot.org/.

ETHICS STATEMENT

The study protocol was approved by the Ethics Committee, Kasetsart University (ACKU-62-VET-002). Written informed consent was obtained from the owners for the participation of their animals in this study.

AUTHOR CONTRIBUTIONS

SP wrote the original article, prepared the figures, and was a major contributor in writing the article. MY, MK, BI, and TP analyzed and interpreted the data. All authors contributed to the article and approved the submitted version.

ACKNOWLEDGMENTS

The authors are grateful to Kasetsart University Veterinary Teaching Hospital, Faculty of Veterinary Medicine, Kasetsart University, for providing facilities for the study. The authors also gratefully acknowledge the cooperation of the peptidomics analysis performed by Narumon Phanakrop, Siriwan Thaisakun, and Sittiruk Roytrakul, without the suggestions, this study would not have been done.

REFERENCES

1. Enriquez-Sarano M, Akins CW, Vahanian A. Mitral regurgitation. *Lancet.* (2009) 373:1382–94. doi: 10.1016/S0140-6736(09)60692-9
2. Lord P, Hansson K, Kvart C, Häggström J. Rate of change of heart size before congestive heart failure in dogs with mitral regurgitation. *J Small Anim Pract.* (2010) 51:210–8. doi: 10.1111/j.1748-5827.2010.00910.x
3. Visser LC, Scansen BA, Schober KE, Bonagura JD. Echocardiographic assessment of right ventricular systolic function in conscious healthy dogs: repeatability and reference intervals. *J Vet Cardiol.* (2015) 17:83–96. doi: 10.1016/j.jvc.2014.10.003
4. Atkins C, Bonagura J, Ettinger S, Fox P, Gordon S, Haggstrom J, et al. Guidelines for the diagnosis and treatment of canine chronic valvular heart disease. *J Vet Intern Med.* (2009) 23:1142–50. doi: 10.1111/j.1939-1676.2009.0392.x
5. Keene BW, Atkins CE, Bonagura JD, Fox PR, Haggstrom J, Fuentes VL, et al. ACVIM consensus guidelines for the diagnosis and treatment of myxomatous mitral valve disease in dogs. *J Vet Intern Med.* (2019) 33:1127–40. doi: 10.1111/jvim.15488
6. Iwanuk N, Wall L, Nolte I, Raue J, Rumstedt K, Pilgram A, et al. Effect of pimobendan on physical fitness, lactate and echocardiographic parameters in dogs with preclinical mitral valve disease without cardiomegaly. *PLoS ONE.* (2019) 14:e0223164. doi: 10.1371/journal.pone.0223164
7. Fahey R, Rozanski E, Paul A, Rush JE. Prevalence of vomiting in dogs with pericardial effusion. *J Vet Emerg Crit Care.* (2017) 27:250–2. doi: 10.1111/vec.12570
8. Le Tourneau T, Deswarte G, Lamblin N. Right ventricular systolic function in organic mitral regurgitation: impact of biventricular impairment. *Circulation.* (2013) 127:1597–608. doi: 10.1161/CIRCULATIONAHA.112.000999
9. Kjaergaard J, Iversen KK, Akkan D. Predictors of right ventricular function as measured by tricuspid annular plane systolic excursion in heart failure. *Cardiac Ultrasound.* (2009) 7:51. doi: 10.1186/1476-7120-7-51
10. Chapel EH, Scansen BA, Schober KE, Bonagura JD. Echocardiographic estimates of right ventricular systolic function in dogs with myxomatous mitral valve disease. *J Vet Intern Med.* (2018) 32:64–71. doi: 10.1111/jvim.14884
11. Haddad F, Hunt SA, Rosenthal DN, Murphy DJ. Right ventricular function in cardiovascular disease, part I: anatomy, physiology, aging, and functional assessment of the right ventricle. *Circulation.* (2008) 117:1436–48. doi: 10.1161/CIRCULATIONAHA.107.653576
12. Desai RV, Meyer P, Ahmed MI. Relationship between left and right ventricular ejection fractions in chronic advanced systolic heart failure: insights from the BEST trial. *Eur J Heart Fail.* (2011) 13:392–7. doi: 10.1093/eurjhf/hfq206
13. Ueda Y, Gunther-Harrington CT, Cruzen CL, Roberts JA, Stern JA. Echocardiographic parameters of clinically normal geriatric rhesus macaques (Macaca mulatta). *J Am Assoc Lab Anim Sci.* (2017) 56:361–8.
14. Lang RM, Badano LP, Mor-Avi V, Afilalo J, Armstrong A, Ernande L, et al. Recommendations for cardiac chamber quantification by echocardiography in adults: an update from the American society of echocardiography and the European association of cardiovascular imaging. *J Am Soc Echocardiogr.* (2015) 28:1–39. doi: 10.1016/j.echo.2014.10.003
15. Bleeker GB, Steendijk P, Holman ER. Assessing right ventricular function: the role of echocardiography and complementary technologies. *Heart.* (2006) 92:i19–26. doi: 10.1136/hrt.2005.082503

16. Rudski LG, Lai WW, Afilalo J, Hua L, Handschumacher MD, Chandrasekaran K, et al. Guidelines for the echocardiographic assessment of the right heart in adults: a report from the American society of echocardiography. *J Am Soc Echocardiogr.* (2010) 23:685–713. doi: 10.1016/j.echo.2010.05.010
17. Geyer PE, Kulak NA, Pichler G, Holdt LM, Teupser D, Mann M. Plasma proteome profiling to assess human health and disease. *Cell Syst.* (2016) 2:185–95. doi: 10.1016/j.cels.2016.02.015
18. Egerstedt A, Berntsson J, Smith ML. Profiling of the plasma proteome across different stages of human heart failure. *Nat Commun.* (2019) 10:5830. doi: 10.1038/s41467-019-13306-y
19. Zarubin T, Han J. Activation and signaling of the p38 MAP kinase pathway. *Cell Res.* (2005) 15:11–18. doi: 10.1038/sj.cr.7290257
20. Yin H, Chao L, Chao J. Kallikrein/kinin protects against myocardial apoptosis after ischemia/reperfusion via Akt-GSK-3 and Akt-Bad-14-3-3 signaling pathways. *J Biol Chem.* (2005) 280:8022–30. doi: 10.1074/jbc.M407179200
21. Yao YY, Yin H, Shen B, Chao L, Chao J. Tissue kallikrein infusion prevents cardiomyocyte apoptosis, inflammation and ventricular remodeling after myocardial infarction. *Regul Pept.* (2007) 140:12–20. doi: 10.1016/j.regpep.2006.11.020
22. Imanaka-Yoshida K. Tenascin-C in heart diseases: the role of inflammation. *Int J Mol Sci.* (2021) 22:5828. doi: 10.3390/ijms22115828
23. Lowry OH, Rosebrough NJ, Farr AL, Randall RJ. Protein measurement with the folin phenol reagent. *J Biol Chem.* (1951) 193:265–75. doi: 10.1016/S0021-9258(19)52451-6
24. Restan AZ, Camacho AA, Cerqueira JA, Zacche E, Kirnew MD, Loureiro BA. Effect of a lactate-guided conditioning program on heart rate variability obtained using 24-Holter electrocardiography in Beagle dogs. *PLoS ONE.* (2020) 15:e0233264. doi: 10.1371/journal.pone.0233264
25. Yuchi Y, Suzuki R, Kanno H, Teshima T, Matsumoto H, Koyama H. Right ventricular myocardial adaptation assessed by two-dimensional speckle tracking echocardiography in canine models of chronic pulmonary hypertension. *Front Vet Sci.* (2021) 8:727155. doi: 10.3389/fvets.2021.727155
26. Emilsson K. Right ventricular long-axis function in relation to left ventricular systolic function. *Clin Physiol Funct Imaging.* (2004) 24:212–5. doi: 10.1111/j.1475-097X.2004.00550.x

Conflict of Interest: The authors declare that the research was conducted in the absence of any commercial or financial relationships that could be construed as a potential conflict of interest.

Publisher's Note: All claims expressed in this article are solely those of the authors and do not necessarily represent those of their affiliated organizations, or those of the publisher, the editors and the reviewers. Any product that may be evaluated in this article, or claim that may be made by its manufacturer, is not guaranteed or endorsed by the publisher.

frontiers in Veterinary Science

ORIGINAL RESEARCH
published: 07 March 2022
doi: 10.3389/fvets.2022.819694

Development of a Loop-Mediated Isothermal Amplification Assay Coupled With a Lateral Flow Dipstick Test for Detection of Myosin Binding Protein C3 *A31P* Mutation in Maine Coon Cats

Pratch Sukumolanan[1], *Kanokwan Demeekul*[2] *and Soontaree Petchdee*[3]*

[1] *Program of Veterinary Clinical Studies, Graduate School, Kasetsart University, Nakorn Pathom, Thailand,* [2] *Department of Cardio-Thoracic Technology, Faculty of Allied Health Sciences, Naresuan University, Phitsanulok, Thailand,* [3] *Department of Large Animal and Wildlife Clinical Sciences, Faculty of Veterinary Medicine, Kasetsart University, Nakorn Pathom, Thailand*

OPEN ACCESS

Edited by:
Zeki Yilmaz,
Faculty of Veterinary Medicine, Turkey

Reviewed by:
Sena Ardicli,
Uludağ University, Turkey
Yu Ueda,
North Carolina State University, United States

***Correspondence:**
Soontaree Petchdee
fvetstr@ku.ac.th

Specialty section:
This article was submitted to Comparative and Clinical Medicine, a section of the journal Frontiers in Veterinary Science

Received: *22 November 2021*
Accepted: *07 January 2022*
Published: *07 March 2022*

Citation:
Sukumolanan P, Demeekul K and Petchdee S (2022) Development of a Loop-Mediated Isothermal Amplification Assay Coupled With a Lateral Flow Dipstick Test for Detection of Myosin Binding Protein C3 A31P Mutation in Maine Coon Cats. Front. Vet. Sci. 9:819694. doi: 10.3389/fvets.2022.819694

Background: Myosin-binding protein C3 *A31P* (*MYBPC3-A31P*) missense mutation is a genetic deviation associated with the development of hypertrophic cardiomyopathy (HCM) in Maine Coon cats. The standard detection of the *MYBPC3-A31P* mutation is complicated, time-consuming, and expensive. Currently, there has been a focus on the speed and reliability of diagnostic tools. Therefore, this study aimed to develop a loop-mediated isothermal amplification assay (LAMP) coupled with a lateral flow dipstick (LFD) test to detect *MYBPC3-A31P* mutations in Maine Coon cats.

Materials and Methods: Fifty-five Maine Coon cats were enrolled in this study, and blood samples were collected. *MYBPC3-A31P* was genotyped by DNA sequencing. Primers for LAMP with a LFD test were designed. The optimal conditions were determined, including temperature and time to completion for the reaction. The sensitivity of *A31P*-LAMP detection was compared between agarose gel electrophoresis (the standard method) and the LFD test. The *A31P*-LAMP-LFD test was randomly performed on seven cats (four with the *A31P* mutation and three wild-type cats).

Results: The *A31P*-LAMP procedure was able to distinguish between cats with *MYBPC3-A31P* wild-type cats and *MYBPC3-A31P* mutant cats. The LAMP reactions were able to be completed in 60 min at a single temperature of 64°C. Moreover, this study demonstrated that *A31P*-LAMP coupled with the LFD test allowed for *A31P* genotype detection at a lower DNA concentration than agarose gel electrophoresis.

Discussions: This new *A31P*-LAMP with a LFD test is a successful and reliable assay with a rapid method, cost-effectiveness, and low requirements for sophisticated equipment for the detection of *MYBPC3-A31P* mutations. Thus, this assay has excellent potential and can be recognized as a novel screening test for hypertrophic cardiomyopathy associated with *MYBPC3-A31P* mutations in felines.

Keywords: loop-mediated isothermal amplification, lateral flow dipstick test, myosin binding protein C3 *A31P*, mutation, Maine Coon cats

INTRODUCTION

Hypertrophic cardiomyopathy (HCM) is the most common hereditary cardiovascular disease in cats (1–4). The HCM phenotype has a prevalence of approximately 15% in cats (5). Moreover, the HCM phenotype in cats is related to an increase in age. Cats with clinical HCM commonly demonstrated left-sided congestive heart failure due to an impairment of diastolic function such as respiratory distress, cardiogenic pulmonary edema, pleural effusion, syncope, hypothermia, and atrial thromboembolism (ATE) (6–9). Specific breeds are highly associated with HCM development, especially the Maine Coon (10) and Ragdoll (11).

Previous research investigated the cause of HCM in cats. Myosin binding protein C3 *A31P* (*MYBPC3-A31P*), a single nucleotide polymorphism (SNP), was possibly associated with HCM development in cats, especially Maine Coon cats (12). *MYBPC3*, the sarcomeric protein in the myocardium, plays a crucial role in heart muscle contraction. Hence, *MYBPC3-A31P* mutation disturbs normal heart function and leads to cardiac concentric hypertrophy (12, 13).

The diagnosis of the HCM phenotype routinely relies on echocardiographic measurements. While detection of the SNP missense mutation *MYBPC3-A31P* is required for genetic screening in Maine Coon cats with familial HCM. However, cats without *MYBPC3-A31P* mutation may develop HCM. For the detection of SNP mutations, DNA sequencing is widely recognized as the gold standard technique (14). However, due to the inconvenience of DNA sequencing, requiring labor-intensive skills, prohibitive cost, and a long time, numerous researchers have developed different methods for SNP detection, such as allele-specific loop-mediated isothermal amplification (AS-LAMP) (15), microarray genotyping (16), molecular beacon genotyping (17), allele-specific polymerase chain reaction (AS-PCR) (18), and high-resolution melting (HRM) (19). Based on advanced genetic research, LAMP is one of the accepted powerful methods for SNP detection. Applying a constant single temperature, LAMP can be used for point-of-care (POC) diagnostic tests owing to the utilization of simple instruments such as thermocyclers, heated blocks, or water baths. The advantages of LAMP are rapid detection with high accuracy because of four to six specific primers used for LAMP and isothermal amplification as a one-step process (20, 21).

In contrast, one disadvantage of LAMP is the challenge of designing a specific primer set. The detection of LAMP products is also usually performed by agarose gel electrophoresis. However, this method uses complex procedures and requires specialized equipment. The other commonly used methods for LAMP product verification are the visualization of colorimetric and lateral flow dipstick (LFD) tests, which are simple and straightforward for carrying out POC tests in a small animal hospital or small laboratory unit (22). Nonetheless, the application of LAMP combined with LFD for the detection of *MYBPC3-A31P* mutations has not yet been reported. Therefore, this study aimed to develop a specific and rapid diagnostic tool for detecting *MYBPC3-A31P* mutations in Maine Coon cats using a LAMP assay coupled with an LFD.

TABLE 1 | Primer sets for *MYBPC3-A31P* genotyping.

Primer	Sequence (5'-3')	Length (bp)	Tm (°C)	GC (%)
A31P forward	AGCCTTCAGCAAGAAGCCA	19	51.1	53
A31P reverse	CAAACTTGACCTTGGAGGAGC	21	54.4	52
F3-*A31P*	CCATTGGCCCATCTCAGTC	19	53.2	58
B3-*A31P*	TGCGTAGGGTCCCTGGTC	18	54.9	67
FIP-*A31P*	CCTCGAACACAGCAGAGC-TCAGCCTTCAGCAAGAAGCC	38		
BIP-*A31P*	Biotin-GGCAGTGACATCAGCGCCA-CTGTCAGAGTGTGCCTCGTG	39		
A31P-probe	6-FAM-AGAGCGGTCAGGAGTAAAGG	20	53.8	55

The underline represents the MYBPC3-A31P SNP area on the A31P-LAMP primer.

MATERIALS AND METHODS

Animals and Sample Collection

Fifty-five Maine Coon cats were recruited into this study. The procedures of animal use were permitted by Kasetsart University Institutional Animal Care and Use Committee, Kasetsart University, Bangkok, Thailand (Approval number: ACKU 62-VET-059). The blood samples were collected from venous vessels for 2–3 ml per cat and stored in an ethylenediaminetetraacetic acid (EDTA) tube. The stored blood was aliquoted and kept at −20°C until DNA extraction. As described previously, the process of DNA extraction was conducted via Blood Genomic DNA Extraction Mini Kit (Favorgen, Taiwan) regarding manufacturer's recommendations (23).

Genotyping of *MYBPC3-A31P* Mutation

The protocol for genotyping of *MYBPC3-A31P* mutation was obtained from a previous study by Godiksen et al. (24). The details of forwarding and reverse primers were represented in **Table 1**. In brief, the steps of PCR included heat activation at 95°C for 15 min, 35 cycles of 3 steps of (i) denaturation at 95°C for 30 s, (ii) annealing at 58°C for 30 s, and (iii) extension at 72°C for 1 min and final extension at 72°C for 10 min. The size of the PCR product was 242 bp. PCR purification was then conducted following manufacturer's protocol (Favorgen, Taiwan). The Sanger sequencing was applied to determine the nucleotide of the *MYBPC3* gene. The mutation of *MYBPC-A31P* was evaluated by using the Bioedit program. After *MYBPC3-A31P* genotyping, the enrolled cats were divided into two groups: wild-type genotype and mutant genotype. Three cats from the wild-type group and four cats from the mutant group were randomly selected, owing to the concentration and purity of DNA extraction for the detection of the *A31P*-LAMP method coupled with LFD test.

A31P-LAMP Primer Design

The *A31P*-LAMP primer set was designed by using Primer Explorer version 5 software (http://primerexplorer.jp/lampv5e/index.html). Based on our experience, the high guanine and cytosine (G/C) nucleotide in the sequence of the *MYBPC3*

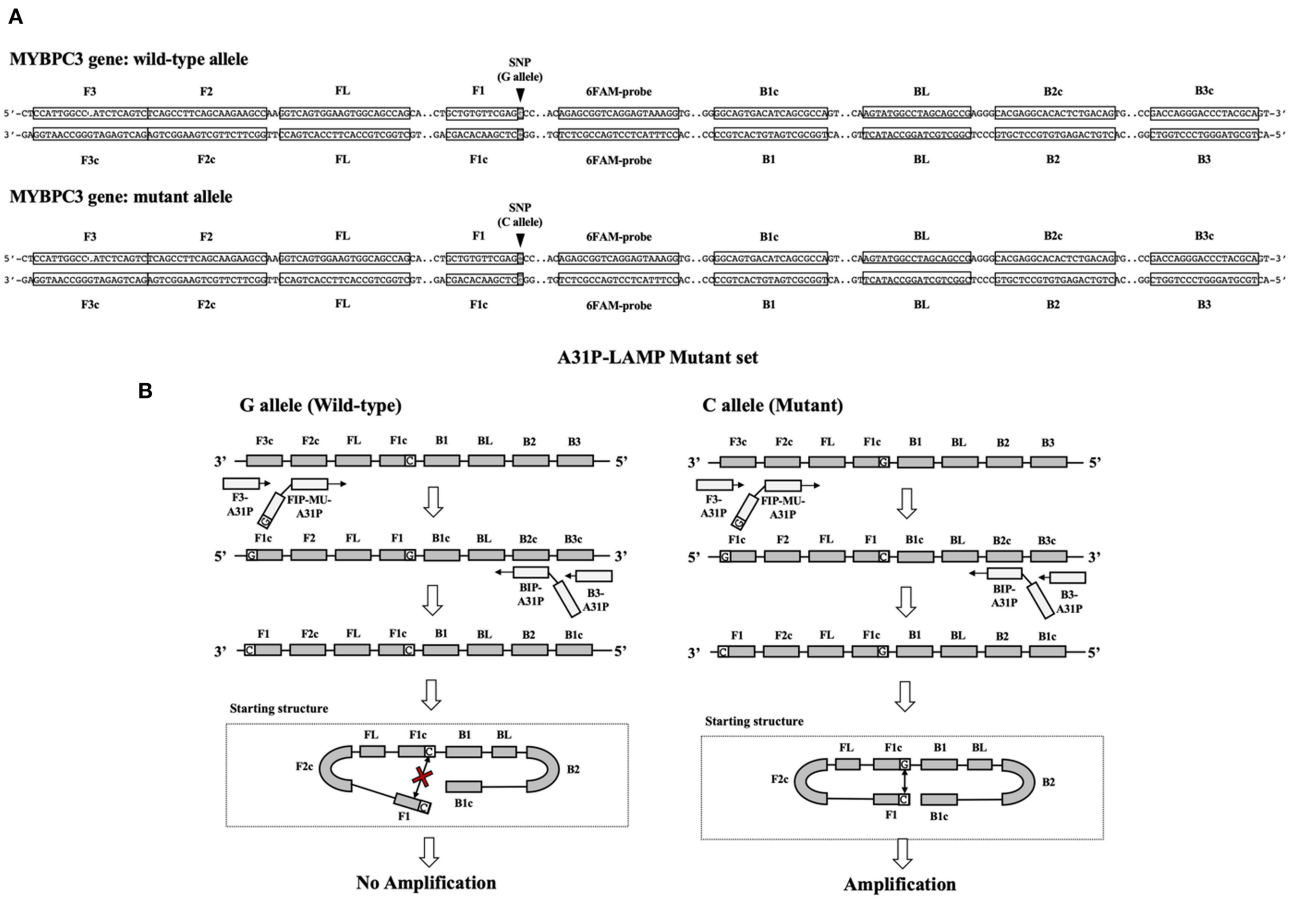

FIGURE 1 | The schematic of target sequence *A31P*-LAMP for detecting the *MYBPC3-A31P* and *A31P* LAMP process. **(A)** The homozygous wild-type and homozygous mutation of the *MYBPC3-A31P* were represented. The target of the *A31P*-LAMP primer regions including outer primer (F3 and B3 primer) and inner primer (FIP and BIP) was demonstrated. The dark triangle symbols pointed to *MYBPC3-A31P* SNP. **(B)** The schematic displayed the *A31P*-LAMP process. The guanine (G) allele from the homozygous wild type was not amplified while the cytosine (C) allele from homozygous mutation was amplified.

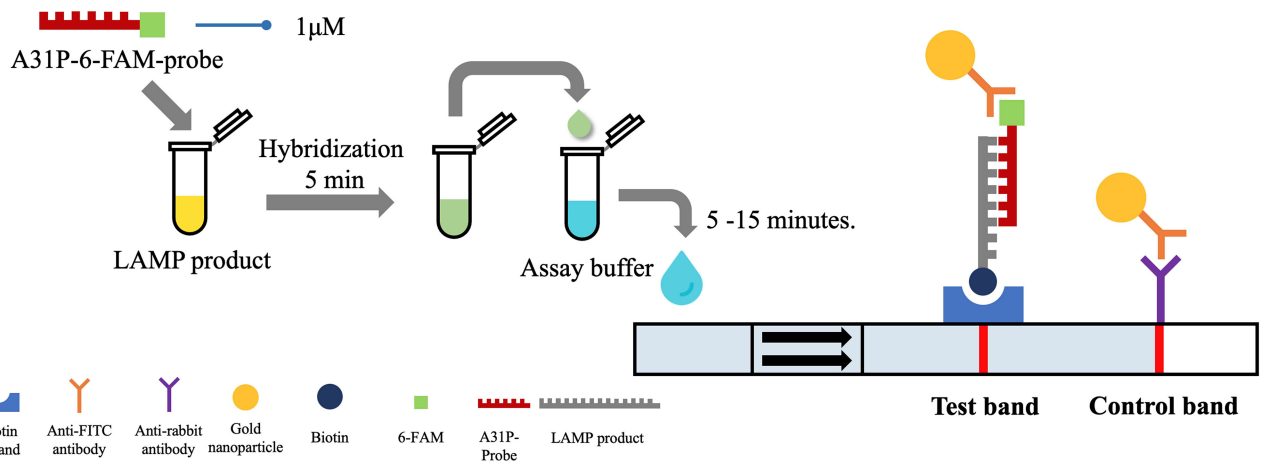

FIGURE 2 | The illustration of the principle of LFD test. The *A31P*-LAMP assay coupled with the LFD test showed the positive purple-red color band in the control line. In homozygous wild-type cats, the band was not represented in the test band while the positive test band appeared in cats with the *MYBPC3-A31P* mutation.

required a manual design of the primer set. The DNA sequence of *MYBPC3* protein was obtained from the National Center for Biotechnology Information (NCBI) database. In this research study, we designed the specific primer set based on the efficiency of recognition of SNP at position *A31P* for specifically selective amplification. The four designed primers can be used to detect mutant allele, cytosine (C), at the *A31P* missense mutation point from the *MYBPC3*. Four specific primers of *A31P*-LAMP, including forwarding inner primer (*A31P*-FIP), backward inner primer (*A31P*-BIP), *A31P*-F3 primer, and *A31P*-B3 primer were designed under the consideration of correlative comparable in the number of base pairs, percentage of G-C components, and melting temperatures. The position of *MYBPC3-A31P* was located at the 5' end of the designed forward inner primer (*A31P*-FIP). The designed primers set in this study were shown in **Table 1**. The illustration of the *MYBPC3*, location of *A31P*-LAMP primer, and steps of the *A31P*-LAMP process are represented in **Figure 1**.

TABLE 2 | Demographic information of animals in this study.

Parameters	Overall cats ($n = 55$)	*A31P*-LAMP-LFD ($n = 7$)
Age (months)	22.54 ± 3.22	24.57 ± 5.94
Weight (kg)	5.73 ± 0.35	5.56 ± 0.48
Male [number (%)]	30/55 (54.55%)	4/7 (57.14%)
MYBPC3-A31P mutation [number (%)]	8/55 (14.55%)	4/7 (57.14%)

A31P-LAMP Condition

A31P-LAMP solution was performed in a total volume of 25 μl per reaction. The mixture of reaction consisted of the following contents: 1X isothermal amplification buffer, containing 20 mM Tris-HCl, 10 mM $(NH_4)_2SO_4$, 50 mM of KCl, 2 mM $MgSO_4$, 0.1% Tween (New England Biolabs, United States), 6 mM of $MgSO_4$ (8 mM in final concentration), 1.4 mM of dNTPs (Thermo Scientific, United States), 0.8 M of betaine (Sigma-Aldrich, United States), 7.5% of DMSO, 0.2 μM of *A31P*-F3 primer, 0.2 μM of *A31P*-B3 primer, 1.6 μM of *A31P*-FIP primer, 1.6 μM of *A31P*-BIP primer, 8 unit of *Bst* 2.0 DNA polymerase (New England Biolabs, United States), 9.4 μl of sterile water, and 2 μl of DNA template. RNase-free water was used as a negative control in each experiment. To optimize the reaction time of *A31P*-LAMP, the initial condition was modified from the manufacturer (New England Biolabs, United States). The

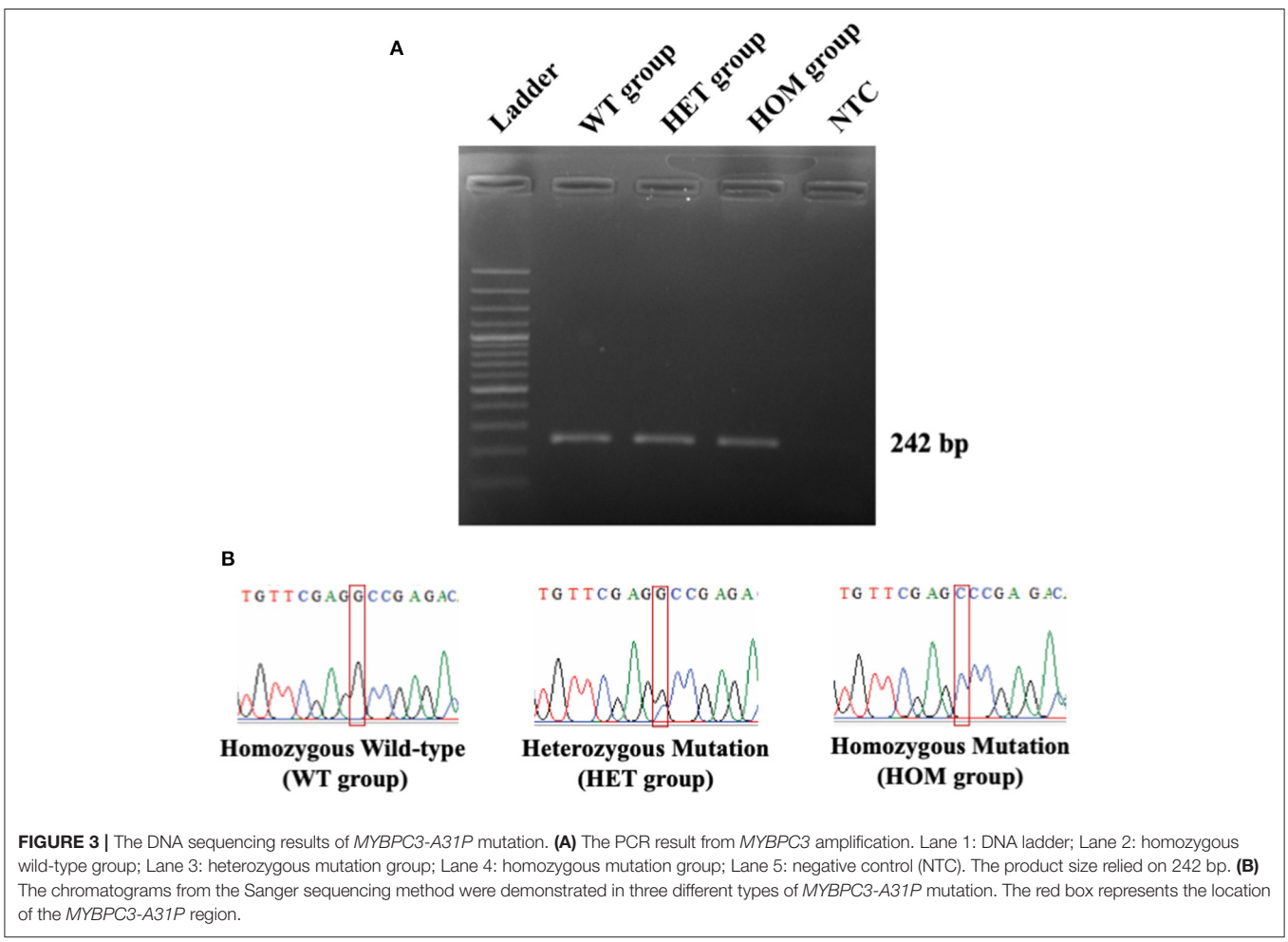

FIGURE 3 | The DNA sequencing results of *MYBPC3-A31P* mutation. **(A)** The PCR result from *MYBPC3* amplification. Lane 1: DNA ladder; Lane 2: homozygous wild-type group; Lane 3: heterozygous mutation group; Lane 4: homozygous mutation group; Lane 5: negative control (NTC). The product size relied on 242 bp. **(B)** The chromatograms from the Sanger sequencing method were demonstrated in three different types of *MYBPC3-A31P* mutation. The red box represents the location of the *MYBPC3-A31P* region.

optimal temperature of the *A31P*-LAMP reaction was evaluated at the gradient temperature, ranging from 60.8 to 68.0°C. Moreover, the mixtures of LAMP reaction were experimented with to incubate with different time points for 30, 45, 60, and 75 min.

Lateral Flow Dipstick Test

After the *A31P*-LAMP protocol was optimized, an LFD test was conducted for validating the test efficacy. Regarding this study, the designed *A31P*-LAMP products were labeled with biotin-tagged BIP. In our experiment, an LFD test was performed according to commercial manufacture protocol (Melinia Genline HybriDetect, GieBen, Germany). In short, the amplificated *A31P*-LAMP product was added with 1 μM of *A31P*-probe which was labeled with a 6-carboxyfluorescein (6-FAM) probe and allowed to hybridize in the same temperature of *A31P*-LAMP amplification for 5 min. The sequence of designed *A31P*-probe is represented in **Table 1**. Then, the 10 μl of hybridized LAMP products were directly dropped on lateral flow test strips. After that, lateral flow test strips were dipped into 80 μl of assay buffer that has been rewarmed at room temperature. Subsequently, the assay solution was emigrated by chromatography method along the test strips. The results of the LFD were observed by the naked eye within 5–15 min (**Figure 2**). A positive result for the MYBPC3-*A31P* mutation was represented by two bands, the control line and the test line, appearing on the strip of the LFD test in a purple-red color. One band, the control line, appeared for homozygous wild-type cats. If no band appeared for the control line, the results of the LFD test were considered invalid.

Verity of the Diagnostic Test for the *A31P*-LAMP Test

The analytical sensitivity of the *A31P*-LAMP test was determined in this study. The DNA of enrolled cats with *MYBPC3-A31P* mutation was diluted in various concentrations, including 10, 1, 0.1, 0.01, 0.001, 0.0001, and 0.00001 ng/μl. *A31P*-LAMP reaction was performed according to the protocol as described above. Then, the *A31P*-LAMP product was detected via (LFD test in comparison with a standard 1.5% agarose gel electrophoresis technique (25).

RESULTS

Descriptive Demographics of the Animals

In this study, 55 Maine Coon cats were recruited to the experiment. The average age of the enrolled cats was 22.54 ± 3.22 months (mean ± SEM). Their average body weight was 5.73 ± 0.35 kg (mean ± SEM). There were 30/55 (54.55%) male and 25/55 (45.45%) female Maine Coon cats. The DNA sequencing results revealed that 8/55 cats (14.55%) had the *MYBPC3-A31P* mutation. Among these, 1/55 (1.82%) was a homozygous mutation and 7/55 (12.73%) were heterozygous mutations. The demographics of the seven randomly selected Maine Coon cats are presented in **Table 2**. **Figure 3** represents the DNA sequencing examination of the *MYBPC3-A31P* mutation.

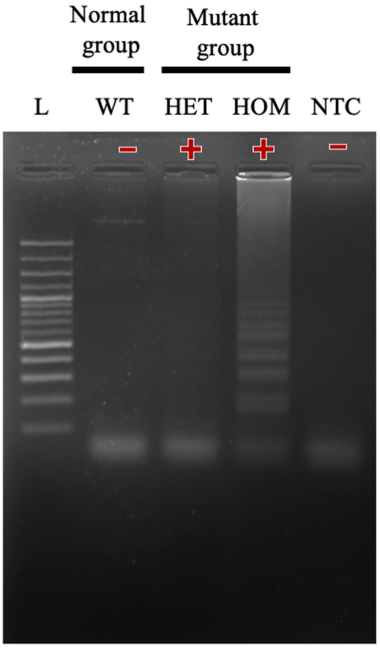

FIGURE 4 | The results of the *A31P*-LAMP reaction for identifying *MYBPC3-A31P* mutation in Maine Coon cats by agarose gel electrophoresis. The results showed a positive amplified band in Lane 3 and Lane 4 from both heterozygous mutation and homozygous mutation. In Lane 1, the cats from the homozygous wild type did not amplify the *A31P*-LAMP.

Design of the *A31P*-LAMP Primer for Detecting the *MYBPC3-A31P* Mutation

In this study, we successfully designed a specific *A31P*-LAMP primer for detecting the mutant allele cytosine (C) of the *MYBPC3-A31P* mutation. *MYBPC3-A31P* is located at the 5' end of the forward inner primer (FIP) to distinguish between the wild-type genotype and mutant genotype in Maine Coon cats. The *A31P*-LAMP reaction on the *MYBPC3-A31P* mutation in cats is demonstrated in **Figure 4**. The mutated allele (C), including the heterozygous mutation (G/C) (Lane 3) and the homozygous mutation (C/C) (Lane 4), was amplified and evaluated via agarose gel electrophoresis as the standard method. However, homozygous wild-type (G/G) was not able to be observed by *A31P*-LAMP detection. Therefore, the designed *A31P*-LAMP primer set is an excellent LAMP primer set for identifying the *MYBPC3-A31P* mutation.

Optimizations of the Designed *A31P*-LAMP Amplification

After designing an effective *A31P*-LAMP primer set, we sequentially optimized the conditions of the temperature and time to perform the *A31P*-LAMP reaction. The optimal temperatures were tested from 60.8 to 68.0°C. We observed that *A31P*-LAMP was successful at 62.4 to 66.2°C (**Figure 5A**). Thus, we selected the temperature of 64°C as optimal for the *A31P*-LAMP reaction. Moreover, the time required for the

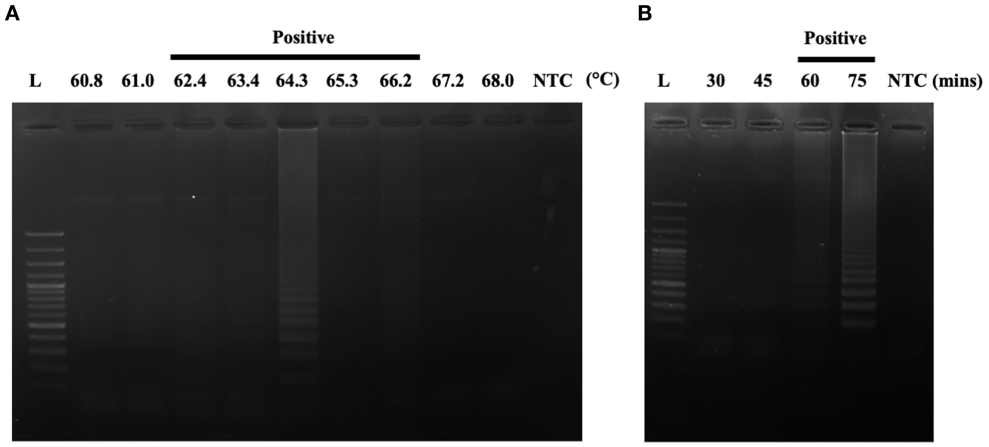

FIGURE 5 | The optimization of the *A31P*-LAMP protocol. **(A)** The optimal temperature was examined from 60.8 to 68°C. **(B)** The optimal temperature was evaluated from 30, 45, 60, to 75 min. The A31P-LAMP product was demonstrated within 60 min.

A31P-LAMP reaction was optimized. We discovered that *A31P*-LAMP had positive results from 60 to 75 min (**Figure 5B**). Therefore, the *A31P*-LAMP reaction at 60 min provided a better experimental outcome based on the higher intensity signal on gel electrophoresis.

Evaluation of *A31P*-LAMP Coupled With Lateral Flow Dipstick Test

A31P-LAMP coupled with the LFD test was operated to detect the designed LAMP products. Biotin was tagged at the backward inner primer (*A31P*-BIP) and 6-carboxyfluorescein (6-FAM) was labeled in the *A31P*-probe. In this experiment, two purple-red color bands for the test line and control line appeared for mutant cats with either a heterozygous or homozygous mutation. However, only one band appeared at the control line in homozygous wild-type cats (**Figure 6**). Overall observations suggested that the *A31P*-LAMP coupled with the LFD test was potentially suitable for detecting *MYBPC3-A31P*.

Verity of a Diagnostic Test for *A31P*-LAMP Test

The sensitivity test of the designed *A31P*-LAMP reaction for detecting *A31P*-LAMP product was investigated using 10-fold serial dilutions of DNA concentration in comparison between agarose gel electrophoresis (standard method) and LFD test. In agarose gel electrophoresis, we found that the lowest DNA concentration to detect LAMP-*A31P* was 0.0001 ng/μl.

In this study, seven out of 55 cats were diagnosed using the *A31P*-LAMP assay coupled with the LFD test, all seven cats were used in various DNA concentrations (from 0.0001 to 0.00001 ng/μl) to detect *A31P* mutation. The results showed that 0.00001 ng/μl of DNA concentration is the minimal amount that was able to detect *A31P* mutation with the LFD test in all seven cats (**Figure 7**). The accumulated finding indicated that the LFD test provided more sensitivity to identify *A31P*-LAMP product than agarose gel electrophoresis.

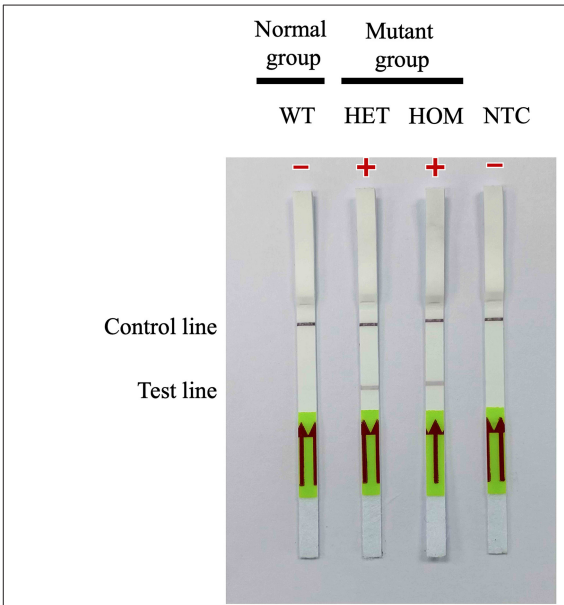

FIGURE 6 | Detection of the DNA (10 ng per μL) of *MYBPC3-A31P* mutation using the recombinase polymerase amplification-LFD test. WT, wild-type cats; HET, heterozygous mutation; HOM, homozygous mutation; NTC, negative control.

DISCUSSION

The *MYBPC3-A31P* mutation is of great concern in Maine Coon cats due to the severity of the pathogenesis and the HCM disease progression (26). According to our findings in the recruited study animals, the *MYBPC3-A31P* mutation rate was 14.55%, which is low. In concordance with our recent prior publication, the mutation rates of *MYBPC3-A31P* and *A74T* in Maine Coon cats accounted for 21.43% in Thailand (23). The prevalence of *MYBPC3-A31P* mutations worldwide (not included in Thailand)

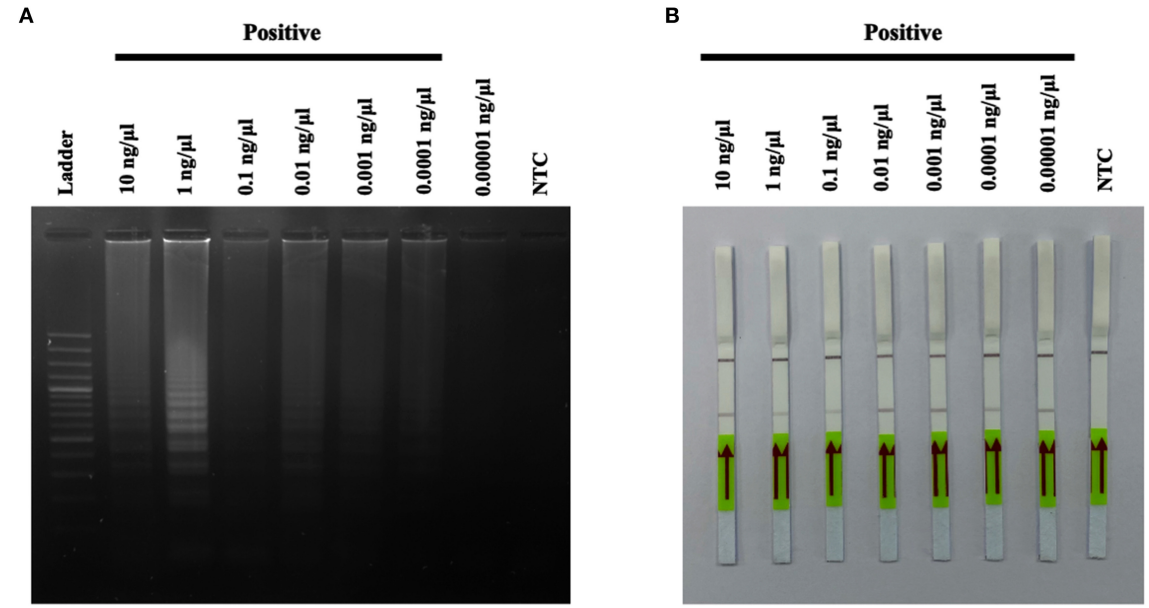

FIGURE 7 | The results of *A31P*-LAMP reaction from various DNA concentrations (10–0.00001 ng per μL) for identifying *MYBPC3-A31P* mutation in Maine Coon cats by agarose gel electrophoresis **(A)**. Detection of the DNA (10–0.00001 ng per μL) of *MYBPC3-A31P* mutation using the recombinase polymerase amplification-LFD test **(B)**. NTC, negative control.

is around 34% (27). Moreover, a study in a large European region showed that the prevalence of Maine Coon cats with the *MYBPC3-A31P* mutation was 41.5% (28).

To date, the gold standard for the detection of *MYBPC3-A31P* mutations is DNA sequencing. However, this method has various limitations, such as complicated processes, time-consuming, a prohibitive cost, and requiring special equipment. Over the past few decades, many researchers have attempted to develop better techniques for detecting SNP gene mutations. There is currently no perfect screening test that can be applied as a simple diagnostic tool for SNP gene mutations, especially *MYBPC3-A31P* mutations in cats.

This is the first study applying a LAMP coupled with an LFD test for screening *MYBPC3-A31P* mutations. Our findings demonstrated that *A31P*-LAMP associated with the LFD test can distinguish between wild-type cats and mutant cats with the *MYBPC3-A31P* mutation (**Figure 6**). Nevertheless, this technique has some limitations due to its inability to differentiate between homozygous and heterozygous mutation carriers.

After successfully developing a specific design of *A31P*-LAMP, the *A31P*-LAMP amplification was optimized for temperature and time (**Figure 5**). We found that the designed *A31P*-LAMP can be amplified in wide ranges of temperatures and with various equipment, such as thermocyclers, heated blocks, and water baths. This is consistent with a previous study, where the researchers developed a LAMP for detecting the *Mycobacterium leprae* pathogen that causes Hansen's disease. The researchers were able to conduct LAMP amplification in both a heated block and a water bath (29). Moreover, in this study, the average time to perform the *MYBPC3-A31P* test with LAMP was ∼110 min, including the process of DNA extraction, DNA amplification, and SNP detection. These data indicated that the designed *A31P*-LAMP required less time than other methods for SNP detection, such as PCR with DNA sequencing. PCR with DNA sequencing takes a long time due to the numerous steps, including DNA extraction, PCR, purification of PCR products, and DNA sequencing methods (30).

The designed *A31P*-LAMP can be clinically utilized as a rapid assay for *MYBPC3-A31P* mutation detection. To reduce the SNP detection time, in future studies, DNA from various samples, such as blood, dry blood spots (DBSs), hair follicles, or buccal swaps, will be extracted with sodium hydroxide (NaOH). This method can save time for DNA extraction owing to its simple DNA extraction procedure (31).

The LFD test is a widely accepted technique for detecting LAMP products. Following numerous lines of previous evidence, a LAMP assay combined with an LFD test was initially used for detecting several diseases not only in animals but also in humans. For instance, LAMP with the LFD test has been reported for use in the detection of the hepatitis B virus in human fields (32). In this publication, the LAMP products were detected by agarose gel electrophoresis, LFD tests, and gold nanoparticles (AuNPs). The three methods had the same accuracy for hepatitis B virus detection. In humans infected with *Plasmodium falciparum*, LAMP with an LFD for specific SNP detection (*Pf*SNP-LAMP-LFD) was applied to investigate malarial disease. It has been reported that malarial disease is associated with antifolate molecular resistance to manage antimalarial drug strategies (33).

LAMP combined with LFD has been applied to detect hepatopancreatic parvovirus in shrimp (34). They documented that this method is more sensitive than one-step PCR with agarose gel electrophoresis due to the lower DNA concentration. In terms of the objective of this study, the combination of LAMP with the LFD test had superior sensitivity for the detection of the designed LAMP product compared with agarose gel electrophoresis at 0.00001 ng/μl (**Figure 7**). Based on these promising results, the designed *A31P*-LAMP coupled with the LFD test is a reliable assay for *MYBPC3-A31P* mutation screening. Similar to the previous study (35), our results showed that the LAMP assay only took 110 min, this method provides on-site detection of a pathogen without requiring complex equipment. The LAMP assay is a rapid, simple, and sensitive test. Therefore, the *A31P*-LAMP assay could be more suitable as a screening point-of-care test for detecting the *MYBPC3-A31P* mutation in Maine Coon cats than the conventional PCR methods. In our pilot study, only 7/55 cats (12.73%) were diagnosed using the *A31P*-LAMP assay coupled with the LFD test, which was a limitation. For future work, it will be useful to increase the number of cats tested; however, we still gained valuable results by using the *A31P*-LAMP-LFD test in this study. Another limitation was that we did not investigate the efficacy of diagnostic examinations, such as the sensitivity and specificity, for *MYBPC3-A31P* diagnosis with the *A31P*-LAMP assay coupled with the LFD test. This should be further investigated in a larger population of Maine Coon cats.

Novel methods for genetic testing of the *MYBPC3-A31P* mutation play a crucial role in reducing the effects of familial HCM in Maine Coon cats (26, 36). According to the American College of Veterinary Internal Medicine (ACVIM) consensus statement guidelines for the classification, diagnosis, and management of cardiomyopathies in cats, *MYBPC3-A31P* screening is suggested to decrease the abnormal gene pool and reduce HCM development in Maine Coon cats (26, 36). In this study, the *A31P*-LAMP method coupled with the LFD test is a rapid diagnostic tool for detecting *MYBPC3-A31P* mutations.

CONCLUSION

Loop-mediated isothermal amplification for the *MYBPC3-A31P* mutation (*A31P*-LAMP) coupled with an LFD test has enormous potential for screening the crucial SNP mutation of the sarcomeric protein in Maine Coon cats with HCM. Due to its high sensitivity and simple evaluation, this technique can be readily applied for on-site routine examinations in pedigree breeding in cats.

DATA AVAILABILITY STATEMENT

The datasets presented in this study can be found in online repositories. The names of the repository/repositories and accession number(s) can be found in the article/supplementary material.

ETHICS STATEMENT

The animal study was reviewed and approved by Kasetsart University Institutional Animal Care and Use Committee, Kasetsart University, Bangkok, Thailand (Approval Number: ACKU 62-VET-059). Written informed consent was obtained from the owners for the participation of their animals in this study.

AUTHOR CONTRIBUTIONS

SP and PS designed the study and wrote the original manuscript and prepared figures. SP, KD, and PS collected all samples and analyzed and interpreted the data. PS performed the experiments of genotyping and LAMP with LFD. SP finalized the manuscript. All authors have read and approved the final version of the manuscript.

FUNDING

This research project was supported by the National Research Council of Thailand (NRCT): NRCT5-RGJ63002-035.

ACKNOWLEDGMENTS

The authors would like to express our sincere thanks to Asst. Prof. Dr. Janjira Phavaphutanon from the Department of Companion Animals Clinical Sciences, Kasetsart University for her advice and suggestions. Also, thanks to Kasetsart University Veterinary Teaching Hospital, Faculty of Veterinary Medicine, Kasetsart University and Biotechnology Laboratory, Kamphaeng Saen Veterinary Diagnostic Center, Faculty of Veterinary Medicine, Kasetsart University for providing the facilities for this research.

REFERENCES

1. Fox PR, Liu SK, Maron BJ. Echocardiographic assessment of spontaneously occurring feline hypertrophic cardiomyopathy. An animal model of human disease. *Circulation.* (1995) 92:2645–51. doi: 10.1161/01.CIR.92.9.2645
2. Ferasin L, Sturgess C, Cannon M, Caney S, Gruffydd-Jones T, Wotton P. Feline idiopathic cardiomyopathy: a retrospective study of 106 cats (1994–2001). *J Feline Med Surg.* (2003) 5:151–9. doi: 10.1016/S1098-612X(02)00133-X
3. Fox PR. Hypertrophic cardiomyopathy. Clinical and pathologic correlates. *J Vet Cardiol.* (2003) 5:39–45. doi: 10.1016/S1760-2734(06)70051-0
4. Granström S, Godiksen M, Christiansen M, Pipper CB, Martinussen T, Møgelvang R, et al. Genotype-phenotype correlation between the cardiac myosin binding protein C mutation *A31P* and hypertrophic cardiomyopathy in a cohort of Maine Coon cats: a longitudinal study. *J Vet Cardiol.* (2015) 17:S268–S81. doi: 10.1016/j.jvc.2015.10.005
5. Payne J, Brodbelt DC, Fuentes VL. Cardiomyopathy prevalence in 780 apparently healthy cats in rehoming centres (the CatScan study). *J Vet Cardiol.* (2015) 17:S244–57. doi: 10.1016/j.jvc.2015.03.008

6. Payne J, Borgeat K, Connolly D, Boswood A, Dennis S, Wagner T, et al. Prognostic indicators in cats with hypertrophic cardiomyopathy. *J Vet Intern Med.* (2013) 27:1427–36. doi: 10.1111/jvim.12215
7. Abbott JA. Feline hypertrophic cardiomyopathy: an update. *Vet Clin North Am Small Anim Pract.* (2010) 40:685–700. doi: 10.1016/j.cvsm.2010.04.004
8. Payne J, Fuentes VL, Boswood A, Connolly D, Koffas H, Brodbelt D. Population characteristics and survival in 127 referred cats with hypertrophic cardiomyopathy (1997 to 2005). *J Small Anim Pract.* (2010) 51:540–7. doi: 10.1111/j.1748-5827.2010.00989.x
9. Baty CJ, Malarkey DE, Atkins CE, DeFrancesco TC, Sidley J, Keene BW. Natural history of hypertrophic cardiomyopathy and aortic thromboembolism in a family of domestic shorthair cats. *J Vet Intern Med.* (2001) 15:595–9. doi: 10.1111/j.1939-1676.2001.tb01598.x
10. Kittleson MD, Meurs KM, Munro MJ, Kittleson JA, Liu S-K, Pion PD, et al. Familial hypertrophic cardiomyopathy in Maine coon cats: an animal model of human disease. *Circulation.* (1999) 99:3172–80. doi: 10.1161/01.CIR.99.24.3172
11. Meurs KM, Norgard MM, Ederer MM, Hendrix KP, Kittleson MD. A substitution mutation in the myosin-binding protein C gene in ragdoll hypertrophic cardiomyopathy. *Genomics.* (2007) 90:261–4. doi: 10.1016/j.ygeno.2007.04.007
12. Meurs KM, Sanchez X, David RM, Bowles NE, Towbin JA, Reiser PJ, et al. A cardiac myosin binding protein C mutation in the Maine Coon cat with familial hypertrophic cardiomyopathy. *Hum Mol Genet.* (2005) 14:3587–93. doi: 10.1093/hmg/ddi386
13. Coulton AT, Stelzer JE. Cardiac myosin binding protein C and its phosphorylation regulate multiple steps in the cross-bridge cycle of muscle contraction. *Biochemistry.* (2012) 51:3292–301. doi: 10.1021/bi300085x
14. Hawkins GA. *Analysis of Human Genetic Variations Using DNA Sequencing. Basic Science Methods for Clinical Researchers.* (2017). p. 77–98. doi: 10.1016/B978-0-12-803077-6.00005-9
15. Ding S, Chen R, Chen G, Li M, Wang J, Zou J, et al. One-step colorimetric genotyping of single nucleotide polymorphism using probe-enhanced loop-mediated isothermal amplification (PE-LAMP). *Theranostics.* (2019) 9:3723. doi: 10.7150/thno.33980
16. Lindroos K, Sigurdsson S, Johansson K, Rönnblom L, Syvänen AC. Multiplex SNP genotyping in pooled DNA samples by a four-color microarray system. *Nucleic Acids Res.* (2002) 30:e70. doi: 10.1093/nar/gnf069
17. Marras SA, Kramer FR, Tyagi S. Genotyping SNPs with molecular beacons. *Methods Mol Biol.* (2003) 212:111–28. doi: 10.1385/1-59259-327-5:111
18. Zhang W, Gianibelli M, Ma W, Rampling L, Gale K. Identification of SNPs and development of allele-specific PCR markers for γ-gliadin alleles in *Triticum aestivum*. *Theor Appl Genet.* (2003) 107:130–8. doi: 10.1007/s00122-003-1223-2
19. Garritano S, Gemignani F, Voegele C, Nguyen-Dumont T, Le Calvez-Kelm F, De Silva D, et al. Determining the effectiveness of high resolution melting analysis for SNP genotyping and mutation scanning at the TP53 locus. *BMC Genet.* (2009) 10:1–12. doi: 10.1186/1471-2156-10-5
20. Notomi T, Okayama H, Masubuchi H, Yonekawa T, Watanabe K, Amino N, et al. Loop-mediated isothermal amplification of DNA. *Nucleic Acids Res.* (2000) 28:e63. doi: 10.1093/nar/28.12.e63
21. Yongkiettrakul S, Kampeera J, Chareanchim W, Rattanajak R, Pornthanakasem W, Kiatpathomchai W, et al. Simple detection of single nucleotide polymorphism in *Plasmodium falciparum* by SNP-LAMP assay combined with lateral flow dipstick. *Parasitol Int.* (2017) 66:964–71. doi: 10.1016/j.parint.2016.10.024
22. Saechue B, Kamiyama N, Wang Y, Fukuda C, Watanabe K, Soga Y, et al. Development of a portable reverse transcription loop-mediated isothermal amplification system to detect the E1 region of Chikungunya virus in a cost-effective manner. *Genes Cells.* (2020) 25:615–25. doi: 10.1111/gtc.12797
23. Sukumolanan P, Phanakrop N, Thaisakun S, Roytrakul S, Petchdee S. Analysis of the serum peptidomics profile for cats with sarcomeric gene mutation and hypertrophic cardiomyopathy. *Front Vet Sci.* (2021) 8:771408. doi: 10.3389/fvets.2021.771408
24. Godiksen MT, Granström S, Koch J, Christiansen M. Hypertrophic cardiomyopathy in young Maine Coon cats caused by the p. *A31P* cMyBP-C mutation-the clinical significance of having the mutation. *Acta Vet Scand.* (2011) 53:7. doi: 10.1186/1751-0147-53-7
25. Günther S, Felten S, Wess G, Hartmann K, Weber K. Detection of feline Coronavirus in effusions of cats with and without feline infectious peritonitis using loop-mediated isothermal amplification. *J Virol Methods.* (2018) 256:32–6. doi: 10.1016/j.jviromet.2018.03.003
26. Fuentes VL, Abbott J, Chetboul V, Côté E, Fox PR, Häggström J, et al. ACVIM consensus statement guidelines for the classification, diagnosis, and management of cardiomyopathies in cats. *J Vet Intern Med.* (2020) 34:1062–77. doi: 10.1111/jvim.15745
27. Fries R, Heaney AM, Meurs KM. Prevalence of the myosin-binding protein C mutation in Maine Coon cats. *J Vet Intern Med.* (2008) 22:893–6. doi: 10.1111/j.1939-1676.2008.0113.x
28. Mary J, Chetboul V, Sampedrano CC, Abitbol M, Gouni V, Trehiou-Sechi E, et al. Prevalence of the *MYBPC3-A31P* mutation in a large European feline population and association with hypertrophic cardiomyopathy in the Maine Coon breed. *J Vet Cardiol.* (2010) 12:155–61. doi: 10.1016/j.jvc.2010.06.004
29. Garg N, Sahu U, Kar S, Ahmad FJ. Development of a Loop-mediated isothermal amplification (LAMP) technique for specific and early detection of *Mycobacterium leprae* in clinical samples. *Sci Rep.* (2021) 11:1–12. doi: 10.1038/s41598-021-89304-2
30. Gharahkhani P, O'Leary CA, Kyaw-Tanner M, Sturm RA, Duffy DL, A. non-synonymous mutation in the canine Pkd1 gene is associated with autosomal dominant polycystic kidney disease in Bull Terriers. *PLoS ONE.* (2011) 6:e22455. doi: 10.1371/journal.pone.0022455
31. Liu X, Zhang C, Zhao M, Liu K, Li H, Li N, et al. A direct isothermal amplification system adapted for rapid SNP genotyping of multifarious sample types. *Biosens Bioelectron.* (2018) 115:70–6. doi: 10.1016/j.bios.2018.05.021
32. Augkarawaritsawong S, Srisurapanon S, Wachiralurpan S, Areekit S, Chansiri K. Comparatively rapid screening tests for diagnosis of hepatitis b virus infection using loop-mediated isothermal amplification (LAMP) paired with lateral flow dipstick (LFD), gold nanoparticles (AuNPs), and real-time turbidimetry. *Sci Technol Asia*. (2019) 45—57. doi: 10.14456/scitechasia.2019.13
33. Yongkiettrakul S, Kolié FR, Kongkasuriyachai D, Sattabongkot J, Nguitragool W, Nawattanapaibool N, et al. Validation of PfSNP-LAMP-lateral flow dipstick for detection of single nucleotide polymorphism associated with pyrimethamine resistance in *Plasmodium falciparum*. *Diagnostics.* (2020) 10:948. doi: 10.3390/diagnostics10110948
34. Nimitphak T, Kiatpathomchai W, Flegel T. Shrimp hepatopancreatic parvovirus detection by combining loop-mediated isothermal amplification with a lateral flow dipstick. *J Virol Methods.* (2008) 154:56–60. doi: 10.1016/j.jviromet.2008.09.003
35. Khan M, Wang R, Li B, Liu P, Weng Q, Chen Q. Comparative evaluation of the LAMP assay and PCR-Based assays for the rapid detection of *Alternaria solani*. *Front Microbiol.* (2018) 9:2089. doi: 10.3389/fmicb.2018.02089
36. Schipper T. An overview of the current genetic and phenotypical selection strategies to reduce the prevalence of feline hypertrophic cardiomyopathy. *Vlaams Diergeneeskd Tijdschr.* (2020) 89:69–80. doi: 10.21825/vdt.v89i2.16355

Conflict of Interest: The research was conducted with a patent application (ID: 2103003416).

The authors declare that the research was conducted in the absence of any commercial or financial relationships that could be construed as a potential conflict of interest.

Publisher's Note: All claims expressed in this article are solely those of the authors and do not necessarily represent those of their affiliated organizations, or those of the publisher, the editors and the reviewers. Any product that may be evaluated in this article, or claim that may be made by its manufacturer, is not guaranteed or endorsed by the publisher.

frontiers in Veterinary Science

ORIGINAL RESEARCH
published: 30 March 2022
doi: 10.3389/fvets.2022.846492

Comparison of Intestinal Microbiota Between Healthy and MMVD Chihuahuas Using 16S rRNA Gene Amplicon Sequencing

Ryuji Araki[1,2,3], *Koji Iwanaga*[2], *Kazunori Ueda*[1], *Ayaka Shima*[4], *Genki Ishihara*[4], *Mitsuhiro Aizu*[4], *Toshiharu Fukayama*[4] *and Mitsuhiro Isaka*[3]*

[1] Yokohama Yamate Dog & Cat Medical Center, Yokohama, Japan, [2] Tokyo Veterinary Cardiology Center, Tokyo, Japan, [3] Department of Small Animal Clinical Sciences, School of Veterinary Medicine, Rakuno Gakuen University, Ebetsu, Japan, [4] Anicom Insurance, Inc., Tokyo, Japan

Myxomatous mitral valve disease (MMVD) is the most common cause of congestive heart failure in dogs, and although complications of MMVD to the lungs and kidneys have been identified, complications to the gut are less well understood. The intestinal microbiota is an important factor in the gut, and although the association between heart disease and the intestinal microbiota has been shown in human medicine, it is unknown in dogs. The study aimed to evaluate the relationship between MMVD and gut microbiota. A total of 69 healthy Chihuahuas and Chihuahuas with MMVD were evaluated for cardiac health by echocardiography and chest radiography and grouped according to ACVIM guidelines. Fecal samples were collected from all cases and 16S rRNA sequencing was used to reveal the intestinal microbiota. There were significant differences in LA/Ao, LVIDd, E vel, VHS, and VLAS with the severity of ACVIM. On the other hand, there were no significant differences in the diversity and composition of gut microbiota among the groups. The present study did not identify the effects of MMVD on the gut microbiota.

Keywords: Chihuahua, fractional shortening, intestinal complication, intestinal microbiota, myxomatous mitral valve disease

OPEN ACCESS

Edited by:
Zeki Yilmaz,
Faculty of Veterinary Medicine, Turkey

Reviewed by:
Kerem Ural,
Adnan Menderes University, Turkey
Sirilak Disatian Surachetpong,
Chulalongkorn University, Thailand

***Correspondence:**
Mitsuhiro Isaka
m-isaka@rakuno.ac.jp

Specialty section:
This article was submitted to Comparative and Clinical Medicine, a section of the journal Frontiers in Veterinary Science

Received: *31 December 2021*
Accepted: *07 February 2022*
Published: *30 March 2022*

Citation:
Araki R, Iwanaga K, Ueda K, Shima A, Ishihara G, Aizu M, Fukayama T and Isaka M (2022) Comparison of Intestinal Microbiota Between Healthy and MMVD Chihuahuas Using 16S rRNA Gene Amplicon Sequencing. Front. Vet. Sci. 9:846492. doi: 10.3389/fvets.2022.846492

INTRODUCTION

Much research has been done on the relationship between heart disease and the gut, and the concept of "Heart-Gut Axis" is well known. An important factor in understanding the function of the gut is the intestinal microbiota. In human medicine, it has been proven that the intestinal microbiota is involved in the pathogenesis of the cardiovascular disease, and it has been reported that lowering the blood concentration of trimethylamine N-oxide, a metabolite of intestinal bacteria, reduces the risk of cardiovascular disease (1–5). In addition, functional and morphological changes in the gut are induced in patients with heart failure, which in turn affects the gut microbiota. In both conditions, heart failure with preserved ejection fraction and heart failure with reduced ejection fraction, there were changes in the gut microbiota (6, 7). It has been reported that changes in the gut microbiota and the effects of heart failure on the intestinal tract can lead to systemic inflammation (8–12). Thus, in human medicine, the relationship between heart disease and intestinal microbiota has been the focus of much research and attention. Although research on the intestinal microbiota in veterinary medicine lags that in human medicine, it has been active in recent years due to

the widespread use of 16S rRNA sequencing (13). The relationship between inflammatory bowel disease and intestinal microbiota has been reported, and the relationship between disease and intestinal microbiota has attracted attention in veterinary medicine, but there have been no reports on heart disease and intestinal microbiota (14).

MMVD is the most common cause of congestive heart failure in dogs. Cavalier King Charles Spaniels, Maltese, and Toy Poodles are reported to be the predominant breeds, and in clinical practice, MMVD is commonly seen in Chihuahuas due to many dogs kept. If MMVD worsens, it can cause fatal complications such as pulmonary edema and arrhythmia. It has been suggested that heart failure due to long-term MMVD can cause decreased blood flow throughout the body, leading to ischemic injury to vital organs such as the kidney and pancreas (15–17). We clarified the intestinal complications of MMVD using intestinal mucosal injury markers (I-FABP and D-Lactate) (18). To further understand the intestinal complications of MMVD, we investigated the fecal samples from MMVD-affected and healthy Chihuahuas using 16S rRNA gene sequencing to reveal the intestinal microbiota.

MATERIALS AND METHODS

Animals

This study was approved by the Rakuno Gakuen University, School of Veterinary Medicine Institutional Animal Care and Use Committee (approval No. VH19A10). Dogs sampled at two institutions, Yokohama Yamate Dogs and Cats Medical Center and Tokyo Veterinary Cardiology Center, from April 2019 to May 2020 were included in the study. The breed was limited to Chihuahuas only. All Chihuahuas that met the following inclusion criteria and came to the hospital during the study period were included: (1) adult dogs; (2) consented to the study; (3) provided a fecal sample; (4) no cardiac disease not associated with MMVD; (5) no fatal comorbidities. Most of the healthy Chihuahuas came to the hospital for checkups and preventive medical care such as rabies vaccines. Patients with diseases secondary to MMVD (e.g., pulmonary hypertension or chronic kidney disease) were included; however, patients with other cardiac diseases (e.g., cardiac tumor or epicardial disease) were excluded. After obtaining the owner's consent, physical examination (weight and body condition score [BCS]), auscultation (presence and intensity of heart murmur), medical history, current medical history, medications, antibiotics, and the usual diet were recorded in all cases. In all the cases, chest radiography and echocardiography were performed to evaluate the heart.

Heart Examination

In all cases, the heart was evaluated by chest X-ray and echocardiography. Echocardiography was performed according to standard techniques, using a Xario (TOSHIBA, probe: PST-50AT, 5MHz) at the Yokohama Yamate Dogs and Cats Medical Center and a LOGIC e9 (GE Health care Japan, probe: 6S) at the Tokyo Veterinary Cardiology Center (19). Data were collected by two examiners, and all examinations were performed in a quiet room. Echocardiography included the subjective evaluation of the valve structure and function; mitral regurgitation (MR) jets on color Doppler examination in four-lumen cross-sectional images, left atrium to aorta ratio (LA/Ao) at diastole, left ventricular septal wall thickness at diastole (IVSd), left ventricular posterior wall thickness at diastole (LVPWd), left ventricular internal diameter at diastole (LVIDd), normalized left ventricular internal diameter (LVIDDN) (20), left ventricular internal diameters in systole (LVIDs), fractional shortening (FS), left ventricular ejection fraction (LVEF), and left ventricular inflow velocity waves (Evel, Avel) were evaluated and recorded.Chest X-rays were taken at maximal right lateral inspiration for the presence of pulmonary edema and a recording of VHS, and VLAS was measured according to previous reports (21, 22). The ACVIM guidelines were used for the severity of MMVD (23).

DNA Extraction From Fecal Samples

Fecal samples were collected using a specimen collection kit (Fecal collection container F, Fujifilm Wako Pharmaceutical) and sent to Anicom Insurance Inc. Add 200 μL of fecal samples and 810 μL of the lysis buffer (containing 224 μg/mL ProtenaseK) provided with the schematic kit to a Precellys 2 mL Soft Tissue Homogenizing Ceramic Beads Kit (KT03961-1-003.2, Bertin Instruments, France), and bead fragmentation (6,000 rpm, fragmentation 20 s, interval 30 s, fragmentation 20 s) was performed with a bead homogenizer Precellys Evolution (Bertin Instruments). The specimens were then lysed with Proteinase K by placing them on a heat block at 70°C for 10 min. Subsequently, Proteinase K was inactivated by placing the specimens on a heat block at 95°C for 5 min. The lysed samples were subjected to automated DNA extraction using chemagic 360 (PerkinElmer) and chemagic kit stool protocol to obtain 100 μL of DNA extract.

16S rRNA Gene Amplicon Sequencing

The DNAs were subjected to 16S rRNA gene amplicon sequencing. The V3–V4 regions of the 16S rRNA gene were amplified by PCR using the primers described in the Illumina 16S Sample Preparation Guide (Illumina, San Diego, CA, USA) as follows: forward, 5′-TCGTCGGCAGCGTCAGATGTGTATAAGAGACAG–CCTACGGGNGGCWGCAG-3′; reverse, 5′-GTCTCGTGGGCTCGGAGATGTGTATAAGAGACA-GGAC TAC- HVGGGTATCTAATCC-3′. PCR amplification was performed using the KAPA HiFi HotStart Library Amplification Kit (Kapa Biosystems, Wilmington, MA, USA). Each PCR product was purified using an Agencourt AMPure XP Beads Kit (Beckman Coulter, Pasadena, CA, USA) and quantified using a Qubit dsDNA BR Assay Kit (Thermo Fisher Scientific, Waltham, MA, USA). One hundred nanograms of each amplicon were subjected to a second PCR round for indexing, using a Nextera XT Index Kit v2 (Illumina). After purification, the PCR products were quantified with a NanoPhotometer (Implen, Westlake Village, CA, USA) and pooled into one tube at a final concentration of 1.6 ng/μl. The concentration of the pooled DNA library was validated using an Agilent 2100 Bioanalyzer (Agilent, Santa Clara, CA, USA). After denaturation

TABLE 1 | Patient characteristics of healthy Chihuahuas (H) and Chihuahuas with myxomatous mitral valve disease divided into three groups (B1, B2, and C/D).

	H ($n = 19$)	B1 ($n = 21$)	B2 ($n = 15$)	C/D ($n = 14$)
Age (years)	7.3 ± 2.6	11.1 ± 2.5	12.0 ± 2.4	11.8 ± 1.9
Sex (M/F)	9/10	11/10	6/9	8/6
Male/Casted male	0/9	2/9	2/4	3/5
Female/Spayed female	0/10	0/10	1/8	1/5
BW (kg)	3.1 ± 1.2	2.8 ± 1.0	3.0 ± 0.9	3.1 ± 1.0
Antibiotics	Nothing ($n = 19$)	Nothing ($n = 20$) Erythromycin ($n = 1$)	Nothing ($n = 15$)	Nothing ($n = 13$) Enrofloxacin ($n = 1$)
Comorbidities	CAD ($n = 1$) CKD ($n = 1$) Epileptic seizures ($n = 1$) Food allergy (n=1)	CAD ($n = 1$) Cholelithiasis ($n = 1$) Hypoadrenocorticism ($n = 1$) Hypothyroidism ($n = 2$)	CAD ($n = 1$) CKD ($n = 2$) Diabetes mellitus ($n = 1$) Hypothyroidism ($n = 1$) Tracheal collapse ($n = 2$)	CKD ($n = 7$) Tracheal collapse ($n = 2$)
Medicine				
ACE-I	$n = 1$	$n = 2$	$n = 10$	$n = 14$
Pimobendan	nothing	$n = 1$	$n = 13$	$n = 14$
Loop-diuretics	nothing	nothing	$n = 3$ (furosemide: 1.1 ± 0.6 mg/kg/day)	$n = 9$ (trasemide: 0.33 ± 0.23 mg/kg/day)

Data are presented as mean ± standard deviation (SD).
BW, body weight; BCS, body condition score; CAD, canine atopic dermatitis; CKD, chronic kidney disease; ACE-I angiotensin-converting enzyme inhibitor.

with NaOH,850 μl of 9pM DNA library and 150 μl of 9p M PhiX were mixed and subjected to pair-end sequencing using Illumina MiSeq with a MiSeq Reagent Kit v3 (600 cycles; Illumina).

Processing of 16S rRNA Gene Amplicon Sequencing

The sequence data were processed using Quantitative Insights into Microbial Ecology 2 (QIIME 2) v2019.4.0 (24). The DADA2 software package v2019.4.0 incorporated in QIIME 2 was used to correct the amplicon sequence errors and to construct an amplicon sequence variant (ASV) table. The ASV table was rarefied. Microbial taxonomy was assigned using a Naïve Bayes classifier trained on the SILVA 132 99 % database.

Microbial Diversity

Metrics of alpha diversity, including Shannon's index (Shannon), and those of beta diversity, including unweighted UniFrac and weighted UniFrac (weighted UniFrac), were examined using QIIME2. These diversity metrics were statistically analyzed by the method described below.

Statistical Analysis

Case data were entered into a spreadsheet, and statistical analysis was performed using SPSS software (SPSS statistics ver 24.0 IBM Japan, Ltd., Tokyo, Japan). Age, weight, and BCS were subjected to a one-way analysis of variance using the Turley-Kramer *post-hoc* test. For gender and medications, Fisher's exact test was used. Values for each group obtained by echocardiography and chest radiography were subjected to a one-way analysis of variance using the Turley-Kramer *post-hoc* test.

RESULTS

Animals

We collected a sample of 69 cases, ranging in age from 3 to 12 years, which were divided into four groups: Healthy chihuahuas (H) ($n = 19$), B1 ($n = 21$), B2 ($n = 15$), and C/D ($n = 14$) (**Table 1**). Of the 14 cases in Group C/D, 3 samples were taken at presentation to the hospital in a hypoxemic crisis of fulminant pulmonary edema. The remaining 11 cases were sampled on stable on medication at a scheduled recheck. There were no cases there that were excluded after sample collection. Group H had a predominantly lower mean age compared to the other groups. One case each in groups B1 and C/D was on antimicrobial medication. They were administered erythromycin and enrofloxacin, respectively. The following comorbidities were observed in each group. Group H: canine atopic dermatitis (CAD) ($n = 2$), chronic kidney disease (CKD) ($n = 1$), epileptic seizures ($n = 1$), and food allergy ($n = 1$). Group B1: CAD ($n = 1$), cholelithiasis ($n = 1$) hypoadrenocorticism ($n = 1$), and hypothyroidism ($n = 2$). Group B2: CAD ($n = 1$), CKD ($n = 2$), diabetes mellitus ($n = 1$), tracheal collapse

TABLE 2 | Patient diet data in healthy Chihuahuas (H) and Chihuahuas with myxomatous mitral valve disease divided into three groups (B1, B2, and C/D).

Group H ($n = 19$)	Group B1 ($n = 21$)
Dry food, Royal canin, RENAL ($n = 1$)	Dry food, Royal canin, satiety renovation ($n = 4$)
Dry food, Royal canin, satiety renovation ($n = 3$)	Dry food, other companies, animal based ($n = 2$)
Dry food, Royal canin, Allergy ($n = 3$)	Dry food, Royal canin, Chihuahua 8 ($n = 1$)
Dry food, Royal canin, Urinary ($n = 1$)	Dry food, Royal canin, Gastrointestinal low fat ($n = 5$)
Dry food, Hill's, z/d ($n = 2$)	Dry food, other companies, animal based (n=6)
Dry food, other companies, animal based ($n = 5$)	Dry food, other companies, plant based ($n = 1$)
Dry food, other companies, plant based (n = 2)	Homemade food ($n = 2$)
Dry food, Royal canin, Skin support ($n = 1$)	Homemade food ($n = 1$)
Group B2 ($n = 15$)	**Group C/D ($n = 14$)**
Dry food, Royal canin, Chihuahua 8 ($n = 3$)	Dry food, Royal canin, RENAL ($n = 4$)
Dry food, Royal canin, Gastrointestinal low fat ($n = 2$)	Dry food, Royal canin, Gastrointestinal low fat ($n = 2$)
Dry food, Royal canin, Cardiac ($n = 1$)	Dry food, Royal canin, Neutered care ($n = 1$)
Dry food, Royal canin, satiety renovation ($n = 1$)	Dry food, Hill's, z/d ($n = 1$)
Dry food, Royal canin, RENAL ($n = 2$)	Dry food, other companies, animal based ($n = 4$)
Dry food, other companies, animal based ($n = 6$)	Homemade food ($n = 2$)

($n = 2$), and hypothyroidism ($n = 1$). Group C/D: CKD ($n = 7$), tracheal collapse ($n = 2$). Owing to worsening cardiac disease, many patients were taking cardiac medications, and all the patients in Group C/D were taking angiotensin-converting enzyme inhibitors (ACI) and pimobendan. The three patients in Group B2 on loop diuretics (furosemide: 1.1 ± 0.6 mg/kg/day) had no history of heart failure and, were being prescribed for cough reduction. Nine patients in Group C/D were taking loop diuretics (trasemide: 0.33 ± 0.23 mg/kg/day). The dietary content is summarized in **Table 2**.

Echocardiography and Chest Radiography

Echocardiography, VHS, and VLAS findings are presented in **Table 2**. LVIDd was higher in groups B2 and C/D than in groups H and B1; however, there was no significant difference between groups B2 and C/D. The E wave also increased with severity, with group C/D having the highest increase. VHS and VLAS were also higher with worsening cardiac disease, with Group C/D having higher values than the other groups.

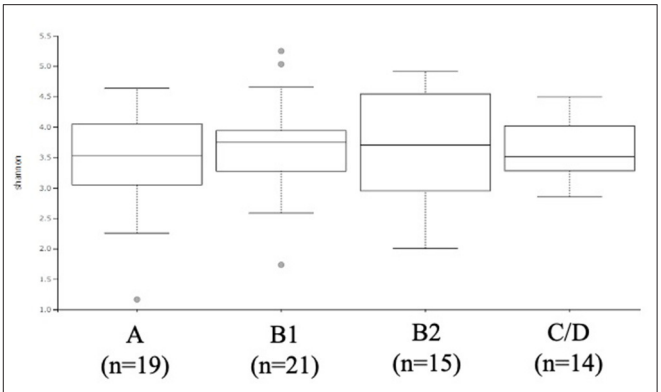

FIGURE 1 | α-diversity: Shannon index based on operational taxonomic unit abundance of healthy Chihuahuas (H) and Chihuahuas with myxomatous mitral valve disease divided into three groups (B1, B2, and C/D).

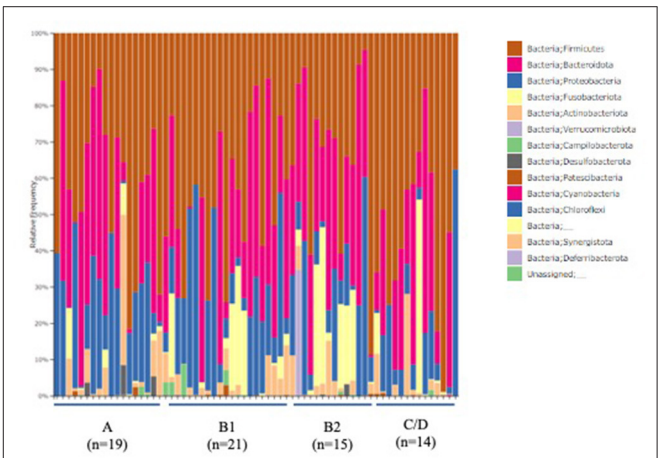

FIGURE 2 | Abundances of taxa in the intestinal microbiota of healthy Chihuahuas (H) and Chihuahuas with myxomatous mitral valve disease divided into three groups (B1, B2, and C/D) (phylum level).

Intestinal Microbiota Analysis

The ACVIM stage classification showed no significant difference in alpha diversity between the groups (**Figure 1**). In terms of the composition of the intestinal microbiota at the phylum level, most cases were dominated by bacterial species in the following order: Firmicutes, Bacteroides, Proteobacteria, Fusobacterium, Actinobacteria (**Figure 2**). There was no significant difference in the composition of the intestinal microbiota at the phylum level between the groups. Firmicutes/Bacteroidetes ratio was 82.6 ± 383.7.

DISCUSSION

As shown in **Table 3**, there was a tendency for the measurements obtained by echocardiography and chest radiography to worsen with increasing severity of MMVD. LA, LA/Ao, E vel, VHS, and VLAS were significantly increased in heart failure dogs compared with other groups, suggesting that they are important items

TABLE 3 | Echocardiographic and radiographic data in healthy Chihuahuas (H) and Chihuahuas with myxomatous mitral valve disease divided into three groups (B1, B2, and C/D).

	H ($n = 19$)	B1 ($n = 21$)	B2 ($n = 15$)	C/D ($n = 14$)	*P*-value for all
LA (mm)	13.2 ± 2.2	15.2 ± 2.7	23.3 ± 6.1 [b,d]	32.0 ± 7.4 [c,e,f]	<0.001
Ao (mm)	9.41 ± 1.0	10.2 ± 1.2	10.9 ± 1.3 [b]	10.5 ± 1.3 [c]	0.005
LA/Ao	1.4 ± 0.2	1.5 ± 0.2	2.1 ± 0.5 [b,d]	3.1 ± 0.9 [c,e,f]	<0.001
IVSDd (mm)	5.2 ± 1.2	5.2 ± 0.8	4.6 ± 0.9	4.4 ± 1.2	0.062
LVPWd (mm)	5.4 ± 0.9	5.6 ± 1.0	5.1 ± 0.8	5.1 ± 1.2	0.292
LVIDd (mm)	17.0 ± 2.6	19.1 ± 3.4	25.5 ± 3.4 [b,d]	27.5 ± 4.1 [c,e]	<0.001
LVIDs (mm)	10.8 ± 2.6	12.0 ± 2.2	14.1 ± 2.3 [b]	15.5 ± 3.6 [c,e]	<0.001
LVIDDN	1.7 ± 0.2	1.8 ± 0.1	1.9 ± 0.1 [b]	1.9 ± 0.2 [c]	<0.001
E vel (m/s)	0.6 ± 0.1	0.7 ± 0.2	0.9 ± 0.2 [b]	1.3 ± 0.5 [c,e,f]	<0.001
A vel (m/s)	0.6 ± 0.2	0.8 ± 0.2 [a]	1.0 ± 0.2 [b]	0.8 ± 0.3	<0.001
MR vel (m/s)	nothing	5.7 ± 0.6	5.4 ± 0.5	5.3 ± 0.6	0.286
FS (%)	35.7 ± 6.3	36.0 ± 6.7	38.8 ± 12.9	44.4 ± 11.0 [c]	0.037
LVEF (%)	68.3 ± 8.4	67.5 ± 7.6	72.0 ± 9.0	72.6 ± 11.7	0.338
VHS (v)	9.2 ± 0.9	9.4 ± 0.8 [a]	10.6 ± 0.7 [b,d]	11.5 ± 1.2 [c,e,f]	<0.001
VLAS (v)	2.0 ± 0.2	2.3 ± 0.3 [a]	3.1 ± 0.3 [b,d]	3.8 ± 0.4 [c,e,f]	<0.001

Data are presented as mean ± standard deviation (SD).

LA, left atrium; Ao, aorta; LA/Ao, maximal diastolic left atrial body-to-aortic root diameter ratio in the right, parasternal, short-axis view of the heart base; IVSTd, interventricular septum thickness in diastole; LVPWd, left ventricular posterior wall thickness in diastole; LVIDd, left ventricular internal diameter in diastole; LVIDs, left ventricular internal diameter in systole; LVIDDN, left ventricular internal diameter in diastole, indexed to the bodyweight; E vel, early wave velocity; A vel, atrium wave velocity; MR vel; mitral regurgitation velocity; FS, shortening fraction; LVEF, left ventricular ejection fraction; VHS, vertebral heart score; VLAS, vertebral left atrial size.

P-value for all: Results of the overall ANOVA F-test.

Pairwise comparisons were made using the Tukey-Kramer test.

[a] *Statistically significant difference between H and B1 ($P < 0.05$).*

[b] *Statistically significant difference between H and B2 ($P < 0.05$).*

[c] *Statistically significant difference between H and C/D ($P < 0.05$).*

[d] *Statistically significant difference between B1 and B2 ($P < 0.05$).*

[e] *Statistically significant difference between B1 and C/D ($P < 0.05$).*

[f] *Statistically significant difference between B2 and C/D ($P < 0.05$).*

indicating the severity of MMVD. LA/Ao and E vel have been reported to be important parameters that can be poor prognostic factors in MMVD, and the results of this study are consistent with previous reports (25). FS and LVEF did not differ significantly, although there was a trend toward increased values due to worsening MMVD. Worsening of MMVD has been reported in the past to increase FS, which was also true in this study, although the difference was not significant (26). FS is influenced by a variety of factors, including age, sex, breed, concomitant disease, preload, post load, and wall stress (20, 27–29). Also, many of the patients in this study were taking pimobendan internally. Pimobendan has been reported to increase FS and may have influenced this study (30). It has also been reported that the more severe the myocardial failure, the less FS that was elevated in MMVD (26). This study is difficult to evaluate because no histological examination of the myocardium was performed, but the influence of such a condition on the results should be considered.

As shown in **Figures 1**, **2**, there was no difference in α diversity or composition of the gut microbiota among the groups classified by the ACVIM guidelines in the gut microbiota analysis. In a study by Sandri et al. (31), the gut microbiota of dog was found to be composed of Firmicutes (43%), Bacteroidetes (19.8–26.9%), Fusobacteria (4.7–11%), and Proteobacteria (1.3–4.3%); in another study, it was found to be composed of Firmicutes (84% of all sequences), Bacteroidetes (2.9%), Fusobacteria (3.2%), Proteobacteria (7.8%) and Actinobacteria (1.7%) (32). These differences are thought to be due to individual and animal differences in intestinal microbiota (33). The intestinal microbiota of each case obtained by this study was consistent with previous reports in dogs. Human medicine has reported changes in gut microbiota composition in heart failure patients (6, 7). In this study, the FS and LVEF of heart failure dogs were normal and there was no obvious decrease in cardiac output. Decreased cardiac output has been reported to reduce blood flow to the intestinal tract and enteric membrane arteries, resulting in changes in the composition of the intestinal microbiota (6, 10). Considering the results of this study, it is possible that there is no obvious change in the composition of the gut microbiota in dogs with heart failure that do not have a reduced cardiac output. Next, we need to study the composition of the gut microbiota in dogs with heart failure due to MMVD with reduced cardiac output.

The intestinal microbiota is said to be affected by various factors such as individual differences and living environment, and it has been reported in dogs that it also changes with age. The age of Group H was lower in this study, and the difference in age between the groups may have affected the results. Chihuahuas are the preferred breed for MMVD, and the Chihuahuas that did not have MMVD tended to be sampled at a relatively young age (34–37). On the other hand, there is no

significant age difference between the groups affected by MMVD (B1, B2, C/D), and comorbidities and medications administered need to be considered. The major difference was the presence of diuretics and the presence of CKD. In Group C/D, 9/14 patients were taking diuretics due to worsening MMVD, and in Group B2, 3/15 patients were taking diuretics. Diuretics in Group B2 were used to reduce cough and were used at lower volumes than in Groups C/D. In human medicine, chronic kidney disease has been reported to affect the intestinal microbiota (38). The accumulation of urea in the blood due to decreased renal function increases urea efflux in the intestine, and urease-containing intestinal bacteria increase ammonia concentration in the intestine, affecting the intestinal microbiota (39). The possibility of intestinal ischemia and acidosis due to uremia has also been suggested. We need to consider the possibility that the dogs in this study had various comorbidities (e.g., CAD, hypothyroidism, etc.) that may have affected the results.

Two cases were taking antibiotics and many cases were taking ACE-I internally. It has been reported that antibiotics and ACE-I affect the intestinal microbiota, which may have influenced the results of this study (40). In addition, the number of cases in group C/D was less than the other groups (H, B1, B2) in this study. It is necessary to consider the possibility that this may have affected the results.

The effect of diet on intestinal microbiota has been reported in dogs (33, 41). Specifically, dogs fed a natural diet have more diverse and abundant microbial composition in the gut microbiota than dogs fed a commercial feed. In this study, there was no uniformity in the diets, as shown in **Table 2**. In addition, the treatment diet contained several dietary fibers, including prebiotics. It is highly possible that the lack of uniformity in diet content and composition affected the gut microbiota, and the results of this study should be discussed in this light.

In this study, we were not able to confirm changes in the gut microbiota according to ACVIM stage. However, because this study was a clinical trial, there were a variety of factors in each case, and the influence of these factors on the results of this study cannot be measured. In the future, it is necessary to conduct a study with uniform conditions.

DATA AVAILABILITY STATEMENT

The original contributions presented in the study are included in the article/supplementary material, further inquiries can be directed to the corresponding author/s.

ETHICS STATEMENT

The animal study was reviewed and approved by the Rakuno Gakuen University, School of Veterinary Medicine Institutional Animal Care and Use Committee (approval No. VH19A10). Written informed consent was obtained from the owners for the participation of their animals in this study.

AUTHOR CONTRIBUTIONS

RA: sample collection, data analysis, and writing the draft. KU and KI: sample collection and data analysis. AS, GI, MA, and TF: data analysis for gut microbiota. MI: study design and data analysis. All authors contributed to the article and approved the submitted version.

ACKNOWLEDGMENTS

We would like to thank Editage (www.editage.com) for English language editing.

REFERENCES

1. Andersen LW, Landow L, Baek L, Jansen E, Baker S. Association between gastric intramucosal pH and splanchnic endotoxin, antibody to endotoxin, and tumor necrosis factor-alpha concentrations in patients undergoing cardiopulmonary bypass. *Crit Care Med.* (1993) 21:210–7. doi: 10.1097/00003246-199302000-00011
2. Emoto T, Yamashita T, Sasaki N, Hirota Y, Hayashi T, So A, et al. Analysis of gut microbiota in coronary artery disease patients: a possible link between gut microbiota and coronary artery disease. *J Atheroscler Thromb.* (2016) 23:908–21. doi: 10.5551/jat.32672
3. Tang WH, Wang Z, Fan Y, Levison B, Hazen JE, Donahue LM, et al. Prognostic value of elevated levels of intestinal microbe-generated metabolite trimethylamine-N-oxide in patients with heart failure: refining the gut hypothesis. *J Am Coll Cardiol.* (2014) 64:1908–14. doi: 10.1016/j.jacc.2014.02.617
4. Wang Z, Klipfell E, Bennett BJ, Koeth R, Levison BS, Dugar B, et al. Gut flora metabolism of phosphatidylcholine promotes cardiovascular disease. *Nature.* (2011) 472:57–63. doi: 10.1038/nature09922
5. Wang Z, Roberts AB, Buffa JA, Levison BS, Zhu W, Org E, et al. Non-lethal inhibition of gut microbial trimethylamine production for the treatment of atherosclerosis. *Cell.* (2015) 163:1585–95. doi: 10.1016/j.cell.2015.11.055
6. Luedde M, Winkler T, Heinsen FA, Ruhlemann MC, Spehlmann ME, Bajrovic A, et al. Heart failure is associated with depletion of core intestinal microbiota. *ESC Heart Fail.* (2017) 4:282–90. doi: 10.1002/ehf2.12155
7. Huang Z, Mei X, Jiang Y, Chen T, Zhou Y. Gut Microbiota in heart failure patients with preserved ejection fraction (GUMPTION Study). *Front Cardiovasc Med.* (2021) 8:803744. doi: 10.3389/fcvm.2021.803744
8. Sandek A, Bauditz J, Swidsinski A, Buhner S, Weber-Eibel J, von Haehling S, et al. Altered intestinal function in patients with chronic heart failure. *J Am Coll Cardiol.* (2007) 50:1561–9. doi: 10.1016/j.jacc.2007.07.016
9. Sandek A, Bjarnason I, Volk HD, Crane R, Meddings JB, Niebauer J, et al. Studies on bacterial endotoxin and intestinal absorption function in patients with chronic heart failure. *Int J Cardiol.* (2012) 157:80–5. doi: 10.1016/j.ijcard.2010.12.016
10. Sandek A, Swidsinski A, Schroedl W, Watson A, Valentova M, Herrmann R, et al. Intestinal blood flow in patients with chronic heart failure: a link with bacterial growth, gastrointestinal symptoms, and cachexia. *J Am Coll Cardiol.* (2014) 64:1092–102. doi: 10.1016/j.jacc.2014.06.1179
11. Pasini E, Aquilani R, Testa C, Baiardi P, Angioletti S, Boschi F, et al. Pathogenic gut flora in patients with chronic heart failure. *JACC Heart Fail.* (2016) 4:220–7. doi: 10.1016/j.jchf.2015.10.009
12. Kamo T, Akazawa H, Suda W, Saga-Kamo A, Shimizu Y, Yagi H, et al. Dysbiosis and compositional alterations with aging in the gut microbiota of patients with heart failure. *PLoS ONE.* (2017) 12:e0174099. doi: 10.1371/journal.pone.0174099

13. Handl S, Dowd SE, Garcia-Mazcorro JF, Steiner JM, Suchodolski JS. Massive parallel 16S rRNA gene pyrosequencing reveals highly diverse fecal bacterial and fungal communities in healthy dogs and cats. *FEMS Microbiol Ecol.* (2011) 76:301–10. doi: 10.1111/j.1574-6941.2011.01058.x
14. Xenoulis PG, Palculict B, Allenspach K, Steiner JM, Van House AM, Suchodolski JS. Molecular-phylogenetic characterization of microbial communities imbalances in the small intestine of dogs with inflammatory bowel disease. *FEMS Microbiol Ecol.* (2008) 66:579–89. doi: 10.1111/j.1574-6941.2008.00556.x
15. Han D, Choi R, Hyun C. Canine pancreatic-specific lipase concentrations in dogs with heart failure and chronic mitral valvular insufficiency. *J Vet Intern Med.* (2015) 29:180–3. doi: 10.1111/jvim.12521
16. Pouchelon JL, Atkins CE, Bussadori C, Oyama MA, Vaden SL, Bonagura JD, et al. Cardiovascular-renal axis disorders in the domestic dog and cat: a veterinary consensus statement. *J Small Anim Pract.* (2015) 56:537–52. doi: 10.1111/jsap.12387
17. Borgarelli M, Haggstrom J. Canine degenerative myxomatous mitral valve disease: natural history, clinical presentation and therapy. *Vet Clin North Am Small Anim Pract.* (2010) 40:651–63. doi: 10.1016/j.cvsm.2010.03.008
18. Araki R, Iwanaga K, Ueda K, Isaka M. Intestinal complication with myxomatous mitral valve diseases in Chihuahuas. *Front Vet Sci.* (2021) 8:777579. doi: 10.3389/fvets.2021.777579
19. Thomas WP, Gaber CE, Jacobs GJ, Kaplen PM, Lombard CW, Mioise NS, et al. Recommendations for standards in transthoracic two-dimentional echocardiography in the dogb and cat. *J Vet Intern Med.* (1993) 7:247–52. doi: 10.1111/j.1939-1676.1993.tb01015.x
20. Cornell CC, Kittleson MD, Torre PD, Haggstorm J, Lombard CW, Pedersen HD, et al. Allometric scaling of M-Mode cardiac measurements in normal adult dogs. *J Vet Intern Med.* (2004) 18:311–21. doi: 10.1111/j.1939-1676.2004.tb02551.x
21. Malcolm EL, Visser LC, Phillips KL, Johnson LR. Diagnostic value of vertebral left atrial size as determined from thoracic radiographs for assessment of left atrial size in dogs with myxomatous mitral valve disease. *J Am Vet Med Assoc.* (2018) 253:1038–45. doi: 10.2460/javma.253.8.1038
22. Buchanan JW, Bucheler J. Vertebral scale system to measure canine heart size in radiographs. *J Am Vet Med Assoc.* (1995) 206:194–9.
23. Keene BW, Atkins CE, Bonagura JD, Fox PR, Haggstrom J, Fuentes VL, et al. ACVIM consensus guidelines for the diagnosis and treatment of myxomatous mitral valve disease in dogs. *J Vet Intern Med.* (2019) 33:1127–40. doi: 10.1111/jvim.15488
24. Bolyen E, Rideout JR, Dillon MR, Bokulich NA, Abnet CC, Al-Ghalith GA, et al. Reproducible, interactive, scalable and extensible microbiome data science using QIIME 2. *Nat Biotechnol.* (2019) 37:852–7. doi: 10.1038/s41587-019-0209-9
25. Borgarelli M, Savarino P, Crosara S, Santilli RA, Chiavegato D, Poggi M, et al. Survival characteristics and prognostic variables of dogs with mitral regurgitation attributable to myxomatous valve disease. *J Vet Intern Med.* (2008) 22:120–8. doi: 10.1111/j.1939-1676.2007.0008.x
26. Borgarelli M, Tarducci A, Zanatta R, Haggstorm J. Decreased systolic function and inadequate hypertrophy in large and small breed dogs with chronic mitral valve insufficiency. *J Vet Intern Med.* (2007) 21:61–7. doi: 10.1111/j.1939-1676.2007.tb02929.x
27. Moise NS, Moise NS, Scarlett J, Mohammed H, Yeager AE. Effect of breed and body weight on echocardiographic values in four breeds of dogs of differing somatotype. *J Vet Intern Med.* (1992) 6:220–4. doi: 10.1111/j.1939-1676.1992.tb00342.x
28. Urabe Y, Mann DL, Kent RL, Nakano K, Tomanek RJ, Carabello BA, et al. Cellular and ventricular contractile dysfunction in experimental canine mitral regurgitation. *Circ Res.* (1992) 70:131–47. doi: 10.1161/01.RES.70.1.131
29. della Torre PK, Kirby AC, Church DB, Malik R. Echocardiographic measurements in greyhounds, whippets and Italian greyhounds–dogs with a similar conformation but different size. *Aust Vet J.* (2000) 78:49–55. doi: 10.1111/j.1751-0813.2000.tb10361.x
30. Kanno N, Kuse H, Kawasaki M, Hara A, Kano R, Sasaki Y. Effects of pimobendan for mitral valve regurgitation in dogs. *J Vet Med Sci.* (2007) 69:373–7. doi: 10.1292/jvms.69.373
31. Sandri M, Dal Monego S, Conte G, Sgorlon S, Stefanon B. Raw meat based diet influences faecal microbiome and end products of fermentation in healthy dogs. *BMC Vet Res.* (2017) 13:65. doi: 10.1186/s12917-017-0981-z
32. Igarashi H, Maeda S, Ohno K, Horigome A, Odamaki T, Tsujimoto H. Effect of oral administration of metronidazole or prednisolone on fecal microbiota in dogs. *PLoS ONE.* (2014) 9:e107909. doi: 10.1371/journal.pone.0107909
33. Kim J, An JU, Kim W, Lee S, Cho S. Differences in the gut microbiota of dogs (Canis lupus familiaris) fed a natural diet or a commercial feed revealed by the Illumina MiSeq platform. *Gut Pathog.* (2017) 9:68. doi: 10.1186/s13099-017-0218-5
34. Guard BC, Mila H, Steiner JM, Mariani C, Suchodolski JS, Chastant-Maillard S. Characterization of the fecal microbiome during neonatal and early pediatric development in puppies. *PLoS ONE.* (2017) 12:e0175718. doi: 10.1371/journal.pone.0175718
35. Masuoka H, Shimada K, Kiyosue-Yasuda T, Kiyosue M, Oishi Y, Kimura S, et al. Transition of the intestinal microbiota of dogs with age. *Biosci Microbiota Food Health.* (2017) 36:27–31. doi: 10.12938/bmfh.BMFH-2016-021
36. Matumoto H, Baba E, Ishikawa H, Hodate Y. Studies in bacterial flora in the alimentary canal of dogs II. Development of the fecal bacterial flora in puppies. *J Vet Med Sci.* (1976) 38:485–94. doi: 10.1292/jvms1939.38.485
37. Mizukami K, Uchiyama J, Igarashi H, Murakami H, Osumi T, Shima A, et al. Age-related analysis of the gut microbiome in a purebred dog colony. *FEMS Microbiol Lett.* (2019) 366:8. doi: 10.1093/femsle/fnz095
38. Gao H, Liu S. Role of uremic toxin indoxyl sulfate in the progression of cardiovascular disease. *Life Sci.* (2017) 185:23–9. doi: 10.1016/j.lfs.2017.07.027
39. Ramezani A, Raj DS. The gut microbiome, kidney disease, and targeted interventions. *J Am Soc Nephrol.* (2014) 25:657–70. doi: 10.1681/ASN.2013080905
40. Doig CJ, Sutherland LR, Sandham JD, Fick GH, Verhoef M, Meddings JB. Increased intestinal permeability is associated with the development of multiple organ dysfunction syndrome in critically ill ICU patients. *Am J Respir Crit Care Med.* (1998) 158:444–51. doi: 10.1164/ajrccm.158.2.9710092
41. Zentek J, Marquart B, Pietrzak T, Ballevre O, Rochat F. Dietary effects on bifidobacteria and Clostridium perfringens in the canine intestinal tract. *J Anim Physiol Anim Nutr (Berl).* (2003) 87:397–407. doi: 10.1046/j.0931-2439.2003.00451.x

Conflict of Interest: AS, GI, MA, and TF were employed by Anicom Inc.

The remaining authors declare that the research was conducted in the absence of any commercial or financial relationships that could be construed as a potential conflict of interest.

Publisher's Note: All claims expressed in this article are solely those of the authors and do not necessarily represent those of their affiliated organizations, or those of the publisher, the editors and the reviewers. Any product that may be evaluated in this article, or claim that may be made by its manufacturer, is not guaranteed or endorsed by the publisher.

Advantages of publishing in Frontiers

OPEN ACCESS
Articles are free to read for greatest visibility and readership

FAST PUBLICATION
Around 90 days from submission to decision

HIGH QUALITY PEER-REVIEW
Rigorous, collaborative, and constructive peer-review

TRANSPARENT PEER-REVIEW
Editors and reviewers acknowledged by name on published articles

Frontiers
Avenue du Tribunal-Fédéral 34
1005 Lausanne | Switzerland

Visit us: www.frontiersin.org
Contact us: frontiersin.org/about/contact

REPRODUCIBILITY OF RESEARCH
Support open data and methods to enhance research reproducibility

DIGITAL PUBLISHING
Articles designed for optimal readership across devices

FOLLOW US
@frontiersin

IMPACT METRICS
Advanced article metrics track visibility across digital media

EXTENSIVE PROMOTION
Marketing and promotion of impactful research

LOOP RESEARCH NETWORK
Our network increases your article's readership